Azobenzenes and Dithiocarbamates in Molecular Film Devices

Inauguraldissertation

zur

Erlangung der Würde eines Doktors der Philosophie

vorgelegt der

Philosophisch-Naturwissenschaftlichen Fakultät

der Universität Basel

von

Federica Reinders

aus Weil am Rhein, Deutschland

Basel, 2012

Genehmigt von der Philosophisch-Naturwissenschaftlichen Fakultät
auf Antrag von

Prof. Dr. Marcel Mayor

Prof. Dr. Catherine Housecroft

Dr. Florian von Wrochem

Basel, den 26.06.2012

Prof. Dr. Martin Spiess

Dedicated to:

Enrichetta and Peter

Acknowledgments

First and foremost I would like to thank my supervisor Prof. Dr. Marcel Mayor for having me in his research group and for the trustful working atmosphere during the continuous learning process in the last four years. Your encouragement was a major contribution in seeing me through this challenge.

I am very grateful to Prof. Dr. Catherine Housecroft and Dr. Florian von Wrochem for being the co-referees of this thesis. Many thanks go to Prof. Dr. Edwin Constable for chairing the examination committee.

My sincere thanks go to Dr. Florian von Wrochem, Dr. William Ford and Dr. Deqing Gao for the pleasant collaboration and the interdisciplinary scientific and enjoyable non-scientific discussions during our meetings. Moreover I thank Prof. Dr. Paolo Samorí and his research group for the fruitful collaboration.

My thanks go to Dr. Daniel Häussinger for performing NMR experiments, Dr. Heinz Nadig for mass spectrometric analyses, Werner Kirsch for elemental analyses and Dr. Markus Neuburger for measuring solid state structures. I also want to thank the technical staff from the 'Werkstatt': Maurus Meier, Alois Schäuble, Andreas Koller, Francis Cabrera and Manuel Hermida. Moreover, I am thankful to Markus Hauri and Roy Lips from the 'Materialausgabe' and the secretaries Brigitte Howald, Audrey Fischer, Marina Mambelli and Beatrice Erismann.

For financial support I acknowledge the Stuttgart Technology Center SONY and the National Center of Competence in Research (NCCR) Nanoscale Science.

For the nice time in the labs and during the group trips I thank with great pleasure the whole Mayor group. I hope you keep treating my memorial hiking shoes with care.

Thank you, Dr. Loïc Lepleux, Dr. Jens Tüxen, Dr. Marcel Müri, Thomas Eaton, Dr. Sergio Grunder and Jens Hermes for proof-reading this thesis.

I really appreciate and I am very thankful for the love and support of my parents, Enrichetta and Peter, and my brother, Alberto. All my friends I thank for the nice times spent together and I am excited about the future gatherings.

Jens, how can I express my thanks without becoming sentimental? For sure, you deserve more than just being acknowledged.

Table of Contents

1 Introduction

The functionalization of surfaces covers a large research area, including medicine,[1,2] biology,[3,4] polymer science[5,6] and catalysis.[7,8] The search for new functional electronic components,[9,10] driven by our computer determined daily life, is a further driving force for the development of modified surfaces. This technology field originates from the electronic industry, where the high economic pressure for the miniaturization of electric components is tremendous. The performance of small silicon semiconducting surfaces has been improved over the last years. This "top-down" approach, however, will become more and more challenging, as the technical fabrication of smaller devices and the decrease in expenses will be difficult to correlate with each other. Thus, scientists are searching for alternatives to produce smaller and faster electronic devices. When applying the "bottom-up" approach towards successful nanotechnology, the interdisciplinary communication of physicists and chemists is required. "Nanotools", i.e. well-defined entities of nanometric size, such as molecules, complexes, particles and clusters, are known to modify the properties of surfaces once functionalized on them.[11] The close examination of the structures of these resulting functional molecular films is essential to understand the factors that dramatically alter the interfacial properties of the surface.[12,13] The advances in synthetic chemistry and the improvement of physical experimental setups to study elemental units like atoms, particles and molecules with appropriate techniques allow for the investigation of new functional molecular-based nanomaterials.[14–17] The use of individual molecular materials adsorbed on metallic substrates to perform functions as today's semiconducting devices is the concept of molecular electronics with the main goal of shrinking electrical circuits.[18–21] In this approach the molecules or molecular films become the electronic components due to their intrinsic electronic properties given by the electron distribution in their structures. The carefully planning of tailor-made molecules can provide the targets to fulfill basic functions, such as rectification, switching and storage.[19,22–24] In order to analyze the electronic properties of the molecules, they have to be attached to a matrix (see section 1.1.1) and especially the investigation of their substrate-molecular film interfaces is crucial. Such test devices are far away from future electronic applications, however, they are necessary to correlate the molecular structure with the electronic properties. This fundamental research of surface functionalization is the basis for the development of future electronic devices based on molecular films.

The research activity within this PhD work is mainly the design, the synthesis and characterization of suitable molecular structures to enrich molecular films junctions with additional electronic properties. Although the modification of surface properties includes the

close collaboration of scientists from different backgrounds, the interdisciplinary work here is presented from a chemist's point of view.

At first an introduction about surface functionalization is given, where the general techniques and requirements are briefly discussed. Afterwards a general overview of azobenzenes and dithiocarbamates will be presented, as these functionalities are considered to be appealing molecular building blocks towards functional surfaces.

The main part deals with the design, synthesis and characterization of molecular scaffolds, which contain azobenzene and dithiocarbamate units, respectively, for the purpose to modify surface properties. The preparation of the corresponding self-assembled monolayers and the subsequent surface investigations will be described. This research activity is geared towards future applications such as data storage, memory devices and organic semiconductors.

1.1 Surface Functionalization

1.1.1 Established Functionalization Techniques

For the functionalization of molecules to substrates two techniques are often used that profit from the self-assembly properties of the molecules to organize the molecular layers:[18] (1) the Langmuir-Blodgett (LB) physisorption technique,[25] used to transfer molecules onto a pre-chosen macroscopic electrode and (2) the technique of covalently bonding molecules to electrode surfaces.[26–29] While the LB-technique profits from the amphiphilic character of the molecules the second technique benefits from the anchoring groups of the molecules that bind directly, often covalently, to a suitable substrate.

The traditional means of forming an organic monolayer film is to spread a compound with a hydrophilic head group and a hydrophobic tail on an aqueous subphase. The film is compressed mechanically with a barrier until the molecules are densely packed and oriented approximately normal to the surface. This monolayer is then transferred to a solid substrate by "dipping" (*Scheme 1A*). The orientation of the molecules in the LB-film originates from the amphiphilic character of the molecule structure at the water-air interface.

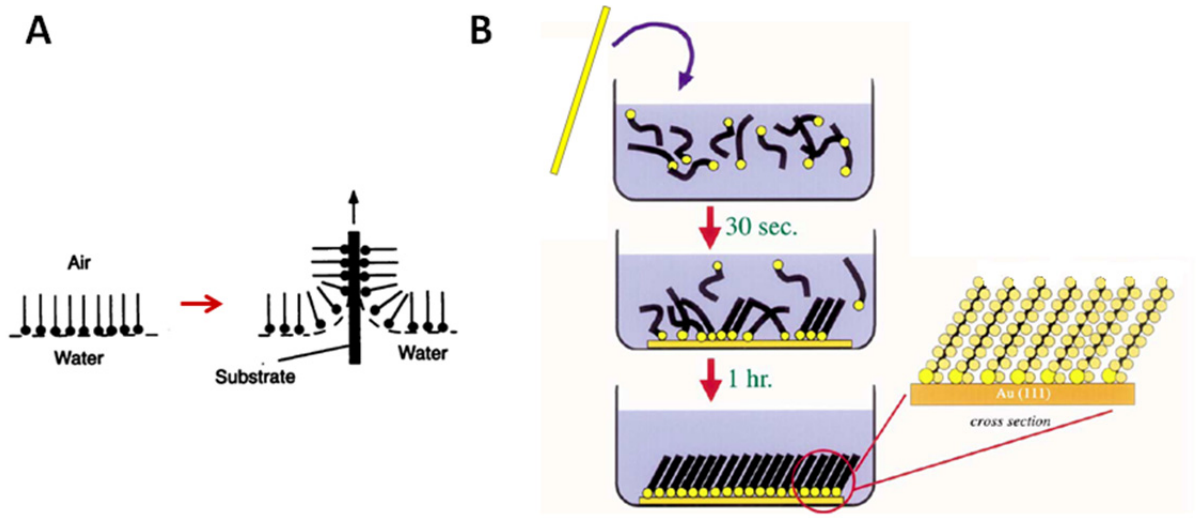

Scheme 1. (A) A sketch adopted from literature of the LB-technique.[25] (B) The self-assembly process of an n-alkanethiol to a gold surface in solution. The scheme is adopted from the literature.[30]

Numerous substrates have been functionalized with different molecules by LB-techniques. LB-monolayers, however, suffer from several drawbacks as model systems for studying interfacial properties. First, they are only metastable and tend to relax into more stable structural forms. Surface properties of LB-films are most easily studied after the film has been transferred to a solid substrate, a procedure that may be complicated by changes in the structure of the monolayer during the transfer process. Second, they are not normally chemically bonded to the substrate and hence are not robust enough to guarantee a stable and reliable device. This is a particular problem for electronic devices as the amphiphilic molecules tend to align in the applied electronic field. Furthermore, for the preparation of LB-films a lipophilic unit is essential, which limits the applicable molecular diversity.

Self-assembled monolayers (SAMs) rely on a strong chemisorbtion interaction between the adsorbate and substrate, which allows driving the spontaneous formation of an ordered molecular monolayer film (Scheme 1*B*). Thus, SAMs have higher chemical and mechanical stability, compared to LB-films.[26] To prepare a SAM, the substrate is simply immersed in a dilute solution of the adsorbate at room temperature for an interval varying from a few minutes to several days, depending on the system. Nowadays, the formation of SAMs is a standard process in surface science and in nanotechnology. However, also here the structural diversity is limited, as only molecular units that exhibit good packing properties are considered to be useful for the formation of SAMs.

1.1.2 Anchoring Groups

The communication between a monolayer and the surface is of great importance in order to achieve a good electronic response through the monolayer and the substrate. With "communication" is meant the charge transport through the potential barrier, i.e. the space between the monolayer and the surface. The interactions between the assembled molecules and the substrate need to be controlled in order to achieve the desired properties of a SAM. For this issue linkers between the monolayer and surface are essential. Preferably, these linkers, which are also called anchoring groups, have to bind strongly and induce low, or even better, no injection barriers.[31,32] Strong bindings of the molecules to the substrate are not only important for the device stability, but also have a significant influence on the conductance of the device.[33] The search for suitable anchoring groups, which combine both, stability and low charge injection barriers at the molecule-metal interface, is an important research field. Calculations and experiments have been performed to find adequate anchoring groups. Amines, isocyanides, selenium, carboxylic acids and pyridines, amongst others, have been studied.[27,34–37] Also different metals, including copper, silver, palladium, platinum, mercury and ruthenium, and silicon, that bind to the molecular films have been investigated.[27,38–40] In *Figure 1* examples of different interactions between a substrate and anchoring groups are depicted.

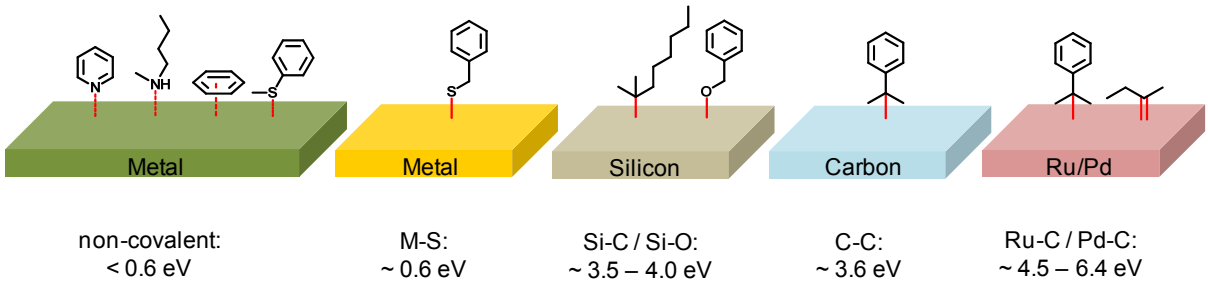

Figure 1. Approximate bonding energies of various types of molecule-substrate interactions.*[27,31,40–43]*

However, the most widely used and examined anchoring group is thiol, which adsorbs on gold (Au) surfaces.[26,27] Thiols are considered to form strong covalent bonds with gold atoms, compared to other anchoring groups, which form weak covalent bond or coordinative bonds with the substrate.[31,35] During the last few years dithiocarbamates as functional linkers between the molecular backbones and gold substrates, forming structurally well defined and densely packed monolayers, have gained considerable interest.[44–47] Dithiocarbamates manifest high chemisorption energies on gold and the corresponding SAMs exhibit several advantages[47,48] compared to the extensively studied thiol-based SAMs. The high stability and robustness of dithiocarbamate-based SAMs and their reduced charge injection barrier across the metal-molecule interface, which causes a decreased contact resistance by about two orders of

magnitude compared to thiolates on gold, are of special interest. This aspect will be introduced in more detail in section 1.3.3.

1.1.3 Changing Surface Properties

Controlling the work function, which is the minimum energy needed to remove an electron from the Fermi level into vacuum, of metal electrodes is an important issue in order to improve device performance.[49,50] The adsorption of organic molecules on different substrates to form SAMs allows influencing the interface energies.[51] Especially, the modification of the metal work function helps to tune the charge injection barriers.[52–54] Although the exact parameters that influence the work function are today still under debate[55,56] several common parameters are known to control the work function.[50] The molecule's architecture itself can alter the metal's work function.[57] The molecule's electronic nature, i.e. electron rich or poor units of the backbone and the anchoring group, influences the electrostatic potential. By choosing suitable building blocks an interface dipole layer can be generated.[51,58,59] Depending on the molecular orientation on the surface this layer induces a work function change to the positive or negative. Also a charge redistribution or transfer upon formation of a chemical bond between the metal and the adsorbate induces a dipole layer.[60] Furthermore, the packing density and packing order of the monolayer is also considered to play a role in altering the work function.[61–63]

Controlling the work function is an issue to be considered when building up molecular rectifiers.[64,21] Rectifiers are one of the fundamental electronic devices, which show an asymmetric current response upon applied bias voltage. In a rectification system the current passes in one direction more easily than in the other. Such systems in industry are the today known diodes, which often are made of p-/n-doped silicon. In molecular electronics rectifiers are metal-molecule-metal junctions. In order to fabricate such a junction, which provides unidirectional current properties, different features have to be considered. Besides the electronic nature of the molecule providing electron acceptor and donor units, also the choice of the metal is crucial.[59] The different work functions of the metals can themselves lead to rectification,[65] which could even dominate over the molecule's effect. Furthermore, having different anchoring groups on each side of the molecule to form a metal-molecule-metal junction, result in an asymmetric current flow.[66] Therefore, the interplay of the molecular structure, anchoring groups and metallic substrates is needed to achieve an overall unidirectional rectifying system.

After controlling the direction of the electric current flowing through a device, the next challenge is to turn reversibly the current on and off. Such molecular switches are necessary to realize

responsive electronic devices.[67–71] By external stimuli, such as a chemical reaction, electricity or light, the conductance can be triggered. A molecular conductance switch requires the alteration of the integrated molecule, which includes its oxidation state, its conformation or its isomerization state. These factors are able, for example, to vary the electron transport distance or change the conjugation of the molecule, leading to a change in the conductance. If these parameters of the corresponding switchable device are externally controllable in a reversible manner, applications in optics, data storage, nanomechanics and electronics could be possible.[68]

1.1.4 Surface Characterization Techniques

Several techniques to characterize SAMs on metal substrates are known. Some of the commonly used setups to characterize the surface energies, the chemical composition and the electronic properties of a sample or device are shortly described.

Contact angle measurements allow for the assignment of the surface energy.[72] The magnitude of the angle between a liquid and a solid, on which the liquid drop is mounted, depends on the intermolecular interactions between the interfacial contacts of the matters. Thus, surface forces, including surface tensions, become important and control phenomena such as wetting and adhesion.

The chemical analysis of surfaces is commonly performed by X-ray photoelectron spectroscopy (XPS). It allows for the chemical identification and the quantification of bound and unbound atoms on surfaces.[73–75] Photons from an X-ray source are focused on the sample surface and electrons from the core levels are excited and emitted from the sample. The counting of the emitted electrons, the simultaneously measurement of their kinetic energies and the known energy of the X-ray source leads to the calculation of the binding energies of the electrons.[76] The elemental composition, the empirical formula and the chemical and electronic state of the studied samples can thus be determined. As for XPS, ultraviolet photoelectron spectroscopy (UPS)[76–78] is based on the photoelectronic effect.[79] But in the case of UPS the electrons are excited from an ultraviolet light source. This low energy source emits the valence electrons of the first atomic layers of the sample surface, which makes UPS extremely surface sensitive. The adsorbed species and their binding to the surface and the orientation on the surface can be assigned. Furthermore, the work function of the material can be obtained by UPS.

The electrical characterization of SAMs and/or the corresponding junctions are often performed with a scanning tunneling microscope (STM).[16,17] The STM allows for an atomically resolved

characterization of surfaces. An atomically sharp probe is placed over a functionalized metal substrate, forming a small gap (0.1 – 1 nm) between tip and surface. A bias voltage is applied leading to a current flow through the gap, as electrons tunnel through. The resulting tunneling current is kept constant and as it is dependent on the probe-surface distance, applied voltage, and local density of state of the material adsorbed at the surface, an image of the surface topography can be recorded.

Another method to electrically characterize formed SAMs in a metal-molecule-metal junction is a mercury (Hg) droplet setup.[80,81] The preparation of this setup is simple and the system takes advantages of the properties of the Hg-electrode. Mercury is highly conductive, it forms well-ordered SAMs and the liquid surface is free of structural defects. Furthermore, the Hg drop adapts itself mechanically to the topography of the solid surface and thus the resulting metal-SAM-metal junction allows for the electrical characterization of the SAMs (*Figure 2*). The irradiation of a photoactive SAM sandwiched between the electrodes under applied potential is an additional attractiveness of a Hg-based junction.[82]

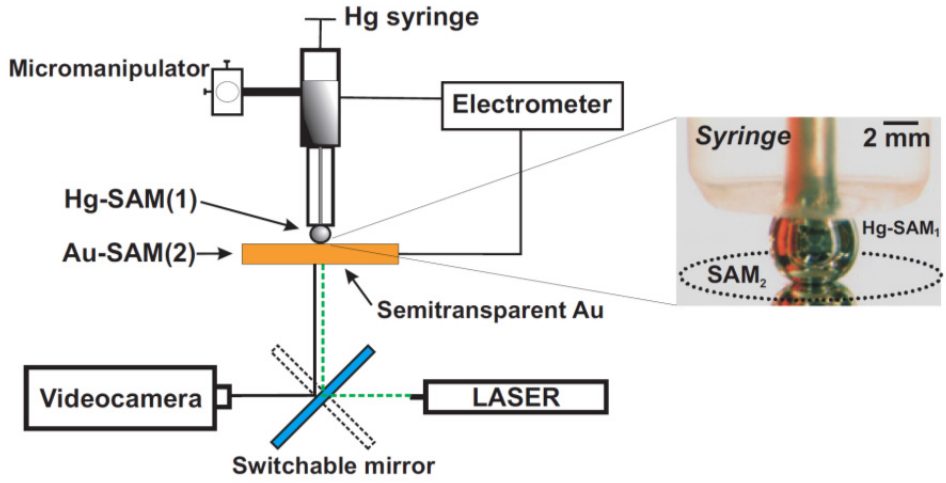

Figure 2. A electrical junction based on a Hg-electrode and the relative picture of the contact area. The junction is formed by a Hg drop covered by SAM(1), usually formed from hexadecane thiol solutions, and a solid semitransparent metal surface (M= Au, silver (Ag)) covered by SAM(2). The two electrodes covered by the SAMs are brought into contact by a micromanipulator. The image of the contact area is collected by a mirror through the semitransparent gold surfaces.[81]

1.2 Azobenzenes

1.2.1 Covering Many Fields

Azo compounds are structures that comprise two nitrogen atoms, which are connected via a double bond (*Figure 3A*). This azo functionality (R-N=N-R) is bound to aliphatic or aromatic units (-R). While aliphatic azo compounds are light and heat sensitive and decompose easily forming radicals, the aromatic derivatives are more stable due to their π-delocalization. As a consequence of the π-delocalization of aromatic azo compounds (azobenzenes or diphenyldiazenes) they are optically seen as colored species, especially colored in red, orange and yellow. Thus, they are used as dyes and pigments. The first azo dyes were produced by Mène in 1861 (Aniline Yellow)[83] and by Martius in 1863 (Bismark Brown)[84] (*Figure 3B*). Today azo dyes are widely used in textile dyeing, paper printing and other industrial processes such as the manufacture of toys and foods.[85,86]

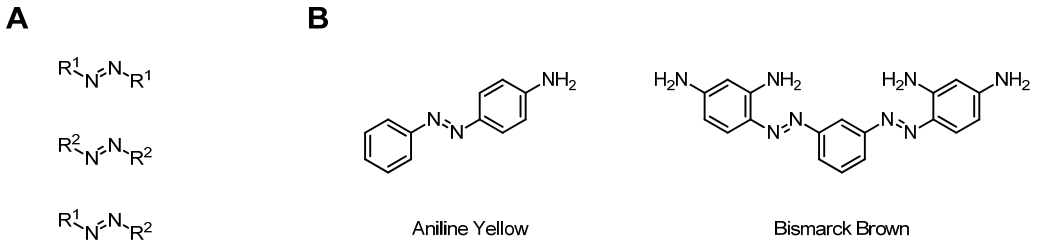

Figure 3. (A) The azo functionality with different substituents, where R^1 = aliphatic rest and R^2 = aromatic rest; (B) The first azo dyes.[83,84]

For the dye industry it is of interest to suppress the photochromism of azobenzene derivatives (section 1.2.2), otherwise the color of a dye would fade or change upon sunlight exposure. However, just because of this intrinsic property of azo derivatives to photoisomerize and thus to chance the structural geometry, refractive index, dielectric constant and dipole moment, azo compounds have been applied and investigated also in many different fields. Azobenzenes derivatives have been incorporated in biological systems,[87] polymer matrices[88] and in supramolecular systems.[89] They can act as photoresponsive molecular sensors,[90] liquid crystals,[91,92] foldamers,[93] ion channels,[94] as well as molecular switches,[95,96] finding applications in data storage,[97,98] molecular machines[99,100] and linear and non-linear optics[101] and many more. The field of photoresponsive molecules on substrates is growing especially fast, leading to "smart" surfaces, which respond to external stimuli.[102] Photoactive azo compounds can be either physisorbed in a planar adsorption geometry or chemisorbed in a vertical arrangement. The aim of the adsorption of azo-based structures on metal surfaces is mainly focused on its capability of switching. The molecular properties of the compounds known from solution are often not retained once absorbed on substrates.[103] However, the investigated

behavior of azobenzene derivatives physisorbed on noble metal surfaces has been reported by many groups.[104–107] These studies provided detailed mechanistic insights into the switching process of individual molecules by local probing techniques under controlled conditions.[102] On the other hand, the vertical chemisorption of azobenzene derivatives on noble metals provides more practical benefits, as such devices are more robust for the fabrication of photoswitchable surfaces due to their intermolecular and packing interactions.[108–110] This concept will be introduced in more detail in section 1.2.4. Furthermore, this concept of switching azo compounds was also carried out on curved surfaces in the three dimensional world of nanoparticles. The assembly of azo-based structures on nanoparticles gained much attention in many groups.[108,111–120] Nanoparticles of noble metals exhibit enhanced reactivity, photochemical activity and electronic properties, due to their high surface-to-volume ratio.[120] Such systems of nanoparticles coated with responsive organic material render them sensitive to changes in environmental conditions and possibly induce their aggregation. The ability to control the aggregation state of coated nanoparticles by stimuli is of interest in exploring their potential for further applications.[119]

1.2.2 Photoisomerism

Although in 1824 the synthesis of the simplest aromatic azo compound (azobenzene) was first described by Mitscherlich,[121] not before 1973 the photochemical *cis* ↔ *trans* isomerization of azobenzene was observed by Hartely.[122] In the following years the photochemistry of azobenzenes drew attention to many scientists.[123–126] Azobenzene and its derivatives can reversibly change their molecular structure photochemically (*trans* ⇄ *cis*) and thermally (*cis* → *trans*) (*Scheme 2*). The *trans*-form is thermodynamically more stable than the *cis*-form (Δ = 50 kJ mol^{-1}) and can be converted into the *cis*-isomer by UV light irradiation. The resultant *cis*-structure can return to the original *trans*-isomer photochemically under illumination with visible light or thermally in the dark. These characteristics of azobenzene derivatives can be monitored by UV/Vis spectroscopy.

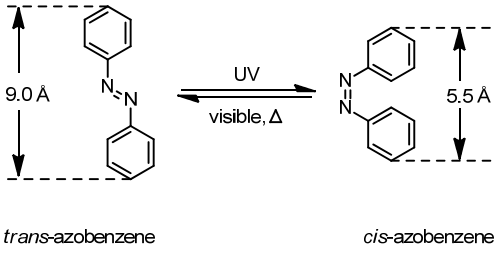

Scheme 2. Photoisomerization of azobenzene.[88]

Typical UV/Vis spectra of the *trans*- and *cis*-azobenzene in an alcoholic solution are shown in *Figure 4*. The highest-energy transition, which appears at 230-240 nm for both azobenzene isomers, is attributed to the σ→σ* process of the azo group. The π-π*-transition of aromatic units also appears in this absorption region.[127] As these two transition bands overlap, the σ→σ*-transition band of the azobenzenes is not very informative for their *cis* ↔ *trans* isomerization process. In contrast, a meaningful absorption band in the UV region (314 nm for *trans*-azobenzene, 280 nm for *cis*-azobenzene) is observed, which corresponds to the π→π*-transition of the azo functionality. The intensity of the *trans*-band is much higher compared to the *cis*-band. This difference is attributed to the non-planar configuration of the *cis*-isomer, whose geometry will be discussed later. In polar solvents these bands undergo bathochromic shifts and the location of the bands is also sensitive to substitution effects on the aromatic units.[125,128] A further band appears at longer wavelengths (400 nm for *trans*-azobenzene, 430 nm for *cis*-azobenzene). For the *trans*-isomer this n→π*-transition is symmetry forbidden, whereas the n→π*-transition is allowed in the *cis*-isomer, showing usually higher intensities. The location of these n→π*-transition bands remains almost unaffected by the substitution pattern of the azobenzene derivatives[128] and the intensities of the n→π*-transition bands of the azobenzenes are not influenced considerably by the substitution on the aromatic units.

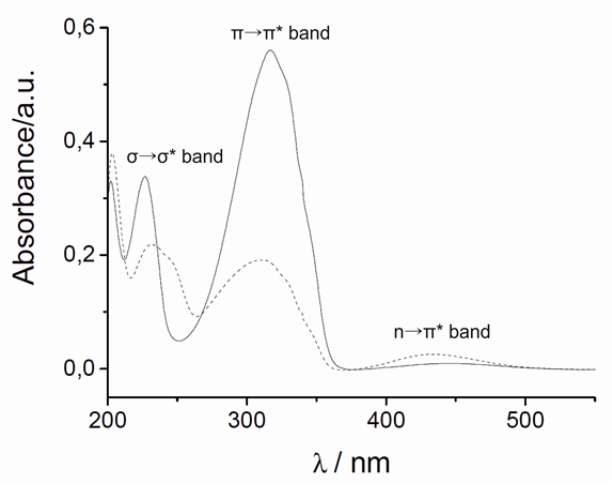

Figure 4. Absorption spectra of azobenzene in an alcoholic solution (solid curve: *trans*-form, dashed curve: *cis*-form).[129]

By irradiating at the π→π*-transition wavelength the azobenzene derivative can be isomerized to the *cis*-isomer and, vice versa, by irradiating at the n→π*-transition band the *trans*-isomer is generated. However, as the π→π*-transition wavelengths of the *trans*- and *cis*-isomers are similar, also the simultaneous re-isomerization to the *trans*-form occurs to a small extent. Therefore, a photostationary equilibrium (about 85%) will be reached. This steady state is wavelength and temperature dependent.[130]

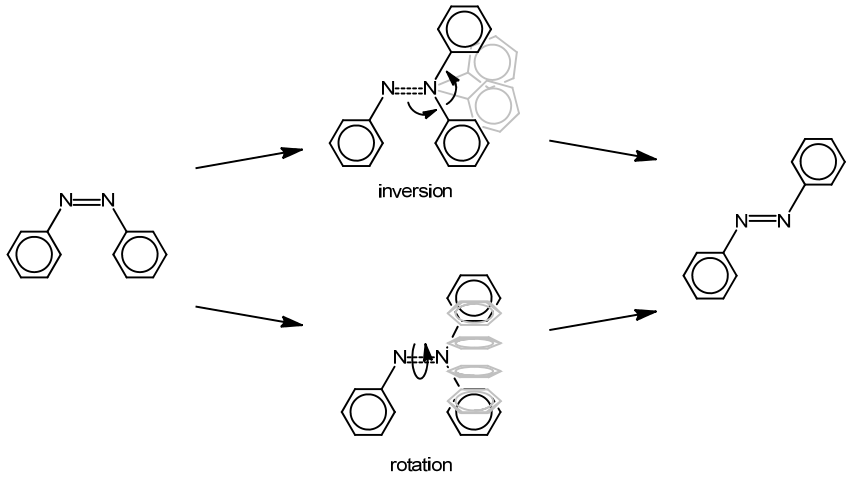

Scheme 3. Two mechanisms (inversion and rotation) of the photoisomerization of aromatic azo derivatives.[131]

Although much interest has been attributed to the photoisomerization process of azobenzenes, the mechanism of the *cis* ↔ *trans* isomerization of azobenzene derivatives is still a subject of debate.[131–135] In contrast, the isomerization mechanism of stilbene derivatives is better understood.[136,137] The difficulty of understanding the *cis* ↔ *trans* isomerization mechanism studies of azobenzenes is most probably attributed to the free electron pairs of the nitrogen atoms, as these free electron pairs induce additional nπ*-states, which stilbenes do not posses, and whose excitation energies are lower than the excitation energies of the σ and π electrons. However, two main mechanisms have been proposed, the rotation mechanism and the inversion mechanism (*Scheme 3*). The former mechanism involves rotation around the N=N bond and the latter comprises the in-plane inversion around the C-N-N angles. Besides the effect of the lone pairs of the nitrogen, as mentioned before, the mechanistic route of isomerization depends also on several other factors, including the solvent (polarity of the reaction medium), the electronic nature of the substituents (covalently bound to one or both phenyl rings) and the geometry of the azobenzenes at the transition states.

Table 1. Physical Properties of the *trans*- and *cis*-azobenzene.

	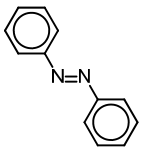 *trans*-azobenzene	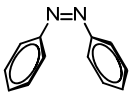 *cis*-azobenzene
N=N distance	1.28 Å	1.25 Å
C-N distance	1.43 Å	1.45 Å
NNC angle	114°	>122°
CNNC angle	>180°	>172°
Symmetry group	C_{2v}	C_{2h}
Dipole moment	0.0 D	3.0 D

However, the geometries of *cis*- and *trans*-azobenzenes in their ground states are well characterized.[138–140] The N=N and C-N bond distances of the *trans*- and *cis*-azobenzene and the corresponding NNC and CNNC angles, and the symmetry groups, which influence the spectroscopic properties of azobenzene, are depicted in *Table 1*. The twist angle of the phenyl rings of cis-azobenzene has a value of 53°. Furthermore, with the isomerization the dipole moment values of the azobenzene isomers change drastically.[141,142] In *Figure 5* a 3D representation of *trans*- and *cis*-azobenzene together with their electrostatic potentials is shown.

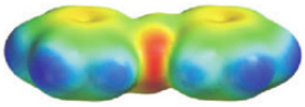

***trans*-azobenzene**

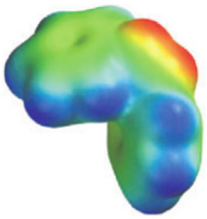

***cis*-azobenzene**

Figure 5. Structures of *trans*- and *cis*-isomers of azobenzene. Spacefilling models are colored by electrostatic potential (red—negative to blue—positive).[87]

1.2.3 Synthesis

The majority of azobenzenes are obtained by the azo coupling reaction, especially for the production of azo dyes in industry.[86] The overall azo coupling reaction is shown in *Scheme 4*. In principle it consists of two main steps: the formation of a diazonium compound (diazotization) followed by the synthesis of the azo dye (the actual azo coupling). The diazotization is the reaction of primary aromatic amines with nitrites, mostly sodium nitrite (**B6**). This reaction is usually performed in an aqueous mineral acid solution at low temperatures, generating the corresponding diazonium salt.

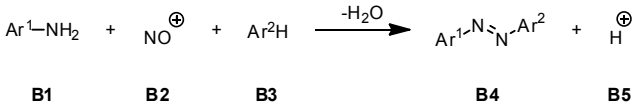

Scheme 4. The overall azo coupling reaction.

Initially, the nitrosating agent (**B2**) has to be liberated *in situ* from sodium nitrite (**B6**). This is done using an acid as shown in *Scheme 5*. The nitrous acid (**B7**) is formed at first and further protonation and water elimination provides the nitrosating agent (**B2**).

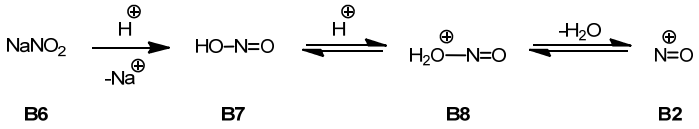

Scheme 5. Formation of the nitrosonium ion ($^{+}$N=O), the nitrosating agent (**B10**).

As $^{+}$N=O is formed the electrophilic nitrosation of the amino group of a primary aromatic amine can occur (*Scheme 6*). The first intermediate is the formation of the N-nitroso derivative **B9**, a tautomer of the diazohydroxide **B10**. A second protonation and water elimination affords the diazonium salt **B11**, which is stabilized by resonance (**B12**).[143]

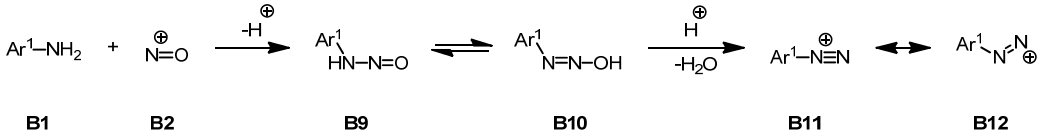

Scheme 6. Formation of a diazonium salt (**B11**) from an aniline derivative (**B1**) and the nitrosonium ion (**B2**).

Diazonium salts are weak electrophiles and react with electron rich species to give azobenzenes. This actual azo coupling is an electrophilic aromatic substitution. Electron rich arenes, having electron donating groups, like amine or hydroxyl, are essential for the azo coupling. The reaction mechanism of the electrophilic aromatic substitution is shown in *Scheme 7* using phenol as an example for the nucleophile. The preferred coupling position on the arene unit is the carbon atom with the highest electron density. Therefore, the substitution reaction normally takes place at the *para* or *ortho* position to the electron donor group on the activated aromatic ring. No coupling occurs if these two positions are occupied.

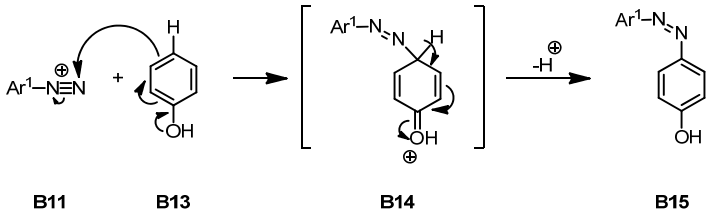

Scheme 7. Reaction mechanism of the electrophilic aromatic substitution of a diazonium salt with an electron rich aromatic unit.

Although the azo coupling is till today the most applied synthetic method for the production of azo dyes in industry, it also bears drawbacks. Previously mentioned, diazonium compounds are relative weak electrophiles, and therefore, the availability of the aromatic coupling partner is limited, as it has to be a rather nucleophilic arene. Thus the usability of the substrates is restricted, as the substituted functionalities and their substitution position have to tolerate the reaction procedure. Beside this issue, the fact that the azo coupling procedure is very pH dependent, the reaction has to be carefully controlled in order to minimize unwanted side

reactions. Furthermore, precautions have to be made, as diazonium salts are highly explosive, since – depending on their counter ion – they decompose above 5 °C.

However, nowadays improvements of the coupling procedure are reported, for example the azo coupling can also be performed in the solid phase.[144] With an anion exchange of the diazonium salt, the diazonium salt can be generated on a polymeric support. The salt then further couples with an electron rich aromatic compound, leading to the corresponding azo compound, which can be isolated without purification or further treatment. The azo coupling has even allowed the introduction of azo functionalities in elaborate architectures as in porphyrins,[145] metacyclophanes[146] and calixarenes[147] (*Figure 6*).

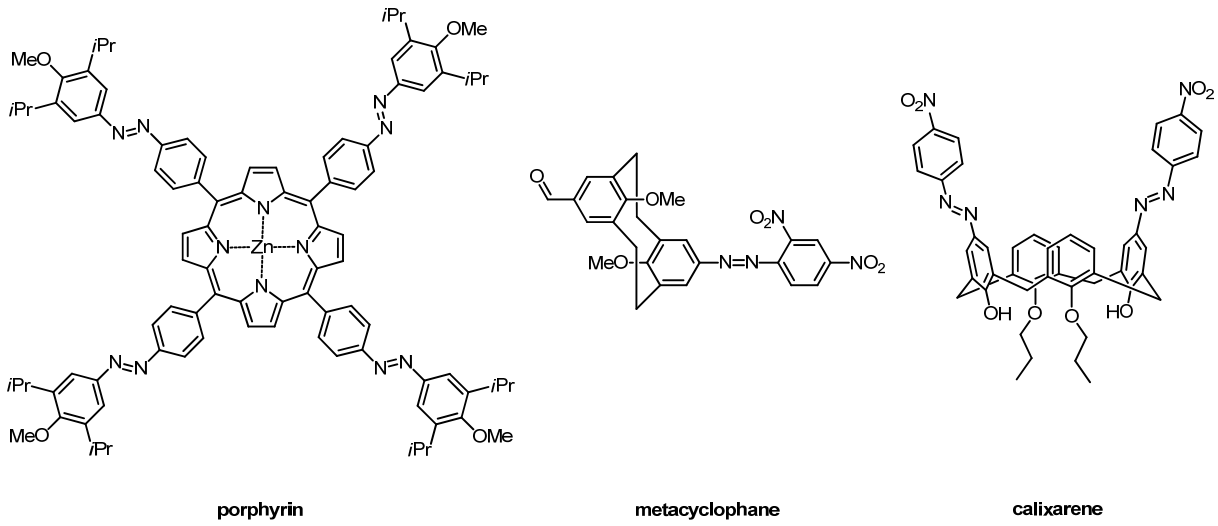

Figure 6. Elaborate architectures with linked azo compounds reported in literature.[145–147]

Other ways to prepare azo compounds include the reductive and oxidative coupling, starting from aromatic nitro derivatives and aniline derivates, respectively, and the Mills reaction. Before introducing the reductive and oxidative coupling methods and the Mills reaction, an overview of possible forming intermediates during reductions and oxidations will be given, which is pictured in *Scheme 8*. The stepwise oxidation intermediates of anilines (**B16**) are aromatic hydoxylamines (**B17**), nitrosobenzenes (**B18**) and nitrobenzenes (**B19**). The other way round, starting from nitrosobenzene (**B19**), the stepwise reduction leads to the same intermediates as just described. The reaction of an aromatic hydroxylamine (**B17**) with a nitroso derivative (**B18**) forms an azoxybenzene (**B20**), which can be further reduced to an azobenzene (**B21**). Azobenzenes are also directly formed from anilines (**B16**) and nitrosobenzenes (**B18**). If an azobenzene is further reduced, a hydrazo derivative (**B22**) is obtained. Clearly one can see that several routes to azo compounds are possible starting from distinct intermediates. The

discussion of all possible routes starting from anilines and nitrosobenzenes would go beyond the scope of the classical methods to prepare azobenzenes. An actual overview of "non classical" methods is given by Merino in the literature.[143]

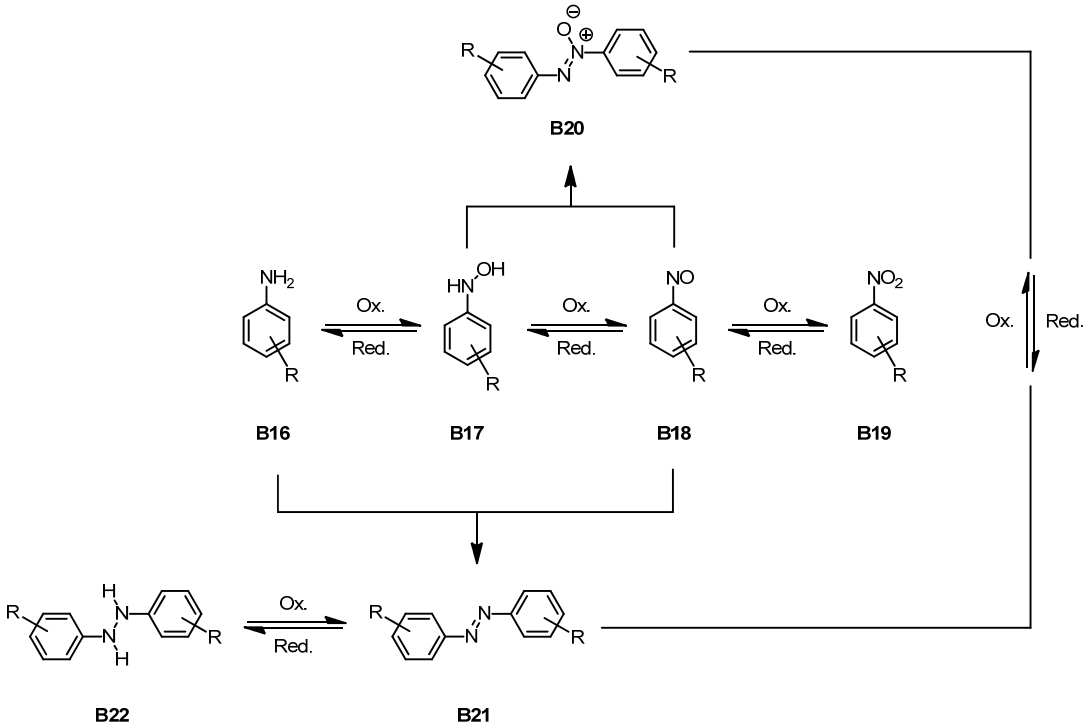

Scheme 8. Overview of possible reduction and oxidation intermediates starting from anilines (**B16**) and nitrobenzenes (**B19**).

Considering the reductive coupling, there are two ways to obtain azobenzenes (**B21**) when starting from the reduction of nitrobenzenes (**B19**). Condensation of the nitroso **B18** and the hydroxylamine **B17** derivatives, which are formed during the reduction of aromatic nitro compounds, results in the formation of azoxy compounds (**B20**). Azoxy compounds (**B20**) in turn can be converted in a further reduction step into azo compounds (**B21**). In principle during the reduction procedure of nitro compounds (**B19**) also amines can be formed, which could react with present nitroso compounds (**B18**) directly to form azo compounds (**B21**). In theory both ways lead to the azo compound. Therefore, depending on the strength of the reducing agent, the stability of the intermediates and the reaction environment both ways may occur. As the formed intermediates are produced *in situ*, such reductive coupling reactions are difficult to control, often leading to by-products. Often used reducing agents are, for example $LiAlH_4$,[148] $NaBH_4$,[149] KOH[150] and Zn/NaOH.[151] However, in industry only one reduction process attained significance for the preparation of azo dyes.[86] Glucose is used as a mild reducing agent in a strong alkaline aqueous medium for the synthesis of the red trisazo dye 25015 (**B26**) from 2-methyl-5-nitroaniline (**B24**) and Nevile-Winther acid (**B23**) (*Scheme 9*).[86] Here, the reaction does not proceed quantitatively up to the azo stage, as the corresponding azoxy derivative is

formed as well. If necessary the subsequent reduction of the azoxy compound to form the azo dye must follow.

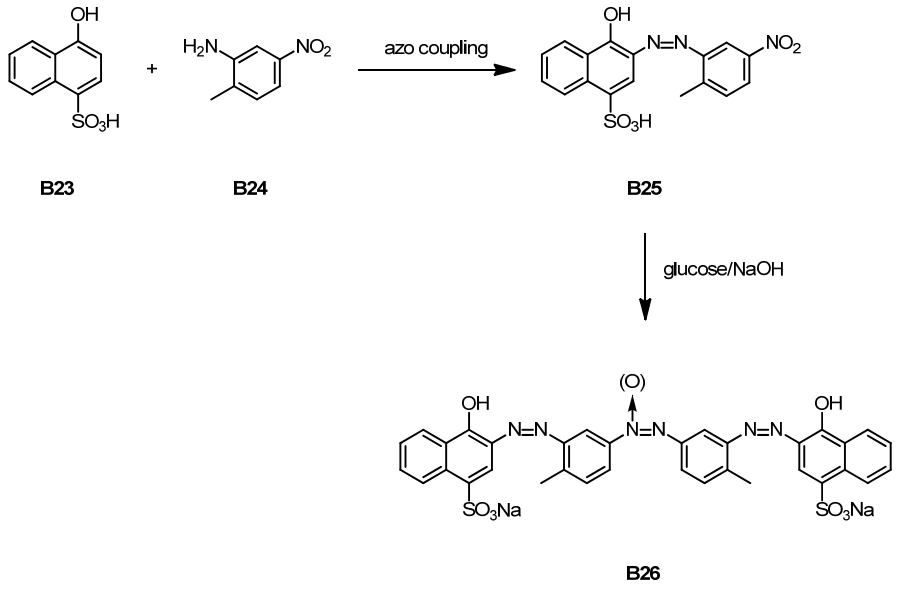

Scheme 9. Industrial synthesis of the red trisazo dye **B26** via an azo coupling followed by a reductive coupling of the nitro derivative **B25**.[86]

The reductive coupling of nitrobenzenes is useful to obtain exclusively symmetrical aromatic azo compounds. In order to obtain asymmetric azobenzenes two different nitro compounds have to be used. The drawback here is the lack of selectivity as statistical mixtures of the azobenzenes are obtained, as well as mixtures of the corresponding azoxy derivatives. The products formed can be isolated with suitable separation methods, but the yields are poor.

As for the reductive coupling of nitrosobenzenes, the oxidative coupling of anilines produces symmetric azo compounds. Furthermore, with two different anilines as starting materials, statistical mixtures of symmetric and asymmetric azo compounds are formed. During the oxidation of the aniline **B16** the nitroso intermediate **B18** formed *in situ*, reacts with the not yet oxidized aniline to form the corresponding azobenzene **B21**. The drawback in this reaction sequence is the generation of azoxy derivatives, either via the over-oxidation of the formed azo product **B21** or the reaction of the oxidation intermediate hydroxylamine **B17** with the nitroso derivative **B18**. The main industrial application for the oxidative linkage of aromatic amines is the synthesis of thiazole-based azo dyes, for example the yellow cotton dye 19555 (*Scheme 10*).[86] It is obtained by treating an aqueous solution of the sodium salt of compound **B27** with sodium hypochlorite (NaClO) in an alkaline medium. Furthermore, oxidizing agents such as $NaBO_3$/AcOH,[152] $H_2O_2/Na_2WO_4/Si_2Cl_6$,[153] MnO_2,[154] $NaBO_3$[155] and O_2/CuCl[156] and many more have been applied in synthetic laboratories for the oxidative coupling of anilines to the corresponding azo compounds.

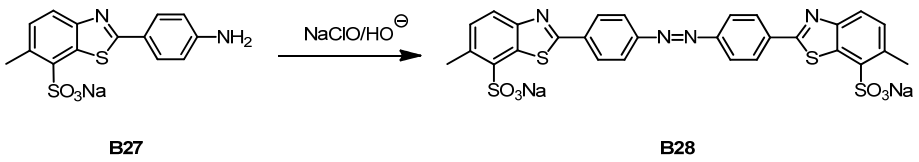

Scheme 10. Synthesis of yellow cotton dye **B28** via oxidation of the amine derivative **B27**.[86]

Considering the limitations of the reductive and oxidative couplings to generate symmetric compounds or statistical mixtures when asymmetric azo compounds are desired, the Mills reaction[157] finds a remedy for an adequate route to unsymmetrically substituted azobenzenes. The Mills reaction requires an isolated nitroso and aniline compound, which are not generated *in situ*, like for the above discussed reductive and oxidative dimerizations. The Mills reaction is performed in an acidic media, preferably in acetic acid. The mechanism of the Mills reaction (*Scheme 11*), which is corroborated by kinetic studies,[158,159] involves the attack of an aniline (**B29**) on an nitroso derivative (**B30**). After the formation of the tautomeric intermediates **B31** and **B32**, dehydration follows to obtain the asymmetric azo compound **B33**.

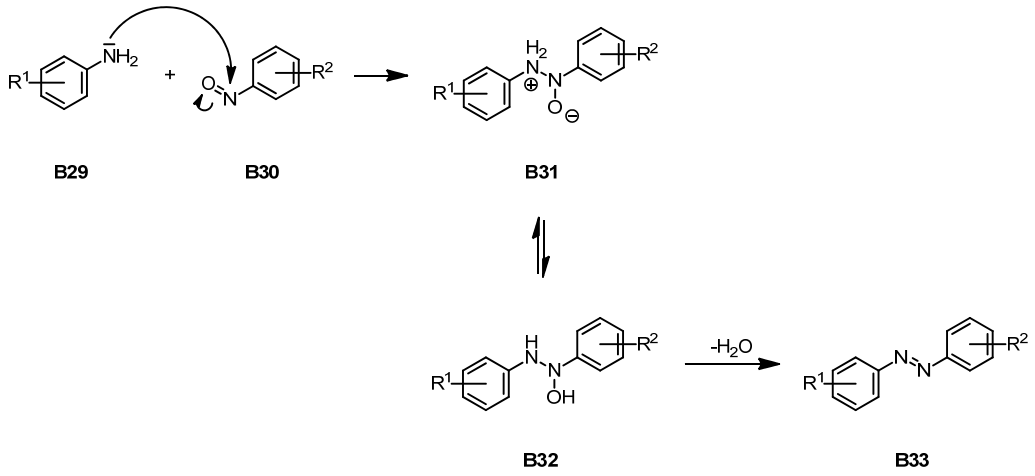

Scheme 11. Reaction mechanism of the Mills reaction to generate asymmetric azo compounds. $R^1 \neq R^2$.

There are several ways to prepare nitroso compounds. Gowenlock and Richter-Addo reported on preparations of C-nitroso compounds[160] amongst others by direct substitution of aromatic protons to the corresponding nitroso group,[161] by the substitution of a functional group to the nitroso group[162] and by the reduction of nitro compounds.[163,164] Besides the preparation of nitrosoarenes from their corresponding hydroxylamines,[165] the preparation from their anilines is also often used. The use of Caro's acid (peroxomonosulfuric acid, H_2SO_5) as oxidizing agent was the first to be employed for the oxidation of primary amines to the nitroso derivatives.[166] Further oxidizing agents such as peracetic acid (CH_3CO_3H),[167] $KMnO_4/CH_2O/H_2SO_4$,[168] 3-chloroperoxybenzoic acid,[169] peroxybenzoic acid[170] and H_2O_2/catalyst[171] have also been applied. However, large scale syntheses of nitrosoarenes from their corresponding aniline

derivatives often fail to give high yields as soon as the aniline starting material has one or more electron withdrawing substituents in the *para* or *meta* position.[172] These less reactive anilines show side reactions during the oxidation process to a greater extent, compared to activated anilines, especially after prolonged reaction times. The possible side reactions during the oxidation of anilines were described before and are shown in *Scheme 8*. If the formation of a specific oxidation stage cannot be controlled, all oxidation products and the aniline itself can be present in the reaction mixture. Besides the condensation to a symmetrically substituted azobenzene a condensation reaction to azoxybenzene can also occur. Indeed, nitrobenzenes and hydroxylamines are also observed as side products in homogeneous and heterogeneous systems. The adoption of a biphasic system improves in the suppression of the mentioned side reactions. In general the less water-soluble nitroso compound can be separated from the water-soluble N-arylhydroxylamine and aniline and thus prevent condensation reactions. Priewisch and Rück-Braun reported on the application of Oxone® as an oxidizing agent in a biphasic system for the oxidation of anilines to nitrosoarenes.[172] This system proved to be suitable for the synthesis of nitrosobenzenes containing electron-withdrawing groups at the *para* position on a large scale. Yu *et al.* expanded the investigations of this Oxone®-system on a wider range of aniline derivatives.[173]

Oxone®, which is a trade name, is also known as Caroat®, another trade name. It is a triple salt with the formula $2KHSO_5 \cdot KHSO_4 \cdot K_2SO_4$, where $KHSO_5$ (potassium peroxymonosulfate) is the potassium salt of peroxymonosulfuric acid (Caro's acid). Caro's acid is a liquid, a very strong oxidant and highly explosive, whereas Oxone® is a stable salt and a mild oxidizing agent. Oxone® has been widely used in swimming pools and spas since the 1970s as a chlorine-free product that eliminates organic contaminants.[174]

In any case, functional groups such as carboxylic acids, esters, nitriles, bromides and alkyl substituents are well tolerated by Oxone® during the oxidation process from the aniline to the nitroso.[172] Nitroso compounds with polar functional groups providing high water solubility lead to inferior results, as these substances may persist in the aqueous layer and thus are prone to further oxidation to the corresponding nitro compounds. However, in some cases the purification of the nitrosoarene is avoided, as nitroso compounds are known to have deficient stability features.[175] Having the unpurified mixture in hand is not a drawback considering the next reaction step (Mills reaction), since small impurities of nitro compounds and azoxybenzenes in the crude reaction mixture do not interfere in the synthesis of the unsymmetrically substituted azobenzenes. The subsequent purification of the azobenzenes proved to be less troublesome,[165] accelerating and simplifying the two step synthesis of azobenzenes. However, the need of an excess of the unpurified nitroso compound has to be considered.

To conclude, the Oxone® mediated oxidation of amines to nitroso compounds in a biphasic system is an efficient large scale method for the preparation of asymmetric azobenzenes. Such azobenzenes were often applied for their investigation as functional units physisorbed on surfaces[176] and in photoswitchable amino acids.[177,178]

Up to this point, some classical methods to prepare azobenzenes have been discussed. However, a novel way to prepare azobenzene derivatives is noteworthy, as it is a mild alternative towards asymmetric azobenzenes.[179] As shown in *Scheme 12* the reaction sequence to the asymmetric azobenzene **B33** starts from an aryl halide (**B34**) that reacts with a Boc-protected hydrazine (**B35**) in a palladium catalyzed Hartwig-Buchwald type reaction[180,181] to afford intermediate **B36**.[182,183] With another palladium catalyzed cross-coupling reaction, subsequently, another haloarene (**B37**) is attached to compound **B36**. The resulting diaryl hydrazine **B38** is then oxidized to the corresponding azobenzene **B33**. A large variety of functional groups, including electron donating (EDG) and withdrawing substituents (EWG), are tolerated. However, poor reaction yields are observed, when sterically demanding substituents are present in the *ortho* or *para* position to the nitrogen.[184,185] Nevertheless, this method has been successfully applied in the synthesis of azo macrocycles.[184]

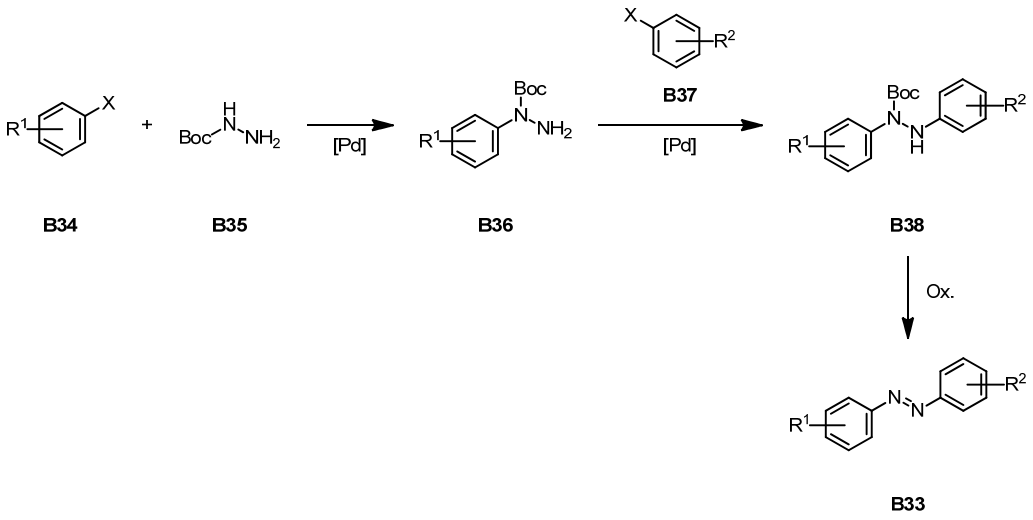

Scheme 12. Three step synthesis towards asymmetric azo compounds via a hydrazine intermediate. X = I, Br, OTf; R^1 = R^2 = EDG or EWG.

Many more ways to prepare azobenzene are known, but are not discussed in detail here. Examples from the literature are the conversion from azoxybenzenes,[186] the dehydrogenation of arylhydrazines,[187] triazene rearrangements[188] and the thermolysis of azides.[189]

1.2.4 Aromatic Azo Compounds on Metal Surfaces

The reversible photoswitching of azobenzene-functionalized molecules on substrates has been widely investigated[92] as such light-powered SAMs can be used as prototypes for future molecular electronic devices.[96] In particular, a promising and common structural motif was often chosen for the research studies: an azobenzene tailgroup (orange) that is linked with an aliphatic spacer (blue) to a sulfur anchoring group (green) (*Figure 7*). The aliphatic spacer is often a long linear alkyl chain for several reasons: 1) one can benefit from the broad knowledge of alkyl chains assembled on surfaces, since alkanethiols on gold are the most intensively studied systems;[27] 2) alkyl chains provide upright ordering on the surface and improve the formation of the SAM;[38,190] 3) the alkyl chain decouples the azobenzene moiety from the surface in order to prevent or limit the quenching of the photo-excited state by the metal substrate and so promotes photoisomerization.[106]

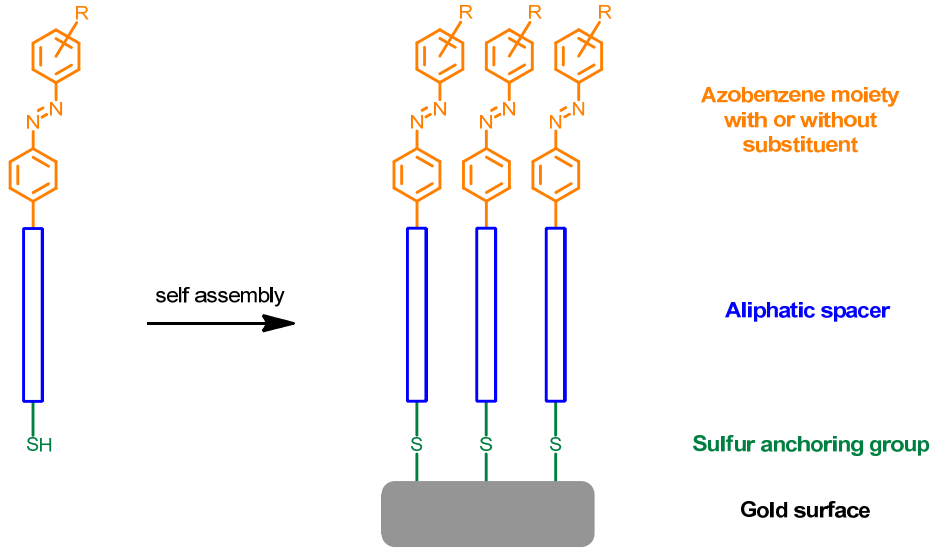

Figure 7. Schematic representation of a common structural motif of functionalized azobenzenes on surfaces for research studies in literature.

At first the structural characterization and packing properties of aliphatic-azobenzene-functionalized SAMs were the focus of interest of several researchers. It was shown that these SAMs exhibit common properties, which are a dense packing of the monolayer and usually a high ordering of the molecules due to the strong *van der Waals* interactions between the neighboring aliphatic chains and π-stacking of the aromatic units.[191–195] In other words: the supramolecular architecture of the SAM is ruled by the balance of adsorbate-substrate and adsorbate-adsorbate interactions.[196] Later, the investigations were concentrated on the reversible photoisomerization of the azobenzene units, which were assembled through a thiol on a gold substrate.[108,112,197–207] Unfortunately, no or low photoresponsiveness of the azobenzene incorporated in the SAM was often observed.[108,208] In order to promote higher

trans ⇄ *cis* photoconversion yields in monolayers, numerous studies from the viewpoint of molecular free space were performed. Since the aliphatic SAMs with azobenzene tailgroups exhibit a high 2D density of packed structures, the azobenzenes are restricted in motion. The *trans* ⇄ *cis* conversion is considered to require free space between neighboring molecules. In order to diminish the steric hindrance of the molecular neighbors for the photoisomerization process, different strategies to enlarge the space between the adjacent molecules and therefore regulate the 2D density of the chromophores were envisaged. One approach to provide more space for the isomerization process was the use of two component systems (mixed monolayers).[108,201,205,207,209,210] In *Figure 8* a sketch of a mixed monolayer is shown, where, besides the azobenzene building block, the second component is an aliphatic chain (*n*-butanethiol).[209] Although photoisomerization was observed in traces, the authors report that in the mixed SAMs the azobenzene molecules are randomly adsorbed within a surrounding matrix of the butanethiol molecules and phase separation was not excluded. Preferred domains with bigger aggregations of the azo compounds are formed, which anew works against the problem of steric hindrance.

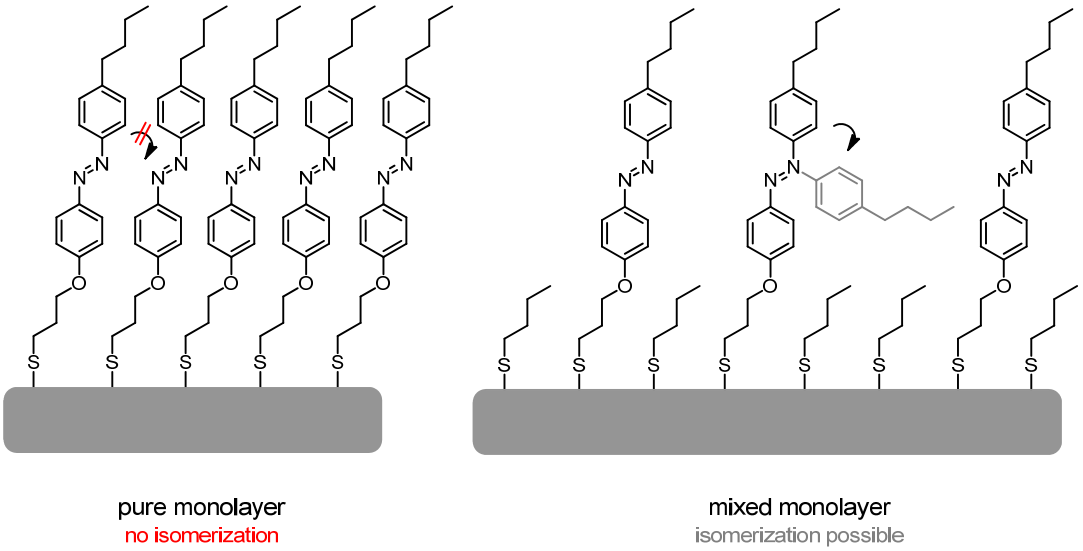

Figure 8. Steric hindrance in a tight packed SAM of azobenzene moieties and a mixed monolayer, where short alkanethiols induce free space for the switching.

In order to control the ratio of the matrix components and thus to guarantee an equal distribution, the asymmetric disulfide strategy was developed.[109,200,202,206] The monolayers were prepared starting from disulfides that contain an alkyl group on one side and an azobenzene-terminated alkyl group on the other side of the disulfide functionality (*Scheme 13*). Thus, phase separation is often better controlled and the azobenzene moieties are diluted by half. In general, the dilution of the switches showed restoration of the photoinduced functionality of the chromophores. However, only moderate switching efficiencies were obtained with this strategy.

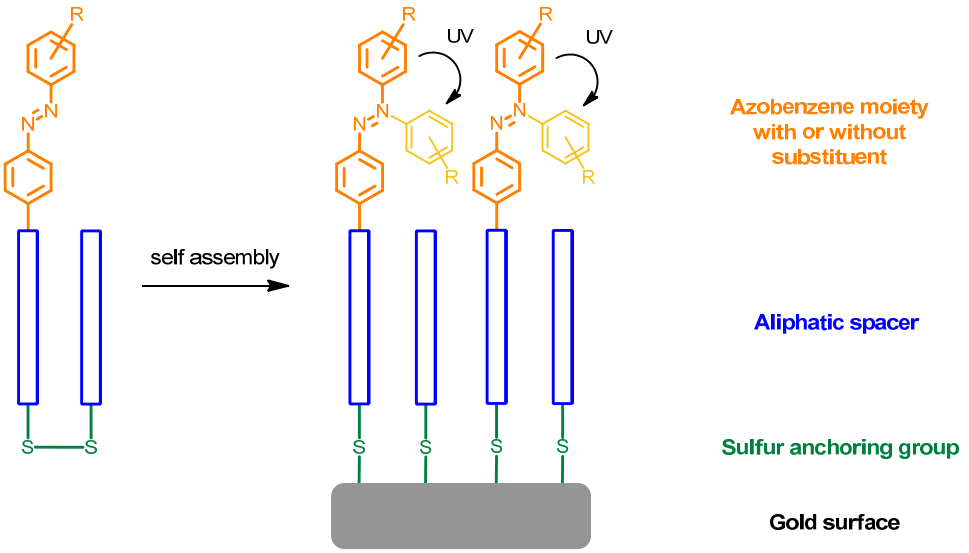

Scheme 13. Asymmetric disulfide strategy for the preparation of mixed SAMs to increase the free space for the switching process of the chromophores.

Other approaches to increase the free space between the chromophores in a one component system have been studied. Modifications on the structure of the molecules were accomplished by introducing bulky substituents[211] or even different headgroups.[212–214] Ito *et al.* introduced spherical *para*-carboranes as spacer units in the alkyl chain, where the corresponding azobenzene-containing SAM showed a pronounced photoisomerization capacity (*Scheme 14A*).[211] Another efficient one component photoswitch is depicted in *Scheme 14B*. Due to the bulky three-legged adamantan-based azo moieties a lateral spacing of the molecules on a gold surface was provided.[213]

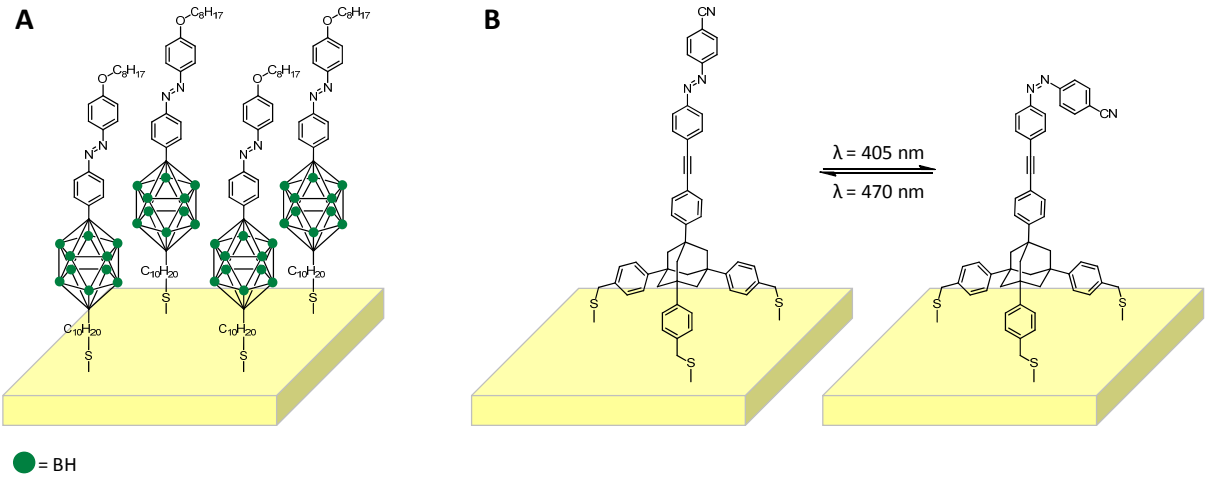

Scheme 14. Introduction of (A) spherical *para*-carboranes as spacer units *[211]* and (B) a tripodal linker system.[213]

Recently, the group of Prof. Herges presented an approach, which is based on the usage of molecular platforms that are formed on Au(111) surfaces (*Scheme 15A*).[215] The platforms are triazatriangulenium (TATA) moieties that allow the attachment of functional units (R') as

demonstrated in *Scheme 15B*. The spacing between each assembled platform on the surface can be tuned by varying the length of the R-groups and consequently allow to better modulate the switching of the chromophores.

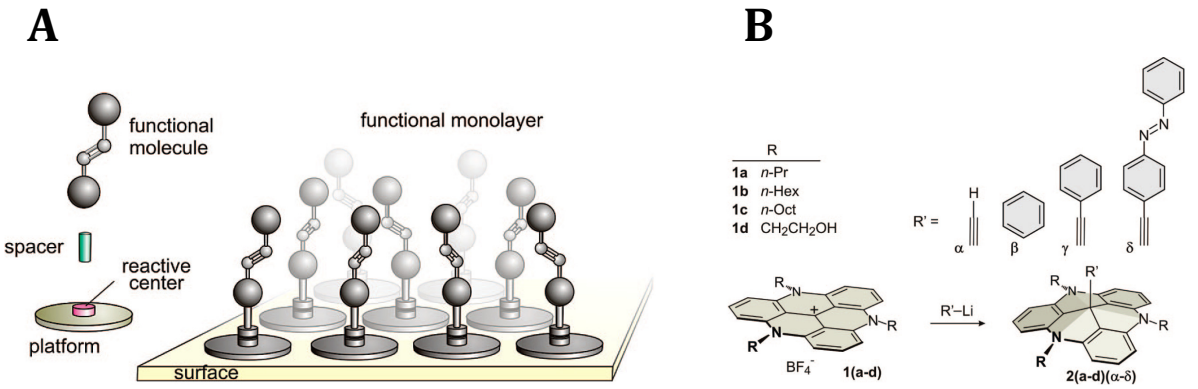

Scheme 15. (A) Schematic view of the "Herges"-platform approach. The size of the platform determines the distance between the functional molecules, the length of the spacer defines the distance from the surface, and the reactive center allows a "click type" attachment. (B) Attachment of functional groups to the TATA platform.[215]

Beside steric hindrance, molecular switches can influence each other by electronic effects,[199,203] resulting in surface quenching and suppression of photoisomerization. Therefore, the interplay of the factors that minimize the photoisomerization of azobenzene-functionalized SAMs has to be considered and explored in greater detail.

For pure azobenzene-based alkanethiol SAMs on gold only a few experiments showed photoinduced changes.[108,200,211,216] However, many applications ask for switching a larger fraction, or better, even a complete fraction of molecules in a one component dense packed monolayer. Recently, Han *et al*. reported on alkyl-based azobenzene-functionalized monolayers with high fraction and reversible photoswitching.[217] Although this structure and all mentioned structures above have one structural similarity - the long (aliphatic) spacer between the chromophore and the anchoring group - until 2007 no azo compound without a spacer showed high isomerization yields upon irradiation. This was achieved with a terminally thiol functionalized biphenyl azobenzene assembled on a gold substrate (*Scheme 16*).[218] This SAM showed a tight packing density and photo-isomerization over the complete surface. The photochemical switching was shown by STM imaging. The switching of the entire molecular 2D crystalline domains of such rigid azo rods on surfaces was not reported till then. The switching mechanism is assumed to have a cooperative character governed by the adjacent structures, where a dense packing character of the monolayer is needed. Such a collective and cooperative switching transformation had not been achieved in aliphatic-based azo SAMs and was not presumed to occur with rigid azo rods.[192,196] However, these assumptions were disproven with this terminally thiol functionalized biphenyl azobenzene.

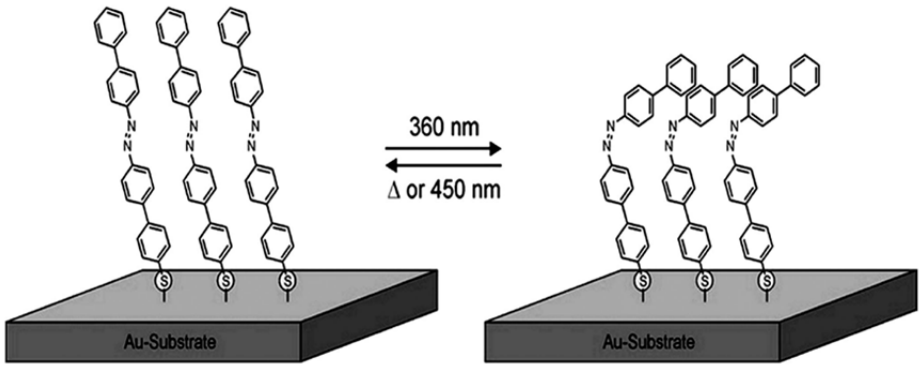

Scheme 16. Terminally thiol functionalized biphenyl azobenzene assembled on a gold substrate and its switching process.[218]

Due to the light-induced properties of this specific assembled compound several adoptions of this rigid and fully conjugated azobenzene[82,218–221] in different devices, such as bistable electrical nano-junctions[219] and a cargo lifter,[82] have been established. Ferri *et al.* were able to incorporate the azobiphenyl in a junction between an Au(111) surface and a Hg drop (*Scheme 17*).[82] Upon irradiation this device was able to lift the Hg drop and to reversibly photoswitch the current flowing through the junction by 1.4 orders of magnitude. Furthermore, contact atomic force microscopy (cAFM) measurements of the azobiphenyl in a metal-azo-metal junction showed a 30-fold decrease in resistance following transformation to the *cis* isomerization state upon irradiation.[220] This proved the expectation that the decrease in the tunneling barrier length is associated with the molecular conformational change of the biphenyl azobenzene.

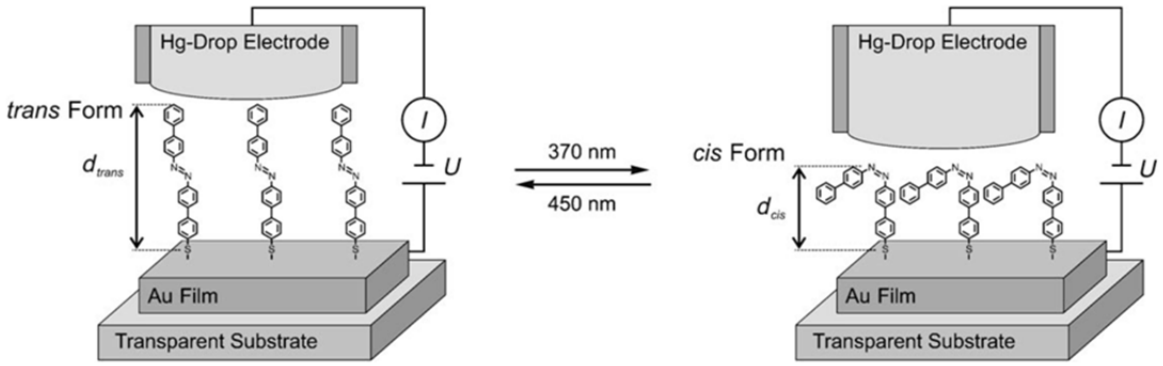

Scheme 17. The terminally thiol functionalized azobiphenyl immobilized between a transparent Au surface and a Hg drop electrode. As a result of the light-triggered isomerization between the rodlike *trans*-isomer (left) and the more compact *cis*-isomer (right), the distance between both electrodes varies, thus providing both an optoelectronic switch and an optomechanical cargo lifter.[82]

The packing tightness of this azobiphenyl on gold was investigated by comparing its properties with an azobiphenyl derivative with two methyl side groups, which act as steric repulsion moieties (*Scheme 18*).[219] Here, the authors claim that the free volume in between the packed

molecules is not necessarily required to fabricate photoswitchable surfaces based on azo compounds, as very similar maximum ratios of the *cis* to *trans* isomers in both azo-SAMs were observed.

Recently, Cohen and coworkers reported on the results of an AFM and atomistic computational study of the change in local stiffness, as induced by the optical *trans* ⇄ *cis* conversion in a SAM of the azobiphenyl.[221] The experimental variations in stiffness showed quantitative agreement with the calculated values and indicate that the stiffer response in the *cis*-form comprises contributions both from the individual molecular bonds and from intermolecular interactions in the film. Such innovative measuring techniques and advanced computational methods demonstrate the qualification in gaining deeper insights.

To summarize, the extensive investigation of the thiol functionalized biphenyl azobenzene on gold substrates, which showed unexpected high yielding switching properties, gave some insights into its skills under influence of light irradiation. This biphenyl-based structure clearly shows different switching properties compared to the common structural motif discussed at the beginning of this section. As very high switching ratios were observed, this biphenyl-based azo structure represents the basic framework of our research activities.

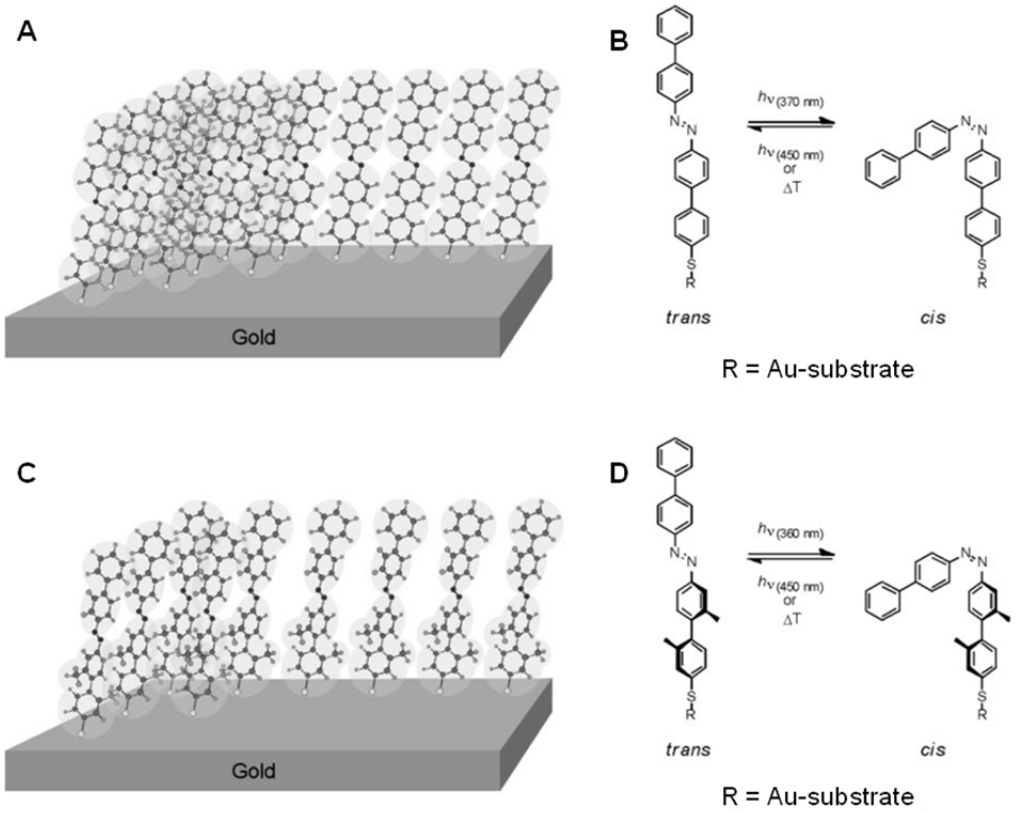

Scheme 18. Schematic representation of the densely packed SAMs of azo derivatives on a gold substrate (A and C) and of their photoisomerization (B and D). The steric requirements of the twisted biphenyl moiety creates additional space (free volume) in the SAM of the second azo derivative.[219]

1.3 Dithiocarbamates

1.3.1 From Biocidal Activity to Surface Chemistry

Dithiocarbamates are structurally the analogues of carbamates, where both oxygen atoms are replaced by sulfur atoms. The general structure of a dithiocarbamate is shown in Figure 9A. In the middle of the 19th century this functional group was first identified[222] and its chemistry has been extensively studied in the middle of the 20th century.[223,48] In bioorganic and medical chemistry the isolation of a dithiocarbamate from cabbage (Brassinin, *Figure 9B*), which was reported to have a cancer chemopreventive activity,[224] encouraged the scientists to gear the dithiocarbamate chemistry towards potential anticancer agents (Sulforamate, *Figure 9*).[225,226] Many efforts have been made and especially dithiocarbamate complexes with tin are of particular interest for biocidal activities.[227] These may have the potential of displacing the clinically common used cisplatin in anti-cancer therapy.[228] Within this research the combination of tin-dithiocarbamate-complexes with piperazine building blocks are suggested, as piperazines also have a broad biological relevance.[229] However, dithiocarbamates and dithiocarbamate complexes have also found applications as herbicides,[230] fungicides,[231] NO-trapping agents,[232] vulcanizers[233] and lubricants,[234] to name a few.

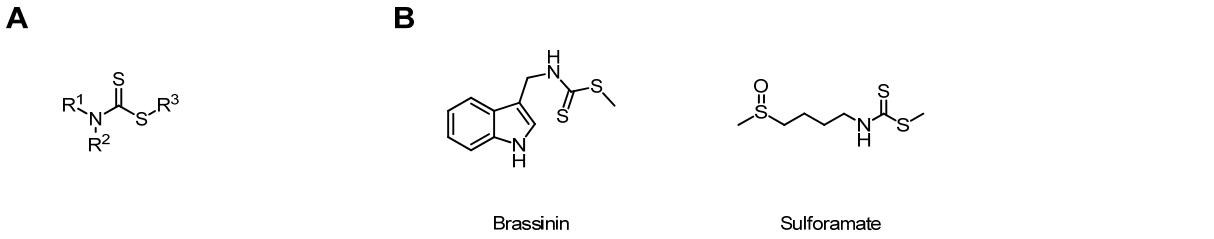

Figure 9. (A) General chemical structure of dithiocarbamates, where $R^1 = R^3$ = H, alkyl, aryl and R^2 = alkyl, aryl; (B) Brassinin: a dithiocarbamate isolated from cabbage. Sulforamate: potential cancer chemopreventive agent.[226]

Dithiocarbamates have also been investigated as metallomesogens, which are metal-containing liquid crystals[235] or transition metal liquid crystals.[236] Hoshino-Miyajima reported the first time on the mesomorphism in metal complexes of piperazine-based dithiocarbamates.[237] Such metal containing complexes were proposed to be interesting, as desired properties, such as high electronic polarizability and paramagnetism, can be introduced in liquid crystalline systems.[238]

The simple synthetic procedure of dithiocarbamate-based metal complexes (see section 1.3.2) was an important encouragement for the formation of multimetallic arrays.[239] The investigation of such multimetallic arrays was geared towards the introduction of transition metals onto the surface of gold nanoparticles for applications in catalysis and sensing.[240] In *Figure 10* an example of a gold nanoparticle with a ruthenium-based structure that was functionalized via dithiocarbamate linkers is depicted.

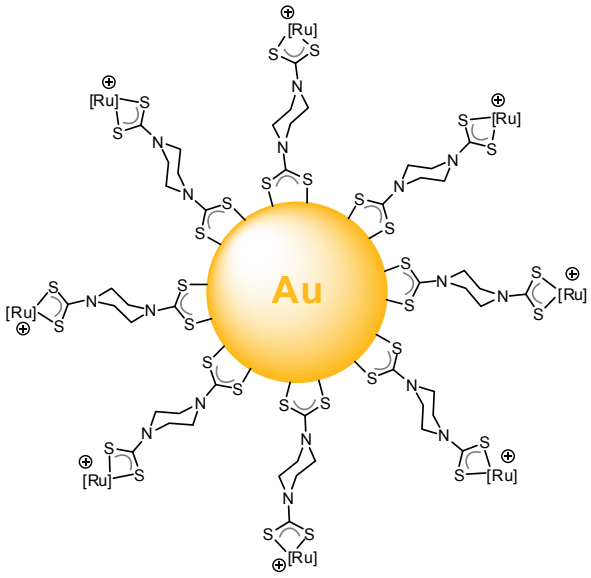

Figure 10. An example of gold nanoparticles, which were functionalized with dithiocarbamate linkers.[240]

Furthermore, inspired by the topological beauty, dithiocarbamates have been used as structural motifs in supramolecular chemistry, such as in macrocycles,[241] cages[242] and catenanes.[243] In *Figure 11* two cyclic structures interlocked with each other, consisting of dithiocarbamates that chelate different metals (gold and copper), are shown. These interlocked chains are considered to be a rare class of mixed-metal [2]catenanes.[243]

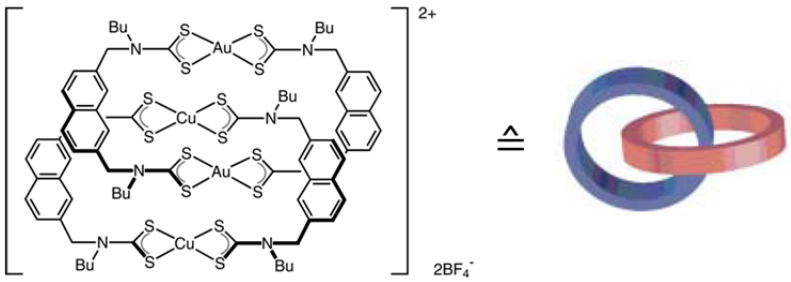

Figure 11. A Cu(II)–Au(III) dithiocarbamate [2]catenane.[243]

The current research on dithiocarbamates is focused on their assembly on gold substrates as versatile linkers.[45–47,244–246] Comparative studies of dithiocarbamates and thiols as anchoring groups are described.[45,47,247] The surface investigations reveal the attractiveness of dithiocarbamates to thiols for self-assembled monolayer experiments and applications (see section 1.3.3). Beside the studies on dithiocarbamate on flat gold surfaces, also the nature of dithiocarbamate-based gold nanoparticles has been described.[44,248–253] In *Figure 12* some examples of investigated dithiocarbamate structures on flat gold surfaces and on gold nanoparticles by Zhao *et al.* are shown. The dispersion properties of some of the corresponding nanoparticles could be modulated. However, as the dithiocarbamate as anchoring group was revisited recently, the scientific experience of it is not as much developed as for the

corresponding thiol linkers. Nevertheless, the gained information of the capabilities of dithiocarbamates points at the potential towards their implementation in electronic circuits (section 1.3.3). A further attractiveness of dithiocarbamates is their simple synthesis and ease of preparing dithiocarbamate metal complexes and dithiocarbamate-based SAMs, which will be discussed in the following section.

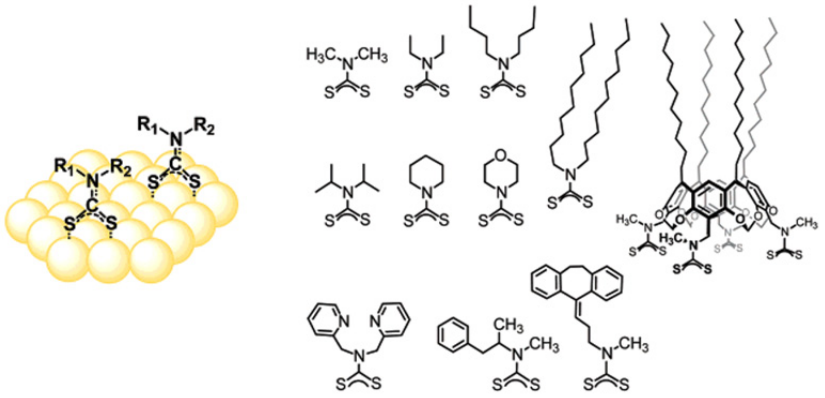

Figure 12. Dithiocarbamate ligands formed on Au surfaces.[44] $R^1 = R^2$ = alkyl, aryl.

1.3.2 Synthesis, Properties and Assembly Methods

In general, dithiocarbamates are formed by the addition of carbon disulfide (**C2**) to primary or secondary amines (**C1**) (*Scheme 19*). The nucleophilic attack of the nitrogen to the electrophilic carbon of carbon disulfide (**C2**) and the proton transfer forms the free dithiocarbamate acid **C3**. The free dithiocarbamate acid **C3** is unstable[254–256] and decomposes back to the starting materials **C1** and **C2**.

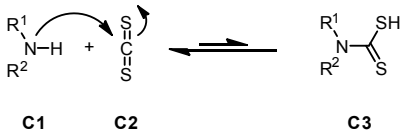

C1 **C2** **C3**

Scheme 19. Formation of the free dithiocarbamate acid **C3**. R^1 = H, alkyl, aryl; R^2 = alkyl, aryl.

Due to the instability of the free dithiocarbamate acid (**C3**), dithiocarbamates are often isolated as the corresponding alkali salts (**C5**), which are formed under strong basic conditions (*Scheme 20*),[222] mainly in sodium hydroxide (**C4**) solutions.

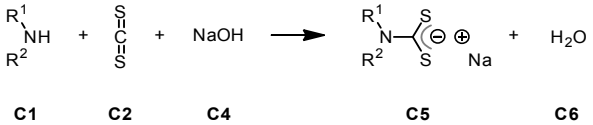

C1 **C2** **C4** **C5** **C6**

Scheme 20. Preparation of the dithiocarbamate salt **C5**, where R^1 = H, alkyl, aryl and R^2 = alkyl, aryl.

Dithiocarbamates derived from primary amines are less stable compared to the corresponding dithiocarbamates prepared from secondary amines. They are susceptible to elimination reactions leading to isothiocyanates (**C9**) (*Scheme 21*).[257,258]

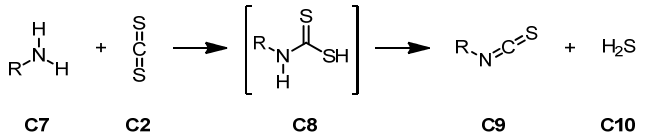

Scheme 21. Elimination reaction of intermediate **C8** to isothiocyanate **C9** when using primary amines. R = alkyl, aryl.

However, the dithiocarbamate anion **C11** forms strong complexes (**C15**) with metals (*Scheme 23*).[238] This is due to the delocalization ability of the dithiocarbamate ligand (*Scheme 22*) and the high electron density of the sulfur donors.[258]

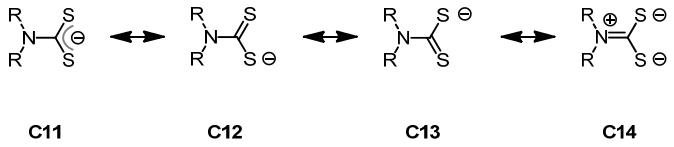

Scheme 22. Resonant structures of the dithiocarbamate ligand

The coordination chemistry of the dithiocarbamate ligands has been extensively studied,[223,259] showing the ability of the dithiocarbamate ligands to stabilize high formal oxidation states, such as iron(IV), copper(III) and nickel(IV).[248]

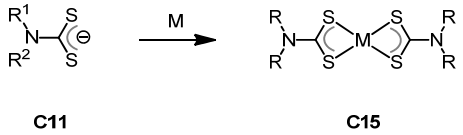

Scheme 23. Formation of dithiocarbamate metal complexes (**C15**) from the dithiocarbamate anions. R = alkyl, aryl, M = metal, from a metal source, as for example $Pd_3(OAc)_6$, $NiCl_2 \cdot 6H_2O$, $CuSO_4 \cdot 5H_2O$ or $Zn(AcO)_2$.[238]

The coordination geometry of dithiocarbamate complexes is influenced by the nature of the metal center. Square planar and octahedral configurations are exemplarily known in the literature.[249,258]

The reaction of diamines, such as piperazines (**C16**), with carbon disulfide generates bis-dithiocarbamate salts (**C17**).[239,240,260,261] Wilton-Ely *et al.* used this property of the zwitterionic piperazine dithiocarbamate (**C17**) to built up multimetallic arrays (see section 1.3.1) in a modular stepwise fashion as shown in *Scheme 24*.[260] The salt **C17** is used to coordinate to a first metal center, while retaining the potential to bind to a second upon deprotonation and

functionalization with carbon disulfide, and so on, leading to oligomers and polymers containing different metals.

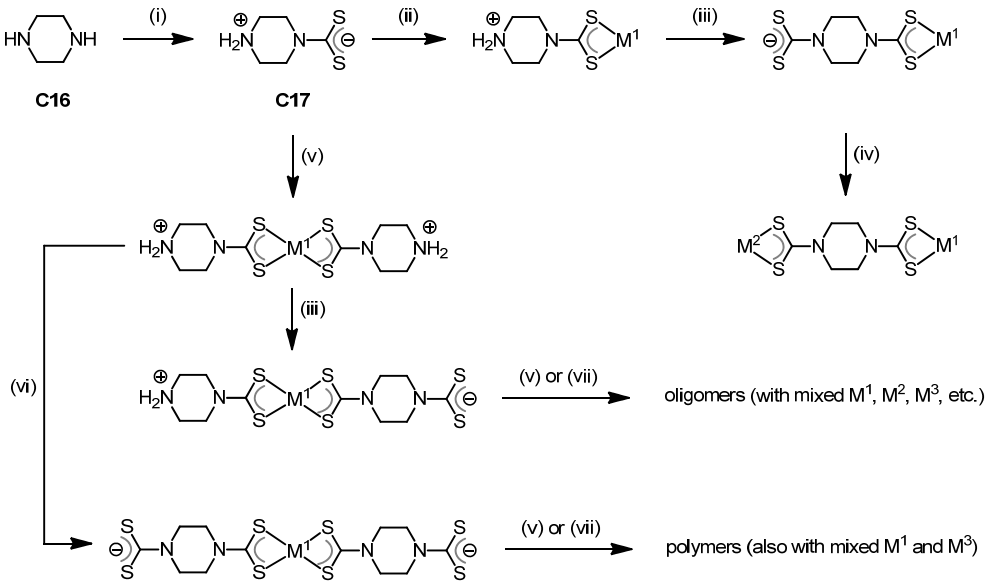

Scheme 24. Multifunctional dithiocarbamates as ligands for the synthesis of polymeric arrays. (i) CS_2; (ii) M^1X; (iii) $2NEt_3$, CS_2; (iv) M^2X; (v) M^1X; (vi) $4NEt_3$, $2CS_2$; (vii) M^2X_2.[239,260]

Dithiocarbamates act as good anchoring groups on gold surfaces (see section 1.3.3), either in the coating of nanoparticles[44,250–253] or to form monolayers on Au(111) surfaces.[45–47,246] Synthetically the functionalization of dithiocarbamates on gold surfaces is often done by the *in situ* formation of the free dithiocarbamate acid starting from an amine (**C18**) and equimolar amounts of carbon disulfide (**C2**) during the assembly process (*Scheme 25*).[75,252] Another procedure for the attachment of a dithiocarbamate on gold substrates is starting from the dithiocarbamate salt **C5** leading to a well defined stoichiometry.[75,262] Alternatively, the assembly of dithiocarbamates on gold surfaces can be achieved directly from thiuram disulfides.[75] Thiuram disulfides (**C20**) can be prepared by the oxidation of the corresponding dithiocarbamate sodium salts (**C5**).[257,263]

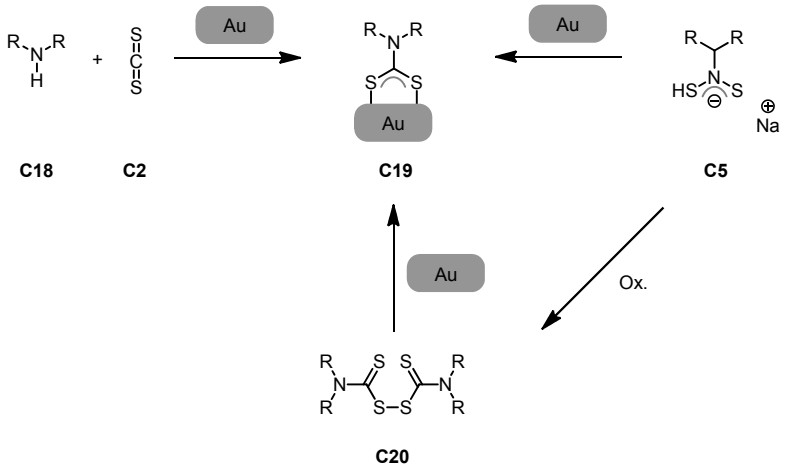

Scheme 25. Possible procedures for the functionalization of dithiocarbamates on gold surfaces.

To summarize, the formation of dithiocarbamates is often performed by a condensation reaction of primary and secondary amines with carbon disulfide. The corresponding stable alkali salts are isolated when working in strong basic media. Dithiocarbamate ligands can form complexes with a wide range of metals. The *in situ* formation of dithiocarbamates for their attachment on gold substrates, by immersing the gold surface into solutions containing carbon disulfide and the corresponding amine precursor, is the most elegant method for the assembly process.

1.3.3 Dithiocarbamates vs. Thiols as Linkers for Surface Functionalization

The functionalization of metal substrates with molecules to modify the metal's properties is of great interest. An intensely studied system is the chemisorption of sulfur-based structures on gold surfaces. Especially, the adsorption of alkanethiols[27] onto the noble metal gold has been widely investigated, due to several advantages. First of all, the high affinity of sulfur to gold facilitates the chemisorption of the molecules on the substrate during the assembly process. Furthermore, alkanethiols are able to pack densely on a metal surface due to the present dispersion forces (*van der Waals* forces) governed by the aliphatic carbon chains. Thus, alkanethiols are ideal compounds for SAM studies. Nevertheless, thiol anchoring groups exhibit a poor electronic coupling to the metal and thus a rather high resistance at the metal-molecule interface hampers the realization of effective molecular electronic devices. Moreover, the low energy barrier for the molecular diffusion and desorption is not beneficial for the device stability. Instead, gold surfaces functionalized with dithiocarbamates show enhanced SAM stability features and a better charge communication at the interface, compared to gold substrates with thiol linkers. Comparative studies of dithiocarbamates and thiols as anchoring groups are described in the literature.[45,47,247] Morf *et al.* studied the binding characteristics and SAM formation of mono- and bifunctional dithiocarbamates on flat Au(111) surfaces.[45] The

investigated structures are depicted in *Figure 13A*. The corresponding SAMs were analyzed by XPS, cyclic voltammetry (CV) and STM. With these measurements it was shown that dithiocarbamates bind as a bi-dentate to Au(111) surfaces and that dithiocarbamate-based molecules form compact SAMs. Nanoparticles have also been interlinked with thiols and dithiocarbamates.[250] The activation energies for the charge transport through the corresponding NP's film were smaller for the dithiocarbamate-based system, which means that the electrical conductivity is enhanced, compared to the thiol-based device. Further comparisons of dithiocarbamate- and thiol-based SAMs were performed by von Wrochem *et al.*.[47] Structures with the same molecular backbone but different anchoring groups were used as comparative systems (*Figure 13B*). XPS data revealed that all dithiocarbamate derivatives chemisorbed to gold formed densely packed monolayers with molecular areas that are very similar to those obtained from the corresponding thiol derivatives. Furthermore, UPS measurements and DFT calculations suggested that due to the electronic structure of the resonant bi-dentate group the electronic coupling between adsorbate and metal is enhanced. This improvement is translated into a low charge injection barrier at the dithiocarbamate-gold interface, which consequently affects the conductance in metal-molecule-metal junctions. Furthermore, thermal desorption experiments manifest higher stability of dithiocarbamates SAMs compared to the corresponding assembled thiols.

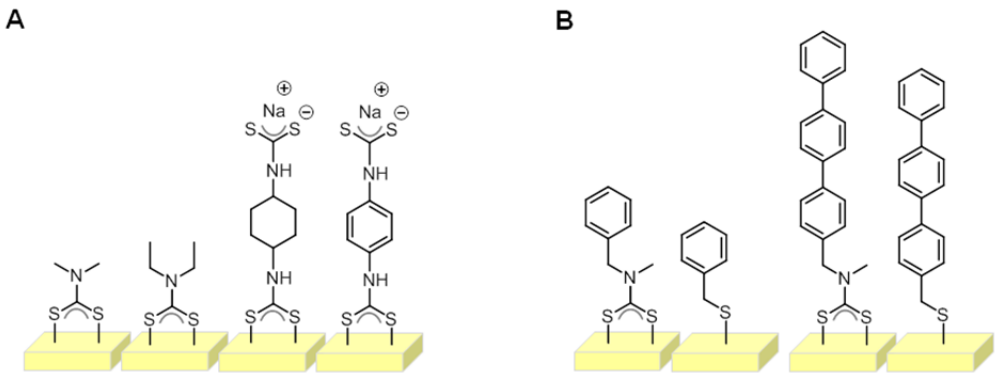

Figure 13. SAMs on gold substrates investigated by (A) Morf *et al.*[45] and (B) von Wrochem *et al.*.[47]

The obtained results of the surface investigations reveal the attractiveness of dithiocarbamates for SAM experiments and applications. Exemplarily, it was reported on "the most stable and robust ruthenium(II) bis-terpyridine complex SAM" (*Figure 14*).[264] Solar cells based on ruthenium polypyridyl complexes are supposed to be stable in order to survive redox cycling without degradation for several years. A strategy to employ highly stable redox-active ruthenium(II) (Ru) polypyridyl SAMs on gold surfaces is to incorporate more robust linkers than the conventional thiol adsorbates. Moreover, the incorporation of a piperazine unit improved the spectroscopic and electrochemical properties of the Ru-complex and additionally enabled the attachment of the robust dithiocarbamate anchoring group. The corresponding SAM showed

excellent reversible redox behavior and exceptional stability, which was not the case for the comparable thiol-based system.

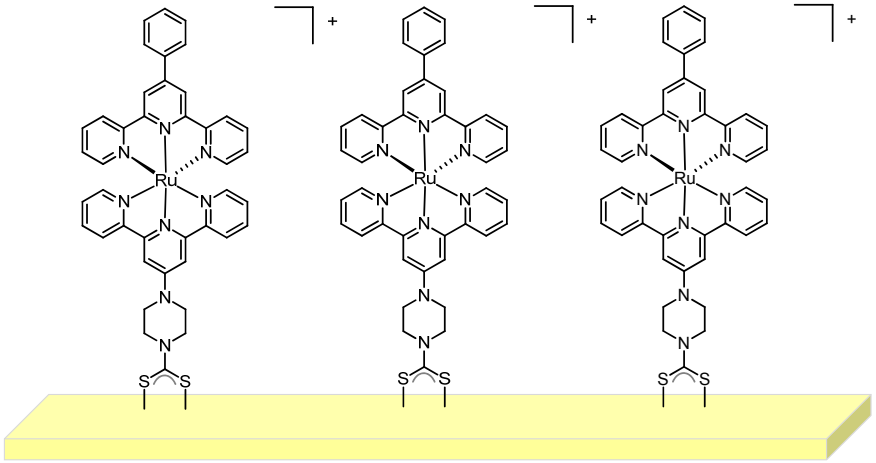

Figure 14. Ruthenium(II) bis-terpyridine complex functionalized gold surface.[264]

To conclude, the electronic structure and bond stability of dithiocarbamates make them promising candidates for their implementation in molecular electronic circuits and optoelectronic devices.

2 Research Project

The “top-down” approach to improve the performance of small electronic devices is becoming more and more challenging due to economic and engineering restrictions. Thus, researchers seek for alternatives towards efficient, smaller and faster devices. The “bottom-up” method, in which molecules or molecular films implement electronic functionalities, is an outstanding challenge for scientists. The functionalization of metals with molecular films changes the metals’ characteristics and thus the tuning of device properties is possible. The fundamental research of exploring functionalized surfaces is the driving force of this PhD-work. In particular, the focus will be set on the electronic communication between two interfaces which have to be considered when gearing towards applications such as organic light-emitting diodes and organic field-effect transistors. The investigations on appropriate metal-molecule and molecule-semiconductor interfaces are crucial to improve the charge transport of a molecular thin film device. The exploration of the metal’s work function is of particular interest and is the main aspect addressed in this work. However, the modulation of the molecular backbone to tune the crystallinity of the self-assembled monolayer and thus the electronic properties of the metal is also investigated within this project.

The design, synthesis and characterization of molecular structures bearing azobenzenes and dithiocarbamates, which are appealing functional units, is presented in this work. Subsequently, the self-assembled monolayers of these structures are prepared and the interdependence of the self-assembled monolayers and the substrate electrodes is investigated. These studies are performed in a close collaboration with the research groups of Prof. P. Samorì, Prof. Dr. B. Doudin, Prof. C. Wöll and Prof. M. A. Rampi and with Dr. F. von Wrochem and Dr. W. Ford from the Material Science Laboratory of SONY Deutschland GmbH. Within this research activity the main aim is to obtain a deeper understanding of the correlation between the structural architecture of molecular films and the overall device’s electronic performance.

3 Biphenyl-Based Azo Compounds Immobilized on Gold Surfaces

The search for highly efficient switching devices based on azobenzenes is of interest in many research groups,[95] as azo compounds are known to perform *trans* ⇄ *cis* isomerization upon irradiation of light and consequently change their physical and chemical properties. In the year 2007, studies with a fully conjugated, terminally thiol functionalized aromatic azobiphenyl compound (*Scheme 26*) showed unexpected properties when assembled on a gold substrate. The corresponding one component monolayer was able to perform a high yielding (up to 98%) isomerization process on the whole 2D crystalline domain. At first, this phenomenon was counterintuitive. The single molecules pack very tightly, due to the π-π-intermolecular interactions. A dense packing of the monolayer would suggest the restriction of conformational change of the azobenzene moieties, as free space for their motion is required (section 1.2.4). However, the efficient switching process can be explained by a cooperative effect of the neighboring molecules. Incorporated in a metal-molecule-metal junction it was demonstrated that upon irradiation und thus isomerization, the current through the junction and the resistance can be triggered.[220] Furthermore, it was shown that the azo molecules can express mechanical work.[82] Due to the interesting properties mentioned this specific azo compound will be investigated in more detail, in order to better understand and consequently to better control its SAM properties.

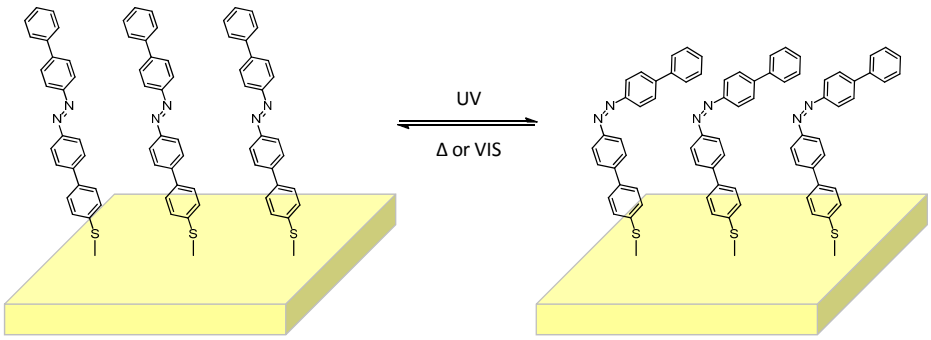

Scheme 26. The terminally thiol functionalized aromatic azobiphenyl compound assembled on a gold surface.

Numerous investigations are proposed to tap the full potential of this terminally thiol functionalized aromatic azobiphenyl compound (*Scheme 26*). In collaboration with Prof. Samorì and Prof. Doudin and their groups this structure will be embedded into different devices. The work function of functionalized gold substrates will be measured applying several microscopy and spectroscopic techniques. The triggable current characteristics of the SAM will be further investigated in an organic field effect transistor (OFET). The question is addressed whether the azo structures will retain their switching capacity and be able to modulate the charge injection of the OFET device by external stimuli. Furthermore, the focus will also be set on the

combination of the photoresponsive properties of the azo structure with the unique properties of metal nanoparticles.

A further approach to better understand the observed properties of the biphenyl azo compound is to investigate on architecturally similar structures. The examination of novel tailor-made azo compounds will give a deeper knowledge to what extent the structural modifications alter the properties of the resulting SAMs. Therefore, the second main focus is set on the design, synthesis and investigation of new biphenyl-based azo structures. In the following sections the novel azo compounds will be presented. Besides comparative studies on the work function of the corresponding assembled gold substrates and on the structural alignment of the monolayer, each individual target structure addresses a specific research goal. These research concepts will be discussed for each single target structure. However, before introducing the new target molecules, an efficient synthetic route towards the terminally thiol functionalized azobiphenyl will be shown and discussed and afterwards the obtained results of the corresponding devices will be presented.

3.1 The “Classical“ Azobiphenyl Compound

The continuous investigations of the properties of the terminally thiol functionalized azobiphenyl depicted in *Figure 15* is discussed in literature within several publications.[82,218–221] Further investigations of this structure incorporated in different setups are envisaged. For the sake of convenience this compound will be entitled the “classical” azobiphenyl (**CABP**) compound.

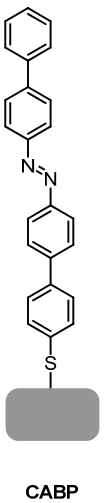

CABP

Figure 15. The ”classical“ azobiphenyl.

3.1.1 An Improved Synthetic Route

Initially the assembly of the "classical" azo biphenyl (**CABP**) onto a gold substrate was accomplished starting from 1,2-di([1,1'-biphenyl]-4-yl)diazene comprising a terminal thiol group (**CABP-SH**).[82,218–220] The synthesis of the **CABP-SH** was developed by Mark Elbing in 2007, which is depicted in *Scheme 27*.[218] The key step of the synthetic pathway was the formation of the azo functionality of compound **8** in a Mills reaction, which enables the formation of asymmetric azo compounds, as already discussed in section 1.2.3. A Mills reaction requires a primary amine and a nitroso derivative. A common way to prepare nitroso compounds is the reduction of a nitro group followed by selective oxidation.[265] Since sulfur atoms are prone to oxidation the precursor towards the nitroso building block **2** has to be free of oxidizable substituents. Therefore the sulfur was introduced in the amine building block **7**. Both, the nitroso and amine intermediates (**2** and **7**, respectively), were synthesized starting from biphenyl moieties (**1** and **3**, respectively), which are commercially available. Their functional groups were exchanged during the synthetic procedure to the desired precursors for the Mills condensation. The detailed discussion of the synthesis of **CABP-SH** is reported in Mark Elbing's Thesis "Funktionale Molekulare Bausteine".[266]

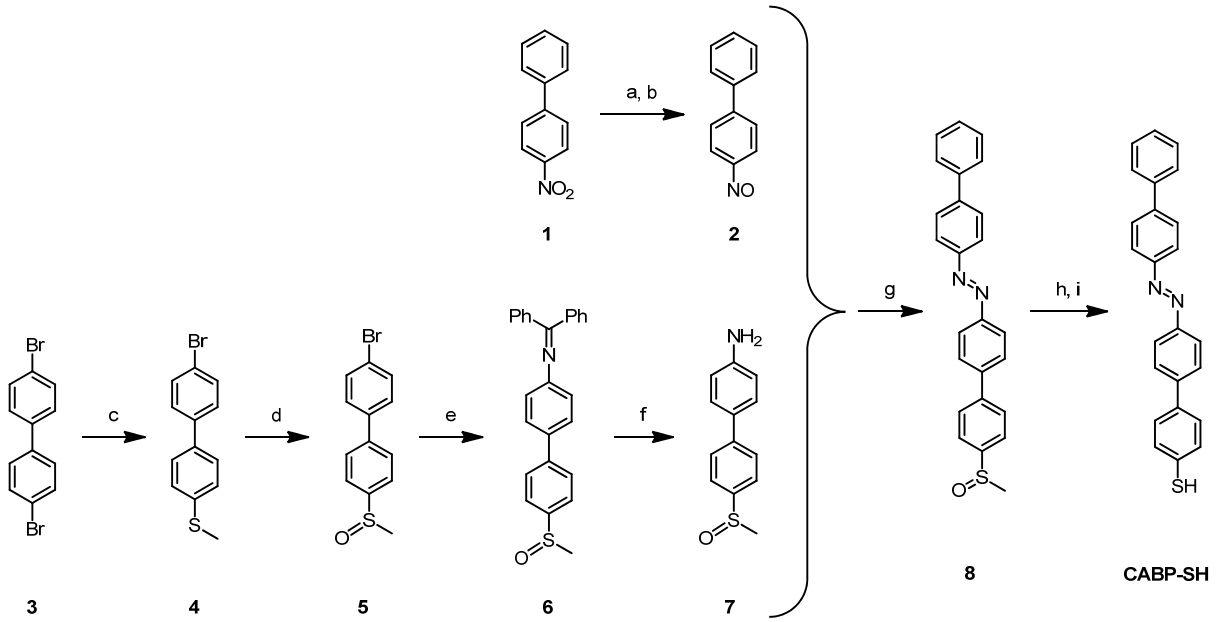

Scheme 27. Synthesis of **CABP-SH**, as described by M. Elbing.[218] *Reagent and conditions:* (a) NH_4Cl, Zn, $MeOCH_2CH_2OH$, H_2O, 35 °C; (b) $FeCl_3$, $MeOCH_2CH_2OH$, H_2O, EtOH, -5 °C, 63% over two steps; (c) NaSMe, DMI, 150 °C, 60%; (d) *m*CPBA, CH_2Cl_2, 0 °C, 89%; (e) $(Ph)_2C{=}NH$, $[Pd_2(dba)_3]{\cdot}CHCl_3$, KO*t*Bu, BINAP, toluene, 80 °C, 77%; (f) $NH_2OH{\cdot}HCl$, NaOAc, MeOH, rt, 95%; (g) AcOH, CH_2Cl_2, 65 °C, 83%; (h) $(CF_3CO)_2O$, toluene, 40 °C; (i) Et_3N, toluene, EtOH, rt, 27% over two steps.

The purification of the obtained sulfur (**CABP-SH**) was, due to its moderate solubility, troublesome. Thus low yields were obtained, affecting dramatically the overall yield of the

synthesis to the **CABP-SH**. Furthermore, the **CABP-SH** is prone to disulfide (**CABP-SS**, *Scheme 28*) formation, which is a further reason for the obtained low yields of the **CABP-SH**. In general disulfides can also be assembled on gold surfaces,[109,200,202,206,267] but in this case the formed disulfide (**CABP-SS**) exhibits very low solubility, which is undesirable for the assembly procedure. Alternatively, SAMs are obtained from acetyl protected precursors.[268] Thus an efficient synthetic access to the acetyl protected azobiphenyl (**CABP-SAc**, *Scheme 28*) was developed. The acetyl protecting group can be easily cleaved *in situ* under basic conditions during the assembly process.

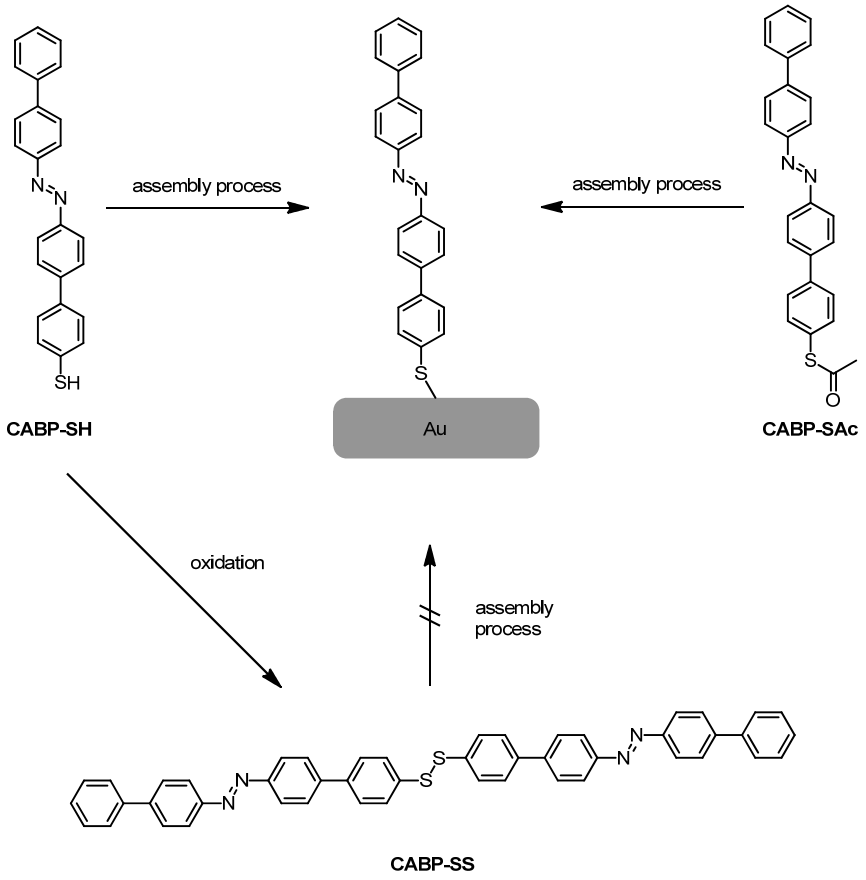

Scheme 28. The assembly of a sulfur terminated compound on gold substrates can be accomplished by their thiol, acetyl and disulfide form, assuming that the compounds are soluble. Here, a schematic overview with the "classical" azobiphenyl (**CABP**) as an example is shown.

The synthetic strategy to the **CABP-SAc** was developed such that the synthetic intermediates can serve as modular building blocks for the preparation of other structurally similar target azo compounds. The importance of this consideration will be reinforced in the next sections. In principle, for the retrosynthetic analysis, the acetyl protected **CABP** can be divided into three main building blocks: the azobenzene middle unit and the outer two aromatic units, where one of them comprises the sulfur functionality with an adequate protecting group (*Scheme 29*). The division of the building blocks was done through the carbon-carbon bonds on purpose, since

metal catalyzed cross-coupling reactions are powerful tools for the formation of carbon-carbon bonds.[269] These couplings involve the formation of the intermediates **9** and **10**, which will be formed in Suzuki-Miyaura cross-coupling reactions.

The sulfur of intermediate **9** should bear a protecting group, which tolerates basic conditions that are used in metal mediated cross coupling reactions. This sulfur protecting group is considered to be transprotected to the basic labile acetyl group in the final step of the synthesis. Compound **10** is suggested to be formed from an asymmetric azo building block (**11**). The asymmetry is of great importance for the selective coupling of the outer aromatic units, in order to minimize statistical coupling reactions. Building block **11** comprises on the aromatic unit in the *para* positions to the azo functionality different halogen substituents. Halogens are known to act as suitable leaving groups in carbon-carbon cross-coupling reactions, where the quality of leaving group increases from Cl to Br to I.[269] The azo functionality in unit **11** is obtained from a condensation reaction between an aniline (**12**) and a nitroso derivative (**13**), the Mills reaction (section 1.2.3). This reaction is introduced in the beginnings of the reaction sequence. The introduction of the Mills reaction at a later stage of the synthetic sequence could be troublesome, if further oxidizable substituents are present during the nitroso formation. Furthermore, as mentioned before, the asymmetric compound **11** is one of the suitable modular building blocks, which can be implied in reaction sequences to other target azo compounds.

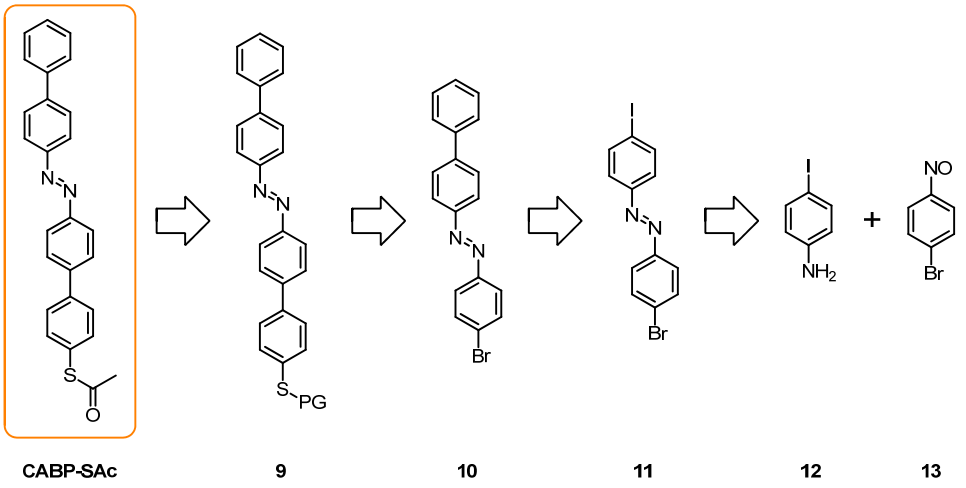

Scheme 29. Retrosynthetic analysis of the **CABP-SAc**.

3.1.2 Synthesis and Characterization

The synthesis to target structure **CABP-SAc** started with the oxidation of 4-bromoaniline (**14**) to 1-bromo-4-nitrosobenzene (**13**) (*Scheme 30*). This was mediated in a biphasic system by Oxone®. The oxidizing agent Oxone® was dissolved in water and added to a solution of

4-bromoaniline (**14**) in dichloromethane and stirred vigorously. The observation of a green reaction mixture indicated the formation of compound **13**, since most nitroso compounds have a deep green color in solution.[175] As thin liquid chromatography (TLC) monitoring showed complete consumption of the starting material **14** the reaction mixture was worked up and the layers were separated. After removal of the solvent the nitroso crude **13** was not further purified, since probable impurities of nitro and azoxy derivatives do not influence the next reaction step to azobenzenes (section 1.2.3). Furthermore, the long storage of nitroso compounds should be avoided due to their limited stability.[270] Acetic acid and 4-iodoaniline (**12**) were added to the crude **13** and stirred at room temperature for two days. After workup and purification by column chromatography azobenzene **11** was isolated as an orange solid in a yield of 79% over two steps. For the further selective coupling 4-iodoaniline (**12**) was chosen in order to obtain an asymmetric azobenzene. As iodide is a better leaving group, compared to bromide,[269] in metal-catalyzed cross-coupling reactions, a selective coupling is possible. In a Suzuki-Miyaura cross-coupling reaction the terminal arene unit was attached to compound **11**.

Besides a halo-compound reagent, a boronic acid derivative is necessary for the Suzuki-Miyaura cross-coupling reaction for the carbon-carbon bond formation. Therefore, phenylboronic acid was chosen. Furthermore, a metallic catalyst and a base are required to promote the coupling. Here, standard Suzuki-Miyaura reagents, i.e. tetrakis(triphenylphosphine)palladium ($Pd(PPh_3)_4$) as catalyst and potassium carbonate as base, were used. 1.3 Equivalents of the commercially available phenylboronic acid, compound **11**, the catalyst and the base were stirred under an inert atmosphere in an ethanol/toluene/water solvent mixture at 50 °C overnight. After workup and purification by column chromatography compound **10** was obtained as an orange solid in a yield of 96%, indicating the efficiency of the selective coupling, which can be controlled by adjusting the temperature. Increasing the reaction temperature could also have led to the coupling of phenylboronic acid at the bromine position, forming the bi-substituted symmetric azo derivative.

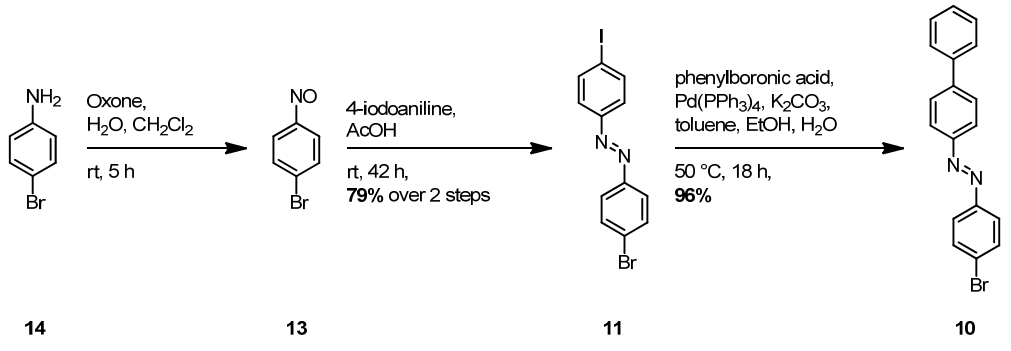

Scheme 30. Synthesis of the azobenzene **10**.

The attachment of the second terminal building block, which comprises the boron and sulfur functionality, to compound **10** is the next step. The sulfur will be protected with an ethyl-trimethylsilane (ethyl-TMS) group, as is known for its stability in basic conditions and its ease of removal with a fluoride source.[271] In a thiol-ene reaction the introduction of the masking group was achieved starting from commercially available 4-bromothiophenol (**15**) (*Scheme 31*). The same reactants and reagents as in a literature procedure of Yu *et al.*,[272] i.e. vinyltrimethylsilane and the radical starter di-*tert*-butyl peroxide, were transferred together with the thiophenol derivative **15** into a pressure tube. The reaction mixture was heated at 100 °C in an oil bath for 5 hours. After basic workup and purification by vacuum distillation, instead of column chromatography as reported in literature,[272] the desired organosulfur compound **16** was isolated as a colorless liquid in a yield of 87%. With compound **16** in hand a halogen-metal exchange with *n*-butyllithium, followed by electrophilic trapping with isopropyl borate to form the corresponding boronic acid after hydrolysis, was performed.[273] After recrystallization from *n*-hexane and drying under high vacuum conditions the boroxine **17**, a cyclotrimeric anhydride of the corresponding boronic acid, was obtained as a colorless solid in 64% yield, and not the free boronic acid as described in literature.[273] Boroxines, as well as boronic acids and boronic esters, can also be employed as substrates for Suzuki-Miyaura cross-coupling reactions.[274]

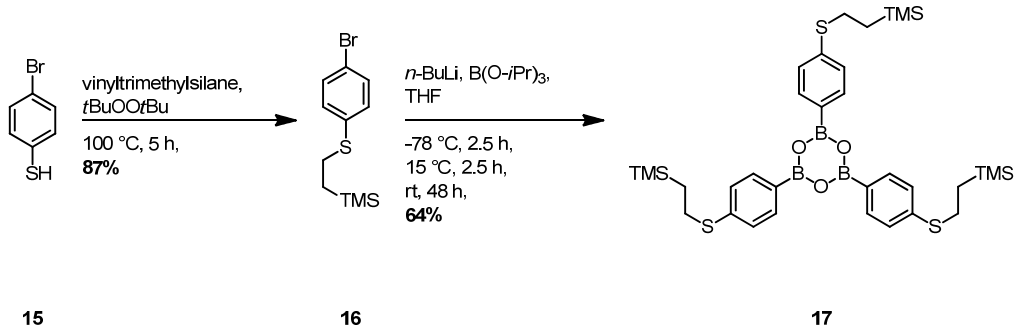

Scheme 31. Two step synthesis of the cyclotrimeric anhydride **17**.

The intermediates **10** and **17** are the reactants for the following Suzuki-Miyaura cross-coupling reaction (*Scheme 32*). The halide **10**, an 1.3-fold excess of the trimeric compound **17** (0.4 equivalents) and potassium carbonate were added to a toluene/ethanol solvent mixture. The solution was degassed and then $Pd(PPh_3)_4$ was added under an inert atmosphere. The resulting reaction mixture was stirred at 60 °C for three hours. After aqueous workup and purification by column chromatography the coupling product **18** was obtained as an orange solid in a yield of 80%. The last step to the desired target structure **CABP-SAc** was the transprotection of the sulfur protecting group to the base labile acetyl group with tetrabutylammounium fluoride in an excess of acetyl chloride in a tetrahydrofuran medium at

room temperature (*Scheme 32*). The target **CABP-SAc** was isolated after workup and purification by column chromatography as an orange solid in a yield of 72%.

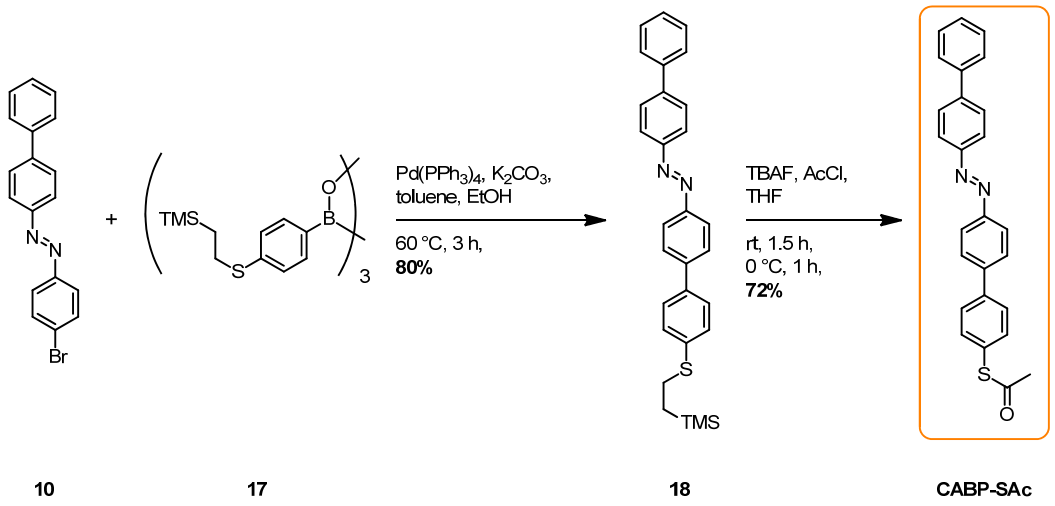

Scheme 32. Synthesis to **CABP-SAc**.

To summarize, with this reaction sequence to the **CABP-SAc** the desired intermediates and the final product are provided in good to excellent yields (between 64% and 96%). The efficiency of a selective coupling of the individual building blocks was shown using an asymmetric azobenzene unit and by applying classical Suzuki-Miyaura cross-coupling conditions. **CABP-SAc** was fully characterized by nuclear magnetic resonance (NMR) spectroscopy (^{1}H, ^{19}F, heteronuclear multiple bond coherence (HMBC) and heteronuclear multiple quantum coherence (HMQC)), electron impact mass spectrometry (EI-MS) and elemental analysis (EA).

3.1.3 Investigations of the Assembled CABP

The synthesized **CABP-SAc** was used as a precursor for the functionalization of gold substrates. With the corresponding fabricated densely packed SAMs, work function measurements using four different experimental techniques, which are Kelvin Probe (KP), Kelvin Probe Force Microscopy (KPFM) electroabsorption (EA) spectroscopy and ultraviolet photoelectron spectroscopy (UPS), were performed.[275] The application of different measurement conditions and different preparation methods helped to get reliable work function values. In order to reinforce the observed experimental results, theoretical calculations were done. KP and KPFM were used to investigate the modification of the surface potential and the work function caused by the chemisorption of the **CABP** on the gold surface. Both measurements were conducted under similar ambient conditions and under the effect of an electric field. While KP maps a macroscopic area, the KPFM features tens of nanometers spatial resolution. The work function

(Φ) of bare polycrystalline gold on a silicon oxide (SiO_x) substrate measured by means of KP, was found to amount to 5.12 eV with a standard deviation lower than 0.02 eV. With this method the work function of the polycrystalline gold substrate, on which the **CABP** is chemisorbed, was measured to be for the *trans*-based SAM Φ_{trans} = 5.15 eV and for the corresponding *cis*-SAM Φ_{cis} = 5.22 eV. Furthermore, the *trans* ↔ *cis* isomerization cycles of the **CABP** on the surface were monitored by KP. *Figure 16* shows the absolute work function values plotted against time during the isomerization process. The wok function of the *trans*-based **CABP**-SAM was recorded before and after irradiating it with UV-light (365 nm). The thermal back reaction (*cis* → *trans*) was monitored in the dark over time. The graph nicely shows an exponential decay during the re-isomerization, which almost reaches "*trans*"-saturation, concluding that most of the *cis*-isomers were converted to the *trans*-form. Unfortunately, a noteworthy switching fatigue is observed in the last cycle.

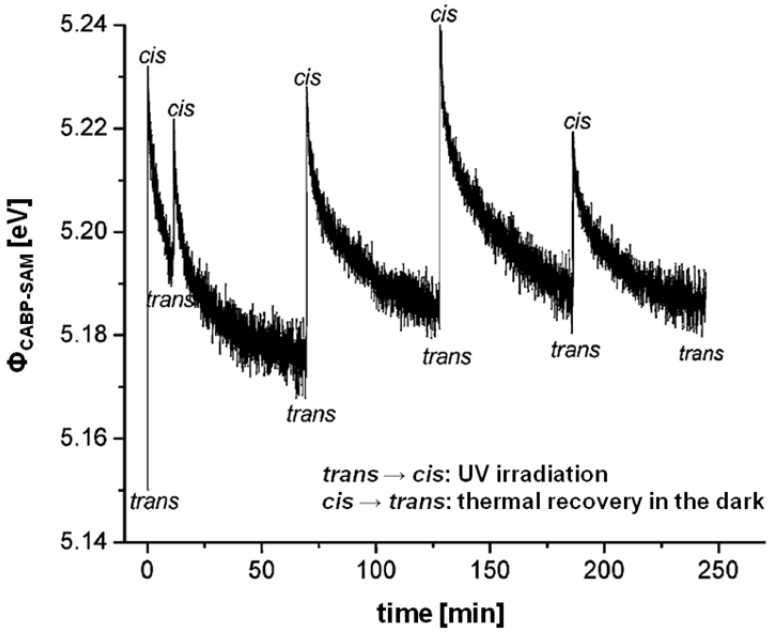

Figure 16. Plot of the $\Phi_{CABP-SAM}$ on gold over time monitored by KP. Work function measurements were performed before (*trans*) and after (*cis*) UV irradiation and the thermal back reaction (*cis* → *trans*) was monitored in the dark.[275]

A very similar work function value of a **CABP**-functionalized Au(111) surface of the initial *trans*-state compared to the KP value, was monitored by KPFM, being Φ_{trans} = 5.17 ± 0.03 eV. The work function difference upon photoswitching was determined to be $\Delta\Phi_{trans\text{-}cis}$ = 116 ± 16 meV, which is comparable to the change measured on samples of the **CABP**-SAM chemisorbed on the polycrystalline gold layers on indium tin oxide (ITO) ($\Delta\Phi_{trans\text{-}cis}$ = 125 ± 15 meV). This small deviation ($\Delta\Phi_{Au(111)\text{-}polycryst.\ Au}$ = 9 meV) can be explained by the direct influence of nature of the gold on the molecule-molecule interactions and thus affecting the packing order of the **CABP** molecules forming the SAM. This different ordering can influence the directionality and yield of the isomerization (i.e. time scale of the switching process). A deeper analysis of the varying work

function values observed for the two different types of gold surfaces (Au(111) on mica and polycrystalline Au on ITO) allowed for a better insight to the switching mechanism of the assembled **CABP**. A stretched exponential function (SEF) was fitted to the experimental data in order to understand the kinetics of the isomerization process. The fittings suggest a strong asymmetry in the time-evolution trend for both substrates. The *trans* to *cis* conversion is faster than the inverse one and presents a work function variation roughly described by a simple exponential trend. An exponential law in kinetics indicates an occurrence of only one mechanism or the simultaneous activation of all sites of the sample. The slower thermal back isomerization (*cis* → *trans*) is explained by the formed herringbone domains of the *cis*-isomers, which were observed by STM.[218] These *cis*-domains are considered to be stabilized by π-π intermolecular interactions, thus leading to the retarded back isomerization. Therefore, it was suggested that the molecular relaxation (*cis* → *trans*) occurs in stages, where the relaxation of a molecule (or molecule cluster) is dependent on the relaxation stage of the molecule's (molecules') neighbors, leading to a serial activation. However, the proposed mechanistic dynamics remain a hypothesis as they cannot be corroborated with experimental evidence, as the resolution of the KPFM images is too low to show anisotropies on the surface.

UPS measurements reveal a work function shift upon isomerization amounting to 80 ± 50 meV (Φ_{trans} = 4.32 eV and Φ_{cis} = 4.40 eV). As expected, the UPS work function values were lower than the KP ones. This is due to the fact that the KP method measures an average of all work function values found in potentially different domains existing under the probe head. On the other hand, UPS is sensitive to the lowest work function in the probed area, as secondary electrons with the lowest kinetic energy are used for the determination.[276,277] However, the observed relative changes in work functions ($\Delta\Phi_{trans\text{-}cis}$) are in good agreement for all three experimental techniques (KP, KPFM and UPS).

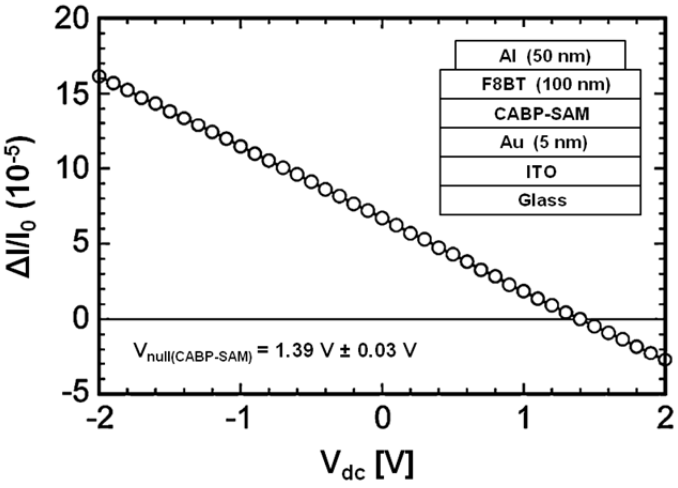

Figure 17. Direct current voltage scans of the EA signal towards positive bias of the ITO/Au/**CABP**-SAM/F8BT/Al device. The zero crossing voltage is 1.39 V, which is translated to a work function value of Φ = 5.15 ± 0.1 eV.[275]

Embedding the *trans*-based **CABP**-SAM in a device allows for EA measurements for a further determination of the work function. The device contained the following components: ITO/Au/**CABP**-SAM/F8BT/Al, where F8BT = poly(9,9'-dioctylfluorene-alt-benzothiadiazole) and Al = aluminium. The linear dependence of the EA signal on the applied bias was used to determine the nulling voltage (V_{null}) across the light-emitting diodes (*Figure 17*). The work function can thus be calculated using the equation $V_{null} = (\Phi_{anode} - \Phi_{cathode})/e$, where Φ_{anode} and $\Phi_{cathode}$ are the work functions of the **CABP**-SAM and the Al substrate, respectively, and e is the electronic charge. Knowing the work function value of aluminium, which was determined in previous KP measurements, the work function of the *trans*-**CABP**-SAM can be extracted from the equation, being Φ_{trans} = 5.06 – 5.22 eV. The similar value obtained by EA compared to the other measurements, shows that the tuning of the work function caused by chemisorption of the **CABP** is not altered once embedded in a device structure. Theoretical quantum-chemical calculations corroborate the observed higher work function values for the *cis*-based SAM and also the work function change between the two forms (Φ_{trans} = 4.04 eV, Φ_{cis} = 4.14 eV, and $\Delta\Phi_{trans\text{-}cis}$ = 100 meV). However, the work function shift between the bare gold surface and the **CABP**-functionalized gold ($\Delta\Phi_{Au\text{-}SAM}$) are much higher than those measured in the present study. Due the actual nature of the gold sample and the presence of contaminants, which can shield the intrinsic work function of the sample in the KP, KPFM and EA measurements, the comparison of the absolute values is restrained. Moreover, according to the calculations performed an additional point is considered: The shift of the work function is dominated by the electronic reorganization upon formation of the gold-sulfur bond (bond dipole) rather than by the difference of dipole moment between the two isomeric forms (molecular contribution).

Table 2. Work function values of **CABP**-SAM determined by different techniques.

Measuring technique	Φ_{Au} [eV]	Φ_{trans} [eV]	Φ_{cis} [eV]	$\Delta\Phi_{trans\text{-}cis}$ [meV]
KP	5.12	5.15	5.22	70
KPFM		5.17 ± 0.03		116 ± 16 (Au on mica) 125 ± 15 (polycryst. Au)
UPS	5.2 (sputtering) 4.50 (polycryst.)	4.32	4.40	80 ± 50
EA		5.06-5.22		
calculation	5.26	4.04	4.14	100

In conclusion, various experimental studies (KP, KPFM, UPS and EA) to determine the work function of **CABP**-based gold substrates were performed. Photoinduced work function changes by isomerization of the monolayer were observed, which were rather small (70-125 meV). In *Table 2* an overview of the obtained work function values is given. However, the comparison

between the techniques allowed getting a deeper insight to the system. Furthermore, quantum-chemical calculations supported the experimental observations.

The **CABP-SAc** was also investigated in an organic field-effect transistor (OFET) device.[278] The **CABP** was assembled on the gold source and drain electrodes of a field-effect transistor setup as shown in *Scheme 33*.[278] As an organic semiconductor *N*,*N*'-1H,1H-perfluorobutyl dicyanoperylenecarboxydiimide (PDIF-CN_2) was used. The choice of the PDIF-CN_2 is due to the advantage that the absorption peaks of the semiconductor do not overlap with the characteristic absorption bands of the azobenzene, and thus the alteration of the electrical properties of the semiconductor during light exposure (UV and visible) are minimized. With the corresponding device, output and transfer measurements were performed during irradiation and non-irradiation cycles. One cycle corresponds to the irradiation of a prepared device with UV-light (365 nm) for 90 minutes and the subsequent keeping of it in the dark for 24 hours. All output curves showed a good field-effect response, as shown in *Figure 18A*. Furthermore, the devices measured after the irradiation time exhibit a higher increase of the maximum source-drain current ($I_{D,max}$) in the output and transfer characteristics of the transistor, compared to the devices measured in the dark (*Figure 18A* and *B*). The source-drain current increases by 20% upon irradiation in the linear regime (source-drain voltage (V_D) = 20V). This observation is also accompanied by a decrease of the threshold voltage (V_{TH}) and the difference in V_{TH} ($\Delta V_{TH(trans\text{-}cis)}$) in the linear and saturation regime. This is an evidence that the charge injection capacity in the device, which was left in the dark, is better. This optical modulation process was found to be reversible as demonstrated in *Figure 18C* and *D*. The modulation of the charge injection capacity is suggested to arise from the isomerization changes of the **CABP**-based device. To demonstrate that the charge injection modulation was indeed caused by the isomerization of the SAM at the interface of the semiconductor and gold electrodes, and not as a result of an alteration of the properties of the device elements, several comparisons and control experiments have to be considered. These considerations are discussed in the next paragraphs.

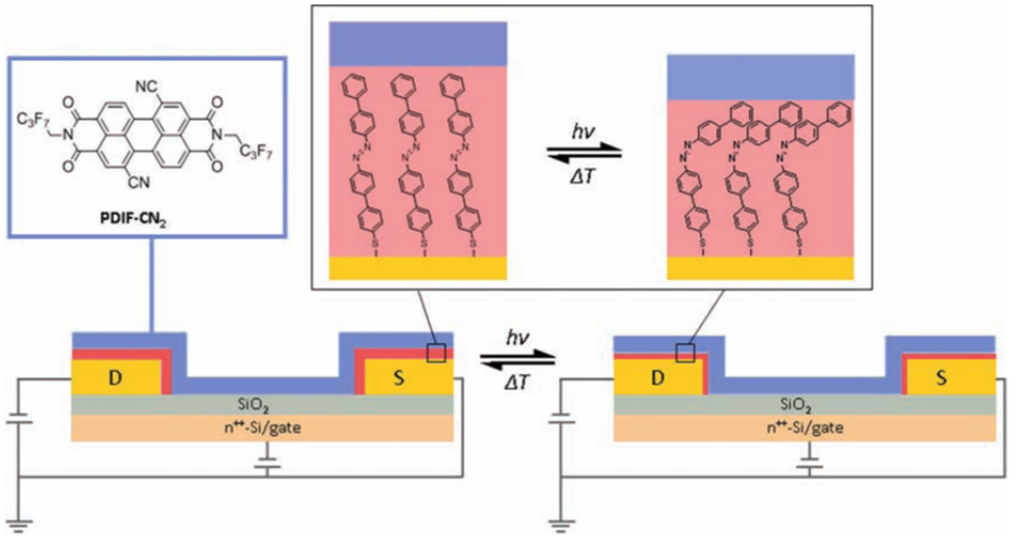

Scheme 33. Schematic representation of the device structure showing the reversible isomerization reaction (*cis* ⇄ *trans*) that takes place at the interface between the semiconductor and **CABP**-functionalized electrodes in an OFET.[278]

Firstly, the current-voltage (I-V) characteristics as described here are in full agreement with previous measurements of the **CABP**-SAM incorporated in two terminal junctions, as studied by cAFM[220] and Hg-drop-based investigations.[82] In these studies it was demonstrated that the modulation of the transport properties relies on the difference in tunneling barrier thickness, which is caused by the variation of the film's height upon structural isomerization. Furthermore, up to four reversible cycles of the **CABP**-based OFET were carried out without significant lost in switching efficiency. Such switching fatigue was also observed on the **CABP**-gold-SAM device used for work function measurements, as reported before.[275] These two comparisons point at the accordance that the observations made strongly depend on the isomerization process of the **CABP**.

In order to demonstrate that the charge injection modulation does not originate from changes in the PDIF-CN_2 film, a control experiment was performed. A spin-coated PDIF-CN_2 film on bare gold electrodes and a spin-coated PDIF-CN_2 film on gold electrodes functionalized with undecanethiol were irradiated at 365 nm for 90 minutes. The electrical characterizations performed on both transistor types did not show any changes in electrical parameters (mobility (μ), V_{TH} and I_D) and no V_{TH} shifts were observed. This excludes an influence of the semiconductor on the charge injection modulation upon irradiation.

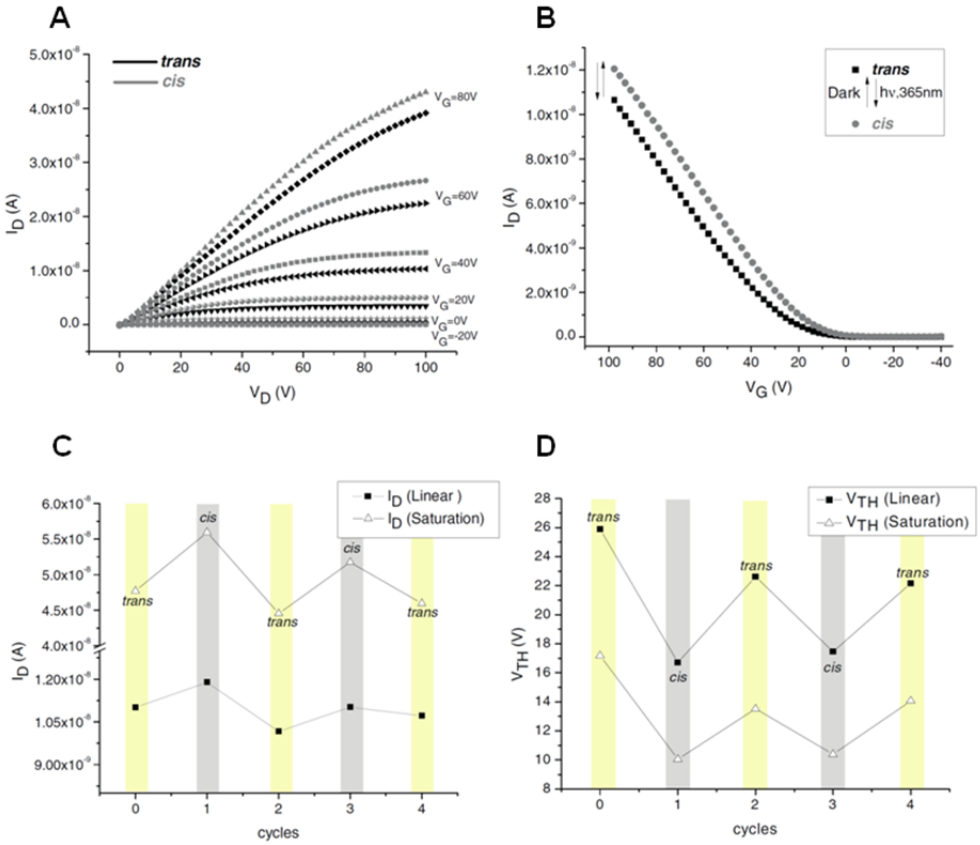

Figure 18. In situ measured (A) output and (B) transfer (linear regime, V_D = 20 V) characteristics for a PDIF-CN_2-film-based device with **CABP**-functionalized electrodes before (*trans*) and after (*cis*) UV irradiation. Variation of (C) $I_{D,max}$ (linear and saturation regime) and (D) V_{TH} (linear and saturation) for consecutive switching cycles of *trans* ⇄ *cis* **CABP**-functionalized electrodes.[278]

The change in electrical properties of the **CABP**-based OFET upon isomerization could also be due to the variation of the film morphology at the interface and/or a change in the work function of the contacts with the electrodes. As reported before, KP measurements of a **CABP**-SAM reveal rather small changes in the work function upon isomerization (Φ_{trans} = 5.15 ± 0.02 eV, $\Delta\Phi_{trans\text{-}cis}$ = 70 meV, $\Phi_{bare\ Au}$ = 5.12 ± 0.02 eV). Therefore, the work function changes cannot represent a major contribution to the electron injection barrier, also due to the different energetic level alignments of the interfaces. It is furthermore known that the nature of a surface can affect the crystallinity and ordering of the semiconducting film physisorbed at the interface and thus the electrical characteristics of the device.[279] Water contact angle measurements show different hydrophobic properties (~16° difference) of the *trans*- and *cis*-based **CABP**-SAM. Such different wettability can influence the interfacial film microstructure and therefore two additional *trans* and *cis* devices were individually prepared in order to get an insight to this consideration. An "*ex-situ*" preparation of a *cis*-based **CABP**-OFET was done, which means that the **CABP-SAc** was dissolved and the corresponding solution was irradiated at 365 nm before the assembly process. The corresponding SAM was continued to be irradiated also during the spin-coating process of the PDIF-CN_2. The preparation of the *trans*-based OFET was performed

in the dark. The output and transfer characteristics of the separated devices show markedly higher drain currents for the *cis*-based transistor compared to the corresponding *trans*, supporting the observed results of the "*in-situ*" prepared device, i.e. irradiation of an initially *trans*-based device. However, the $I_{D(cis)}/I_{D(trans)}$ ratio extracted from the *ex-situ*-based experiment was 2.4, which is a significant increase compared to the *in-situ*-based one, leading to a more pronounced device performance. This is attributed to an improved morphology of the interface for the films separately spin-coated on the two isomeric **CABP**-SAMs. Even more important than this morphological factor might be the improved switching efficiency when the *cis*-SAM is prepared *ex-situ*, resulting in larger amounts of *cis* domains and hence in a higher electrical transport difference in the OFET device.

In conclusion, with a **CABP**-PDIF-CN_2–based transistor device using gold source and drain electrodes it was possible to optically and reversibly modulate for the first time the charge injection at the electrode-semiconductor interface. In this device the source-drain current through the channel can be gated electrically (through gate control) as in a conventional OFET, and optically (through photochemical control). A better charge injection capacity in the *cis*-based device was observed. This is explained by the smaller thickness of the SAM, i.e. a decrease in the tunneling barrier thickness from *trans* to *cis*. Attempts to improve the cyclability and time response of the switch are currently ongoing.

Numerous reports on photosensitive gold and silver nanoparticles (AuNPs, AgNPs), whose surfaces are coated with azobenzene molecules, are known.[108,111–119] Also the **CABP** structure has made it in the AuNP's rubric.[120] AuNPs stabilized with hexylamine with a particle diameter of about 25 nm size were prepared. A ligand-exchange reaction with an excess of the **CABP-SAc** was performed under basic conditions, enabling chemisorption of the deprotected thiol groups to the Au particle surface. After workup of the **CABP**-coated AuNPs ^{1}H-NMR and UV/Vis spectroscopy revealed the attachment of the **CABP** onto the Au surface. A correlation between the solubility of the **CABP** coated particles and the isomerization state of the chemisorbed molecules was observed. As a result of the exposure time to both UV and visible light, the **CABP**-AuNPs were found to form a colloidal dispersion in toluene, when **CABP** groups are in their *cis*-form, or as a precipitate, when the **CABP**s are in their *trans*-conformation (*Scheme 34A*). In particular, the *trans*-**CABP** groups exposed on adjacent **CABP**-AuNPs were found to interdigitate, yielding aggregation and precipitation of the nanoparticles. Upon exposure of the same **CABP**-AuNPs to 366 nm light, a phase transition from solid to a colloidal phase was observed. Upon subsequent irradiation with 450 nm light the photochemical back isomerization was accomplished, leading to the re-precipitation of the **CABP**-AuNPs. By successive stepwise irradiation with UV and visible light the precipitation-dispersion phenomenon was

demonstrated to have a reversible character. This process could also be visible to the naked eye, as shown in *Scheme 34B*.

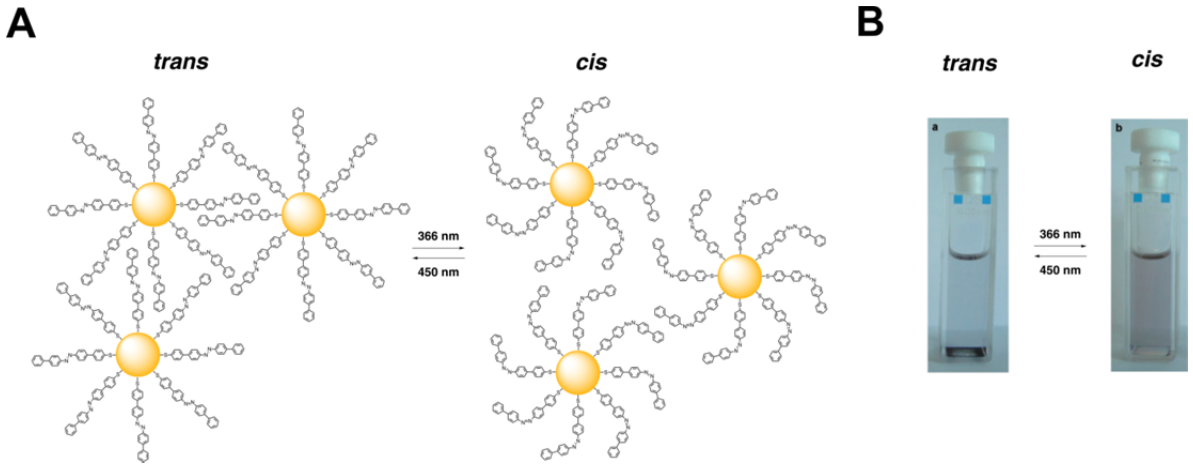

Scheme 34. (A) Schematic representation of the inter-**CABP**-AuNP interactions, where in the *trans*-form the adjacent NPs interdigitate, leading to aggregation and precipitation of the **CABP**-AuNPs. The *cis*-based **CABP**-AuNPs do not interdigitate, forming a colloidal dispersion of the NPs in solution. (B) A photograph of the **CABP**-AuNPs in a toluene solution in the *trans*- (precipitate) and *cis*-form (colloidal solution).[120]

These precipitation-dispersion results were corroborated by comparing the UV/Vis spectra (*Figure 19*) of the **CABP**-AuNPs sample upon irradiation. When the coated azobenzene shell undergoes isomerization from *trans* to *cis* a decrease of the absorbance around 600 nm and an increase around 530 nm was observed. This is due to a change in the Surface Plasmon Resonance (SPR), which is a result of structural changes in the nanoparticle ensemble system, like coagulation, assembly or destruction of the nanoparticles inside the sample. The enhanced peak at about 530 nm corresponds to the SPR of single nanoparticles, which matches with the fact that the **CABP**-AuNPs disperse in solution when the *cis*-form is present.

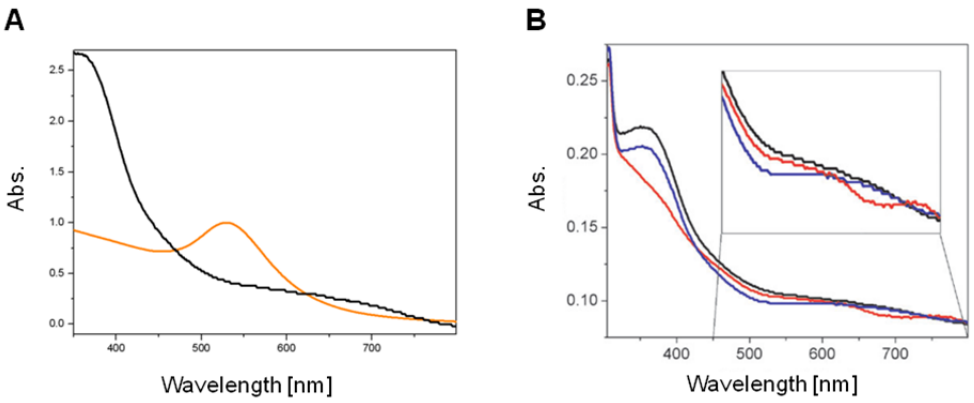

Figure 19. (A) UV/Vis spectra of Au coated NPs with hexylamine before (orange line) and after (black line) substitution with the **CABP**. (B) UV/Vis spectra of the **CABP**-AuNP sample upon irradiation: black line, before irradiation; red line, after irradiation with UV light at 366 nm; blue line, after irradiation with visible light at 450 nm.[120]

Furthermore, the aggregation change as a result of photoisomerization was revealed by scanning transmission electron microscopy (STEM) imaging as shown in *Figure 20*. The images provide evidence that the **CABP**-AuNPs in their *trans*-form feature very strong aggregation propensities, forming micrometer sized disordered 3D aggregates, whereas in the *cis*-form the NPs are rather well dispersed. Here, a method to optically and reversibly modulate the solvation and precipitation of AuNPs, coated by a single molecular component (**CABP**), in organic media was devised. This finding could be of importance to control on demand aggregation of AuNPs and also the density and spatial distribution of NPs in a nanostructured material.

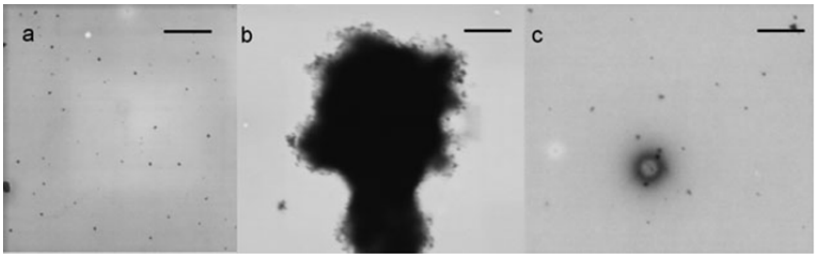

Figure 20. STEM images of the AuNPs (a) before substitution with **CABP** molecules. **CABP**-AuNP (b) in the *trans*-form, (c) in the *cis*-form as obtained upon UV-light irradiation of the sample in (b). Scale bar: 1 μm.[120]

One of the major challenges in molecular electronics is the design of reliable and stable devices. In this frame, a basic question remains to be addressed: How can one best exploit the intrinsic property of a molecule once it is incorporated between electrodes? The use of metallic nanoparticles as building blocks in electronic devices has been successfully demonstrated, since NPs allow bridging the size gap, separating bottom-up and top-down nanofabrication routes. Examples with metal cluster of 3-30 nm in size, trapped between electrodes,[280] or self-assembling in 2D networks that are macroscopically electrically addressable[281,282] are known. However, in these studies, electrical transport is complicated by Coulomb blockade effects, combined with percolation in a 2D network. The design of circuits with single and larger bridging nanoparticles could therefore be advantageous.[283] With this idea in mind the fabrication of bigger spheres coated with functional molecules was envisaged. The aim was to apply this device concept to the photoactive **CABP** (*Scheme 35*)**.** For this purpose, silica particles, which were coated with 30 nm of nickel followed by 30 nm of gold, were prepared. These microspheres were functionalized by chemisorption of the **CABP** and subsequently deposited on a gap (100 nm) of two electrodes. These two electrodes making the nanotrench are made of a nickel layer protected by gold of similar thickness. Afterwards the electrodes were also functionalized with a **CABP** monolayer. The preparation of the potential electronic circuit samples were patterned over UV transparent optical microscopy coverslip glass and an integrated light emitting diode source focused on the samples was switched between 365 and 455 nm.

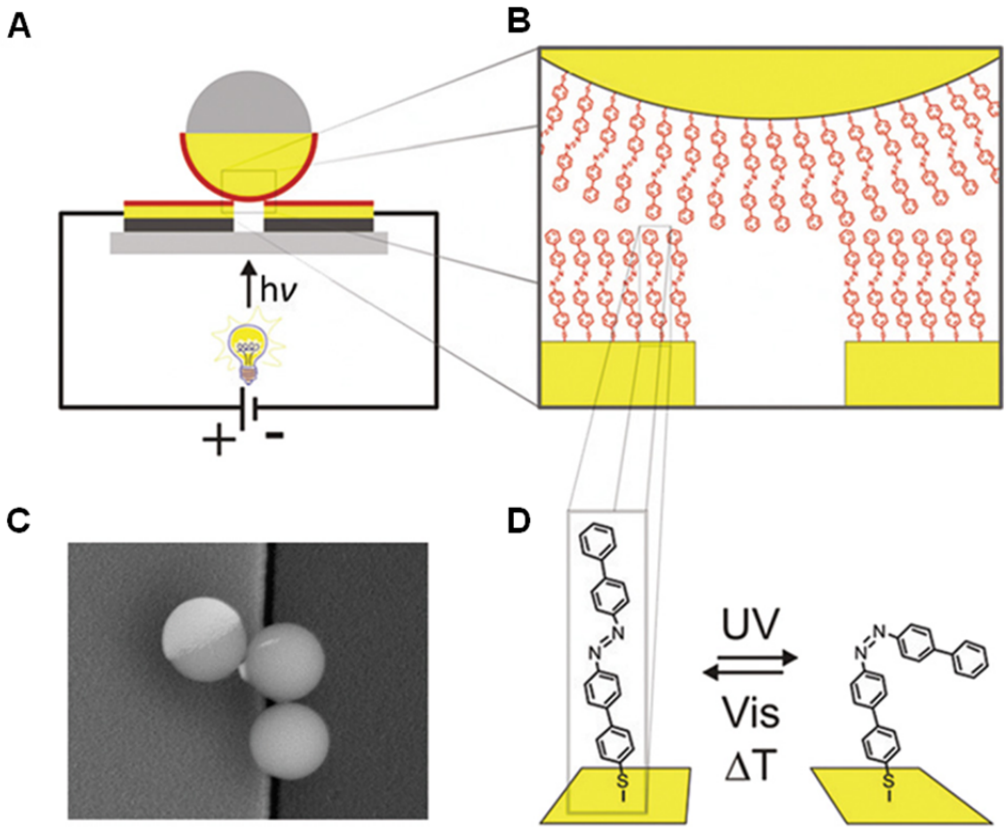

Scheme 35. (A) Schematics of the molecular circuit design. The Au hemisphere of the particle and the electrodes are coated with a chemisorbed **CABP** layer. (B) Cartoon of the interaction between molecules in the specific device geometry used. (C) Scanning electron microscopy view of 1 µm diameter microsphere trapped over an 80 nm trench. (D) The *cis* ⇄ *trans* isomerization of the **CABP**.[284]

The devices exhibit changes of conduction related to light-induced modifications of the molecular films. *Figure 21* displays the current-voltage characteristics of the junction upon switching of the azobenzene units. Typical observed conduction ratio spanned values between 1.1 and 3 (R_{trans}/R_{cis}). Samples were categorized as "switching" when reversible changes of conductance exceeded 10%. A statistical analysis of multiple experiments with the **CABP** films and a comparison with junctions containing photoinactive dodecanethiol SAMs gave good evidence that the devices exhibit changes of conduction related to light-induced modifications of the molecular films, confirming that the observed resistance value originates from molecular interconnects.

With this functionalized microsphere circuit it was affirmed that the observed electrical transport originates from charges transfer through molecules, with a 90% confidence ratio. Furthermore, the time evolution of the I-V curves indicates a time scale of 10^3 s to reach the other conduction state value, in line with other experiments of the **CABP**-based device in the vertical geometry.[82,220] Devices lasted a minimum of several hours, with reproducibility and stability reaching day's periods under ambient atmosphere. Up to several tens of switching

events were realized without any process optimization. Thus, the described studies make long-term systematic studies on switching molecular devices possible.

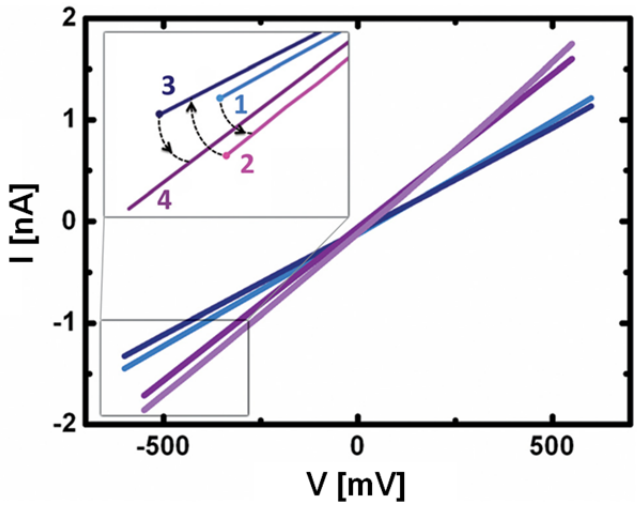

Figure 21. I-V curves showing reversible optically modulated current switching in the junction. Curve 1 corresponds to initial junctions, expected to correspond to molecules in *trans* configuration. Curve 2 results from UV irradiation (365 nm) of enhanced conductance, due to the occurrence of *cis* configurations. Curve 3, after 455 nm illumination, illustrates the reversibility of the switching, similarly to curve 4, switching again to *cis* after re-illumination with UV light.[284]

A further application of **CABP**-functionalized gold nanoparticles is their integration in a novel OFET design.[285] As described previously, the **CABP** was already used as functional building block in an OFET, where **CABP**-based SAMs were chemisorbed on the planar source and drain electrodes of an OFET device. However this device suffered from a photoinduced current change of only 20% and the occurrence of fatigue. As shown in *Scheme 36*, the new design is based on a blend of the p-type polymeric semiconductor poly(3-hexylthiophene) (P3HT) and AuNPs coated with a **CABP** monolayer. A higher photoresponse was proposed due to the enhanced active surface of the nanoparticles as compared to the **CABP**-functionalized gold source and drain electrodes. The semiconductor was chosen to be poly(3-hexylthiophene) (P3HT) as it combines a good solubility in organic solvents and large field-effect mobilities in thin films.[286] The particles were blended with the P3HT matrix and spin-coated on pre-patterned gold electrodes. For comparative studies the following device was prepared: An OFET device, in which the AuNPs are coated with a non-photoresponsive monolayer from a mixture of dodecanethiol and a conjugated thiol-based oligo phenylenes ethynylene (*Scheme 36A*) structure (≙ OPE-AuNP/P3HT).

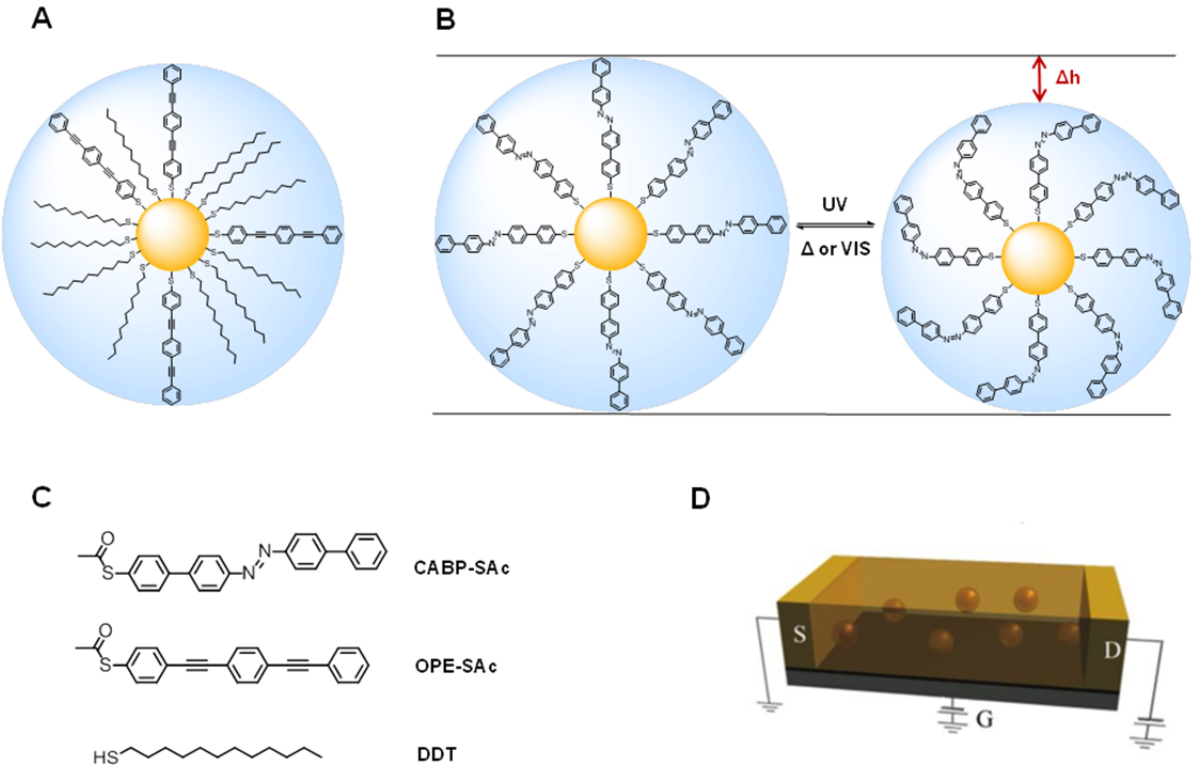

Scheme 36. Scheme of the differently coated gold nanoparticles: (A) OPE-AuNP and (B) **CABP**-AuNP in its *trans*- and *cis*-form. (C) Chemical structures of the acetyl protected "classical" azobiphenyl (**CABP**-SAc), S-(4-((4-(phenylethynyl)phenyl)ethynyl)phenyl) ethanethioate (OPE-SAc) and dodecanethiol (DDT). (D) Scheme of the bottom-contact bottom-gate field-effect transistor in which S, D and G are the three terminals (source, drain and gate). The semiconducting material is a blend of P3HT and the coated AuNPs.

Before studying the device performance the adequate NP's concentration in the P3HT-blend had to be adjusted. It was found that the devices incorporating differently coated AuNPs exhibited a gate-effect up to a given threshold concentration (C_{TH}) of the NPs in the blend. Above that concentration the aggregation propensity of the NPs increased, resulting in a decrease in the source-drain current (I_D). This is likely due to the disruption of the conjugation in the π-π-stacked architectures of the P3HT, which largely affects the charge transport. Thus, to allow data comparison for different binary systems, devices were prepared using the highest amount of NPs that, once blended with P3HT, showed a gate response. Consequently, the threshold concentration amounted for the *cis*-**CABP**-AuNP-based device C_{TH} = 18 wt% and only C_{TH} = 1 wt% for the *trans*-form. The high aggregation propensity of the initially *trans*-prepared SAM was already observed and discussed previously.[281] For comparison reasons the same C_{TH} as for the *cis*-**CABP**-AuNP-based device was used for the OPE-AuNP device. The surface morphology of the blend films was visualized by AFM in intermittent contact mode and by Transition Electron Microscopy (TEM) (*Figure 22*). The tendency of the *trans*-**CABP** containing films to form aggregates is clearly shown. Furthermore, similar morphologies were observed for

the *cis*-**CABP** and OPE-based films, which reinforced to use these two systems as comparative models.

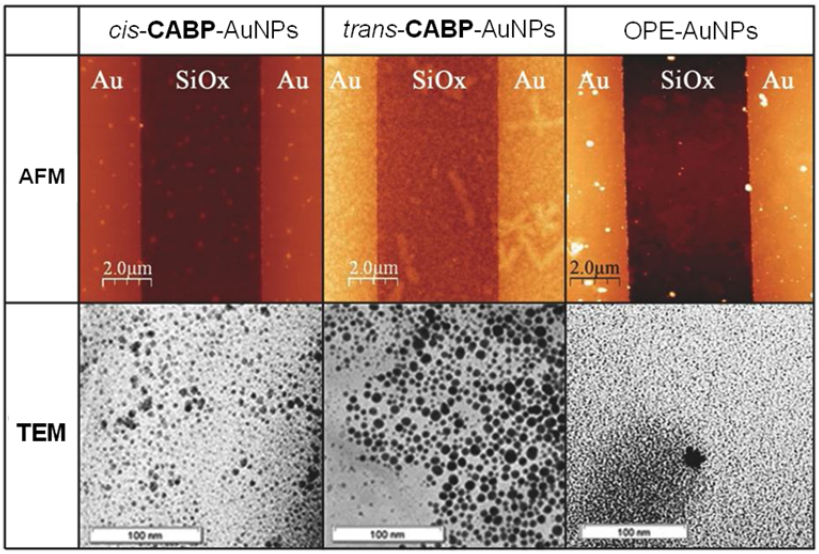

Figure 22. Top: AFM (intermittent contact mode) topographical images of the spin-coated AuNPs/P3HT films on the pre-patterned gold electrodes/SiO_2. Bottom: TEM images of the *cis*-**CABP**-AuNP/P3HT, *trans*-**CABP**-AuNP/P3HT and OPE-AuNP/P3HT blends supported on carbon coated copper grids.

With the now regulated NP's concentration the electrical characterization of the devices (pure P3HT, OPE-AuNP/P3HT, *trans*-**CABP**-AuNP/P3HT and *cis*-**CABP**-AuNP/P3HT) was performed. In *Table 3* a summary of the obtained experimental values of all four devices is given. The strong value discrepancies of the *trans*-based **CABP**-device are explained by the strong aggregation propensities of the resulting NPs. Therefore, in this context this device will not be further discussed in detail.

Table 3. Obtained experimental values of all four FET devices.

		P3HT	**OPE-AuNPs/P3HT**	***trans*-CABP-AuNPs/P3HT**	***cis*-CABP-AuNPs/P3HT**
C_{TH}		/	18%	1%	18%
μ_{mean} [$cm^2 V^{-1} s^{-1}$]		$3.9 \cdot 10^{-3} \pm 1.6 \cdot 10^{-3}$	$9.2 \cdot 10^{-4} \pm 4.8 \cdot 10^{-5}$	$1.2 \cdot 10^{-6} \pm 8.4 \cdot 10^{-7}$	$1.1 \cdot 10^{-3} \pm 9.2 \cdot 10^{-4}$
μ_{max} [$cm^2 V^{-1} s^{-1}$]		$6 \cdot 10^{-3}$	$9.9 \cdot 10^{-4}$	$2.2 \cdot 10^{-6}$	$2.6 \cdot 10^{-3}$
V_{TH} [V]		5.7 ± 4.9	4.1 ± 4.4	-0.1 ± 16.8	-10.0 ± 7.8
Hysteresis [V]	dark	0.4 ± 0.3	1.2 ± 0.5	5.5 ± 4.5	3.4 ± 1.3
	UV	3.6 ± 3.4	10.7 ± 0.8	20.5 ± 9.5	12.2 ± 4.6
	Δ	3.2 ± 3.7	9.5 ± 1.3	15.0 ± 14.0	8.8 ± 5.9
Max number of irradiation cycles		> 25	> 25	3-5	> 25

The incorporation of AuNPs in the film is accompanied by a decrease of the drain currents, including the $I_{D,max}$ measured at the highest V_D and V_G, of up to three orders of magnitude when compared to monocomponent P3HT-based FETs. After irradiation with UV light, the I_D in the *cis*-**CABP**-AuNP/P3HT devices is increased by a factor 7 compared to the OPE-AuNP/P3HT devices. Such high current in the *cis*-**CABP**-AuNP/P3HT devices may be attributed to both the conjugated nature of the SAM and to its reduced thickness,[220] leading to a lower tunneling barrier.[287] *Table* 3 summarizes the average FET parameters extracted for each system before irradiation. The mean charge carrier mobility (μ_{mean}) values are in trend with the morphology of the film, showing the largest μ_{mean} for the bare P3HT and the lowest for the *trans*-**CABP**-AuNPs/P3HT. The *cis*-**CABP**-AuNP/P3HT and OPE-AuNP/P3HT devices revealed similar magnitudes of μ_{mean}.

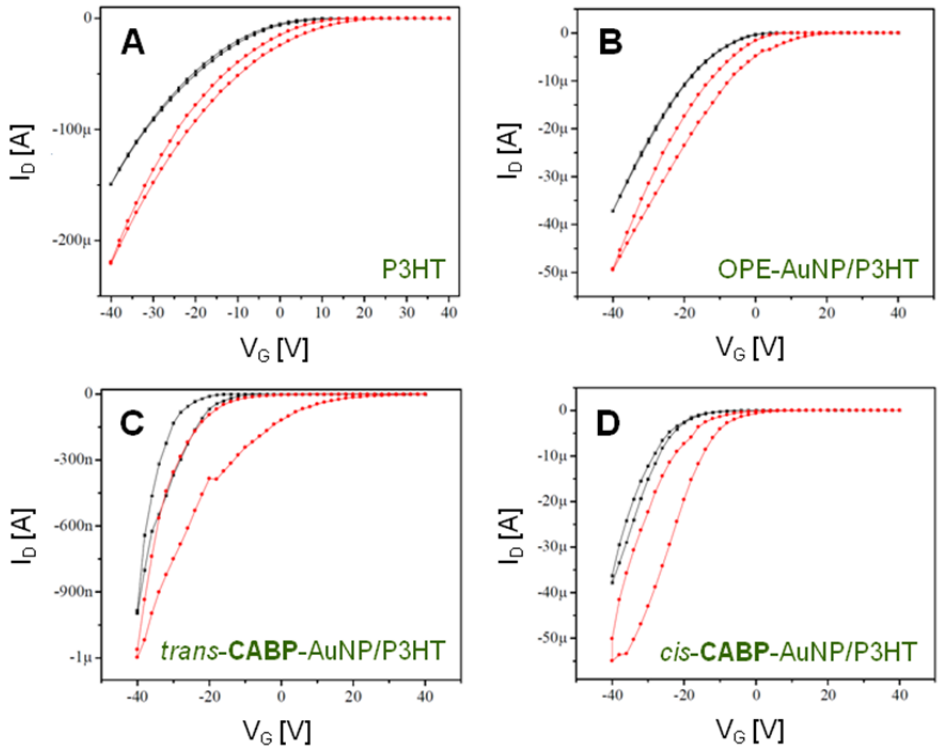

Figure 23. Transfer characteristics (V_D = -30 V) obtained for the four different devices. Black curves: devices in dark. Red curves: devices under UV light (the measurements were recorded after 5 min of irradiation). (A) P3HT, (B) OPE-AuNP/P3HT, (C) *trans*-**CABP**-AuNPs/P3HT, and (D) *cis*-**CABP**-AuNPs/P3HT.

The effect of the different AuNP's coating on the efficiency of charging and releasing is reflected in the observed relative hysteresis as displayed in *Figure 23*. The values of the maximum hysteresis extracted from the difference between the backward and forward transfer curves are reported in *Table 3.* The P3HT device exhibits the lowest hysteresis. The nanoparticles-based devices show higher hysteresis due to their intrinsic charge storage capability and to the inhomogeneous nature of the film. *cis*-**CABP**-AuNPs and OPE-AuNPs showed a similar hysteresis, due to their more homogeneous morphology featuring a reduced aggregation propensity. Among them, the OPE-AuNPs revealed a smaller hysteresis determined by the dodecanethiol's

capacity to disperse well the AuNP in P3HT.[288] In addition, the hydrophobic nature of the alkanethiol SAMs can enhance the crystallinity of the film, which will promote less trapping centers in the P3HT film yielding a lower hysteresis.

The photoswitching capacity and reversible nature of the **CABP**-based devices is illustrated in *Figure 24*. A markedly higher variation was detected for the **CABP**-based device. The observed increase of the $I_{D,UV}/I_{D,dark}$ ratio for the *cis*-**CABP**-AuNPs with time can be attributed to a higher percentage of **CABP** molecules converted to the *cis*-form and a modulation of the device threshold voltage with the UV light.

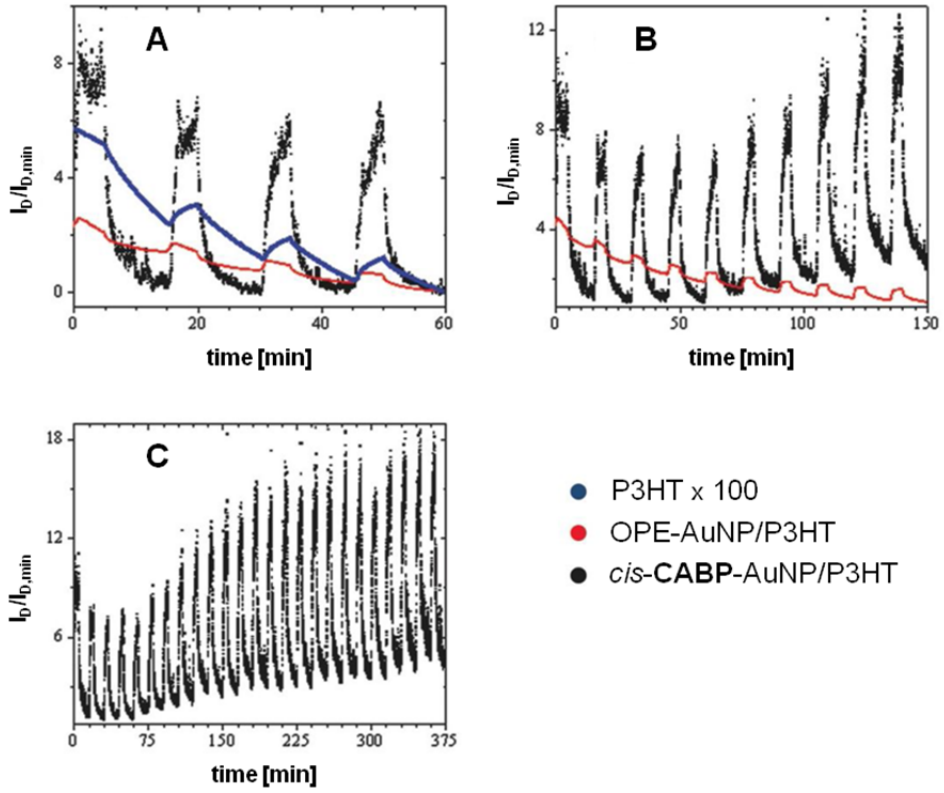

Figure 24. Photoresponsive cycles over time of P3HT (in blue), OPE-AuNPs/P3HT (in red) and *cis*-**CABP**-AuNPs/P3HT (in black). For the P3HT device the $I_D/I_{D,min}$ was multiplied by 100 to allow a better comparison. (A) 4 cycles (B) 10 cycles, and (C) 25 cycles. V_G-V_{TH} = -4 V and V_D = -10 V.

In conclusion, the light-modulation of the current in an OFET based on AuNPs blended with P3HT has been demonstrated to be greatly enhanced when the AuNPs are functionalized with the **CABP**-based SAM. The light-induced isomerization between the *trans*- and *cis*-states of the molecules coating the AuNPs implies a variation of the tunneling barrier (decreasing from *trans*- to *cis*-isomer), which plays a crucial role in the efficiency of the charge trapping/detrapping process within the film. Thus this approach makes it possible to confer a dual functionality to an organic transistor as it provides a means to gate the source-drain current through the channel both electrically (through gate control), as in a conventional transistor, and optically (through

photochemical control). It also represents an innovative approach to digital commuting between optical and electric signals. Finally, such a modulable transistor might be useful for applications in UV sensing.

To summarize, different device setups have been used in order to tap the full potential of the assembled photoresponsive **CABP**. Preliminary investigations on the metal's work function after functionalizing it with the **CABP** were performed. Although the gold's work function was not increased dramatically, it could be demonstrated that upon isomerization of the **CABP** a work function shift occurs. The shift relies on the different tunneling barrier lengths between the two isomeric forms of the azo compound, rather than a contribution of the different dipole moments of the azo structures. Furthermore, the dispersion and precipitation of gold nanoparticles coated with a **CABP** monolayer could be modulated by irradiation of light of different wavelengths. The coating of larger nanoparticles (microspheres) and their incorporation into an electronic device proved anew the capability of the **CABP** to trigger the charge transport through the junction/device upon external stimuli. The **CABP** was also embedded into field-effect transistor devices. One device was based on plane gold source and drain electrodes functionalized with a **CABP**-SAM and another on **CABP**-functionalized gold nanoparticles. With the latter the photoinduced current change was enhanced and the switching fatigue was decreased, compared to the other OFET device. In both OFETs the source-drain current through the channel could be gated electrically and optically. The potential of azobenzene-type structures as reversible photochromic molecular elements could be again amplified.

The next investigation aims are the design, synthesis and surface characterization of novel biphenyl-based azo compounds that are architecturally similar to the **CABP**. This will be reported in the next two sections.

3.2 Structural Modifications of the CABP

Surprisingly, as mentioned in section 1.2.4 , the **CABP** was the first compound to fully switch on surfaces over the whole 2D domain.[218] In order to broaden the scope of such compounds the **CABP** was structurally modified, initiating the investigation of new compounds that will enable a better insight as to what extent the modifications alter the properties of the corresponding SAMs. The following new **AZO** compounds depicted in *Figure 25* have been proposed, where the **CABP** is in terms of structural architecture the "mother compound". Once synthesized, the corresponding assembled structures will be subjected to preliminary investigations considering the structural packing properties, i.e. the crystallinity of the monolayer, and the correlation between the molecule's dipole moment and the metal's work function. The surface

measurements of the three azo compounds depicted below (**AZO 1**, **AZO 2** and **AZO 3**) will be performed in the groups of Prof. Wöll, Prof. Samorì and Prof. Rampi.

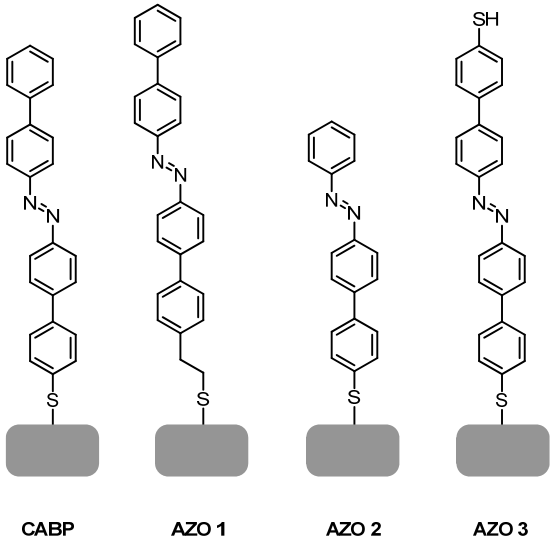

Figure 25. The „classical" azobiphenyl (**CABP**) and new the target structures (**AZO 1** – **AZO 3**).

Azobenzenes linked to a gold surface by an alkanethiol are widely investigated by many different research groups (see section 3). The alkyl chain lengths and the substitution on the azobenzene moiety are often varied. On the other hand, the common structural motif is the single benzene unit on each side of the azo functionality. Most of these corresponding "non-mixed monolayers" show no or low isomerization upon irradiation - as the authors basically claim - due to the steric and tight packing issues. The assembled **CABP** shows a high ratio of reversible switching over the entire surface, even though the SAM packs tightly on Au(111).[218] The reason for this, most probably, arises from the interactions of the two biphenyl moieties with the biphenyls of the adjacent azo compounds. The first envisaged new target compound **AZO 1** (*Figure 25*) should therefore keep the two biphenyls as base structure. Additionally, it should exhibit an alkyl spacer. Here an ethylene spacer is chosen, since oligo phenylenes show the best packing properties with such an alkyl chain length.[289,290] To the best of our knowledge, such structures for surface functionalization with two aromatic units on each side of the azo functionality and alkyl chains as spacers have not been described until now. It is assumed that **AZO 1** will pack more tightly on a Au(111) surface than the **CABP**. Will the neighboring π-π-interactions induce anew a collective switching effect as for the **CABP**?[218]

The investigation of this collective switching effect is also the driving force for the consideration of **AZO 2** (*Figure 25*). The question came up, what would happen if the top aromatic unit of the **CABP** is removed forming a shorter **AZO** compound? The sum of π-π-stacking strength of the adjacent molecules should diminish compared to the **CABP**. But, would then the π-π-stacking still have a strong effect on the switching, also leading to a cooperative effect?

The idea behind **AZO 3** (*Figure 25*) addresses a different issue: In 2007 Schäfer *et al.* demonstrated that the photosimomerization process of individual polymer chains incorporating azobenzenes can perform mechanical work.[291] They repored that the force for each single molecule to express the mechanical work amounts to 10^{-12} Newton. An average of a minimium force of about 10^{-14} Newton of a single biphenly azobenzene is predicted to be needed to lift up a mercury droplet.[82] This indicates that the cargo lifter system of Ferri *et al.* is still far from exploiting its full potential. In order explore the capability of the real power of an azobenzene derivative to express work, a new target structure, **AZO 3**, is proposed. **AZO 3** is functionalized with an additional sulfur group, forming a symmertrical azo compound. If the *cis*-isomer of **AZO 3** is anchored to a gold surface at both ends, is **AZO 3** still able to photoisomerize to the *trans* state (*Scheme 37*)? Are the N=N groups with its neighbouring surroundings able to express a force of 1-2 nN,[37,292] which is needed to release the thiol from the substrate by breaking the Au-S bond?

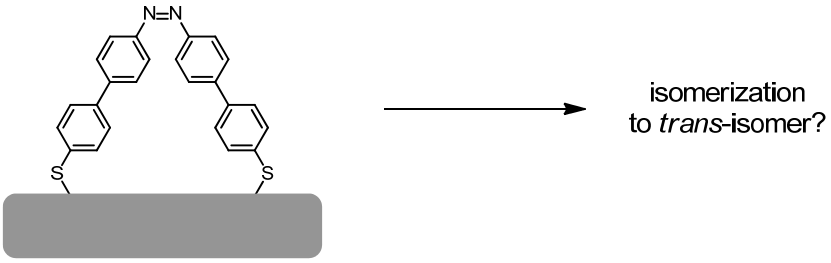

Scheme 37. Assembly of the cis-isomer of **AZO 3** on a gold substrate.

3.2.1 Synthesis and Characterization

The azo precursors (≙ **AZOP**s) for the assembly processes will be delivered as free thiols or as the corresponding acetyl protected forms. In *Figure 26* the targeted **AZOPs** are shown. For all **AZOPs** the synthetic strategy was maintained as for the synthesis of **CABP-SAc** (section 3.1.2). In principle, an unsymmertically *para*-substituted azobenzene is proposed to be the starting point for each synthesis sequence. Due to the asymmetry of the azo building block a selective cross-coupling for the attachment of other arene units in metal mediated cross-coupling reactions is possible. Once all desired building blocks are attached the deprotection or the transprotection of the sulfur finalizes the synthesis of the target structure.

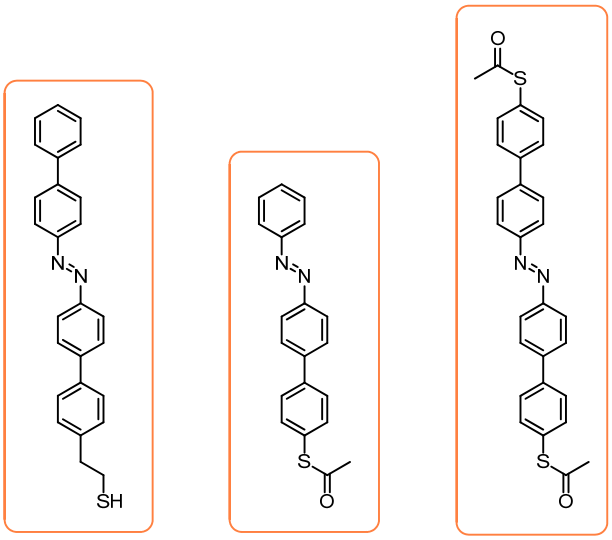

Figure 26. Target structures **AZOP 1**, **AZOP 2** and **AZOP 3.**

The synthesis of **AZOP 1**, **AZOP 2** and **AZOP 3** strongly profits from several building blocks (compounds **10**, **11** and **17**) that were already synthesized for the formation of the **CABP-SAc** (section 3.1.2). As for the synthesis of the **CABP-SAc** the Suzuki-Miyaura cross-coupling reaction was the metal mediated coupling of choice for the carbon-carbon attachment of the aryl units.

*Synthesis of **AZOP 1***

With a modular building block in hand, which was synthesized for the synthesis of the **CABP-SAc** (compound **10**), the reaction sequence to target compound **AZOP 1** was started. The bottom arene unit with a new functional group had to be attached. A sulfur functionality can be introduced via a thiol-ene reaction with an ethene and a radical starter. Therefore, the cross-coupling partner of building block **10** for the Suzuki-Miyaura reaction was the commercially available 4-vinylbenzeneboronic acid (*Scheme 38*). Compound **10** and 1.5 equivalents of 4-vinylbenzeneboronic acid were stirred with potassium carbonate as base, and $Pd(PPh_3)_4$ as catalyst, in an toluene/ethanol mixture at 60 °C for 45 minutes. The desired terminal olefin **20** was obtained after aqueous workup and purification by column chromatography as an orange solid in a yield of 90%. For the following thiol-ene reaction olefin **20** was reacted with 1.5 equivalents of the commercially available 2-trimethylsilylethanethiol in the presence of 0.5 equivalents of the radical starter di-*tert*-butyl peroxide in toluene in a sealed tube. The reaction mixture was heated to reflux in an oil bath over three days. After removal of the solvent and purification of the crude by column chromatography the protected sulfur derivative **21** was obtained as an orange solid in a yield of 54%.

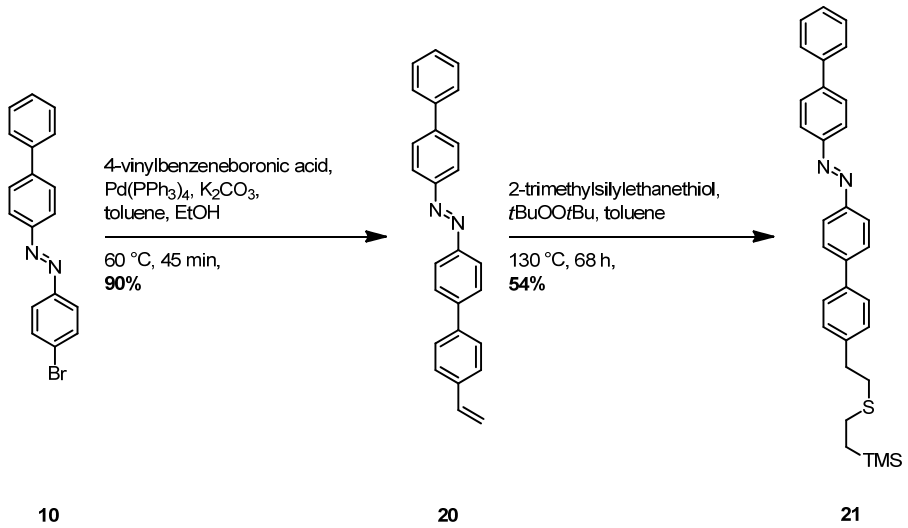

Scheme 38. Synthesis to the ethyl-TMS protected compound **21**.

Since the self-assembly of organosulfur compounds on gold substrates can be accomplished either from the thioacetate or the free thiol, both compound classes were envisaged. Therefore, structure **21** was first converted to the acetyl protected precursor **22** and then to the free thiol **AZOP 1**. Using literature approved reagents,[293,294] the ethyl-TMS protecting group was easily substituted by an acetyl group. Compound **21** was stirred with 3.0 equivalents of silver tetrafluoroborate and with an excess of acetyl chloride (*Scheme 39*) in dichloromethane at room temperature for three hours. The acetyl sulfanyl derivative **22** was obtained after workup and purification by column chromatography to obtain an orange solid in a yield of 80%. Adapting a procedure from Holmes and Snow[295] the thioacetate functionality of compound **22** was deprotected using catalytic amounts of tetrabutylammonium cyanide (TBACN). This method proved to be efficient for a series of aliphatic thioacetates. Target structure **AZOP 1** was successfully synthesized with the above mentioned reagents. Compound **22** was dissolved in dry methanol and dry chloroform and the solution was degassed. After the addition of catalytic amounts of tetrabutylammonium cyanide the reaction mixture was stirred at room temperature for 22 hours. After workup and purification by column chromatography **AZOP 1** was obtained as an orange solid in a yield of 72%.

To summarize, target compound **AZOP 1** was synthesized in seven reaction steps in an overall yield of 21%. The first three steps to compound **10** were already accomplished in the synthesis of the **CABP-SAc** (section 3.1.2), pointing out the advantage of modular building blocks for the preparation of structurally similar azo compounds. Compound **22** and **AZOP 1** were fully characterized by NMR spectroscopy (^{1}H and ^{13}C), EI-MS, EA and UV/Vis spectroscopy.

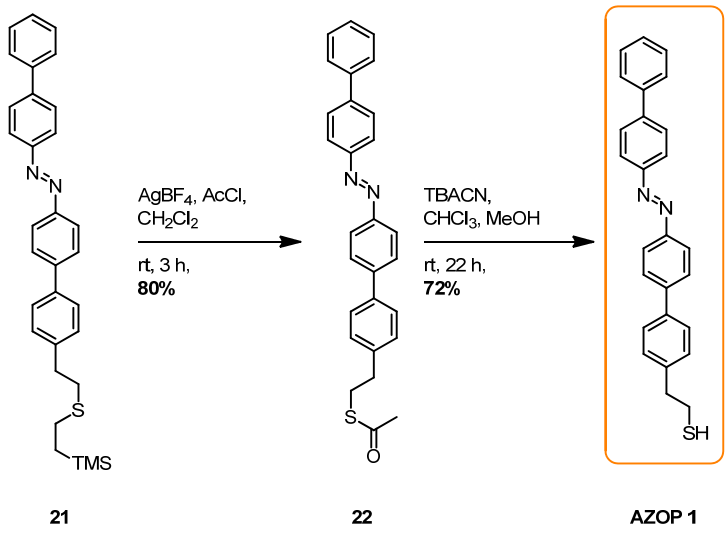

Scheme 39. Last two steps to the synthesis of target structure **AZOP 1**.

*Synthesis of **AZOP 2***

The synthesis to **AZOP 2** began with the oxidation of aniline (**23**) to nitrosobenzene (**24**) with Oxone® in a biphasic solvent mixture of dichloromethane and water (*Scheme 39*). The reaction mixture was stirred at room temperature for 16 hours. After workup the greenish crude **24** was immediately transferred to the next reaction step. Nitrosobenzene **24** was dissolved in acetic acid and then 4-bromoaniline (**14**) was added. After stirring at room temperature for three days the formed azo compound **25** was purified by column chromatography and isolated as an orange solid in a yield of 57% over two steps.

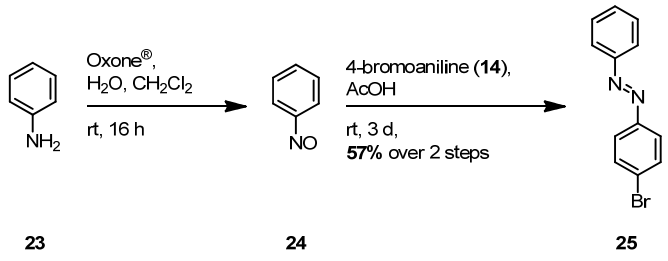

Scheme 40. Two step synthesis to the azobenzene derivative **25**.

In the next two steps the reaction types and reaction conditions, respectively, were adapted as for the **CABP-SAc** synthesis (*Scheme 41*): First, an 1.3-fold excess of the trimer **17** (0.4 equivalents), whose synthesis was reported in section 3.1.2, was coupled with azo compound **25** in a Suzuki-Miyaura reaction leading to intermediate **26**. After workup and purification by column chromatography compound **26** was obtained as an orange solid in a yield of 93%. The ethyl-TMS protection group of **26** was exchanged to the acetyl to afford the target

structure **AZOP 2** after workup and purification by column chromatography as an orange solid in a yield of 50%.

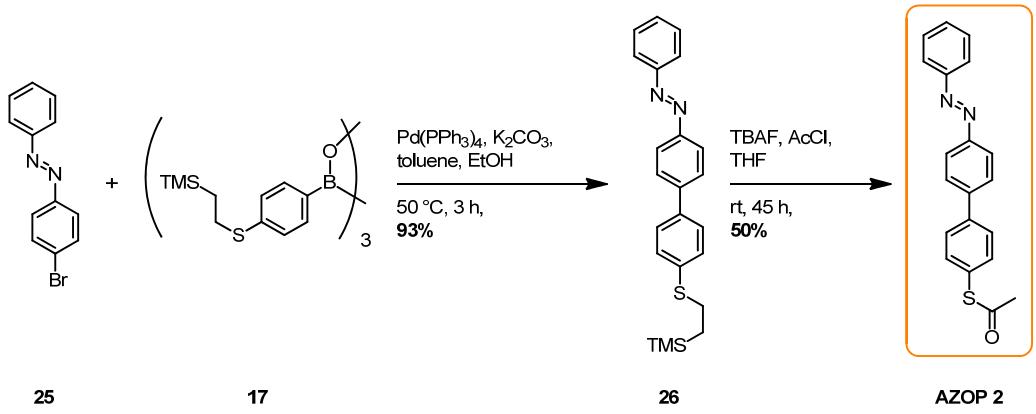

Scheme 41. A Suzuki-Miyaura cross-coupling to azo compound **26** and subsequent transprotection to target structure **AZOP 2**.

Target compound **AZOP 2** was obtained in six steps. Intermediate **17** could be applied for a modular synthetic pathway to **AZOP 2**, as it was already prepared for the synthesis of **CABP-SAc**. **AZOP 2** was characterized by NMR spectroscopy (^{1}H and ^{13}C), EI-MS, EA and UV/Vis spectroscopy. Furthermore, the solid state structure was determined by X-ray crystallography (section 3.2.2).

*Synthesis of **AZOP 3***

With the modular building blocks **11** and **17** in hand the reaction sequence to **AZOP 3** was initiated. The boroxine **17** and the dihalide **11** were reacted in a Suzuki-Miyaura cross-coupling reaction to the bi-substituted azo compound **27** (*Scheme 42*). Compound **11** and 0.8 equivalents of boroxine **17** were stirred with the catalyst $Pd(PPh_3)_4$ and the base potassium carbonate in a toluene/ethanol mixture at 70 °C for 22 hours. After workup and purification by column chromatography the intermediate **27** was obtained as an orange solid in a yield of 72%. Here it was important to raise the reaction temperature above room temperature, which was used previously for selective Suzuki-Miyaura reactions with iodide as leaving group, since the coupling of the boronic derivative **17** had to occur not only at the iodine but also at the bromine position of **11**.

The last step included the transprotection of the sulfur protecting group from the ethyl-TMS to the thiol ester with 20 equivalents of tetrabutylammonium fluoride and an excess of acetyl chloride in tetrahydrofuran. The desired symmetric **AZOP 3** was obtained as an orange solid in a yield of 35% after workup and purification by column chromatography.

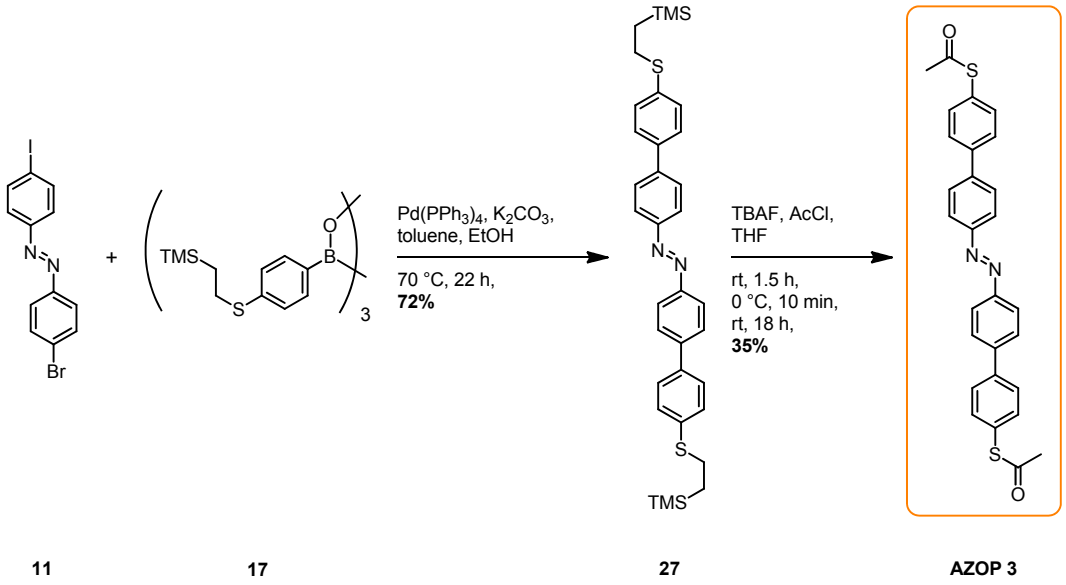

Scheme 42. Synthesis of **AZOP 3**.

To summarize, with building block **11** and **17** in hand only two further reaction steps were necessary to obtain target structure **AZOP 3**. **AZOP 3** was fully characterized by NMR spectroscopy (^{1}H and ^{13}C), EI-MS, EA and UV/Vis spectroscopy.

3.2.2 UV/Vis, ^{1}H-NMR and X-Ray Analyses

UV/Vis measurements of the target compounds **22**, **AZOP 1**, **AZOP 2** and **AZOP 3** were performed, showing the time dependent photoisomerization process of the azo compounds in solution. Furthermore, the four compounds were analyzed by ^{1}H-NMR spectroscopy before and after irradiation at 365 nm and subsequently the *trans*/*cis* amounts were calculated. For **AZOP 2** the solid state structure could be measured by X-ray analysis.

UV/Vis Spectroscopy

Azo compound **22**, **AZOP 1**, **AZOP 2** and **AZOP 3** were analyzed by UV/Vis spectroscopy. The UV/Vis spectra for these azo compounds are shown below (*Figure 27A-D*). The azo compounds were prepared as a 10^{-5} molar solution in chloroform. The two characteristic bands of the azo compounds are observable. The bands at around 350 nm are attributed to the π-π*-transition and the weak bands (see zoom in) at around 450 nm to the n-π*-transition. By irradiating the initially prepared *trans*-form samples at 366 nm, which is the region of high absorption of the *trans*-isomer, the isomerization process towards the *cis*-isomer is initiated. A decrease of the

π-π*-transition band and an increase of the n-π*-transition band is observed with irradiation time. After around 30 to 45 minutes no significant change was observed anymore, so that the photostationary state was about to be reached.

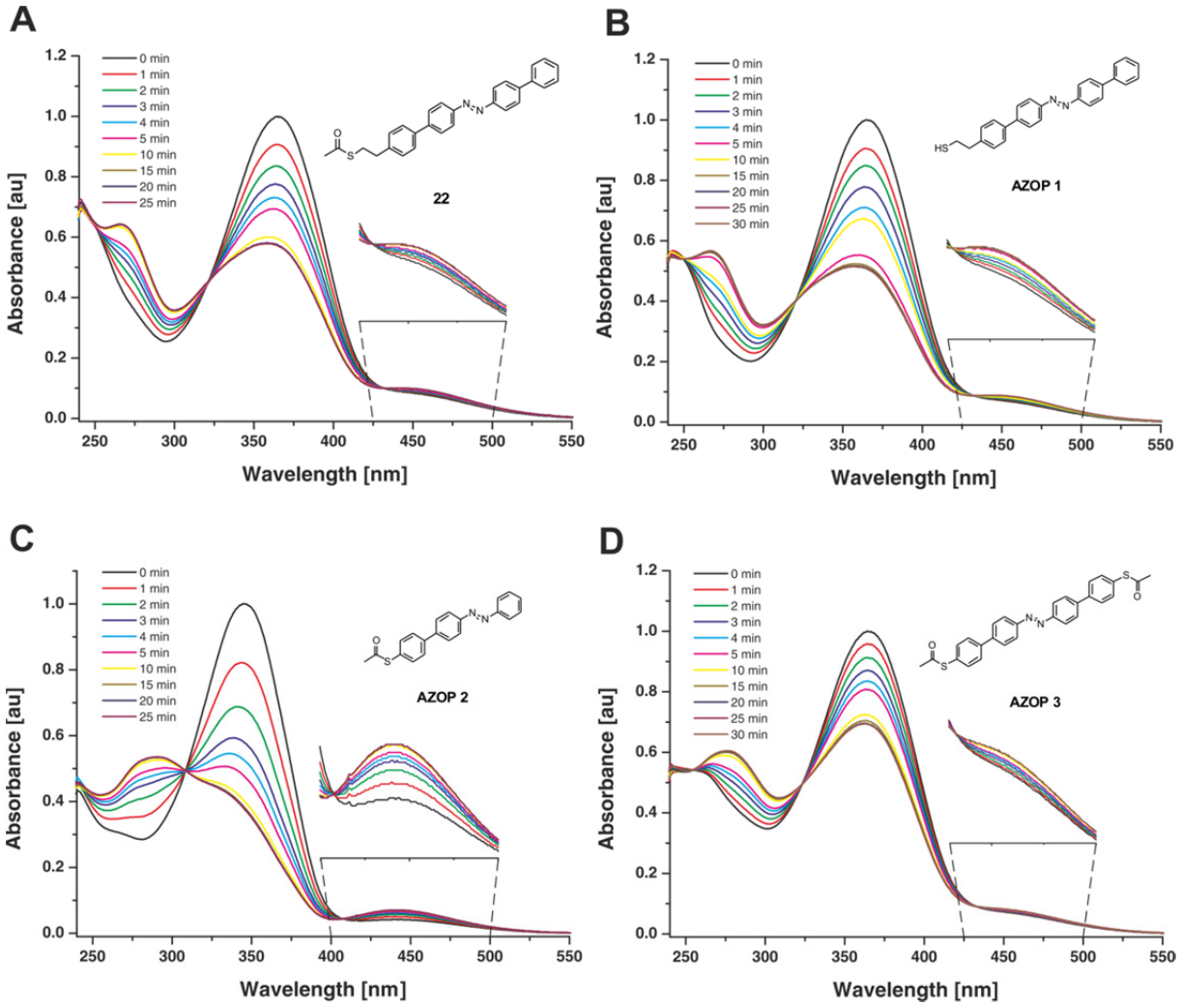

Figure 27. (A)-(D): Time dependent photoinduced *trans* → *cis* switching experiments of **22**, **AZOP 1**, **AZOP 2** and **AZOP 3**, which are recorded by UV/Vis spectroscopy. Irradiation wavelength: 366 nm; solvent: chloroform; lamp power: 8 Watt.

[1]H-NMR Spectroscopy

The *trans* to *cis* photoisomerization of compound **22**, **AZOP 1**, **AZOP 2** and **AZOP 3** were monitored by ^{1}H-NMR spectroscopy. The freshly prepared samples in CD_2Cl_2 (without exclusion of day light) were measured after about 5 minutes. The ^{1}H-NMR spectra are shown in green (*Scheme 43* and *Scheme 44*). Each sample was then irradiated at 365 nm for 45 minutes and afterwards directly measured. The spectra after irradiation are shown in red. The green spectra correspond to the initial state, where about 96% of the *trans*-isomer and 4% of the *cis*-isomer

are observed in each spectrum before irradiation. After irradiation **22**, **AZOP 1**, **AZOP 2** and **AZOP 3** exhibit 64%, 87%, 54% and 79% of the *cis*-isomer, respectively. These results were calculated by means of the integrals of clearly defined peaks. The chosen peaks are marked with the colored dots. For azo compounds **22**, **AZOP 2** and **AZOP 3** the protons of the methyl groups of the structures were chosen as reference and for **AZOP 1** the protons of the methylene group next to the aryl unit.

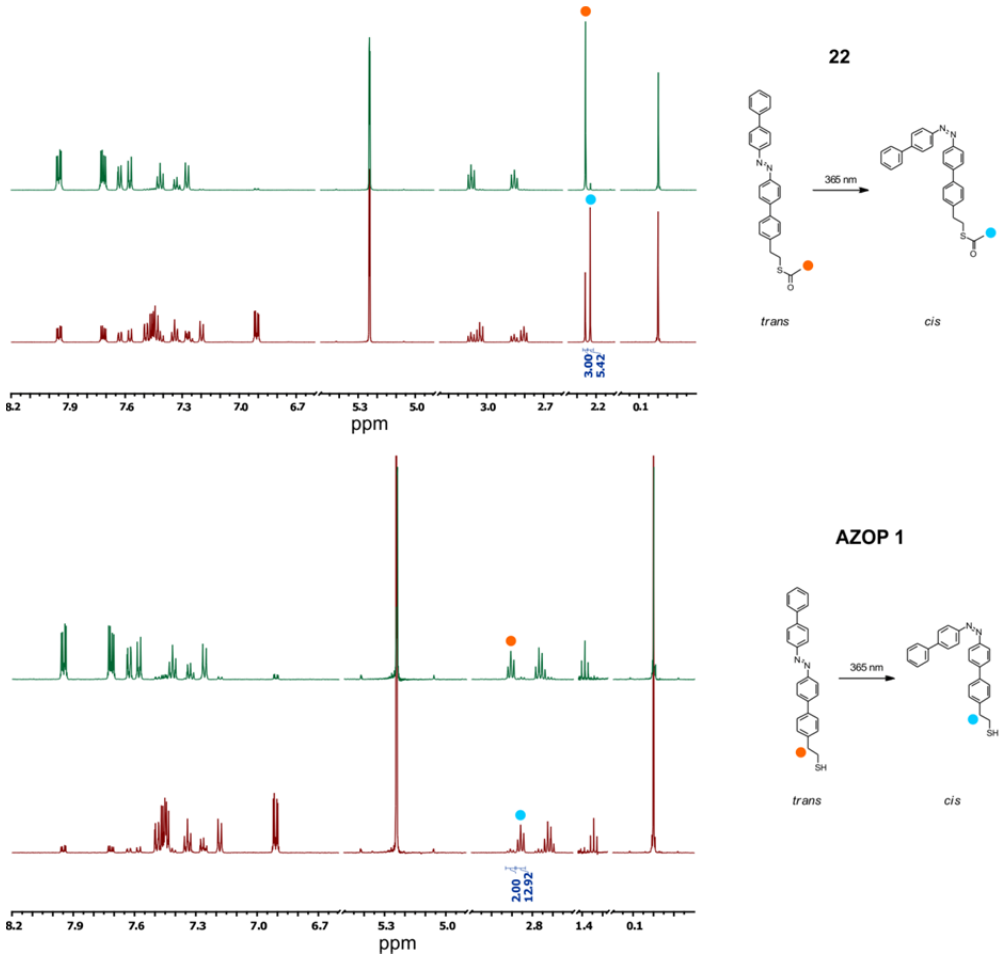

Scheme 43. ^{1}H-NMR spectra of azo compound **22** and **AZOP 1** in CD_2Cl_2 recorded on a 500 MHz instrument. Green spectra correspond to freshly prepared samples (predominantly the *trans*-isomer is observed). The red spectra correspond to the samples measured after 45 minutes irradiation at 365 nm. Each green spectrum is compared to the corresponding red spectrum to demonstrate the increasing amount of the *cis*-isomer after irradiation. The colored dots indicate the peaks used for the assignment of the amount of *cis*-isomer. The peaks at 5.24 ppm and 0.00 ppm correspond to the solvent CD_2Cl_2 and the reference tetramethylsilane, respectively. The power of the lamp was 8 Watt.

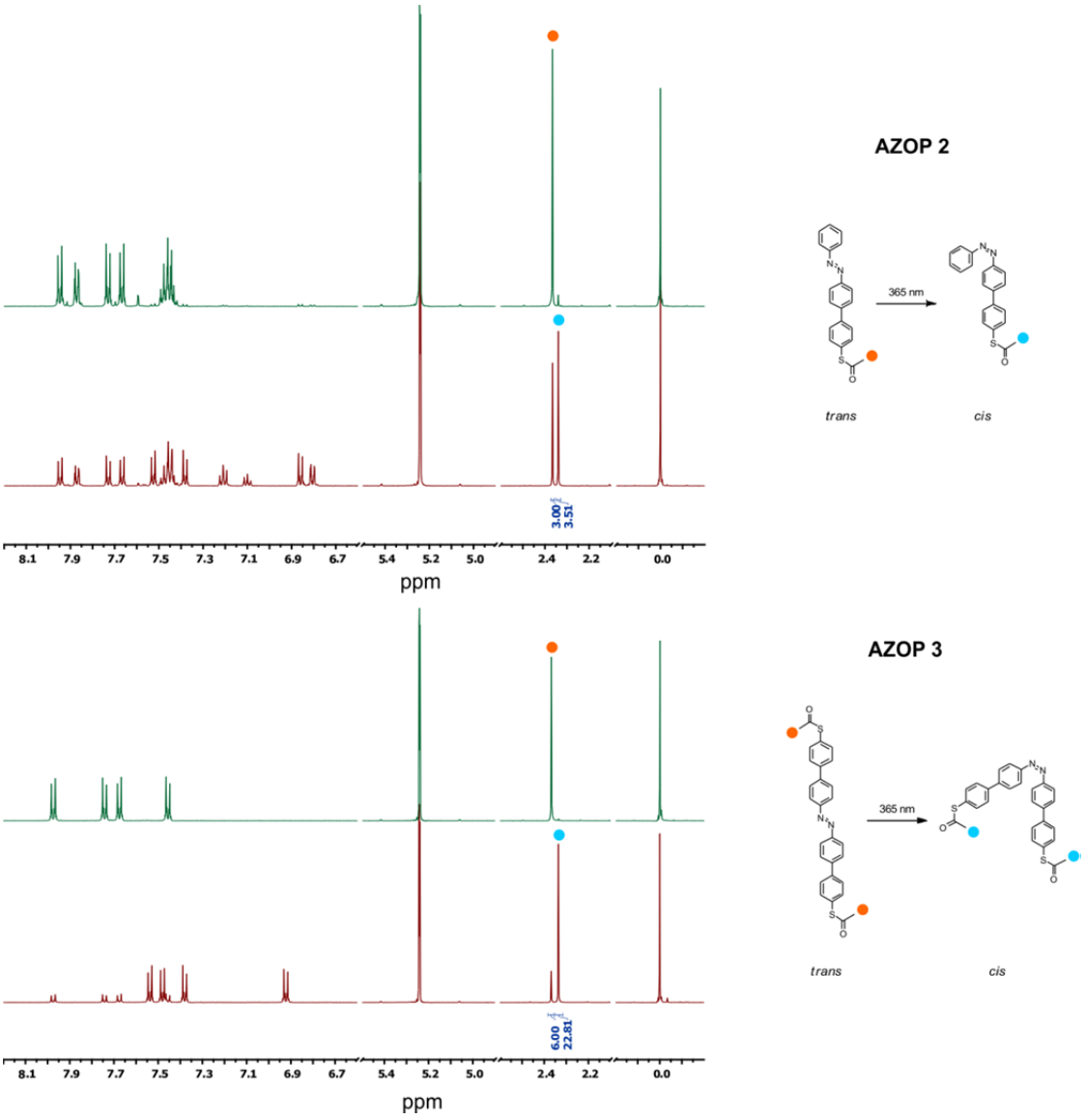

Scheme 44. ^{1}H-NMR spectra of azo compound **AZOP 2** and **AZOP 3** in CD_2Cl_2 recorded on a 500 MHz instrument. Green spectra correspond to freshly prepared samples (predominantly the *trans*-isomer is observed). The red spectra correspond to the samples measured after 45 minutes irradiation at 365 nm. Each green spectrum is compared to the corresponding red spectrum to demonstrate the increasing amount of the *cis*-isomer after irradiation. The colored dots indicate the peaks used for the assignment of the amount of *cis*-isomer. The peaks at 5.24 ppm and 0.00 ppm correspond to the solvent CD_2Cl_2 and the reference tetramethylsilane, respectively. The power of the lamp was 8 Watt.

*Solid State Structure of **AZOP 2***

Single crystals suitable for X-ray analysis were obtained for **AZOP 2** in its *trans*-form by slow evaporation of a saturated chloroform solution. In *Figure 28* several perspectives of the structures are shown. Noteworthy is the almost completely planar arrangement of the conjugated π-system. The azo functionality lies also in the plane. The acetyl group is the only moiety which is out of plane. As visualized on the right hand side in *Figure 28A*, the structures

are aligned in a herringbone fashion. In *Figure 28B* the distances of the arene centers of the neighboring molecules are shown in red. The marked distances have a length of about 4.85 Å, which is a value that is comparable to an optimized calculated value in the literature (4.96 Å) for a T-shaped arrangement of two arenes.[296] In the case of **AZOP 2**, the black colored hydrogen bonds point towards the ring centers of the adjacent molecules, although here they are not perpendicular as in the calculated model. The lengths depicted in red support the consideration that the structures are stabilized by arene-arene-T-shaped interaction, which would explain the moderate solubility of the compound in solution.

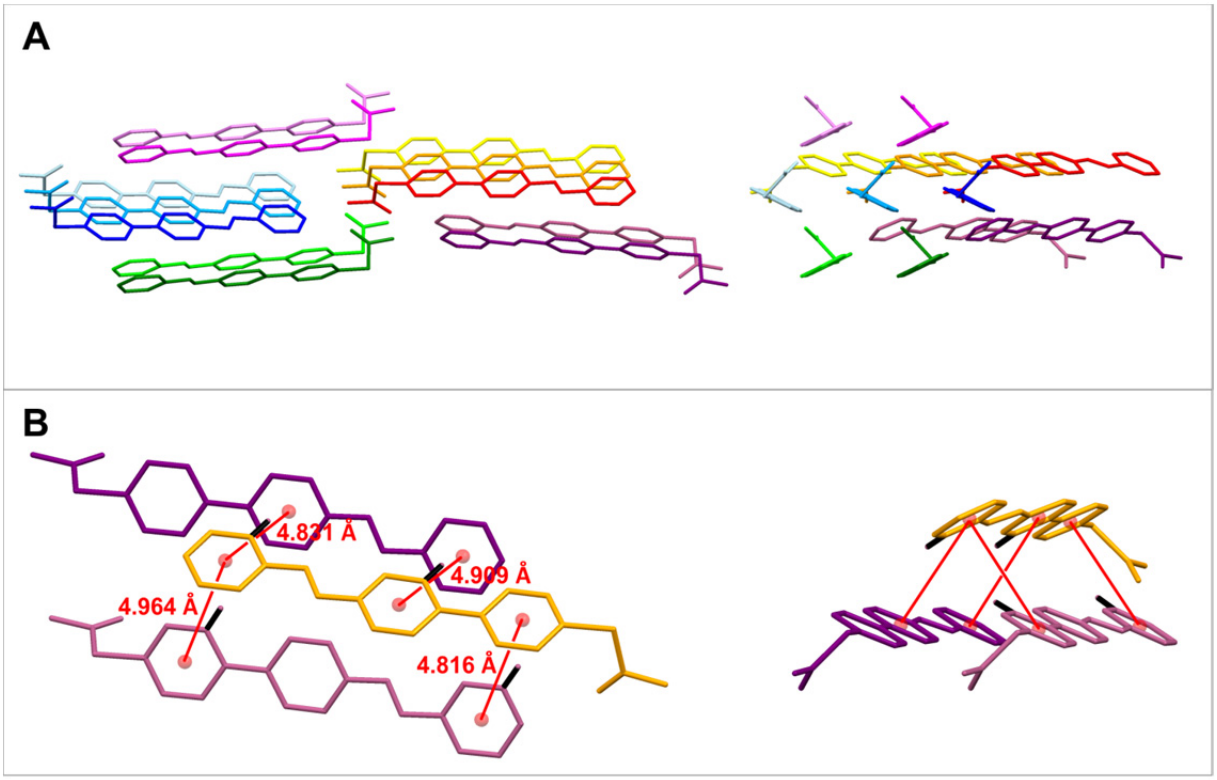

Figure 28. Solid state structure of the *trans*-**AZOP 2** in several perspectives. (A) The packing alignment. (B) Visualization of the almost T-shaped arrangement of adjacent phenylene units.

3.3 Fluoroarene-, Thiophene- and Pyridine-Based Azo Compounds

In order to enlarge the scope of thiol functionalized azobenzenes on gold substrates several other structures are proposed, i.e. two fluorinated azo structures, a bithiophene- and a pyridine-based azo compound (*Figure 29*). Here the investigations on the molecules' dipole moments and thus their correlation with the metal's work function are envisaged. Furthermore, similar structural elements as commonly used in organic semiconductors are incorporated into the azo molecules. This is for the enhanced charge communication at the interfaces in, for example, organic field-effect transistors. The characterization of the inter- and intramolecular interactions of the packed structures in the monolayer are also of interest for the novel azo compounds, especially the influence of these interactions on the crystallinity of the corresponding monolayer. With the corresponding SAMs it is expected to obtain a better insight to what extent the structural modifications of the azo compounds alter the switching behavior of the assembled azo compounds and the charge transport through the SAMs and the devices, respectively.

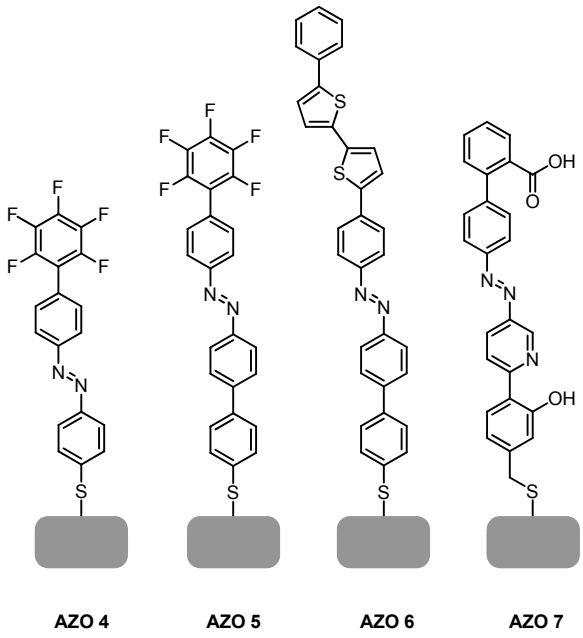

Figure 29. Envisaged architectures for the investigation of the corresponding SAMs.

The idea to incorporate fluorinated benzene units (**AZO 4** and **AZO 5**) originates from the fact that alternating fluorinated and non-fluorinated benzene moieties like to stack with each other.[297,298] This effect is nicely observable to the naked eye: When benzene is mixed with hexafluorobenzene in equimolar quantities a solid of the two components is formed. Benzene (BZ) and hexafluorobenzene (FBZ) have similar melting points (5.4 °C and 5.0 °C, respectively), while the formed "complex" has a melting point of 23.7 °C. The considerable increase of the melting point of the 1:1 solid mixture, compared with those of the pure components, is due to a favorable electrostatic interaction. X-ray and neutron diffraction analysis of the "complex"

demonstrated that the molecules are stacked in columns of alternating BZ and FBZ, whose molecular planes lie parallel to each other.[299,300] In contrast, the crystals of neat BZ and neat FBZ have herringbone structures.[301,302] The sandwich like stacking of the 1:1 solid mixture of BZ and FBZ arises from a quadrupole-quadrupole interaction.[296,303,304] The quadrupole moments of BZ and FBZ are nearly equal in magnitude but opposite in sign. In 2005 Tsuzuki *et al.* reported on ab initio calculations of the intermolecular interaction between BZ and FBZ.[305] They claim that dispersion is also an important factor for the attraction of these two liquids. As depicted in *Figure 30*, the intermolecular distances and the interaction complexes are estimated. The sandwiched and slipped models – both have a parallel character – suggest higher interaction energies, compared to the two T-shaped structures. The electrostatic interaction destabilizes the T-shaped FBZ-BZ complex, whereas the dispersion interaction enhances the relative stability of the slipped-parallel hexafluorobenzene-benzene complex, which is the reason for the slight higher stabilization energy, compared to the sandwich-parallel model. The authors conclude that both electrostatic and dispersion interactions stabilize the slipped-parallel hexafluorobenzene-benzene complexes.

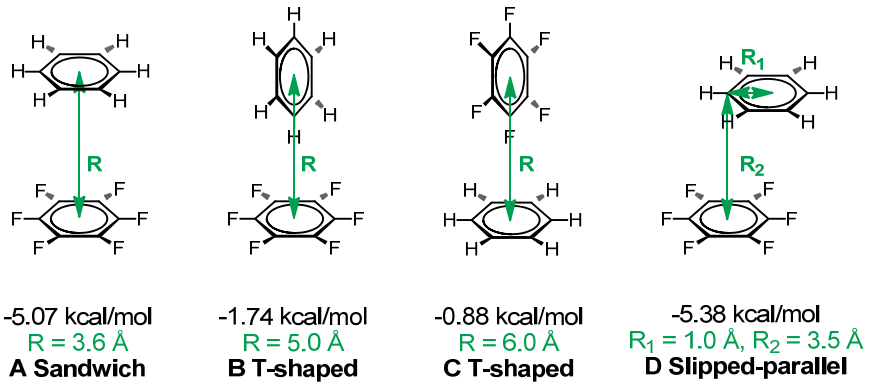

Figure 30. Schematic representation of the computed structures of the hexafluorobenzene-benzene complexes.[305] The ab initio calculation values of the intermolecular distances in complexes A-C and horizontal and vertical displacements in complex D at the potential minima are shown. The estimated interaction energies of the complexes are also depicted.

As already mentioned, the high affinity of electron rich and electron poor aromatic units is obvious.[304] Thus we would like to incorporate this affinity in our studies of the switching mechanism and strength of azobenzene units. **AZO 4** has a fluorinated top arene unit and a single aromatic unit at the other side of the azo functionality (*Figure 29*). Here the question appears, whether the corresponding SAM is able to reversibly switch back to the *trans* isomerisation state or are the interactions between the fluorinated unit and the benzene unit of the adjacent packed molecule in the *cis*-state too strong to allow the back switching? And what differences can be observed if **AZO 4** is elongated by one arene unit, resulting in a fluorinated azobiphenyl? This gives the second fluorinated target structure (**AZO 5**). A further idea to

incorporate a fluorinated arene unit at the tail of the azo structure relies on the effect that fluorinated compounds generally cause an increase on the metal's work function when they form a monolayer on the metal.[53,306] For example, the charge injection into the organic semiconductor from the source-drain electrodes could be improved by the use of a pentafluorobenzenethiol-SAM, as the metal's work function was considerably modified.[306] The combination of a fluorinated unit and a switchable azobenzene into one structure (**AZO 4** and **AZO 5**) is therefore interesting. It is expected that the work function of the functionalized metal can be tuned upon irradiation. If an isomerization process occurs, then the different molecular dipole moments of the isomers can induce a work function change.

Nano-junctions based on azobenzenes that exhibit conductance switching via *cis* ⇄ *trans* photoisomerization have been published.[82,201,207,220,275,278,284] Mativetsky *et al*. reported on a conductance change upon configurational change of the **CABP**, which was demonstrated by cAFM.[220] The measured conductance switch was attributed to a change in height of the azo-based SAM during isomerization rather than to an intrinsic conductance switching.[82,96,220] An intrinsic conductance would arise from the change in the electronic structure of the molecular junction that leads to a modification of the resistance. Recently, it has been reported on an azobenzene-bithiophene-based SAM, showing a high on/off conductance switching ratio.[307,308] The structure of this compound is shown in *Figure 31*. The authors propose that this high photoinduced on/off ratio is a synergistic result of SAM thickness variation and modification of the energy offset between the LUMO and the electrode Fermi energy.[308] The latter is attributed to the thiophene moiety, as thiophene building blocks possess remarkable electronic properties.[309–312] Furthermore, thiophenes have well-defined molecular structures, which lead to their synthetic reproducibility.[311] Due to the mentioned properties of thiophenes we suggested to incorporate a bithiophene unit to the **CABP** (**AZO 6**). The comparison of the corresponding SAM with the neat **CABP**-SAM and their conductance switch, respectively, is of interest. If the new structure **AZO 6** exhibits improved electronic properties its incorporation in an OFET, as was done for the **CABP**,[278] is also suggested. As common organic semiconductors comprise thiophene moieties the structural similarity of **AZO 6** will help to improve the charge mobility through the interfaces and thus through the device when **AZO 6** and the semiconductor are brought in contact to each other.

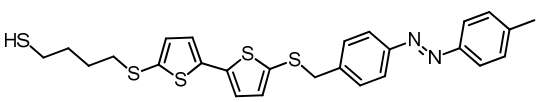

Figure 31. Azobenzene-bithiophene based structure that shows a high on/off conductance switching ratio once assembled on a gold substrate.[307,308]

Intermolecular interactions between adjacent molecules chemisorbed on surfaces are known to stabilize the monolayer's structure and influence the packing density. A widely investigated system is the functionalization of alkanethiols on gold surfaces, where *van der Waals* interactions of the aliphatic chains affect the packing density and stability of the monolayer.[27] Beside *van der Waals* interactions also hydrogen bonding interactions affect the crystallinity of the SAM.[313–318] Numerous studies in the literature are known, where this binding motif is exploited. Exemplarily, the incorporation of hydrogen bond acceptors and donors was used to increase the thermal stability of a monolayer.[319] The lateral hydrogen bonding of an amide group in the vicinity of a terminal hydroxyl group retains a higher degree of order of the SAM within a broader range of temperatures compared to non-hydrogen bonded analogues. Furthermore, it was reported on the phase separation of a SAM from a binary mixture of adsorbates.[320] One adsorbate was a *n*-dodecanethiol and the other an amide-containing alkanethiol of similar chain length. The introduction of a hydrogen-bonding functionality induced the formation of single-component domains, i.e. *n*-dodecanethiol domains separated from the amide-derivative domains. This is a further evidence for the capability of intermolecular hydrogen bond interactions to influence the patterning and structure of thin films. Besides intermolecular hydrogen bonding interactions, intramolecular effects can occur. Bandrara *et al.* reported on azobenzene derivatives that increase a barrier to photoisomerization, due to strong intramolecular hydrogen bonds (*Scheme 45*).[321] Theoretical calculations demonstrate that these hydrogen bonds prevent isomerization, which experimentally was confirmed by the elimination of these hydrogen bonds by changing the substituents. However, these isomerization experiments were performed in solution. To the best of our knowledge no attempts of isomerization inhibition on azobenzene containing SAMs have been introduced in literature. Therefore, we would like to investigate the isomerization effects on a tailor-made azo structure.

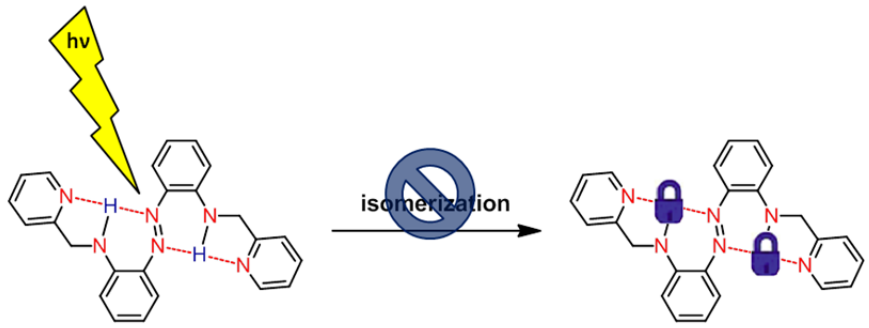

Scheme 45. Mechanism studies of the photoisomerization of an azo compound in solution.[321]

The new target structure **AZO 7** consists of a biphenyl system on one side of the azo functionality and on the other side a phenylpyridine moiety. As shown in *Scheme 46*, the pyridine unit may enforce intramolecular hydrogen bonding in the *cis* conformational state with

the carboxylic and alcoholic substituents. To what extent the stabilization of the *cis*-state influences the packing properties of the monolayer, is of interest here. Furthermore, the question arises whether the formed hydrogen bonds prevent the back isomerization to the *trans*-state.

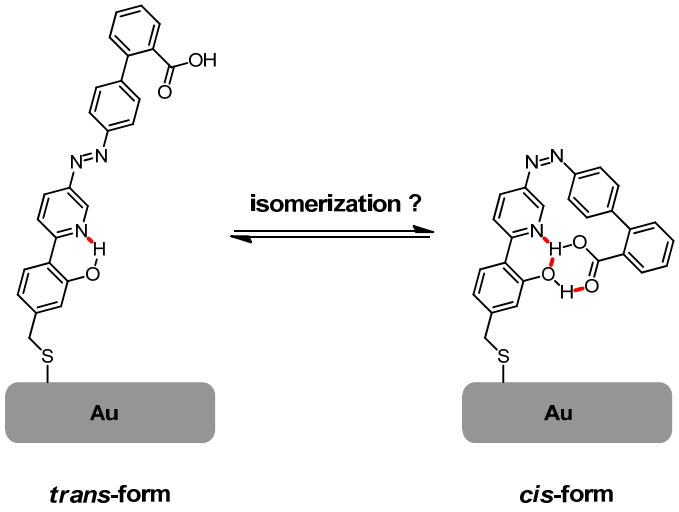

Scheme 46. Probable locking of the *cis*-isomer due to the intramolecular hydrogen bonds of **AZO 7**.

3.3.1 Synthesis and Characterization

As for **AZO 1-3**, the starting materials for the assembly process of the azo compounds will be delivered as free thiols or as the corresponding acetyl protected forms (**AZOP**s) as shown in *Figure 32*.

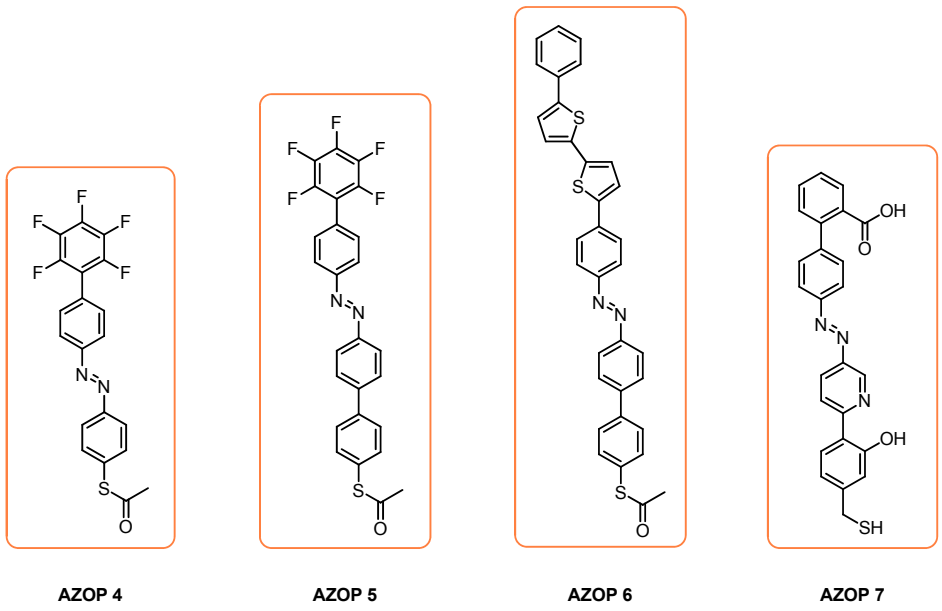

Figure 32. Target structures **AZOP 4**, **AZOP 5**, **AZOP 6** and **AZOP 7.**

*Synthesis of **AZOP 4***

Apart from the fluorinated arene unit in **AZOP 4** the most important structural difference, compared to the other **AZOP**s reported till now in this work, is that the "linker" between the sulfur and the azo functionality is shortened by one aromatic unit. This means – if keeping the synthetic strategy as described above (section 3.1.1) – that the nitroso supply for the Mills reaction inevitably has to come from the unit that does not contain the sulfur functionality (*Scheme 47*). During the oxidation of an amine to the corresponding nitroso a functionalized sulfur would be oxidized, too. Therefore, the organosulfur unit **29** should bear the amine for the subsequent Mills condensation to the corresponding azo compound **28** (*Scheme 47*).

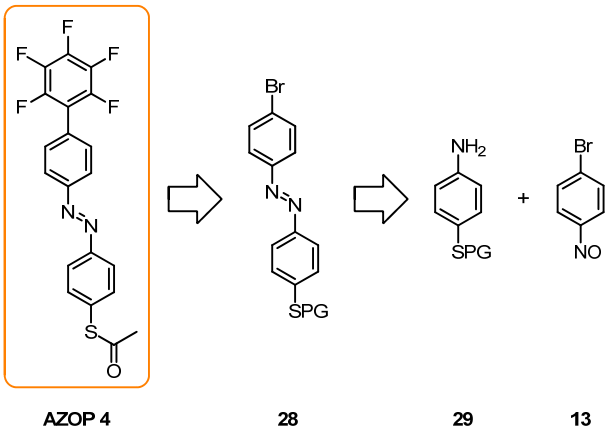

Scheme 47. Retrosynthetic analysis to target compound **AZOP 4**.

The two steps sequence to the sulfur-based aniline **29** was started with the already available (section 3.1.2) bromide **16**. The transformation of an organic halide to the corresponding amine is often accomplished in the lab via a Gabriel reaction with the help of potassium phthalimide. Usually potassium phthalimide is *N*-alkylated with a primary alkyl halide to give the corresponding *N*-alkylphthalimide, but the reaction with aryl halides takes place with difficulty.[322] The presence of copper(I) salts accelerates the reaction with aryl halides.[323,324] A procedure of Sato *et al.*, where halobenzenes were condensed with phthalimide in the presence of copper(I) oxide to give the corresponding *N*-substituted phthalimide, was adapted.[324] This first reaction sequence of the Gabriel reaction, which was performed in 2,4,6-collidine with compound **16**, 1.2 equivalents of phthalimide and 0.6 equivalents of copper(I) oxide at 170 °C for 30 hours, gave the desired intermediate **30** (*Scheme 48*). After workup and purification by column chromatography compound **30** was obtained as a yellowish solid in a yield of 77%. The second step of the Gabriel synthesis is the hydrolysis with hydrazine monohydrate. When using hydrazine for the liberation of the amine the method is called the Ing-Manske procedure.[325] This reaction was performed in a dichloromethane/tetrahydrofuran/methanol solvent mixture with 10 equivalents of hydrazine monohydrate. After 30 minutes of stirring at 50 °C, workup and

purification by column chromatography the corresponding aniline **31** was obtained quantitatively as a colorless liquid. Aniline **31** was then condensed with 1-bromo-4-nitrosobenzene (**13**) in acetic acid to the corresponding azo compound **32**. After workup and purification by column chromatography compound **32** was isolated as an orange solid in a yield of 40%.

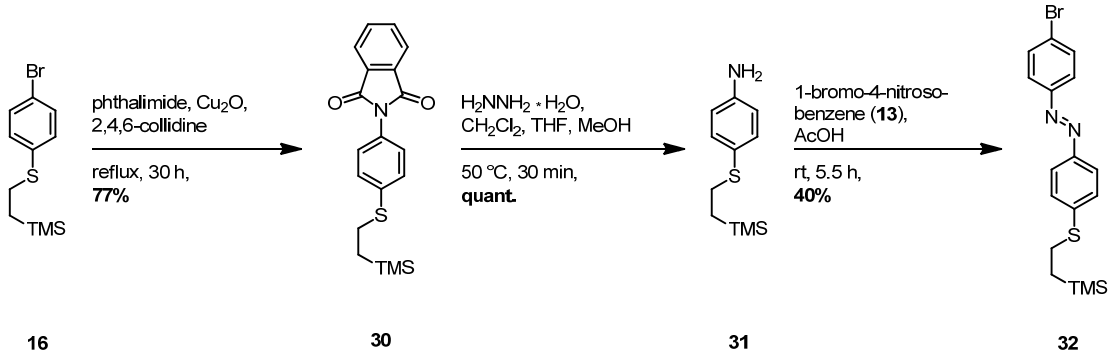

Scheme 48. Synthesis to azo intermediate **32**.

The coupling of azo compound **32** with pentafluorophenylboronic acid was the next envisaged step. The commonly applied reagents and solvent mixture ($Pd(PPh_3)_4$, potassium carbonate, toluene/ethanol) and conditions for the Suzuki-Miyaura cross-coupling reaction proved not to be adequate for the coupling of pentafluorophenylboronic acid (**34**) with compound **32** (*Scheme 49*). This is most probably due to the strong electronegativity of the fluorine atoms on the arene unit, which make the boronic acid an inactive substrate under usual reaction conditions.[326,327] The transmetalation of the highly electron deficient C_6F_5-group to the palladium center proceeds only with difficulty. Korenaga *et al.* optimized the conditions, so that pentafluorophenylboronic acid (**34**) was no longer an inactive substrate for the Suzuki-Miyaura cross-coupling reaction.[328] The usage of tris(dibenzylideneacetone)dipalladium ($Pd_2(dba)_3$), tri-*tert*-butylphosphine ($P(t\text{-}Bu)_3$), cesium fluoride and silver oxide in *N*,*N*-dimethylformamide showed the best results for reactions of aryl bromides and pentafluorophenylboronic acid (**34**). Especially the combination of cesium fluoride and silver oxide was essential for promoting these reactions, since it is considered to accelerate the transmetalation step. Under these conditions it was proposed to react compound **32** with pentafluorophenylboronic acid (**34**), but unfortunately the desired coupling product **33** was not observed (*Scheme 49*). Here the fluoride source from cesium fluoride, most probably, deprotected the sulfur making it a thiolate, which consequently is able to undergo nucleophilic aromatic substitutions on the fluorinated arene unit.[329]

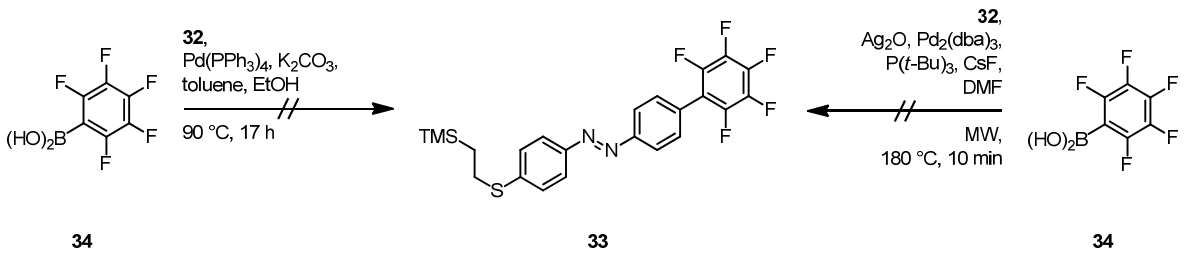

Scheme 49. Attempts of a Suzuki-Miyaura cross-coupling of pentafluorophenylboronic acid (**34**) with the halide **32**.

In order to avoid the cleavage of the ethyl-TMS group under the conditions adapted from Korenaga *et al.,* the sulfur protecting group was replaced with the fluoride stable *tert*-butyl group. This had the consequence that the *tert*-butyl derivative of **32** had to be synthesized first. The synthetic strategy was kept as before for that of compound **32**. 1-Fluoro-4-nitrobenzene (**35**) was the starting point to the *tert*-butyl intermediate **38** (*Scheme 50*). Following a procedure of Błaszczyk *et al.*[330] the sulfur group was introduced via a nucleophilic aromatic substitution with sodium *tert*-butyl sulfide. Compound **35** and 1.7 equivalents of sodium *tert*-butyl sulfide were stirred in *N,N*-dimethylformamide at room temperature for two hours and after workup and purification by column chromatography *tert*-butyl(4-nitrophenyl)sulfane (**36**) was obtained as an orange solid in a yield of 93%. In the second step the nitro functionality was reduced to the corresponding amine **37** with hydrochloric acid and tin powder. After workup and purification by column chromatography aniline **37** was obtained as a yellowish solid in a yield of 83%. Nitroso **13** and aniline **37** underwent a condensation reaction (Mills reaction) in acetic acid at room temperature. After workup and purification by column chromatography the desired *tert*-butyl azo intermediate **38** was obtained in a yield of 40%.

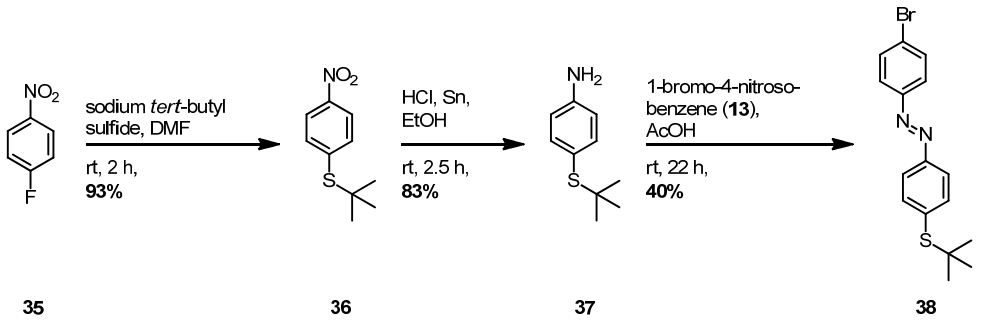

Scheme 50. Synthesis to the *tert*-butyl-based azo intermediate **49**.

Now the Suzuki-Miyaura cross-coupling reaction with 1.1 equivalents of pentafluorophenyl-boronic acid (**34**) in the presence of cesium fluoride as base was performed with the *tert*-butyl protected azo derivative **38** (*Scheme 51*). A satisfying yield of 74% of the desired coupling product **39** (orange solid) was obtained after workup and purification by column

chromatography, showing the effectiveness of the catalyst/base system reported by Korenaga *et al.*. In contrast to the procedure of Korenaga *et al.*, where conventional heating was applied, we performed the reaction under microwave irradiation (10 min), which improved the time efficiency. The final step to the target compound **AZOP 4** was the transprotection of the *tert*-butyl to the acetyl group. The procedure was adapted from Stuhr-Hansen,[331] which comprises the usage of boron tribromide in the presence of an excess of acetyl chloride in toluene. Compound **39** and an excess of acetyl chloride were dissolved in toluene and then 2.0 equivalents of boron tribromide were added dropwise. After stirring at room temperature for three hours, workup and purification by column chromatography, **AZOP 4** was obtained as an orange solid in a yield of 42%.

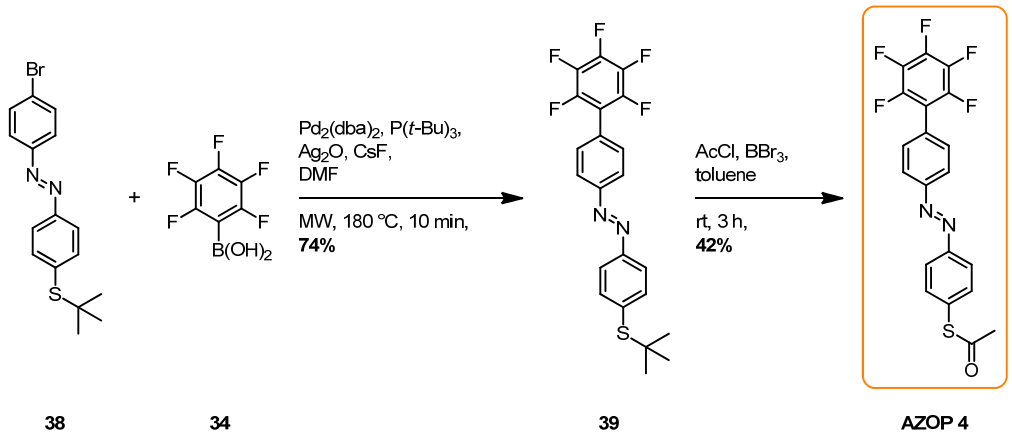

Scheme 51. Last two steps to the synthesis of target compound **AZOP 4**.

To summarize, the presence of an ethyl-TMS sulfur protecting group is not compatible when using the applied conditions (i.e. Ag_2O, $Pd_2(dba)_3$, $P(t\text{-}Bu)_3$, cesium fluoride, *N*,*N*-dimethylformamide) for the reaction of aryl bromide **32** with pentafluorophenylboronic acid (**34**), which is inactive with classical Suzuki-Miyaura conditions for the cross-coupling reaction. Due to the fluoride source the ethyl-TMS protection group of compound **32** was cleaved. With the change of the protecting group to the *tert*-butyl the synthesis to target structure **AZOP 4** could be successfully completed in a total of five steps in an overall yield of 11%. **AZOP 4** was characterized by NMR spectroscopy (^1H, ^{19}F, HMBC and HMQC), EI-MS and UV/Vis spectroscopy and EA.

*Synthesis of **AZOP 5***

AZOP 5 is structurally very similar to the **CABP-SAc**, as only the top arene unit is fully fluorinated and the rest of the structure is maintained. Note here that the general synthetic strategy reported in section 3.1.1 is slightly modified, as the Mills reaction towards **AZOP 5** is introduced at the later stage of the synthetic procedure and not at the very beginning as reported till now. In the course of the synthesis of **AZOP 4** a pentafluorophenyl moiety was successfully introduced to a sulfur containing derivative in a Suzuki-Miyaura cross-coupling reaction only when using a fluoride-stabile protecting group. In order to be flexible in the choice of sulfur protecting groups the fluorinated arene unit was introduced at first, as this reaction is considered to be delicate.

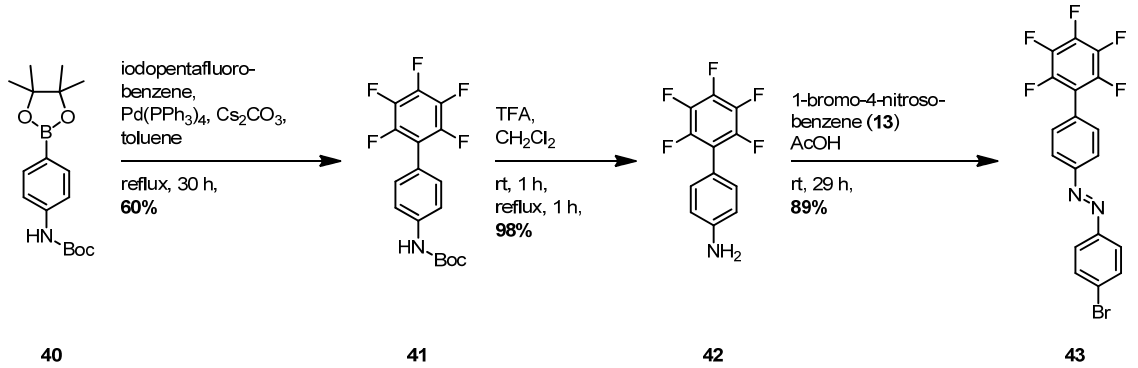

Scheme 52. Synthesis of the azo building block **43**.

The synthesis to the fluorinated unit was initiated with a Suzuki-Miyaura cross-coupling reaction with the commercially available 4-(*N*-Boc-amino)phenylboronic acid pinacol (**40**) and iodopentafluorobenzene. The coupling with cesium carbonate as base and $Pd(PPh_3)_4$ as catalyst in toluene at reflux for 30 hours gave the corresponding product in a yield of 60% (*Scheme 52*). Cesium bases such as cesium carbonate and cesium hydroxide exhibit a greater accelerating effect than sodium or potassium salts.[269] Furthermore, the presence of water or of hydrated inorganic bases is reported to greatly accelerate the reaction, too.[269] In this case, the coupling of compound **40** and iodopentafluorobenzene by the addition of cesium carbonate improved the reaction yield and the addition of water did not. Previous attempts with sodium carbonate as base, with and without the addition of small amounts of water and longer reaction times gave lower yields. However, the following acidic removal of the Boc-protecting group with an excess of trifluoroacetic acid and the subsequent treatment of the crude product with the base triethylamine, gave after workup and without further purification the free amine **42**. It was isolated as a colorless solid in almost quantitative yield. The following condensation reaction of amine **42** with the nitroso **13** in acetic acid gave azo compound **43**. The reaction mixture was

stirred at room temperature overnight and after workup and purification by column chromatography it was isolated as an orange solid in a yield of 89%.

The coupling partner of the azo compound **43** is envisaged to be a boronic acid derivative, which comprises a sulfur moiety at the *para* position to the boron. The sulfur is considered to be protected with a *tert*-butyl group, as it can be transprotected to the acetyl group, as in the synthesis to **AZOP 4**. The synthesis of the sulfur building block was achieved starting from 4-bromothiophenol (**15**) (*Scheme 53*). The free thiol was protected by the *tert*-butyl moiety using 2-chloro-2-methylpropane.[332] The reaction was catalyzed by aluminum trichloride. After stirring at room temperature for 2 hours the reaction mixture was quenched and a subsequent workup led to (4-bromo)phenyl-*tert*-butylthioether (**44**) as a yellowish oil in a yield of 96%. Compound **44** was then converted to the boronic acid derivative **45**. *n*-Butyllithium was added to a cooled solution of compound **44** in tetrahydrofuran. The reaction mixture was then treated with triisopropyl borate and stirred overnight at room temperature. After hydrolysis and workup the boronic acid formed was isolated. The crude product was recrystallized from hexane and dried under high vacuum to give the boroxine **45**, which is formed under loss of water, as a colorless solid in a yield of 61%.

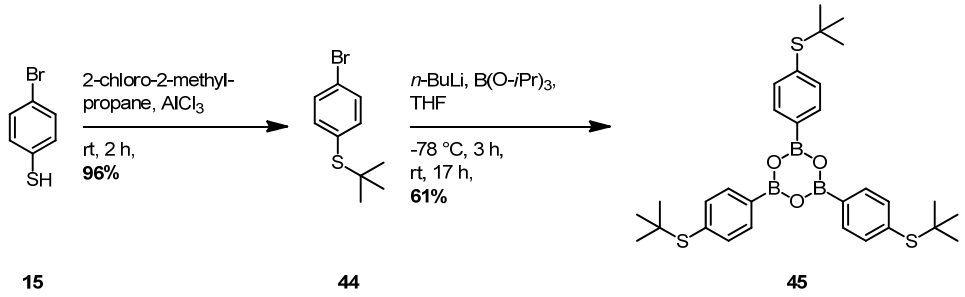

15 **44** **45**

Scheme 53. *Tert*-butyl protection of 4-bromothiophenol (**15**) and the subsequent borylation to boroxine **45**.

With boroxine **45** in hand, the *tert*-butyl derivative **46** was synthesized in a Suzuki-Miyaura cross-coupling reaction (*Scheme 54*). The halide **43** and an 1.3-fold excess of the trimeric boronic derivative **45** (0.4 equivalents) were stirred with the base potassium carbonate and the catalyst $Pd(PPh_3)_4$ in an toluene/ethanol solvent mixture at 60 °C for one hour. After aqueous workup and purification by column chromatography the coupling product **46** was obtained as an orange solid in a yield of 96%. The attempt to transprotect compound **46** to target structure **AZOP 5** with boron tribromide in the presence of acetyl chloride in toluene did not lead to **AZOP 5**. At room temperature the starting material was not converted, as judged by TLC. After the addition of further amounts of boron tribromide the same was observed. At a prolonged reaction time (overnight) the starting material was completely converted, but none of the formed products was assigned to **AZOP 5**. In addition, the side products could not be identified. Here, the

transprotection from the *tert*-butyl to the acetyl group did not show similar reaction characteristics as for the same type of transprotection reported for the synthesis of **AZOP 4**. As an alternative route, the transprotection of an ethyl-TMS group to the acetyl derivative in the last step of the synthesis towards **AZOP 5** was chosen.

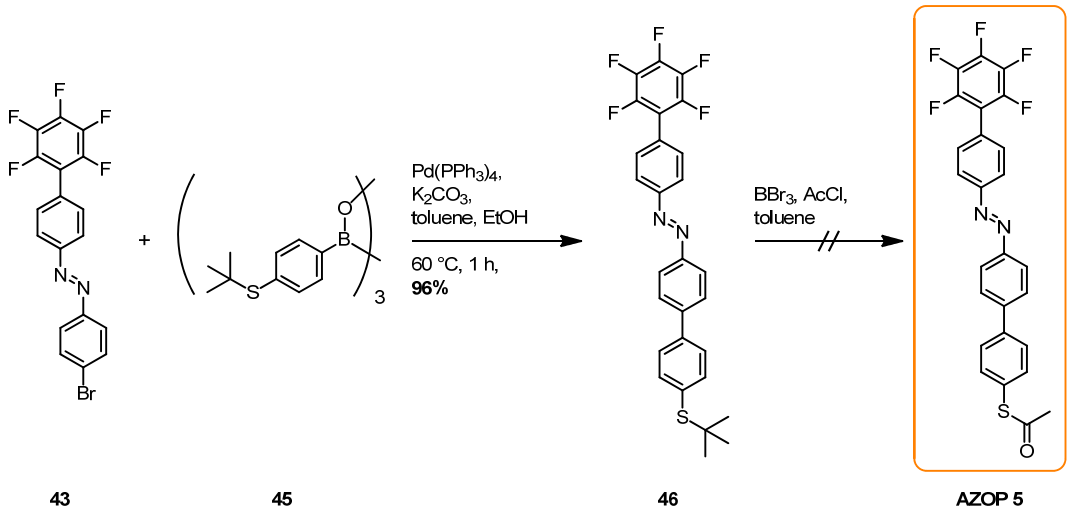

Scheme 54. Synthesis of the *tert*-butyl-based azo compound **46** in a Suzuki-Miyaura cross-coupling reaction and the subsequent transprotection attempt to the acetyl-based compound **AZOP 5**.

As the boroxine **17** was already available (section 3.1.2), it was reacted with azo compound **43** in a Suzuki-Miyaura cross-coupling reaction ($Pd(PPh_3)_4$, K_2CO_3, toluene/ethanol, 60 °C, 45 min). The reaction afforded the precursor **47** after workup and purification by column chromatography as an orange solid in a yield of 98% (*Scheme 55*). The last step towards the target structure **AZOP 5** was the transprotection of the ethyl-TMS protecting group to the acetyl group. As reported in section 3.1.2, the cleavage of the ethyl-TMS group is easily achieved with tetrabutylammonium fluoride in tetrahydrofuran. Therefore, the same procedure was envisaged for the transprotection to **AZOP 5**.

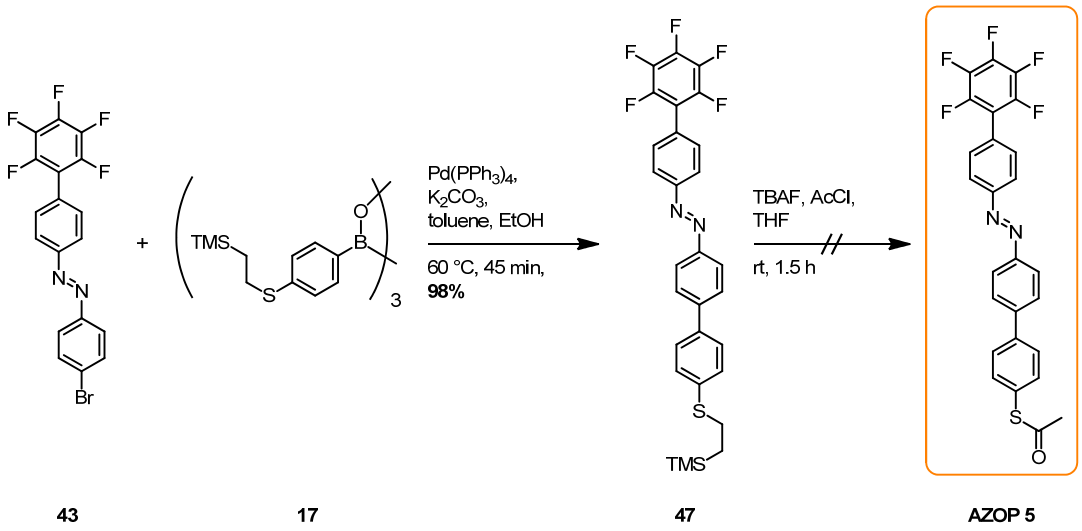

Scheme 55. Synthesis of azo compound **47** and the subsequent attempt to transprotect the sulfur functionality of structure **47**.

Compound **47** was dissolved in tetrahydrofuran and the solution was degassed and then treated at room temperature with an excess of tetrabutylammonium fluoride for 1.5 hours (*Scheme 55*). Then an excess of acetyl chloride was added and stirred for a further 45 minutes. After quenching and workup an orange solid was obtained that was not soluble in any kind of common organic solvent. Thus, neither ^{1}H-NMR analysis nor mass analysis (electron impact (EI), fast atom bombardment (FAB), matrix-assisted laser desorption/ionization time of flight (MALDI-ToF)) were possible. Infrared (IR) spectroscopy did not show any characteristic carbonyl peaks, which indicates the absence of the acetyl protection group. Thus it can be concluded that the insoluble orange solid is not target structure **AZOP 5**. Assumptions are made that either the corresponding disulfide **48** or polymer **49** was obtained (*Figure 33*). The formation of the disulfide **48** would have been the consequence of an oxidative process and the formation of the polymer **49** could be due to the nucleophilic attack of the *in situ* formed thiolate on the pentafluorophenyl. The nucleophilic attack of a sulfur to a polyfluoroarene, even without the addition of a base for the deprotonation of the thiol, is reported by Shaw *et al.*.[333]

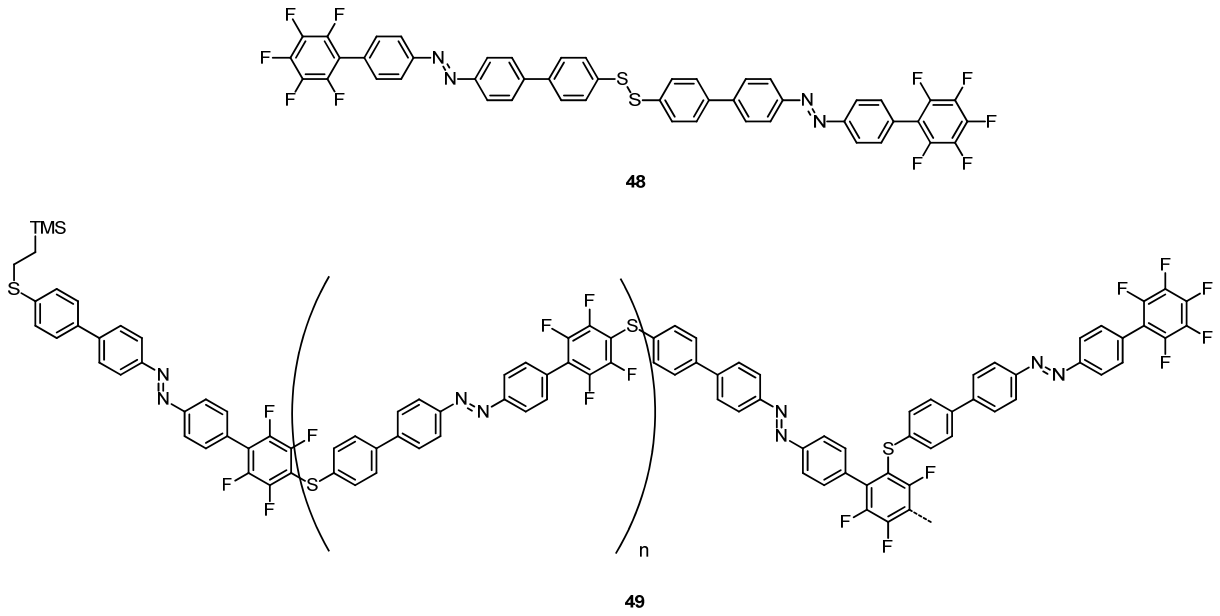

Figure 33. Possible formed undesired side products during the transprotection attempt of compound **47** to **AZOP 5**.

In order to prevent the possible disulfide formation the reaction was repeated again, but this time the degassing time was increased considerably. Also the freeze-pump-thaw method was tried. Unfortunately, the same observations as before were made.

To avoid the probable formation of the polymer **49** the reaction was performed again, by adding first acetyl chloride to the dissolved starting material **47** and subsequently tetrabutylammonium fluoride. It was suggested that by the addition of tetrabutylammonium fluoride the formed thiolate would immediately react with the present acetyl chloride to afford **AZOP 5**. In this way the thiolate would not have the chance to undergo a nucleophilic aromatic substitution with a further molecule of the starting material **47** during prolonged reaction times. Unfortunately, this reaction did not show any conversion of compound **47**, even after prolonged reaction times. However, with another fluoride source, silver tetrafluoroborate, the ethyl-TMS groups can also be cleaved.[293,294] Intermediate **47** was dissolved in dichloromethane in the presence of an excess of acetyl chloride. Afterwards also an excess of silver tetrafluoroborate was added and an immediate color change, from the initial orange solution to a dark blue and then dark red, showed the termination of the reaction. The reaction mixture was stirred for a further 20 minutes at room temperature, then quenched with water and worked up. The target structure **AZOP 5** was isolated after purification by column chromatography as an orange solid in a yield of 83% (*Scheme 56*).

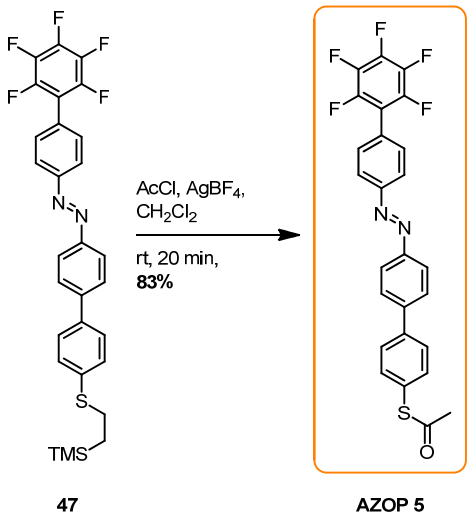

Scheme 56. Last step to target structure **AZOP 5**.

To summarize, the synthetic strategy to **AZOP 5** was slightly modified as compared to the strategy reported of **AZO 4**, i.e. the introduction of the Mills reaction was performed at a later stage of the synthesis. The target structure **AZOP 5** was obtained in a total of seven steps. Furthermore, the deprotection of the ethyl-TMS group was accomplished with silver tetrafluoroborate. **AZOP 5** was characterized by NMR spectroscopy (^{1}H, ^{19}F, HMBC and HMQC), EI-MS and UV/Vis spectroscopy.

*Towards the Synthesis of **AZOP 6***

The structural difference of **AZOP 6**, compared to the **CABP-SAc**, is the insertion of a bithiophene unit into the **CABP-SAc**. A bithiophene building block and the azo unit were synthesized in parallel, which then should afford the target structure's precursor in a Suzuki-Miyaura cross-coupling reaction.

The synthesis of the bithiophene moiety was initiated by adapting a literature procedure.[334] The commercially available 2,2'-bithiophene (**50**) was monobrominated in an acid catalyzed electrophilic aromatic substitution with one equivalent of *N*-bromosuccinimide (*Scheme 57*). The reaction was performed in chloroform and acetic acid at -35 °C for 1.5 hours. After the removal of the precipitated succinimide a basic workup was performed. NMR studies revealed the formation of the monobrominated product **51** and the dibrominated by-product **52**. Furthermore, not all starting material **50** was converted. Thin layer chromatography of the reaction mixture showed three spots (**50**, **51**, and **52**), which had similar R_f-values using *n*-hexane as eluent. As the purification by column chromatography in a gram scale was

troublesome and the desired monofunctionalized compound **51** is already fully characterized in the literature,[335] the crude mixture was used for the next reaction step.

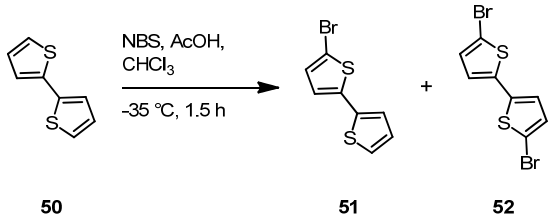

Scheme 57. Formation of a mixture of products during the reaction of bithiophene **50** with *N*-bromosuccinimide in acetic acid and chloroform.

Slightly modifying a literature procedure of Hotta and Katagiri[334] the crude mixture of compounds **50, 51** and **52** was heated at 110 °C for 2.5 hours in the presence of phenylboronic acid, $Pd(PPh_3)_4$ and an aqueous sodium carbonate solution in toluene (*Scheme 58*). This Suzuki-Miyaura cross-coupling reaction afforded, beside the desired structure **53**, also the symmetric bithiophene **54**. After purification by column chromatography compound **53** was isolated in a yield of 42% over two steps.

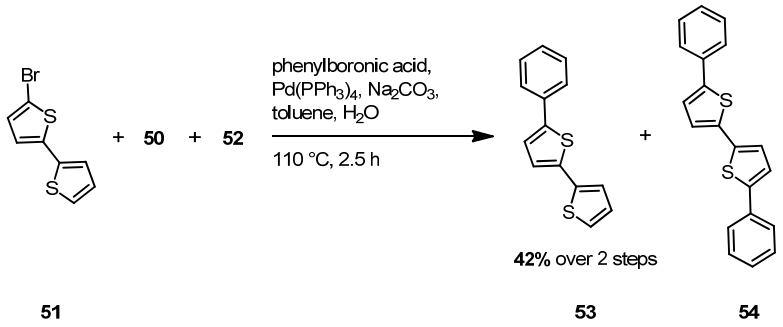

Scheme 58. The crude product mixture (**50**, **51** and **52**) was reacted with phenylboronic acid to obtain compounds **53** and **54** in a Suzuki-Miyaura cross-coupling reaction.

The bromination of 5-phenyl-2,2'-bithiophene (**53**) was proceeded as for the bromination of 2,2'-bithiophene (**50**) (*Scheme 59*).[334] Thiophene **50** dissolved in chloroform was cooled to -35 °C and then one equivalent of *N*-bromosuccinimide and catalytic amounts of acetic acid were added and cooled for a further 2 hours. The formed succinimide was filtered off and the reaction mixture was washed with an aqueous sodium hydroxide solution. After the removal of the solvent and purification by column chromatography, the desired brominated product **55** was obtained in a yield of 72%. The bithiophene-based derivative **55** was then converted to its boronic ester derivative **56**. Compound **55** was dissolved in tetrahydrofuran and after cooling down the solution to -78 °C *n*-butyllithium was added. After the addition of 2-isopropoxy-4,4,5,5-tetramethyl-1,3,2-dioxaborolane and stirring for 2.5 hours the reaction mixture was

quenched. Workup and purification by column chromatography afforded the boronic ester **56** as a dark green solid in a yield of 23%.

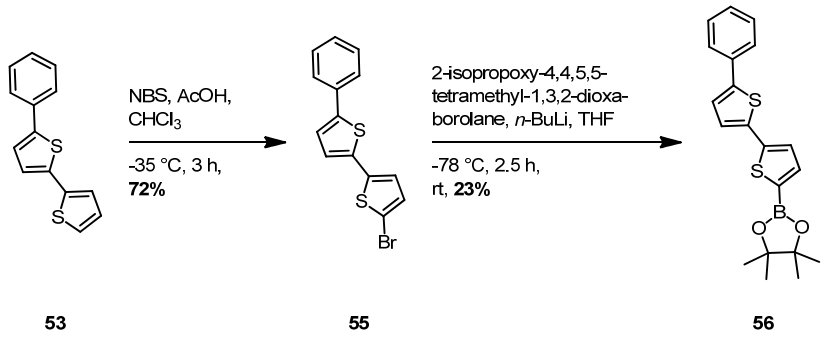

Scheme 59. Formation of the boronic ester derivative **56**.

With bithiophene intermediate **56** in hand the synthesis of its coupling partner had to be performed. With the already available intermediates **11** and **17** a selective Suzuki-Miyaura cross-coupling reaction was performed, where only the iodide acted as leaving group. The asymmetric azo compound **11** was stirred with an 1.3-fold excess of the trimeric boronic derivative **17** (0.4 equivalents) and with $Pd(PPh_3)_4$ as catalyst and potassium carbonate as base in a toluene/ethanol mixture. The mixture was heated to 50 °C for 24 hours and the azo compound **19** was obtained after workup and purification by column chromatography as an orange solid in a yield of 96%. Here, the effectiveness of the selective Suzuki-Miyaura cross-coupling reaction was demonstrated once again.

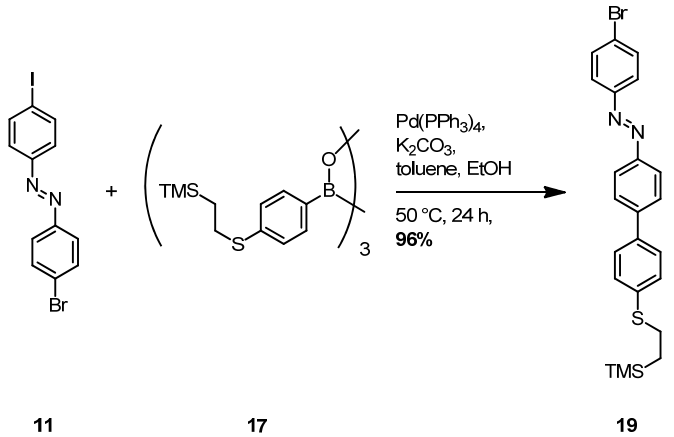

Scheme 60. Selective coupling of boroxine **17** with azo compound **11** to afford the desired product **19**.

The Suzuki-Miyaura cross-coupling reaction of bithiophene moiety **56** and azo building block **19** was performed with the same reagents and similar conditions as the previous reaction. A slight excess of boronic ester **56** was used. Here an orange solid with very low solubility was isolated. This solid was analyzed by MALDI-ToF mass spectrometry and EI-MS. Both mass spectra showed two main peaks. One corresponded to the desired product **57** and the other one had the

mass of compound **58** (*Scheme 61*). ^{1}H-NMR spectroscopy could not verify the by-product **58** as it is known to be very insoluble.[336] Furthermore, its color is also orange as for most azo compounds. The only interpretation of the formation of compound **58** is the homocoupling of compound **56** during the reaction. The attempt to separate compound **57** and by-product **58** with a Soxhlet extractor, as both products could have a different solubility factor, was not successful. However, with the mass analysis and a generous interpretation of the ^{1}H-NMR spectrum the presence of the desired compound **57** was confirmed.

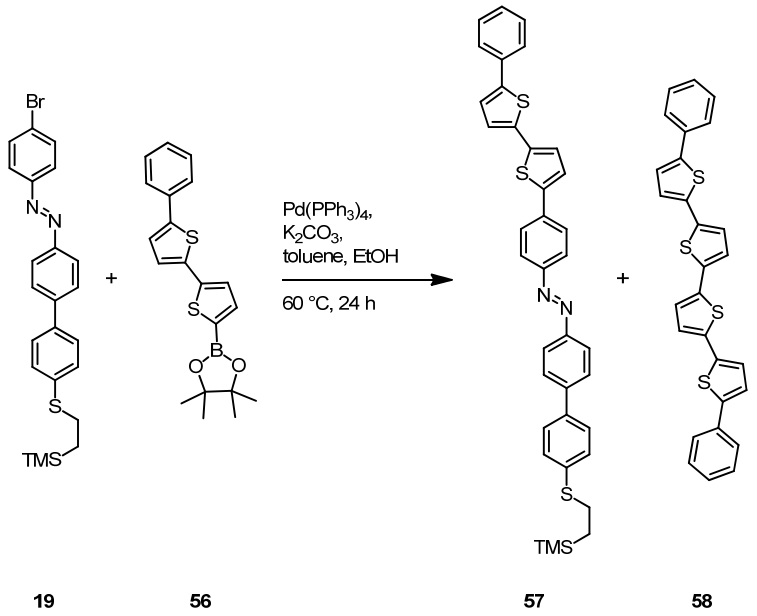

Scheme 61. Reaction to the desired product **57** and the by-product **58**.

In order to avoid the formation of the homocoupled side product **58** the strategy towards **AZOP 6** was modified. The synthesis to intermediate **61** was envisaged (see *Scheme 62*), which would be coupled with boroxine **17** to precursor **57**. Two possible synthetic routs were considered to azo compound **61**. The first route involves the formation of the boronic ester-based azo compound **59**, which would undergo a selective coupling reaction with the thiophene derivative **60**. The second possible route would be the Mills reaction with 1-bromo-4-nitrosobenzene (**13**) and compound **62** to intermediate **61**.

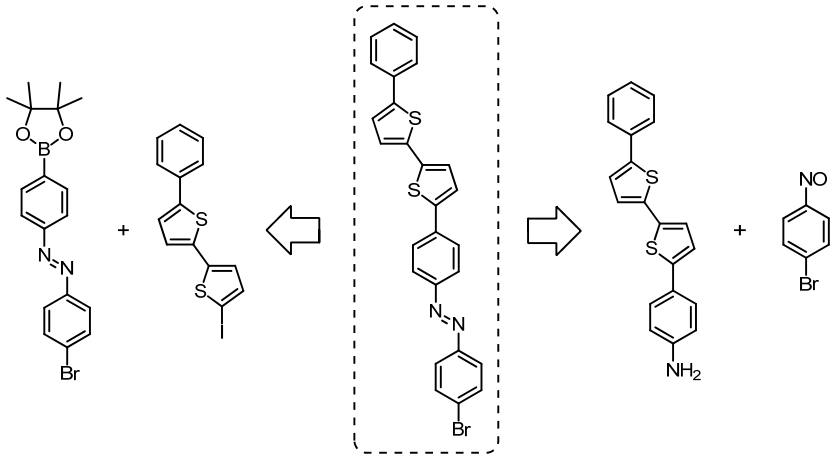

Scheme 62. Two routes to intermediate **61**.

The first possible route started with the condensation reaction of 1-bromo-4-nitrosobenzene (**13**) and the commercially available 4-(4,4,5,5-tetramethyl-1,3,2-dioxaborolan-2-yl)aniline (**63**) in acetic acid. The reaction mixture was stirred at room temperature for 20 hours. After workup and purification by column chromatography the asymmetric azo compound **59** was isolated as an orange solid in a yield of 15% over two steps. Probably the troublesome purification by column chromatography led to the low yield, as the product streaked on the column. However, as the asymmetric compound **59** could be successfully synthesized, its coupling partner **60** was envisaged. The starting point of the synthesis to bithiophene derivative **60** was 2,2'-bithiophene (**50**). Following a literature procedure[337] the diiodinated bithiophene **64** was synthesized (*Scheme 63*). 2,2'-Bithiophene (**50**) was treated with 2.5 equivalents of *N*-iodosuccinimide and acetic acid in methanol at room temperature for 7 hours. The formed colorless precipitate was filtered off and washed with cold methanol. This product was not further purified, yielding 5,5'-diiodo-2,2'-bithiophene (**64**, 87%) as a colorless solid. Compound **60** was obtained by reacting bithiophene **64** with 0.5 equivalents of phenyl boronic acid, $Pd(PPh_3)_4$, potassium carbonate in a toluene/methanol reaction mixture under microwave irradiation at 100 °C for 8 minutes. After workup and purification by column chromatography a yellowish solid of compound **60** was isolated in a yield of 32%.

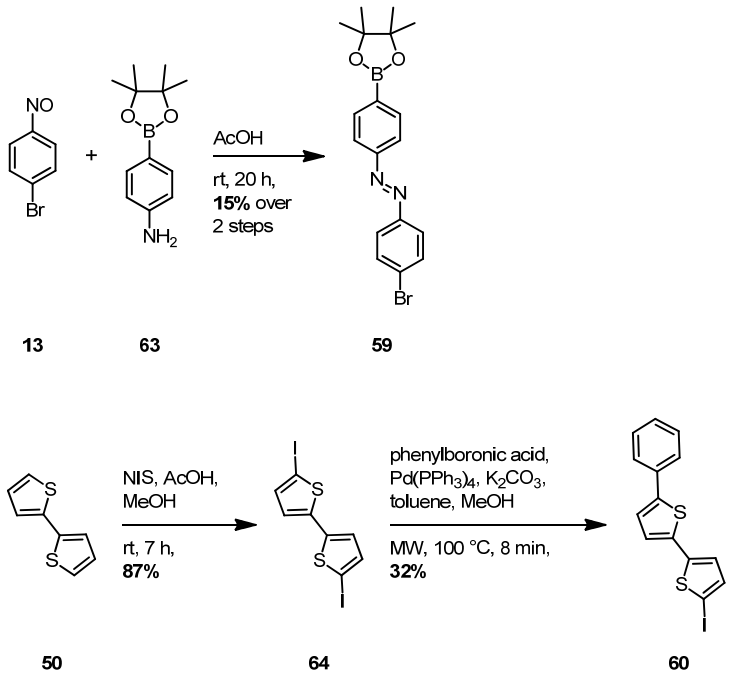

Scheme 63. Syntheses of the coupling partners **59** and **60**.

With building blocks **59** and **60** in hand the selective Suzuki-Miyaura cross-coupling was performed. Compound **59** and one equivalent of bithiophene derivative **60** were stirred with the catalyst bis(triphenylphosphine)palladium chloride ($Pd(PPh_3)_2Cl_2$) and the base potassium carbonate in a toluene/ethanol reaction mixture (*Scheme 64*). For the previously reported selective Suzuki-Miyaura cross-couplings, a maximum temperature of 50 °C was used. For precaution reasons for an effective selective coupling of compound **59** with **60** the reaction was firstly performed at room temperature. If no coupling was observed the temperature would have been risen step by step. The reaction mixture was stirred for 3 days and an orange precipitate was observed. It was then collected by filtration and washed with a variety of common organic solvents. At this point it could be observed that the solid was not very soluble. ^{1}H-NMR studies did not verify the product, due to the low solubility. Beside the formation of target structure **61** also a reaction between two molecules of compound **59** could have had occurred. Furthermore, oligomer or polymer structures of structure **59** could also be present. To ascertain this consideration the reaction could be repeated at lower temperatures and shorter reaction times or the strategy to compound **61** can be changed. The other route to **61** was proposed (see *Scheme 62* or *Scheme 65*), avoiding the selective cross-coupling reaction.

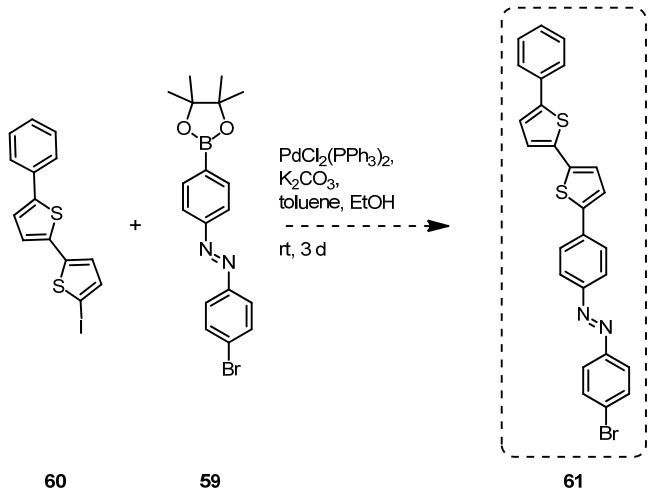

Scheme 64. Selective coupling to bithiophene derivative **61**.

The second proposed route started with the coupling of the already available bithiophene derivative **55**. It was coupled with the commercially available *tert*-butyl-*N*-[4-(4,4,5,5-tetra-methyl-1,2,3-dioxaborolan-2-yl)phenyl]carbamate (**65**) (*Scheme 65*). The well applied reagents and solvent were reused ($Pd(PPh_3)_4$ and potassium carbonate in a toluene/methanol mixture) and the reaction mixture was stirred at 80 °C for one hour. After workup and purification by column chromatography the amine protected bithiophene derivative **66** was obtained as a yellowish solid in a yield of 31%. The subsequent removal of the amine Boc-protecting group was performed with an excess of trifluoroacetic acid in dichloromethane at 45 °C. The free amine **62** was obtained as a greenish solid in a yield of 60%. A successful Mills reaction of the amine **62** and 1-bromo-4-nitrosobenzene (**13**) would exclusively lead to intermediate **61** and no other products are expected. Therefore, amine **62** and nitroso **13** were stirred in acetic acid at room temperature for 27 hours. The orange formed precipitate was removed from the reaction mixture and was washed with several common organic solvents. Indeed, also here the orange solid was not very soluble. This orange solid was strongly considered to be azo compound **61**, as no other possible product is expected for this reaction, as just mentioned. The observation of the orange insoluble solid affirmed that the obtained product before (see *Scheme 64*) could have also been the azo compound **61**. The insight, that the orange solid could only be the azo compound **61** and that this solid suffers low solubility, is a drawback. The further synthesis towards **AZOP 6** will be hard to fulfill, due to solubility issues. If intermediate **61** already suffers insolubility, target structure **AZOP 6** is expected to show even lower solubility. The insolubility of these compounds is not desired for the assembly process on metal surfaces.

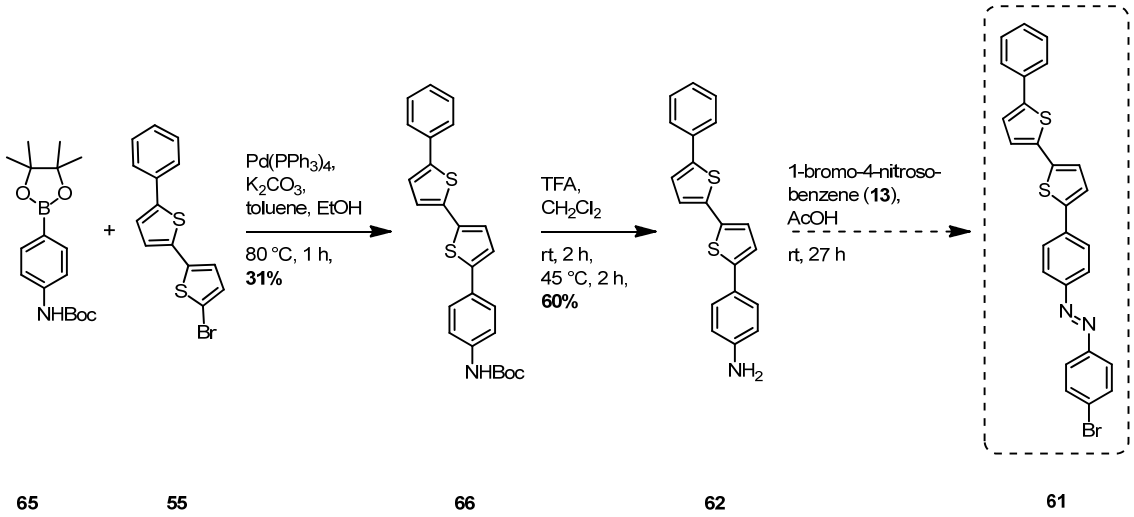

Scheme 65. Second route to intermediate **61**.

A way to increase the compound solubility is the attachment of long apolar alkyl chains to the target structure. Considering the investigation aims of **AZOP 6** the only conceivable position of the attachment of alkyl chain(s) is on the molecule's tail. The lateral attachment of chains would disturb the packing interactions of the molecule neighbors. With this consideration in mind, a modified structure of **AZOP 6** was proposed. At the tail of the actual target structure an alkyl chain of a length of eight carbon atoms is envisaged, as shown in *Figure 34* (**AZOP 6a**).

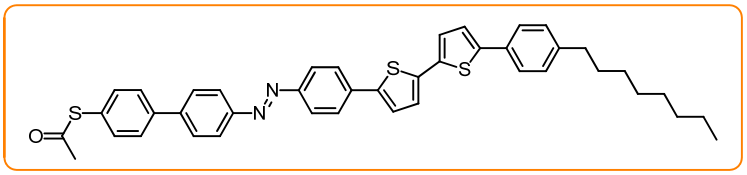

AZOP 6a

Figure 34. Modified structure in order to increase the solubility.

Profiting from the already available building blocks the synthesis towards **AZOP 6a** was initiated with the commercially available 1-bromo-4-octylbenzene (**67**), which was converted to the boronic ester derivative **68** (*Scheme 66*). This was achieved first by generating the free boronic acid. Compound **61** was treated with *n*-butyllithium at -78 °C for 40 minutes and then with trimethyl borate for one hour before quenching with an acidic solution. After workup and drying the crude (free boronic acid) was treated with 2,2-dimethyl-1,3-propanediol in dry dichloromethane at room temperature for 2.5 hours. The solvent was removed and purification by column chromatography afforded the desired boronic ester **68** as a colorless solid in a yield of 20%. Boronic ester **68** was then reacted with the already available 5,5'-diiodo-2,2'-bithiophene (**64**) in a Suzuki-Miyaura cross-coupling reaction. Compound **68** and 1.1 equivalents of compound **64** were added into a flask with potassium carbonate, toluene and

ethanol. After degassing the reaction mixture catalytic amounts of $Pd(PPh_3)_4$ were added. The reaction mixture was stirred at room temperature for 20 hours and after workup and purification by column chromatography the desired product **69** was isolated as a greenish solid in a yield of 17%.

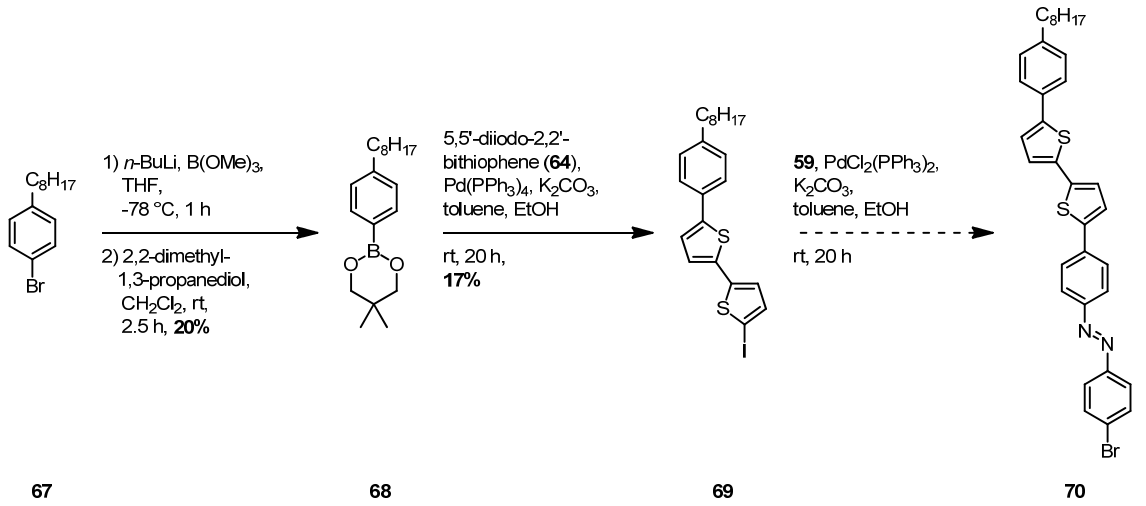

Scheme 66. Synthesis of bithiophene intermediate **70**.

The subsequent selective coupling towards compound **70** was performed as for the selective coupling of its derivative without the alkyl chain (see *Scheme 64*). But the reaction time was shortened to 20 hours. As it was considered that the product **61** in *Scheme 64* was obtained (instead of any oligomer/polymer), a successful selective coupling was consequently suggested. Therefore, the obtained orange precipitate in the reaction of its alkyl derivative was ascribed to the desired intermediate **70**. Unfortunately, this orange solid showed very low solubility in any common organic solvent. However, ^{1}H-NMR spectra could be recorded, but an accurate characterization was not possible due to the low solubility of the product in dichloromethane-d2 (CD_2Cl_2). However, the interpretation of the visible peaks could be ascribed to the desired compound **70**. At this point the synthesis towards **AZOP 6a** was not continued, as the strategy to introduce an alkyl chain to increase the solubility did not simplify and improve the synthesis proceedings. Furthermore, as the introduction of even more or longer alkyl chains to the **AZOP 6** structure would conflict with the initial investigation aims, the bithiophene project in the framework of a conductance switching was at this point put on hold.

To summarize, due to the low solubility of the intermediates used for the synthesis of **AZOP 6**, the bithiophene project was not further pursued. The introduction of long alkyl chains to the **AZOP 6** structure did not improve the solubility of the intermediates.

*Towards the Synthesis of **AZOP 7***

Target structure **AZOP 7** is divided into three building blocks: the carbonyl unit (blue), the azo unit (pink) and the sulfur unit (green) as shown in *Scheme 67*. These three building blocks were synthesized in parallel. The blue and pink building blocks were designed such in order to profit from selective cross-coupling reactions. These two units are supposed to be attached first to each other in a selective Suzuki-Miyaura cross-coupling reaction with iodide as leaving group. Subsequently, the bottom unit is planned to be attached in a further cross-coupling reaction. Furthermore, the protecting groups of the alcohol, sulfur and carboxylic acid functionalities have to be base tolerant, in order to survive the Suzuki-Miyaura cross-coupling reactions.

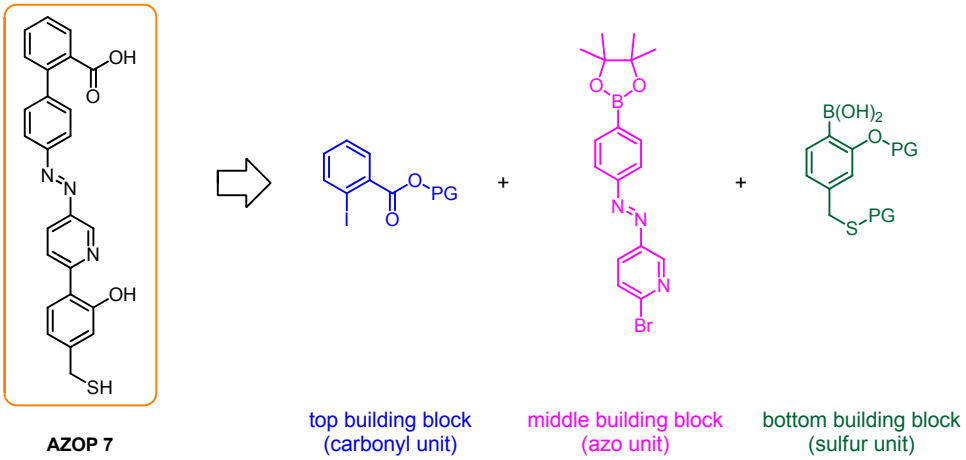

Scheme 67. Synthetic strategy of target structure **AZOP 7**. PG = protecting group.

The carbonyl unit was synthesized in two steps following a patented procedure (*Scheme 68*).[338] 2-Iodobezoic acid (**71**) was converted into 2-iodobenzoic chloride (**72**) by the reaction of oxalyl chloride in dichloromethane, initiated by a drop of *N*,*N*-dimethylformamide. *N*,*N*-Dimethyl-formamide attacks oxalyl chloride to form after the release of carbon monoxide and carbon dioxide the iminium derivative (Me_2N^+=CHCl). The iminium then reacts with the carboxylic acid (**72**), abstracting an oxide and regenerating the dimethylformamide catalyst. This catalyzed reaction was carried out at room temperature and after removal of the solvent and excess of the oxalyl chloride the remaining yellowish liquid was transferred directly to the next reaction step. The crude of compound **72** was dissolved in tetrahydrofuran and was added to a previously prepared cooled solution of *tert*-butanol and *n*-butyllithium in tetrahydrofuran. After stirring at -78 °C and then at room temperature the reaction mixture was quenched and worked up. The crude was purified by column chromatography to obtain the protected carboxylic acid **73** as a yellowish oil in a yield of 96% over two steps.

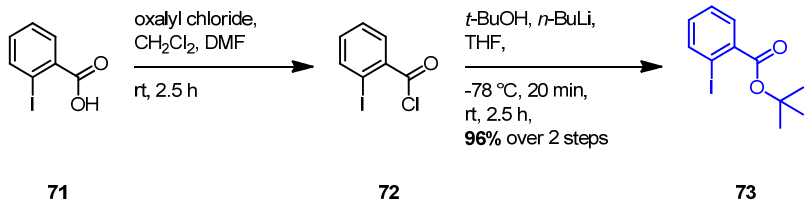

Scheme 68. Formation of the carboxylic ester **73** in two steps starting from 2-iodobezoic acid (**71**).[338]

As already mentioned before, the top building block **73** (in blue) is supposed to undergo a selective coupling with the middle unit **76** (in pink). This azo unit was synthesized in two steps. 3-Amino-6-bromopyridine (**74**), which is commercially available, was treated with Oxone® in a biphasic water/dichloromethane mixture at room temperature for 19 hours. The usual workup, that included the washing of the separated organic layer with aqueous hydrochloric acid solution, aqueous saturated sodium bicarbonate solution, water and brine, was modified. The aqueous workup with hydrochloric acid, which was used to transfer the unreacted amine into the aqueous phase, was avoided here, as the protonation of the nitrogen of the pyridine could also transfer the nitroso derivative into the aqueous layer. Beside the advantage of not transferring the nitroso into the aqueous layer a small disadvantage is that unconverted starting material **74** could be present in the crude. This would lead in the subsequent Mills reaction to symmetrically azo compounds and probably a more challenging separation of the symmetric and asymmetric azo compounds. Therefore, the crude was purified by column chromatography, but not further analyzed, as a slow color change of the green solid to brown displayed decomposition of the unstable nitroso derivative **75**. The following Mills reaction with nitroso **75** and the commercially available amine **63** was performed in acetic acid at room temperature. The reaction mixture was stirred for three days and after workup and purification by column chromatography the desired asymmetric azo compound was obtained as an orange solid in a yield of 12% over two steps. The low yields are probably due to the decomposition of the nitroso derivative **76** during its purification by column chromatography after the first reaction step.

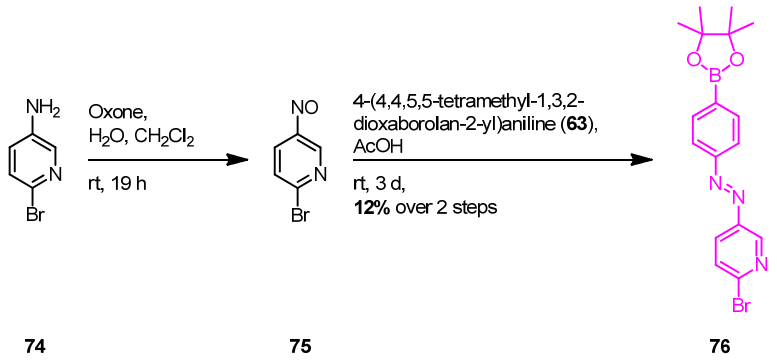

Scheme 69. Formation of the nitroso derivative **75** and subsequent condensation to intermediate **76**.

However, with sufficient amounts of the azobenzene derivative **76** the selective coupling to the previously synthesized ester **73** was performed (*Scheme 70*). The reaction was done under microwave heating.

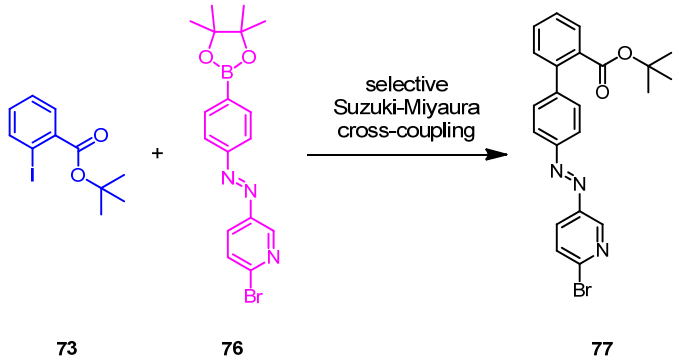

73 **76** **77**

Scheme 70. Selective cross-coupling reaction to form azo compound **77**.

Several test reactions were performed until the desired product **77** was obtained in satisfactory yields. In *Table 4* the reagents and conditions are summarized. The first test reaction implied the re-usage of the promising reagents and solvent mixture ($Pd(PPh_3)_4$, potassium carbonate, toluene/ethanol). Five equivalents of the iodine derivative **73** were added and the reaction mixture was heated in the microwave at 80 °C for 45 minutes (1st entry). After workup and purification by column chromatography only traces of the desired azo compound **77** were isolated. Instead by-products were formed, which could have occurred from the multiple coupling of compound **76**, as the temperatures were probably too high for a selective coupling with the iodine derivative **73**. In the second test reaction the catalyst, base and solvent mixture were changed to $PdCl_2(PPh_3)_2$, sodium carbonate and tetrahydrofuran/water, respectively (2nd entry). The reaction temperature and the time were decreased to 40°C and 30 minutes, respectively. Furthermore, the amount of equivalents of the iodine unit **73** was increased to ten. Here the target structure **77** was isolated as an orange solid in 27% yield. An improved yield of 43% of compound **77** was reached by maintaining the reagents and solvent mixture and by increasing the reaction time by 15 minutes (3rd entry). A considerable change in the parameters was the addition of 30 equivalents of the starting material **73**. The crude product **77** was purified by column chromatography.

Table 4. Test reactions to azo compound **77**.

Entry	76	73	Catalyst	Base	Solvent mixture	Temp.	Time	Results
1	1.0 eq.	5.0 eq.	0.23 eq. $Pd(PPh_3)_4$	1.7 eq. K_2CO_3	toluene, EtOH	80 °C	45 min	Traces of **77**; by-products; recovery of **73**
2	1.0 eq.	10 eq.	0.05 eq. $PdCl_2(PPh_3)_2$	271 eq. Na_2CO_3	THF, H_2O	40 °C	30 min	27% of **77**; recovery of **73**
3	1.0 eq.	30 eq.	0.05 eq. $PdCl_2(PPh_3)_2$	97 eq. Na_2CO_3	THF, H_2O	40 °C	45 min	43% of **77**; recovery of **73**

With azobenzene derivative **77** in hand its coupling partner, i.e. the sulfur unit (green, see *Scheme 67*), had to be synthesized. The alcohol was considered to be protected with a *tert*-butyldimethylsilyl (TBDMS) group and the sulfur with a trityl group. The reaction sequence was started with the bromination of methyl 3-hydroxybenzoate (**78**). An electrophilic aromatic substitution was performed with the addition of one equivalent of bromine to the dissolved compound **78** in acetic acid.[339] After stirring at room temperature for 5.5 hours, workup and purification by column chromatography, the desired methyl 4-bromo-3-hydroxybenzoate (**79**) was obtained as a colorless solid in a yield of 36% (*Scheme 71*). Following a patented procedure the ester of the brominated compound **79** was reduced to the corresponding alcohol **80**.[340] 3.3 Equivalents of diisobutylaluminium hydride were added to an ice cooled suspension of compound **79** in dichloromethane. Afterwards the reaction mixture was stirred at room temperature for three hours. After workup with potassium sodium tartrate, for dissolving the emulsion produced, and with an aqueous ammonium chloride solution, the desired alcohol **80** was obtained in a yield of 86% without any need of further purification. The bromination of benzylic alcohols can be performed with phosphorus tribromide. Benzylic alcohol **80** was suspended in chloroform and 0.5 equivalents of phosphorus tribromide were added to the ice cooled suspension.[340] After stirring at 0 °C for one hour and at room temperature for two hours the reaction mixture was worked up. After purification of the crude product by column chromatography the benzylic bromide derivative **81** was obtained as a colorless solid in a yield of 78%.

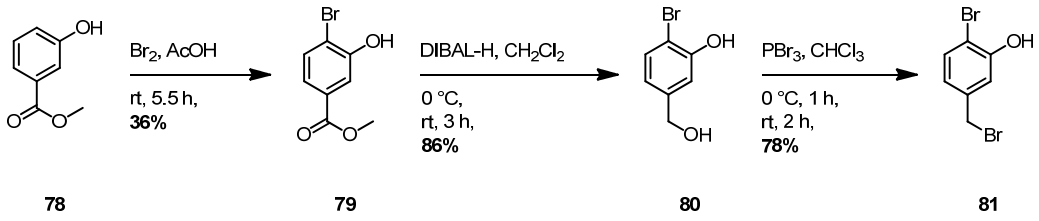

Scheme 71. Reaction sequence to intermediate **81**.

The alcohol functionality of compound **81** was protected with a TBDMS-group. The silylation agent *tert*-butyldimethylsilyl chloride (1.2 equivalents) was added to a solution of compound **81** in *N*,*N*-dimethylformamide (*Scheme 72*). With the further addition of 2.5 equivalents of imidazole the reaction was initiated. The reaction proceeds via *N*-*tert*-butyldimethylsilylimidazole, which is a reactive silylating agent. The desired silylether **82** was obtained as a colorless liquid in a yield of 49% after purification by column chromatography. The formation of the benzylic bromide was accomplished in order to introduce a protected sulfur moiety via an S_N2-reaction. Triphenylmethanethiol was deprotonated with an excess of sodium hydride in tetrahydrofuran and the thiolate formed could attack at the benzylic position of structure **82** releasing bromide. After stirring at room temperature for two hours the reaction mixture was quenched, worked up and the crude product was purified by column chromatography to afford the trityl derivative **83** as a colorless viscous liquid in a yield of 87%.

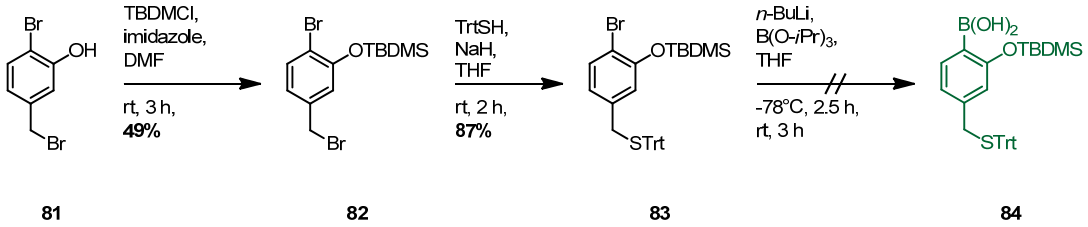

Scheme 72. Synthesis of intermediate **83** and subsequent attempt to afford the boronic acid **84**.

The transformation of the bromide in compound **83** to the corresponding boronic acid, would lead to the third building block (green). The synthesis towards the boronic acid **84** was accomplished using a standard procedure for the formation of boronic acids from the corresponding bromides, i.e. cooling the bromide in a tetrahydrofuran solution to -78 °C, addition of *n*-butyllithium and then a borate reagent, stirring for a specific time at -78 °C afterwards at room temperature and finally quenching with an aqueous hydrochloride solution to from the free acid (*Scheme 72*). For the reaction towards compound **84** the quenching with an aqueous hydrochloride solution was avoided, in order to not deprotect the trityl and TBDMS groups, instead water was used. The purification of the reaction mixture by column chromatography gave several by-products, which were interpreted by ^{1}H-NMR studies and which are depicted in *Scheme 73*. The main product was the dehalogenated form **85** of the

starting material **83**. The second main product was the corresponding alcohol **86**. The silyl deprotected form **87** and its dehalogenated derivative **88** were also observed in traces. Boronic acids are often not apolar enough to be purified by column chromatography using silica gel, as they stick on the base line. Therefore, if the desired intermediate **84** was formed, it probably could not have been isolated by column chromatography. However, no noticeable amount of a present product on the baseline of the TLC plate was observed.

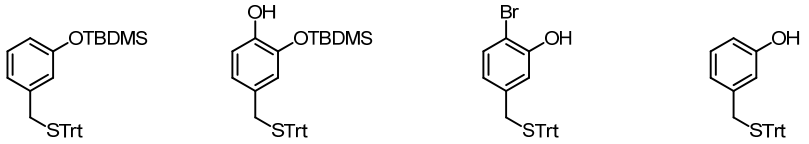

85 **86** **87** **88**

Scheme 73. By-products of the reaction of compound **83** towards intermediate **84**.

Nevertheless, in order to be able to isolate the sulfur moiety as the bottom building block, a boronic ester derivative was envisaged. Borylations are often performed with an aryl halide and diboronyl reagents in a metal-catalyzed coupling reaction using a base and, if necessary, a ligand.[274] Here the borylation was performed with compound **83** and bis(pinacolato)diboron (*Scheme 74*).

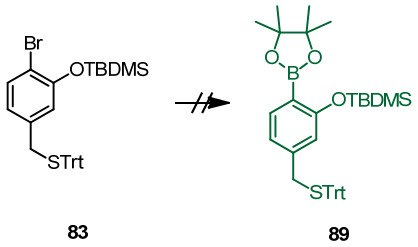

83 **89**

Scheme 74. Borylation attempt of compound **83** towards the corresponding boronic ester **89** with bis(pinacolato)diboron.

Several test reactions were performed, each one using different reagents and solvent media. The results are summarized in *Table 5*. Burns *et al.* reported on an experimental procedure for the borylation of an aryl bromide, which comprises two TBDMS-groups.[341] There they used bis(pinacolato)diboron as diboronyl reagent, triethylamine as base, palladium acetate as catalyst, tri-*o*-tolylphosphine as ligand and toluene as solvent. They performed the reaction at 100 °C and isolated the desired boronic ester in high yields. Applying the same conditions and reagents the aryl bromide **83** was not transformed to the corresponding boronic ester **89**. Instead, an unknown by-product was isolated. Furthermore, the second main by-product was the dehalogenated derivative **85** (1st entry). An often applied system of the borylation with bis(pinacolato)diboron is potassium acetate, [1,1-bis(diphenylphosphino)ferrocene]-

dichloropalladium ($PdCl_2$(dppf)) in dimethyl sulfoxide.[274] This system was employed for our purpose under microwave irradiation. After 30 minutes at 120 °C the starting material was completely converted. The isolated product was the deprotected alcohol derivative **87** (2nd entry). Another literature procedure was found, were the authors use potassium *tert*-butoxide as base.[342] The TBDMS-group is known to tolerate potassium *tert*-butoxide.[271] The applied reagents were used (3rd entry) and the reaction mixture was heated to 50 °C for 30 minutes in the microwave. Unfortunately, the main by-product formed was also here the deprotected alcohol **87**. The reaction with cesium carbonate as base and $PdCl_2$(dppf) as catalyst also did not lead to the desired ester **89** (4th entry). Almost the complete bromo starting material **83** was recovered, showing that the used reagents did not activate the borylation.

Table 5. Borylation attempts to compound **89**.

Entry	Base	Catalyst	Ligand	Solvent	Results
1	NEt_3	$Pd(OAc)_2$	tri-*o*-tolylphosphine	toluene	unknown product and **85**
2 (microwave)	KOAc	$PdCl_2$(dppf)	-/-	DMSO	main product: **87**
3 (microwave)	*t*-BuOK	CuI	*n*-Bu_3P	THF	main product: **87**
4 (microwave)	Cs_2CO_3	$PdCl_2$(dppf)	-/-	toluene	recovery of **83**; traces of **87**

Obviously for this specific starting material **83** the question of a proper base for the borylation with bis(pinacolato)diboron is not the only issue to be considered. However, as for the reactions to the boronic acid **84** and the boronic ester **89,** either dehalogenation and/or deprotection of the alcohol occurred, it was decided to introduce another alcohol protecting group. The alternative phenol protecting group was chosen to be a benzylic group. Oriyama *et al.* reported on direct conversions of aryl silyl ethers into aryl alkyl ethers.[343] Following their reaction conditions compound **83** was transprotected to the corresponding benzyl ether **90**. To a solution of cesium fluoride, which acts as a fluoride source that cleaves the TBDMS group, in *N*,*N*-dimethylformamide, compound **83** and benzyl bromide were added successively. The reaction mixture was stirred at room temperature for 3 days. After quenching with a phosphate buffer, workup and purification by column chromatography the desired transprotected product **90** was obtained as a yellowish solid in a yield of 83%. The aryl bromide **90** was then transformed *in situ* to the corresponding aryl lithium intermediate (with *n*-butyllithium) and subsequent electrophilic trapping with trimethyl borate was performed. The addition of the reagents was done at -78 °C and afterwards the reaction mixture was stirred at room temperature. After quenching with an aqueous saturated ammonium chloride solution and workup the crude product was purified by column chromatography. Besides the by-products

formed, interestingly, this time, the free boronic acid (compound **91**) could be isolated by column chromatography using silica gel as stationary phase. Compound **91** was obtained as a colorless solid in a yield of 12%.

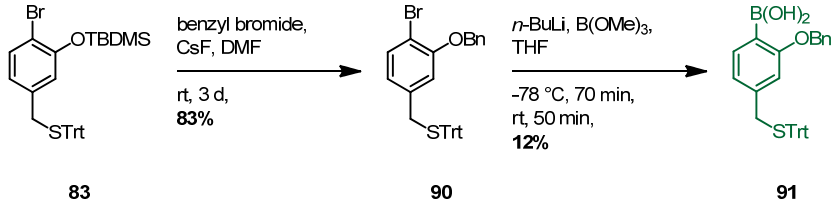

83 **90** **91**

Scheme 75. Transprotection of the phenol derivative **83** and subsequent formation of the boronic acid derivative **91**.

The third building block was successfully synthesized and now it was left to attach it to azo compound **92** in a Suzuki-Miyaura cross-coupling reaction (*Scheme 76*). The in this work successfully applied reagents and conditions were reused ($PdCl_2(PPh_3)_2$ and potassium carbonate in a toluene/ethanol solvent mixture). The reaction mixture was stirred at 65 °C overnight, worked up and purified by column chromatography to obtain the desired intermediate **93** as an orange solid in a very good yield of 98%. In order to increase the amounts of compound **93** the boronic acid **91** was resynthesized, but this time the purification of compound **91** by column chromatography was avoided, since during the purification considerable amounts of the boronic acid **91** were lost. The crude was directly used for the subsequent cross-coupling reaction and again good yields of 94% were obtained for precursor **93**.

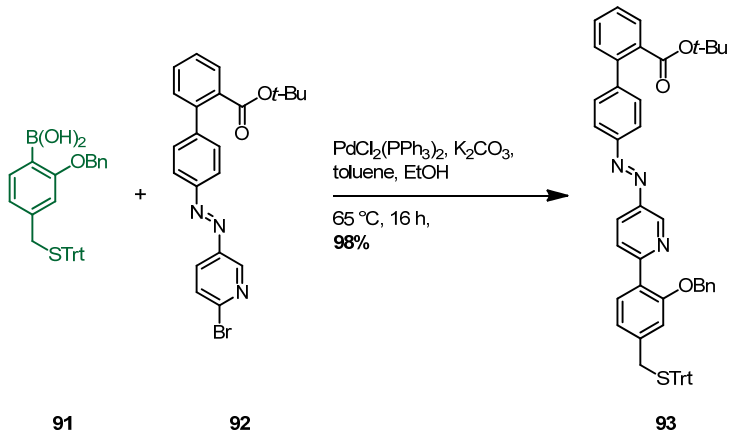

91 **92** **93**

Scheme 76. Suzuki-Miyaura cross-coupling to azo intermediate **93**.

The last steps towards target structure **AZOP 7** is the cleavage of all protecting groups, i.e. the *tert*-butyl, the benzyl and the trityl group. All three protective groups are known to be cleavable with trifluoroacetic acid.[271] Generally, the reactions are proceeded in the presence of cation scavengers, as the formation of *tert*-butyl and/or benzyl carbonium ions during acid-catalyzed

deprotection often leads to *tert*-butylation and/or benzylation of aromatic species present.[344,345] Triethylsilane is known to be an efficient carbocation scavenger,[346] which can trap *tert*-butyl and trityl carbocations. Therefore, intermediate **93** was treated with trifluoroacetic acid and triethylsilane in a dichloromethane solution. After stirring at room temperature for 1.5 hours the reaction mixture was quenched with an aqueous saturated sodium hydrogen carbonate solution. After purification by column chromatography the main product isolated was compound **94** (*Scheme 77*). Under the used conditions only the trityl group was removed. This is probably due to the low concentration of trifluoroacetic acid (4% v/v to dichloromethane) used. The removal of the *tert*-butyl would need a higher concentration of trifluoroacetic acid.[346] However, with compound **94** in hand, deprotection with trifluoroacetic acid was considered anew. This time the cation scavenger triethylamine was replaced by thioanisole, which is an effective scavenger of *tert*-butyl and benzyl groups during acid-promoted deprotections.[347,348] The reaction was performed in pure trifluoroacetic acid and at room temperature for three hours. After quenching and purification by column chromatography the two main products, which had the same R_f-value, were isolated. ^{1}H-NMR spectroscopy studies suggested that one of the two products was the free carboxylic acid- and benzyl-based derivative. The other product could not be identified.

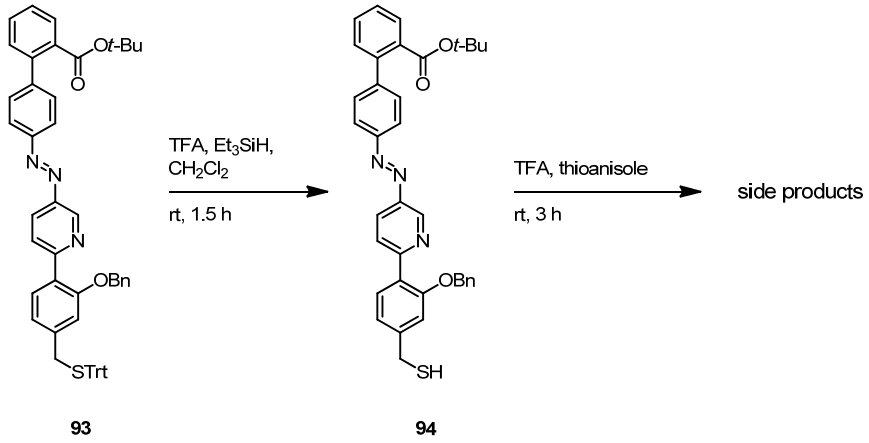

Scheme 77. Attempts to cleave all three protecting groups with trifluoroacetic acid.

The next attempt was the simultaneous deprotection of all three protecting groups of intermediate **93** with trifluoroacetic acid in the presence of two cation scavengers, i.e. triethylsilane and anisole. The reaction mixture was stirred at room temperature for six hours. During these six hours the amount of trifluoroacetic acid was continuously increased, till TLC-monitoring revealed new products formed. One isolated product was identified to be compound **95** as shown in *Scheme 78*. ^{1}H-NMR spectroscopy and mass spectrometry (MALDI-ToF) corroborated the presence of compound **95**.

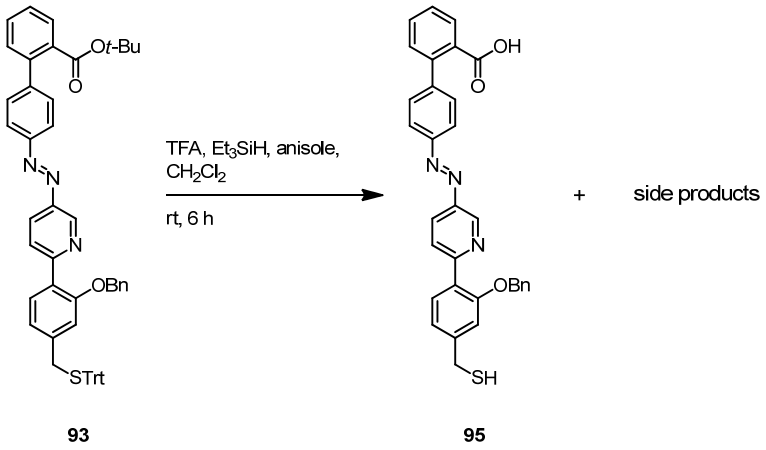

93 **95**

Scheme 78. Further attempts to cleave all three protecting groups with trifluoroacetic acid.

These reactions showed that the attempts to deprotect all protecting groups with trifluoroacetic acid left the benzyl protecting group untouched. Therefore, as an outlook, the deprotection of the alcohol functionality of compound **93** at first was considered, leaving the carboxylic acid's and sulfur's protecting groups intact (*Scheme 79*). Akiyama *et al.* reported on an aluminium trichloride-*N*,*N*-dimethylaniline ether cleavage reagent.[349] This reagent tolerates ester and sulfide functional groups. A successful benzyl deprotection of compound **93** to intermediate **96** would encourage retrying the deprotection of the remaining groups with trifluoroacetic acid in the presence of triethylsilane and anisole towards target structure **AZOP 7**.

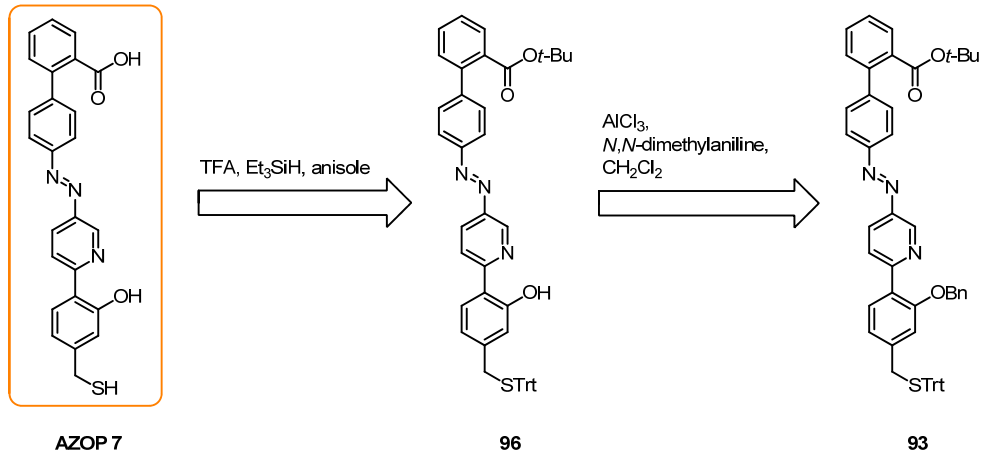

AZOP 7 **96** **93**

Scheme 79. Outlook towards desired target structure **AZOP 7**.

To summarize, the division of the target structure **AZOP 7** in three building blocks and the selective attachment of these units in Suzuki-Miyaura cross-coupling reactions afforded the fully protected precursor **93**. First attempts to remove the deblocking groups have been performed. However, compound **AZOP 7** was until now not synthesized, but a promising synthetic outlook towards **AZOP 7** is given.

3.3.2 UV/Vis, ^{1}H-NMR and X-Ray Analyses

UV/Vis measurements of target compounds **AZOP 4** and **AZOP 5** were performed. The time dependent photoisomerization process of the azo compounds in solution was analyzed. ^{1}H-NMR spectra of each compound (**AZOP 4** and **AZOP 5**) before and after irradiation at 365 nm were recorded. With the shown decrease of the peaks intensities, which correspond to the *trans*-structures, and the increase of the peaks of the *cis*-isomers the *trans*/*cis* amounts of the corresponding isomers were calculated. For **AZOP 4** the solid state structure could be measured by X-ray analysis.

UV/Vis Spectroscopy

Azo compounds **AZOP 4** and **AZOP 5** were analyzed by UV/Vis spectroscopy. The UV/Vis spectra for these azo compounds in a 10^{-5} molar chloroform solution are shown in *Figure 35*. As for compounds **22** and **AZOP 1-3**, **AZOP 4**'s and **AZOP 5**'s characteristic bands are observed at around 350 nm (π-π*-transition) and at 405 nm (n-π*-transition). By irradiating the initially prepared *trans*-form samples at 366 nm, the isomerization process towards the *cis*-isomer is initiated. A decrease of the π-π*-transition band and an increase of the n-π*-transition band is observed with increasing irradiation time. After around 30 to 45 minutes the photostationary state is about to be reached.

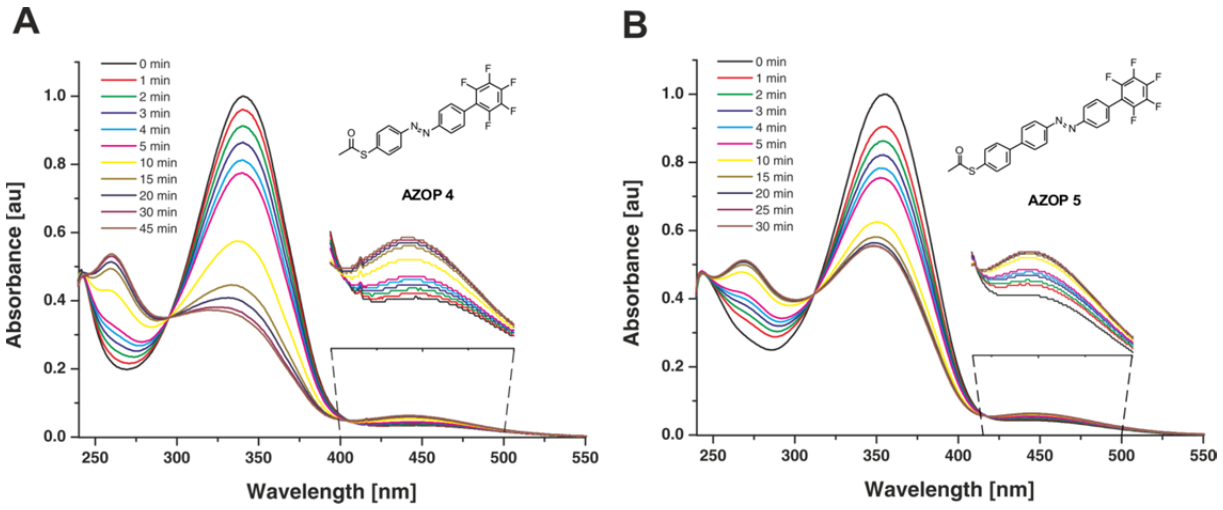

Figure 35. (A) & (B): Time dependent photoinduced *trans* → *cis* switching experiments of **AZOP 4** and **AZOP 5**, which are recorded by UV/Vis spectroscopy. Irradiation wavelength: 366 nm; solvent: chloroform; lamp power: 8 Watt.

^{1}H-NMR Spectroscopy

The *trans* to *cis* photoisomerization of **AZOP 4** and **AZOP 5** were monitored by ^{1}H-NMR. The freshly prepared samples in CD_2Cl_2 (without exclusion of day light) were measured after about five minutes. (green spectra in *Scheme 80*). Each sample was then irradiated at 365 nm for 45 minutes and afterwards directly measured (red spectra in *Scheme 80*). The green spectra correspond to the initial state, where about 99.3% of the *trans*-isomer and 0.7% of the *cis*-isomer are observed in each spectrum before irradiation. After irradiation, **AZOP 4** and **AZOP 5** exhibit 35% and 34% of the *cis*-isomer, respectively. These results were calculated by means of the integrals of clearly defined peaks. The chosen peaks are marked in *Scheme 80* with colored dots. For the azo compounds the protons of the methyl groups were chosen as reference signals.

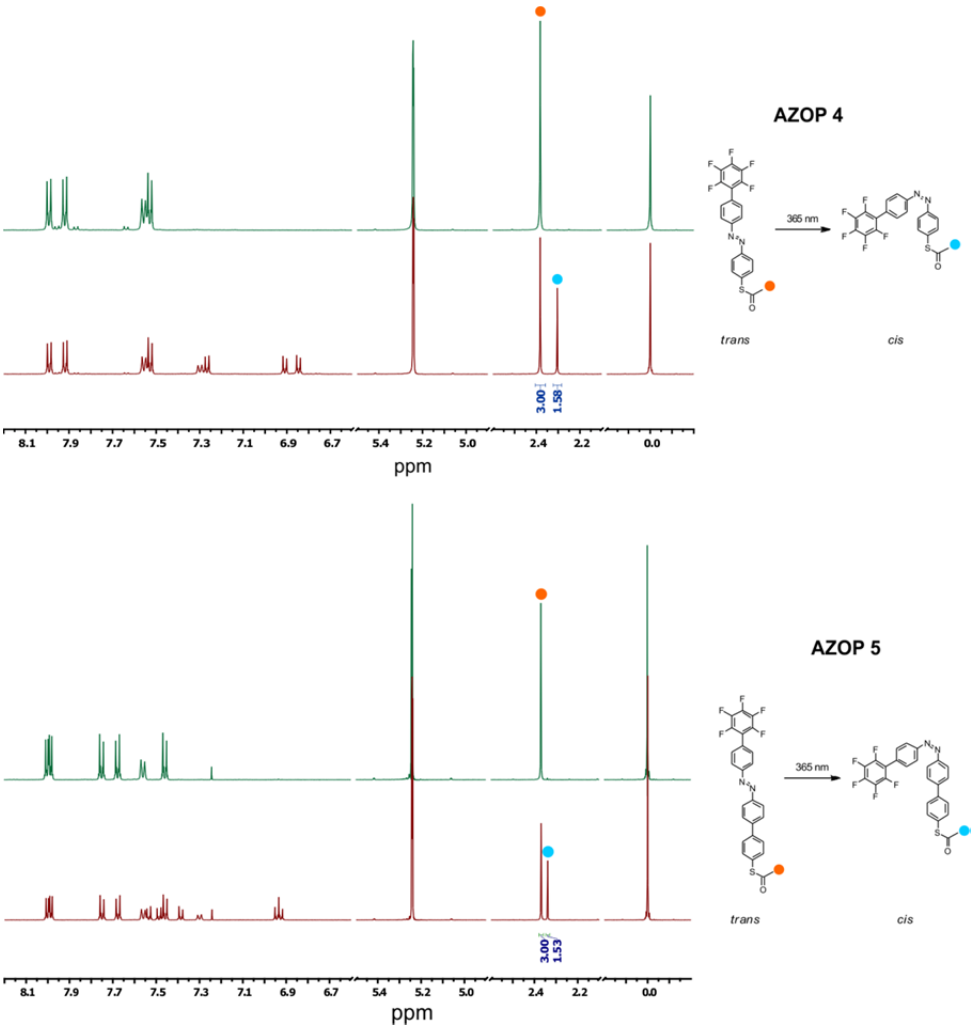

Scheme 80. ^{1}H-NMR spectra of azo compound **AZOP 4** and **AZOP 5** in CD_2Cl_2 recorded on a 500 MHz instrument. Green spectra correspond to freshly prepared samples (predominantly the *trans*-isomer is observed). The red spectra correspond to the samples measured after 45 minutes irradiation at 365 nm. Each green spectrum is compared to the corresponding red spectrum to demonstrate the increasing amount of the *cis*-isomer after irradiation. The colored dots indicate the peaks used for the assignment of the amount of *cis*-isomer. The peaks at 5.24 ppm and 0.00 ppm correspond to the solvent CD_2Cl_2 and the reference tetramethylsilane, respectively. The power of the lamp was 8 Watt.

*Solid State Structure of **AZOP 4***

Single crystals suitable for X-ray analysis were obtained for **AZOP 4** in its *trans*-form by slow evaporation of a saturated deuterated chloroform solution. In *Figure 36* several perspectives of the structures are shown. None of the single phenylene units lay in the same plane. This is the striking difference compared to **AZOP 2** (section 3.2.2), where nearly the whole molecule lies in the same plane. This difference most probably arises from the fluorinated arene units: In section 3.3 the π-π-stacking of fluorinated and non fluorinated arene units was discussed. An example of optimized calculated values was shown in *Figure 30*, where sandwich-like conformations of the two rings, i.e. parallel to each other lying rings, have the lowest energy. The ring distances were calculated to be between 3.5 and 3.6 Å. As one can see in *Figure 36B*, the distances in the solid state structure of **AZOP 4** are 3.696 Å (shown in red). In order to obtain such a conformation with π-π-stacking interactions of fluorinated and non-fluorinated units, the phenyl rings are forced to twist. This could be the reason for the better solubility of **AZOP 4**, compared to the **AZOP 2** reported previously, which has an almost completely planar arrangement of the aromatic moiety.

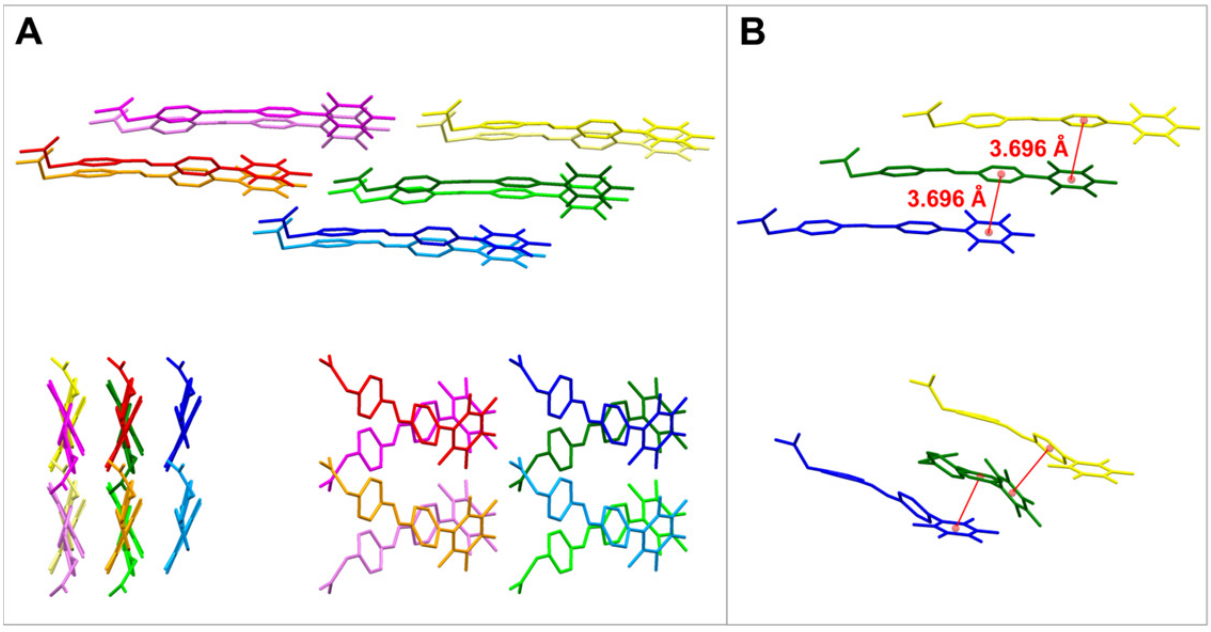

Figure 36. Solid state structure of trans-**AZOP 4** in several perspectives. (A) The packing alignment. (B) π-π-Stacking distances shown in red.

3.3.3 Surface Investigations of AZO 4

The *trans* to *cis* isomerization process of **AZOP 4** in solution was monitored by UV/Vis absorption spectroscopy as shown in section 3.3.2. After about 45 minutes the photostationary state of the **AZOP 4** was reached by irradiating the chloroform solution (10^{-5} M) of **AZOP 4** at a wavelength of 366 nm. The complete back isomerization was achieved with white light within 15 minutes.[350] UV/Vis absorption spectroscopy is also used to monitor the preparation of SAMs.

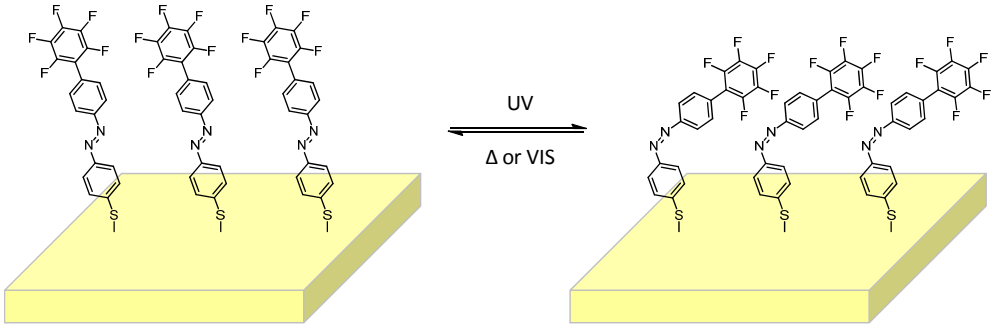

Scheme 81. Schematic representation of the *trans* ⇄ *cis* switching of **AZO 4** on a gold substrate.

The preparation of the **AZO 4**-SAM was accomplished by immersing a freshly evaporated gold substrate in a 0.1 mM solution of **AZOP 4** in chloroform for 48 hours. In order to obtain the *trans*-based **AZO 4**-SAM the SAM preparation was carried out in the dark. After the immersion time the gold substrate was removed from the solution, rinsed with chloroform and dried under a gentle nitrogen stream. The functionalized SAM was characterized by UV/Vis absorption spectroscopy and the corresponding spectrum was compared with the spectrum of the non-functionalized gold substrate (*Figure 37*). The bare gold substrate shows a non-symmetric broad band (black line) centered at about 510 nm. This band is attributed to the gold surface Plasmon resonance (SPR) band.[351] The intensity of this band decreases upon chemisorption of the **AZO 4** onto the gold surface (red line). The decrease of this band intensity is attributed to the formation of the gold-sulfur bond. Furthermore, the spectrum of the functionalized gold substrate reveals a new band with a maximum at 345 nm, which is attributed to the π-π*-transition of the **AZO 4** in the *trans*-state. This new band indicated the presence of **AZO 4**. The decrease of the SRP band and the appearance of a new band at 345 nm indicated the successful formation of an **AZO 4**-SAM.

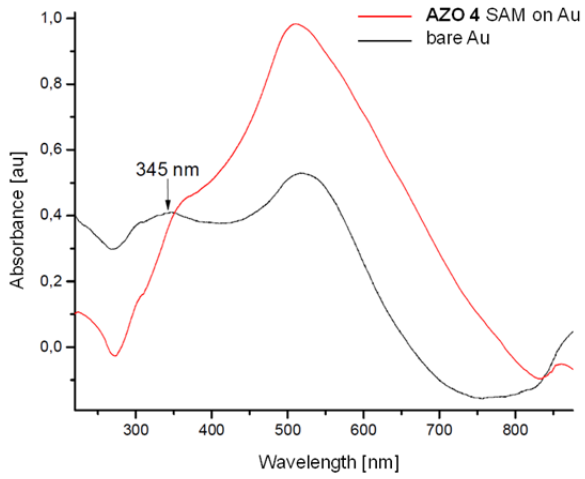

Figure 37. UV/Vis spectra of the bare gold substrate (black curve) and of the **AZO 4**-functionalized gold substrate (red curve).[350]

The **AZO 4**-SAM-formation was also analyzed by water contact angle measurements. A freshly prepared *trans*-**AZO 4**-SAM revealed a strong hydrophobic nature, where the contact angle values were 94.0 ± 2.3°. This value is in agreement with other fluorinated SAMs reported in literature.[352] Furthermore, the *trans* to *cis* isomerization of the chemisorbed **AZO 4** was investigated by this technique. A freshly prepared *trans*-**AZO 4**-SAM was exposed to 365 nm irradiation for two hours and the measured contact angle value changed to 88.0 ± 0.8°. The small difference observed between the contact angle values measured before and after irradiation does not unambiguously prove the occurrence of the *trans* to *cis* isomerization of the chemisorbed molecules, but on the contrary, it does not exclude the possibility that the isomerization change is observable. A hypothesis for the small difference in contact angle values is that the fluorine atoms of the top aromatic unit of **AZO 4** do not completely point to the inside of the monolayer when the molecules adopt the *cis* conformation. Thus, the not hidden fluorine atoms still have an influence on the interactions of the monolayer with the water drop and therefore only a minor change in the wettability is observed. This observation is supported by DFT calculations, which suggest the exposure of some of the fluorine atoms in the *cis*-SAM.

The work function (Φ) of the gold substrate coated with the **AZO 4** monolayer was investigated experimentally and theoretically. It was determined by KP measurements, KPFM, photoelectron spectroscopy (PS) under atmospheric conditions and by EA. In *Table 6* the work function values obtained by the different measuring techniques are summarized.

Table 6. Work function values of **AZO 4**-SAM determined by different techniques.

Measuring technique	Φ_{trans} [eV]	Φ_{cis} [eV]	$\Delta\Phi_{trans\text{-}cis}$ [meV]
EA	5.8 ± 0.1		
KP	5.78 ±0.02	5.75 ± 0.02 (*in-situ*)	30
PS	5.36 ±0.02	5.25 ± 0.02 (*ex-situ*)	110
KPFM	5.50 ± 0.01	5.41 ± 0.01 (*in-situ*)	90
calculation	5.28	5.06	220

The first work function value of the *trans*-based **AZO 4**-SAM was determined by a direct current (DC) voltage scan of the EA signal towards positive bias (*Figure 38*) of a device in which the **AZO 4**-SAM is embedded. The detailed device description can be found in literature (section 3.1.3).[275] The zero crossing voltage (V_{null}) for the **AZO 4**-SAM is 2.20 ± 0.06 eV, which corresponds to Φ = 5.8 ± 0.1 eV. In comparison, a work function value of 5.15 ± 0.10 eV was found for the *trans*-based **CABP**-SAM (section 3.1.3),[275] whose corresponding V_{Null} value is smaller, revealing a large work function shift caused by the fluorinated terminal benzene ring. Macroscopic KP measurements of the *trans*-**AZO 4**-SAM showed a large work function shift of 5.78 ± 0.02 eV when compared to the work function of the bare gold substrate (Φ = 5.12 eV).[275] The work function value is in perfect agreement with the EA results. As demonstrated in *Table 6*, the absolute work function values of the *trans*-**AZO 4**-SAM and *cis*-**AZO 4**-SAM (Φ_{trans} and Φ_{cis}, respectively) and their corresponding changes ($\Delta\Phi_{trans\text{-}cis}$) vary depending on the applied measuring technique (KP, PS and KPFM). For example, as expected, the work function obtained by PS is a few hundreds of meV lower than those measured by KP. This is due to the fact that the KP method measures an average of all work function values and the PS method is sensitive to the lowest work function in the probed area.[276,277] Furthermore, the $\Delta\Phi_{trans\text{-}cis}$ obtained from the different measuring techniques have to be considered independently, as the preparation of the *cis*-based SAM was performed either "*in-situ*" or "*ex-situ*". The *ex-situ* SAM-preparation includes the initial UV-irradiation of the **AZOP 4** in a chloroform solution before starting with the assembly process. However, all techniques displayed higher work function values for the *trans*-isomer-based SAM compared to the corresponding *cis*.

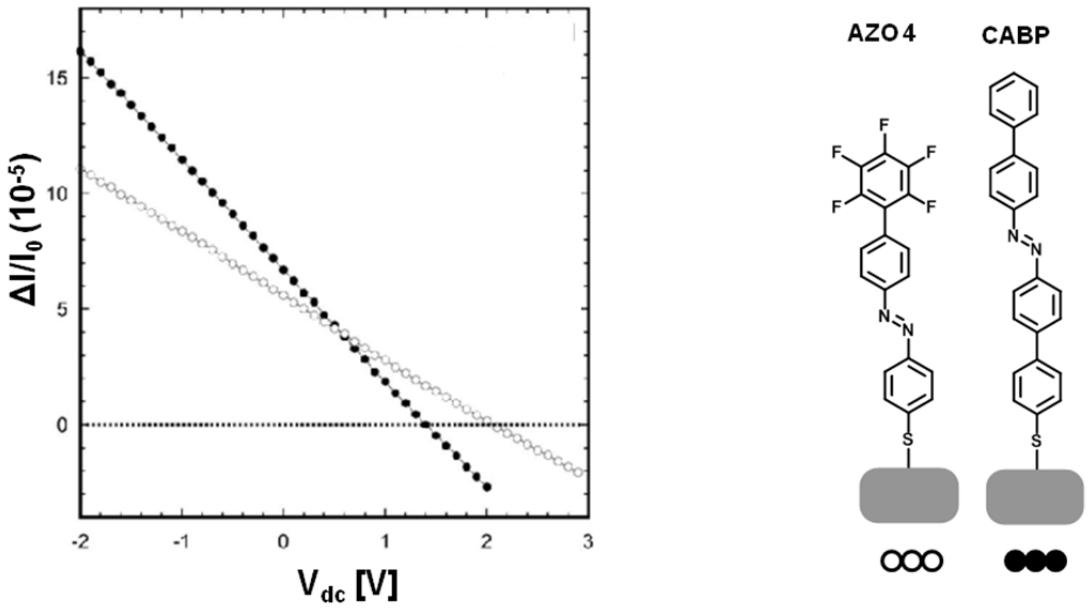

Figure 38. Direct current voltage scans of the EA signal towards positive bias of the ITO/Au/**CABP**-SAM/F8BT/Al device (black circles) and the ITO/Au/**AZO 4**-SAM/F8BT/Al device (white circles). The zero crossing voltages are 1.39 V (translated to Φ = 5.15 ± 0.1 eV) for the **CABP**-SAM and 2.20 V (translated to Φ = 5.80 ± 0.1 eV) for the **AZO 4**-SAM.[350]

Calculated plane average potential profiles associated to the optimized structures of the unit cell for the *trans*- and *cis*-isomers suggest a work function value of 5.28 eV for the *trans*-based SAM and 5.06 eV for the *cis*-based SAM. The trend that the *trans*-SAM-value is higher than the corresponding *cis* supports the experimental measurements. Furthermore, the calculations suggest that the bond dipole induces a counter-acting contribution to the work function compared to the molecular contribution.

In conclusion, it was demonstrate that the energetic and wettability properties of the gold surface can be modified by the functionalization with a fluorinated azobenzene-based monolayer. Moreover, the surface characteristics, especially the work function could be tuned photochemically. The work function trends for the **AZO 4**-based SAM (*trans* vs. *cis*) are opposite compared to the previous findings of the **CABP**-SAM. The absolute work function values of the *cis*-**CABP**-SAM were higher compared to the corresponding *trans*-SAM. Instead, in the here described **AZO 4**-SAM, the gold substrate functionalized with the *trans*-isomer exhibits the higher work function compared to the *cis*-**AZO 4**-SAM. This is attributed to the fluorinated terminal phenyl unit, which features strong electron-withdrawing characteristics. With the experimental measurements used here and the obtained results it could be demonstrated that a proper design of the functional molecules forming the corresponding SAM is crucial to drive the device properties into a specific desired direction.

The investigations of the **AZO 4** were extended revealing further interesting features. Nowadays, two main approaches are followed to increase the efficiency of organic light-emitting diodes (OLEDs): synthesis of conjugated polymers with high photoluminescence efficiency and engineering of device architectures, including electrodes optimization. The latter strategy was pursued by incorporating an **AZO 4**-SAM based gold anode into a polyfluorene-based LED. The device was built up as following: ITO/Au/**AZO 4**-SAM/F8BT/Ca-Al, which is similar as reported previously for the setup for the work function measurements via EA. Additional reference samples were also prepared: a device without a gold film (ITO/F8BT/Ca-Al), a device with a gold film (ITO/Au/F8BT/Ca-Al) and a device which involves a **CABP**-layer functionalized on the gold substrate (ITO/Au/**CABP**-SAM/F8BT/Ca-Al). The first observation was that the functionalization of a gold electrode with the **AZO 4** monolayer influenced the external quantum efficiency (EQE) of the corresponding light-emitting diode. In *Figure 39* the current density (J) and luminance (L) measurements as a function of the driving voltage (V) for all four devices are shown. In both graphs it is clearly observable that as soon as the gold substrate is functionalized, either with the **CABP** or the **AZO 4** layer, the current density and the luminance increases dramatically. The extracted EQEs of the devices are highest for the **AZO 4**-based device (EQE_{ITO} = 0.018%; $EQE_{ITO/Au}$ = 0.006%; $EQE_{ITO/Au/\mathbf{CABP}}$ = 0.004%; $EQE_{ITO/Au/\mathbf{AZO\ 4}}$ = 0.18%;), which represents a ten-fold increase compared to the device of pure ITO and 30 times higher compared to the ITO/Au-based device. In addition, the luminance turn-on voltage (V_{on}),[275] improves for the **AZO 4**-based device, which is associated with the high work function increase of the gold compared to the **CABP**-device. The higher work function values were shown in the EA measurements reported previously ($\Phi_{\mathbf{AZO\ 4}}$ = 5.8 eV), which induce a reduction of the hole injection barrier at the anode. Consequently, the electron(-)-hole(+) balance in the F8BT layer is improved, leading to an increase of the EQE and a reduction of V_{on}.

A further observation was that no alteration in the photoluminescence (PL) and electroluminescence (EL) spectra were detected for all four LED devices. The characterization of the temporal decay of the PL provides evidence that both azo-SAMs do not lead to formation of additional emissive species.

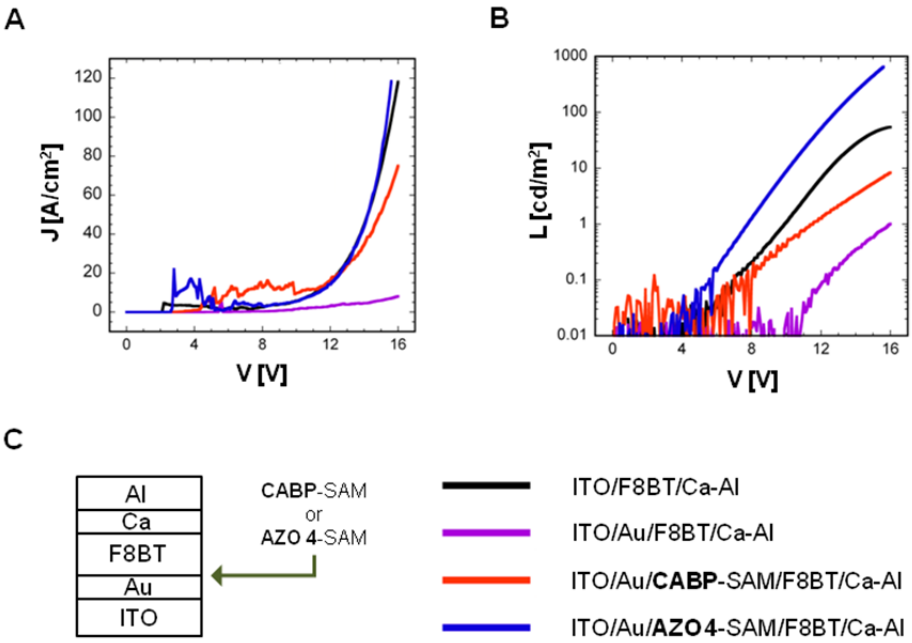

Figure 39. Current density - voltage (A) and (semi-logarithmic) luminance - voltage (B) plots for all four OLEDs. (C) Schematic build up of the OLED devices and corresponding color codes for the specific devices.

The transport properties of the **AZO 4**-SAM were also investigated by incorporating it in between a flat Au(111) surface supported on mica and a liquid compliant eutectic alloy of gallium-indium (GaIn) counter electrode, which forms an oxide layer (Ga_2O_3) in ambient conditions (*Figure 40*). The electrical characterization confirmed that the **AZO 4**-SAM layer only contributes to enhance the hole injection at the anode, without rectifying the current.

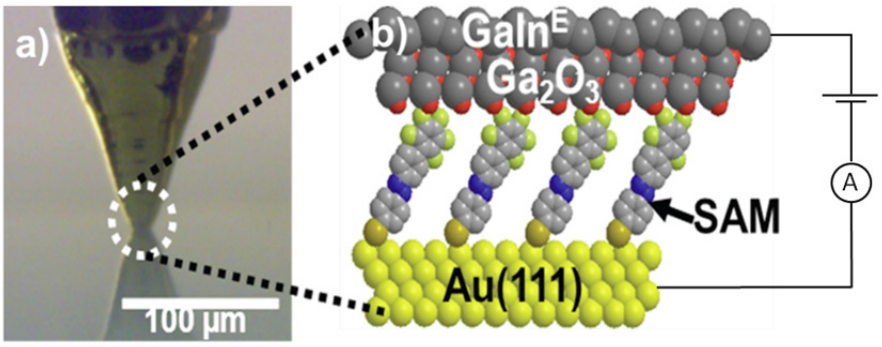

Figure 40. (a) Image of the $GaIn^E$ tip in contact with the **AZO 4**-SAM on Au(111). (b) Schematic representation of the constituents of the Au/**AZO 4**-SAM/Ga_2O_3||$GaIn^E$ junction with the bias' conditions.

In conclusion, the functionalization of a multilayer ITO/Au anode with the **AZO 4**-SAM increased the efficiency of OLEDs based on F8BT. These results, together with the unique property of azo-based SAMs of optically switching the electrode work function, pave the way to the integration of photo-responsive properties into state of the art OLEDs.

3.4 Comparison of UV/Vis Measurements

In *Figure 41* the spectra of the target compounds **AZOP 1-5** in their initial *trans*-form are compared. **AZOP 1** and **AZOP 3** have a similar absorption curve, as both systems bear two biphenyl systems. Their absorption maxima are located at 364 nm. The absorption maxima of **AZOP 2** and **AZOP 4** instead are sifted hypsochromically, due to the smaller conjugation systems, as both have only one biphenyl system. A small difference in the position of the absorption maxima of **AZOP 2** ($\lambda = 345$ nm) and **AZOP 4** ($\lambda = 340$ nm) is observed. This is attributed mainly to the geometry of the aryl units. As in **AZOP 4** the conjugated π-system is planar, where as the system in **AZOP 2** is twisted. These geometries could be seen in the solid state structures of **AZOP 2** and **AZOP 4** by X-ray analysis (section 3.2.2, *Figure 28* and section 3.3.2, *Figure 36*, respectively). The absorption maximum of **AZOP 5** lies in between the biphenyl structures (**AZOP 1** and **AZOP 3**) and the shorter structures (**AZOP 2** and **AZOP 4**), as it combines the properties of a large conjugated system and a presumably non-planar configuration of the π-system.

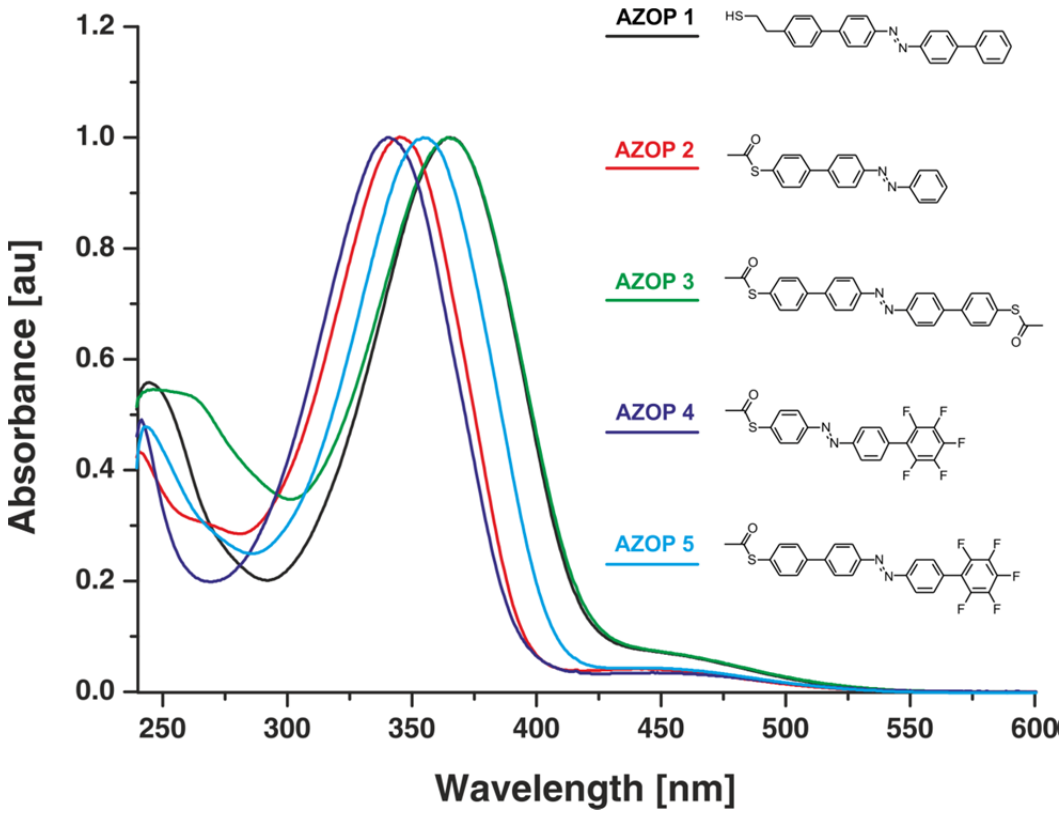

Figure 41. Comparison of the absorption maxima location of the *trans* **AZOP 1**, **AZOP 2**, **AZOP 3**, **AZOP 4** and **AZOP 5**.

3.5 Summary and Conclusion

A new and efficient route to the thiol functionalized azobiphenyl was developed. This "classical" azobiphenyl (**CABP**) was synthesized in the acetyl protected form (**CABP-SAc**), where the Mills reaction to form the asymmetric azobenzene (step b) led to an important modular building block (*Scheme 82*). This asymmetric azo moiety was designed such that selective metal mediated cross-coupling reactions for the attachment of further building blocks can be performed. The **CABP-SAc** was used as precursor for the assembly of the corresponding monolayers on different gold-based devices. Upon photoisomerization of the **CABP** it was shown that the corresponding SAM devices revealed a change in work function, conductance and charge injection barrier. Furthermore, the precipitation and dispersion of **CABP**-coated AuNPs were triggered by light. The coating of microspheres and their incorporation into an electronic device proved anew the capability of the **CABP** to trigger the charge transport through the junction upon external stimuli. The **CABP** was also embedded into field-effect transistor devices, where the source-drain current through the channel could be gated electrically and optically.

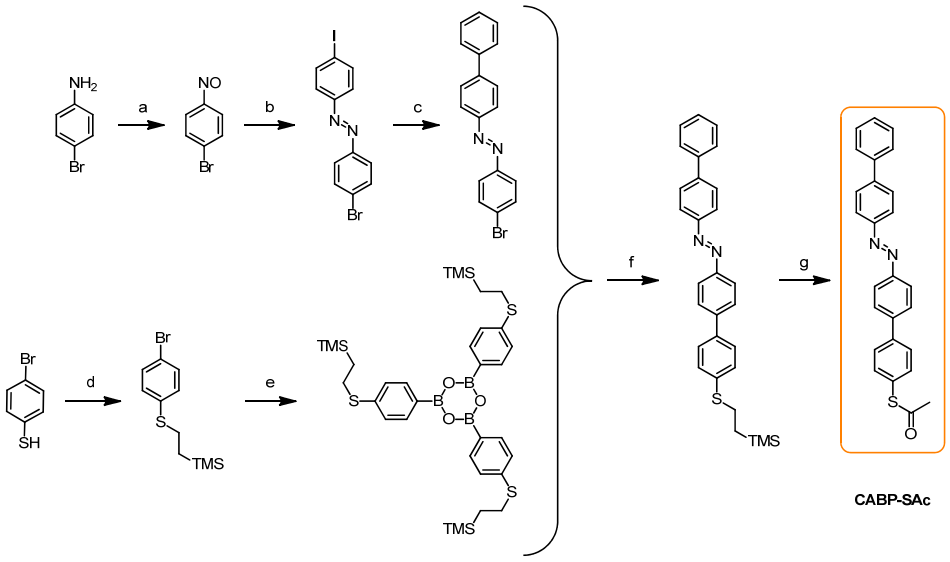

Scheme 82. Synthesis of **CABP-SAc**: *Reagent and conditions:* (a) Oxone®, H_2O, CH_2Cl_2, rt, 5 h; (b) 4-iodoaniline, AcOH, rt, 42 h, 79% over two steps; (c) phenylboronic acid, $Pd(PPh_3)_4$, K_2CO_3, toluene, EtOH, H_2O, 50 °C, 18 h, 96%; (d) vinyltrimethylsilane, di-*tert*-butyl peroxide, 100 °C, 5 h, 87%; (e) *n*-BuLi, $B(O\text{-}iPr)_3$, THF, -78 °C, 2.5 h → -15 °C, 2.5 h → rt, 48 h, 64%; (f) $Pd(PPh_3)_4$, K_2CO_3, toluene, EtOH, 60 °C, 3 h, 80%; (g) tetrabutylammonium fluoride, AcCl, THF, rt, 1.5 h → 0 °C, 1 h, 72%.

Furthermore, several structural modifications of the **CABP** compound have been suggested. Investigation aims such as the crystallinity character of the monolayers, inter- and intramolecular interactions, switching efficiency and metal work function and conductance measurements are proposed. **AZOP 1**, **AZOP 2**, **AZOP 3**, **AZOP 4** and **AZOP 5** were successfully synthesized applying a synthetic strategy that profits from modular building blocks. **AZOP 4**

showed that upon functionalization on gold substrates the metal's work function could be tuned photochemically and that the efficiency of an **AZO 4**-based OLED could be increased. The other synthesized target compounds are under investigation in different research groups. The precursor of **AZOP 7** could be obtained and the synthesis towards the target compound can be seen optimistically. **AZOP 6** could not be synthesized due to solubility issues. The structure as it was first proposed would need dramatic modifications to increase the solubility, which would be in conflict with the scope of investigation aims.

With the surface investigations of the target structure based SAMs we hope to better estimate what kind of molecular components are necessary to fulfill specific desired properties of the devices in order to better control future applications.

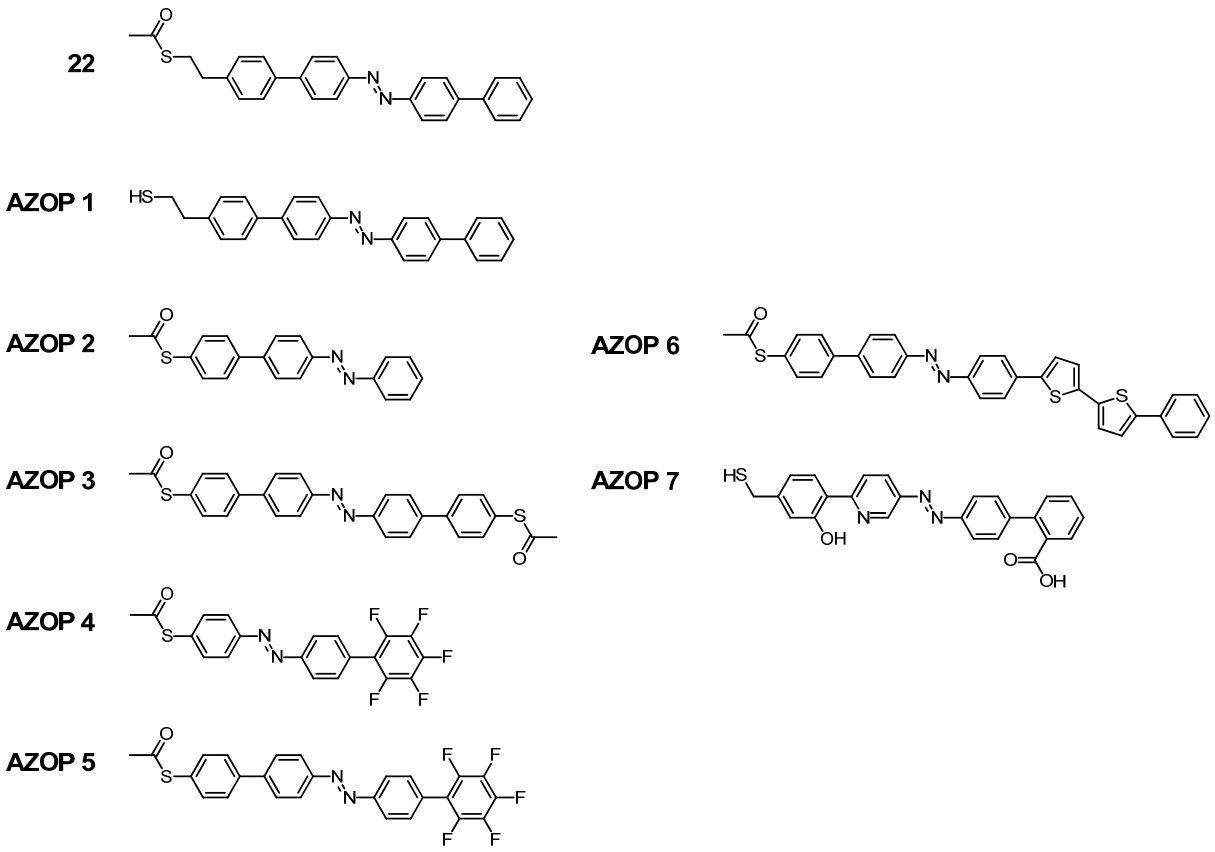

Figure 42. On the left hand side: Synthesized structures. On the right hand side: Synthesis of **AZOP 7** was not completed and synthesis of **AZOP 6** was halted.

Moreover, UV/Vis spectra of compounds **22** and **AZOP 1**-**AZOP 5** were shown, briefly discussed and compared with each other. ^{1}H-NMR studies of the structural isomers of the same compounds were performed, showing the *trans*/*cis* ratios of the corresponding azo compounds after irradiation at 365 nm. The solid state structures of **AZOP 2** and **AZOP 4** could be analyzed by X-ray crystallography.

4 Surface Functionalization with Dithiocarbamates

Dithiocarbamates as anchoring groups have been revisited recently, showing interesting SAM properties. The combination of high thermal and mechanical stabilities of the dithiocarbamate-based SAMs and good electronic coupling of the linker with the metal, make dithiocarbamates appealing functional units for their integration in electronic devices.[47] Although dithiocarbamates have been applied as structural motifs in supramolecular chemistry when forming complexes with transition metal ions,[353,354] until now the investigated diversity of the dithiocarbamate-based molecule architectures on flat gold substrates is very limited.[44–47,247,264] Here, we report on the design, synthesis and characterization of tailor-made derivatives for the tuning of the electronic properties of dithiocarbamate-based SAMs. In particular the variation of the molecular backbone's architecture is envisaged. A screening of the contribution of the molecule's dipole moment to the work function of a functionalized metal is considered. Furthermore, with some of the target structures the investigations will be extended to the exploration of rectification properties in metal-molecule junctions. For this purpose an appealing new junction set-up for the electronic characterization of a metal-film/film-metal junction is designed. The research activity of the surface functionalization with dithiocarbamate-based structures was done in collaboration with the Material Science Laboratory of SONY Deutschland GmbH. The synthesis of the desired structures is performed in the group of Prof. Marcel Mayor and the physical measurements and surface characterizations, including XPS, UPS and STM, are performed in Stuttgart at the Material Science Laboratory SONY by Dr. F. von Wrochem and Dr. W. Ford.

In the following sections the target structures of SONY Deutschland GmbH will be introduced. The molecular backbone variations will give an insight to what extent the corresponding SAMs tune the metal's work function. Furthermore, rectification concepts in a novel setup are presented. The aim of this project is the screening of suitable building blocks for modulating the metal's work function and the search for applicable concepts to enrich molecular film devices with additional electronic properties. With the benefits it is expected to increase the luminance and efficiency of OLEDs and to reduce the injection barrier between the source/drain electrodes and the organic semiconductor in thin film transistors (TFTs).

4.1 Work Function Tuning of Gold Substrates

In order to improve the device performance of molecular film junctions it is important to control the metal's work function. Several aspects influence the metal's work function when functionalizing the metal with a monolayer. There are two major contributions of the SAM that affect the metal's work function. The shift of the work function can be induced firstly upon formation of the metal-linker bond, as electronic reorganization occurs implying a bond dipole. Secondly, a molecular contribution arising from the overall dipole moment of the molecular structure is able to modify the metal's work function. The investigation on the latter contribution is of interest in this project, as the contribution to the work function induced by the metal-linker bond will be similar for all target structures as they all bear a dithiocarbamate anchoring group. The work function depends as follows on the dipole moment of the molecular structure: A negative dipole moment (i.e. the partial negative part of the molecule is located at the SAM's outer surface) induces an upward shift of the E_{vac} (outside) relative to the E_{vac} (metal) and thus a positive work function shift. Instead, a positive dipole moment of the molecule induces a negative work function change. The Material Science Laboratory of SONY Deutschland GmbH has performed preliminary work function investigations of gold substrates, which were assembled with dithiocarbamate-based structures. The experimental work function values obtained by UPS measurements are plotted against the calculated dipole moment values of the corresponding structures as shown in *Figure 43*. A trend of an increasing work function value with decreasing the dipole moment is observed. The goal here is now to enlarge the scope of possible structures that modulate the work function values. Exemplarily, acetylene-phenylene-piperazine-based structure with a trifluoropyridinium borate tail group (**DTC 1**, *Figure 44*) is depicted in the plot of *Figure 43*. The calculated dipole moment value of μ = -12.66 D is expected to contribute to a work function value of Φ = 5.6 eV, which is about 0.5 eV higher than the value of a clean gold electrode.

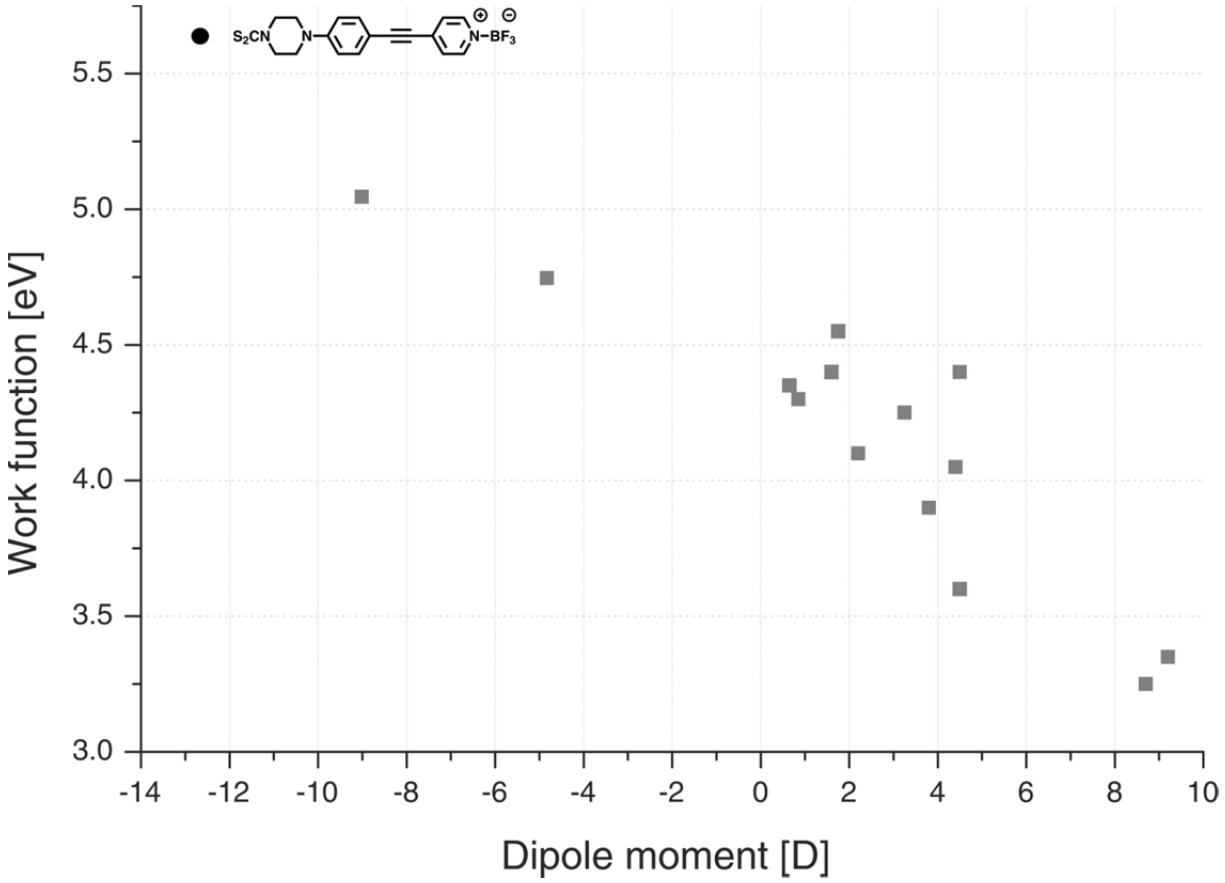

Figure 43. Preliminary work function investigations of gold surfaces with dithiocarbamate based monolayers performed by the Material Science Laboratory of SONY Deutschland GmbH. Plot of the work function against the calculated dipole moment. The work function value of the black structure (circle) is estimated and the work function values of the gray squares are obtained by UPS measurements.

Based on these studies, the synthesis, assembly and subsequent surface measurements of the new target compounds, which are shown in *Figure 44*, are envisaged. The molecular tail group is varied by introducing different substituents. Depending on their electronic nature they will induce a more negative or positive dipole moment. The trifluoropyridinium borate derivative **DTC 1** and the nitro derivative **DTC 2** are considered to induce negative dipole moments as they bear electron withdrawing substituents at the tail and therefore the work function of the gold substrate should be increased. In contrast, the amino **DTC 3**, the julolidine **DTC 4** and the alkoxy **DTC 5** derivatives are calculated to have a positive dipole moment. The aim here is a deeper understanding of the tunability of the metal's work function.

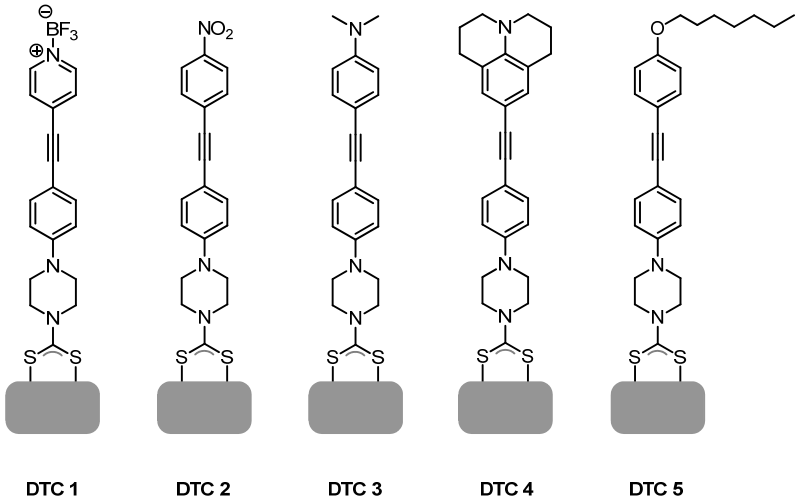

Figure 44. Envisaged target structures for tuning the metal's work function.

4.1.1 Synthesis and Characterization

The target structures will be delivered as free piperazine derivatives, as shown in *Figure 45*. These dithiocarbamate precursors (≙ **DTCP**s) will be transformed *in situ* with carbon disulfide during the assembly process to the corresponding final dithiocarbamates (**DTC**s).

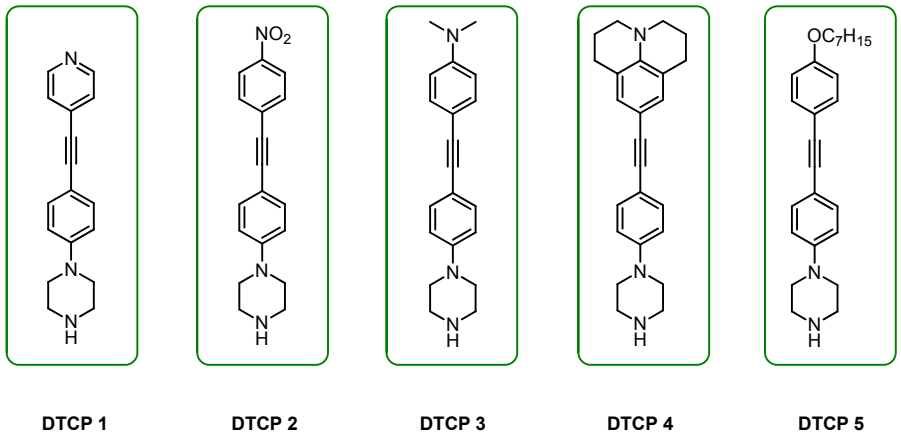

Figure 45. Target compounds for work function investigations.

All dipolar **DTCP** compounds bear the same structural motif, which is the acetylene-phenylene-piperazine building block. Therefore, a modular synthetic pathway towards the target structures is proposed (*Scheme 83*). There are two possible ways to the target structure **97**, both starting from the commercially available 1-(4-bromophenyl)piperazine (**98**). The direct Sonogashira cross-coupling reaction to give target **97** starting from compound **98** with an acetylene building block **99** is one possible route. The acetylene unit **99** will bear the desired substituent, preferably with strong electron donating properties, as in Sonogashira cross-coupling reactions

the acetylene acts as the "organic nucleophile". The other pathway is mechanistically profitable when the haloarene **101** bears a strong electron deficient substituent in *para* the position to enhance the oxidative addition in the catalytic cross-coupling cycle. Theoretically both pathways are possible, but the choice of which route to take is not only affected by the nature of the substituents. The advantages of the availability of the building blocks and the commercial starting materials will also be considered.

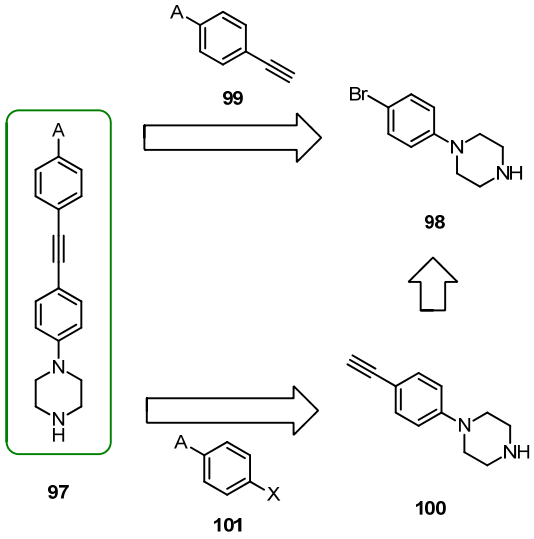

Scheme 83. General synthetic strategy to the **DTCP** compounds, where X = halogen and A = desired substituent. Two possible routes towards the general structural motif **97** are possible.

*Synthesis of **DTCP 1***

DTCP 1 bears a pyridine unit at the end of the acetylene-phenylene-piperazine building block. After assembling this structure to a surface it will be treated with boron trifluoride etherate in order to attach the BF_3-unit *in situ* to the pyridine moiety to obtain **DTC 1** (*Figure 44*).

The route via intermediate **99** starting from compound **98** was chosen for the synthesis of **DTCP 1**, as 4-ethynylpyridine is known to decompose fast and as it has to be synthesized first in two steps.[355] Furthermore due to the electronic nature of the pyridine it is suggested to be a suitable organic electrophile in the haloarene unit.

The piperazine of starting compound **98** will first be protected. Piperazine derivatives are soluble in aqueous media as well as in specific organic solvents. Thus the protection of the free amine of the piperazine assures the solubility of the compound only in the organic media and consequently facilitates aqueous workup steps. Furthermore, the protected piperazine can easily be purified by column chromatography using silica gel as the stationary phase. The elution of the

deprotected species is namely known to be slow even when using very polar solvents. The piperazine was therefore protected with a Boc-group, as it is easily introduced with the corresponding anhydride and removed efficiently under acidic conditions.[271] Thus, the commercially available 1-(4-bromophenyl)piperazine (**98**) was dissolved in dichloromethane and while cooling the solution it was treated with di-*tert*-butyl dicarbonate and stirred for 1.5 hours (*Scheme 84*). The crude was purified by column chromatography to obtain the protected intermediate **102** quantitatively as a colorless solid.

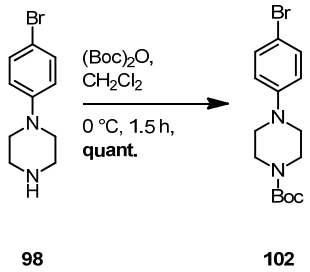

98 **102**

Scheme 84. Protection of the free amine of the piperazine derivative **98**.

The next step is the introduction of the acetylene moiety. This is suggested to be performed in a Sonogashira cross-coupling reaction with trimethylsilylacetylene. Standard Sonogashira cross-coupling conditions include the presence of an amine base, a palladium catalyst and of the co-catalyst copper iodide. Here it was proposed to avoid the co-catalyst for two main reasons: First of all, the presence of copper iodide is known to promote the catalytic reaction in Sonogashira cross-coupling reactions, but it also favors the homocoupling of trimethylsilylacetylene in the presence of traces of oxygen. Copper(I) is known to catalyze the formation of diacetylenes, in a Glaser coupling.[356] Furthermore, the related Hay coupling, where the catalyst is a copper complex, also forms diacetylenes.[357] The copper complex is often formed from copper(I) (or even copper(II)) and aliphatic tertiary amines, as for example tetramethylethylenediamine (TMEDA) and pentamethyldiethylenetriamine (PMDTA) (see *Scheme 85*).[358] TMEDA and PMDTA are often used as bi- and tridentate ligand, respectively, for better solubility of the copper(I) in organic solvents. As substituted piperazines bear two tertiary amines, which are connected to each other aliphatically, a possible complexation of the copper with the piperazine derivative **102** may be possible.

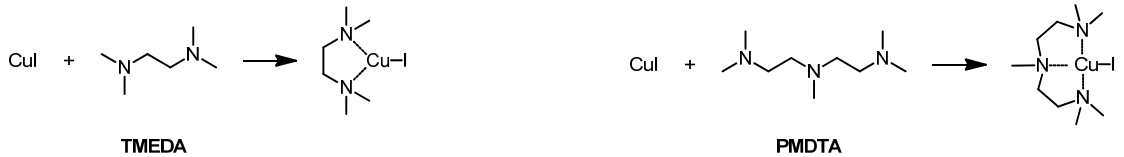

Scheme 85. Copper(I) complexes with tetramethylethylenediamine (TMEDA) and pentamethyldiethylenetriamine (PMDTA).

Therefore, in order to avoid the possible formation of diacetylenes and the complexation of the copper(I) species and these by hindering the Sonogashira cross-coupling reaction, the reagents of the envisaged attachment of trimethylsilylacetylene to compound **102** were modified. Alami *et al.* reported on a rapid copper free reaction of aryl halides with terminal alkynes to give aryl acetylenes when using a palladium catalyst and pyrrolidine as base.[359] These conditions were applied for the reaction of compound **102** with trimethylsilylacetylene. To the reactants, which were dissolved in *N*,*N*-dimethylformamide, $Pd(PPh_3)_4$ and pyrrolidine were added (*Scheme 86*). The reaction mixture was stirred at 70 °C for two days. After workup and purification by column chromatography the desired intermediate **103** was obtained as a yellowish solid in a yield of 79%. The TMS-protecting group of compound **103** was cleaved in the presence of potassium carbonate in a methanol solution. After stirring for 1.5 hours at room temperature, workup and purification by column chromatography the desired free acetylene **104** was isolated as a colorless solid in a yield of 94%.

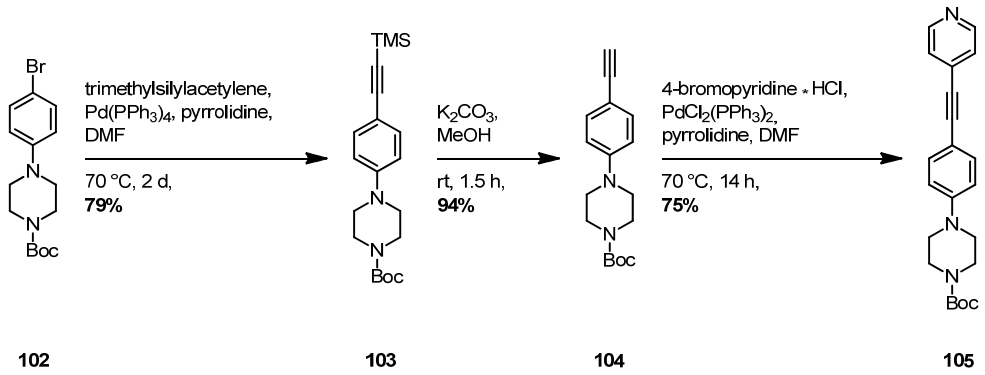

Scheme 86. Synthesis of compound **103** with copper free conditions and subsequent cleavage of the TMS-group of compound **103** for the Sonogashira cross-coupling reaction with 4-bromopyridine to intermediate **105**.

The pyridine moiety was attached in a Sonogashira cross-coupling reaction using the commercially available 4-bromopyridine hydrochloride. Similar copper free conditions as described above were applied and the catalyst was changed from $Pd(PPh_3)_4$ to $PdCl_2(PPh_3)_2$. The desired pyridine derivative **105** was formed and it was isolated after workup and purification by column chromatography as a yellowish solid in a yield of 75%.

The last step towards the target structure **DTCP 1** is the deprotection of the piperazine. The Boc-protecting group is often cleaved with trifluoroacetic acid.[271] Under these conditions compound **105** was stirred with trifluoroacetic acid in tetrahydrofuran for 3 hours at room temperature. The target molecule **DTCP 1** was not formed. Instead, ketone **106** was isolated after workup and purification by column chromatography as the main isolated product (*Scheme* 87).

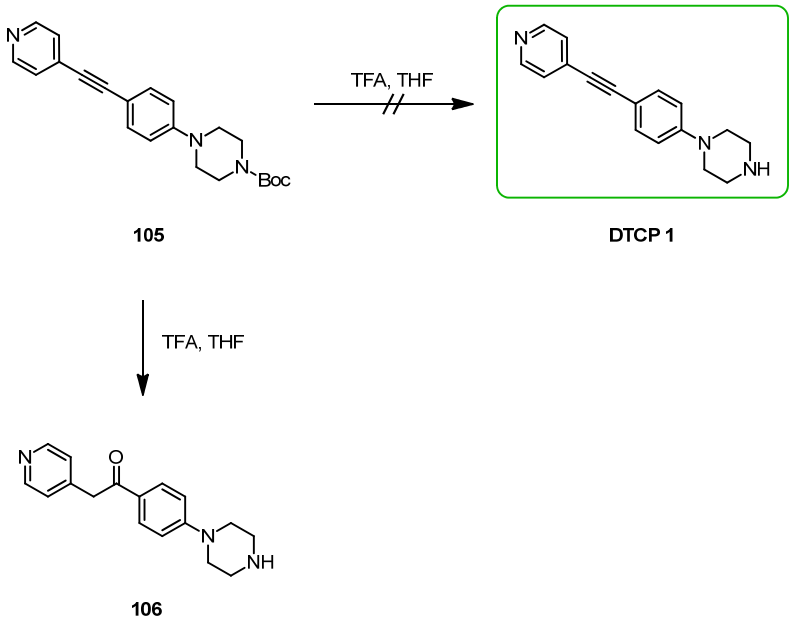

Scheme 87. Formation of the side product **106** during the attempt to deprotect compound **105** with trifluoroacetic acid.

The formation of this by-product is the consequence of an addition-hydrolysis reaction. Beside the cleavage of the Boc-protecting group, trifluoroacetic acid can also attack the triple bond of the acetylene, especially when the aryl moieties attached to the ethynylenes are electron rich.[360] The proposed addition-hydrolysis reaction is shown in *Scheme 88*. After the hydrolysis of intermediate **107** to form compound **108**, keto-enol tautomerism leads to the compound **106**. Furthermore, the deprotection of the Boc-group with other acids, as for example hydrochloric acid, did not lead to the desired acetylenes. The formed by-products could not be completely identified, but NMR-spectroscopy (^{1}H- and ^{13}C) revealed that the triple bonds were not maintained. However, the assembly of compound **106** onto a gold substrate and its work function measurements is also considered. With the corresponding measurements insights to this new compound class can be obtained.

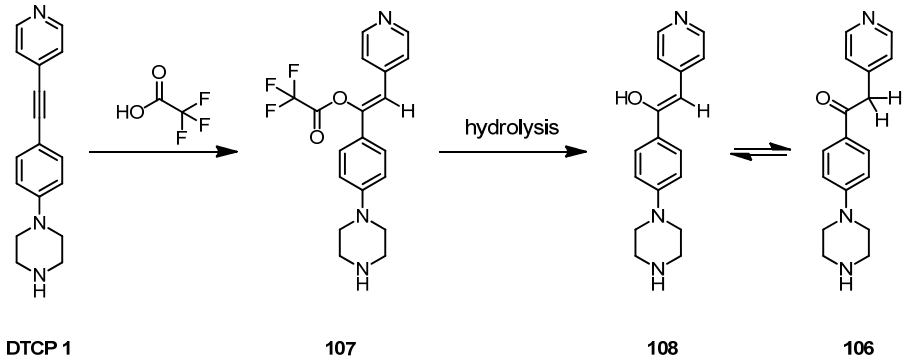

Scheme 88. Proposed mechanism for the formation of the product **121**.

At this stage, as the other **DTCP**s (**DTCP 1**-**5**) with different aryl moieties attached to the ethynylene unit also have to be synthesized in the course of this work, another strategy towards the target structures was considered. A modular synthetic procedure was still desired and thus it was decided to repeat the whole reaction sequence without protecting the piperazine at the beginning. The deprotection of the Boc-group in the last step towards the target structures can thus be avoided.

As the copper free conditions from Alami *et al.* were successfully applied before, it was envisaged to reuse them. Hence, starting material **98** was reacted with trimethylsilylacetylene using $PdCl_2(PPh_3)_2$ as catalyst and pyrrolidine as base in *N*,*N*-dimethylformamide (*Scheme 89*). Stirring at 65 °C for 20 hours led after workup and purification by column chromatography to the desired free piperazine intermediate **109** as a yellow solid in a yield of 80%. The TMS-group of structure **109** was cleaved with potassium carbonate in methanol at room temperature in two hours. Workup and purification by column chromatography gave the free acetylene **100**, which was isolated as a yellowish solid in a yield of 74%. The last coupling step of intermediate **100** and 4-iodopyridine in a Sonogashira cross-coupling reaction led to target structure **DTCP 1**. Compound **100** and pyrrolidine were dissolved in dry *N*,*N*-dimethylformamide and the solution was degassed. Under an inert atmosphere 1.3 equivalents of 4-iodopyridine and subsequently catalytic amounts of $PdCl_2(PPh_3)_2$ were added and the resulting reaction mixture was heated to 50 °C for two hours. After extraction and workup the crude product was purified by column chromatography to afford the desired target structure **DTCP 1** as a yellowish solid in a yield of 84%.

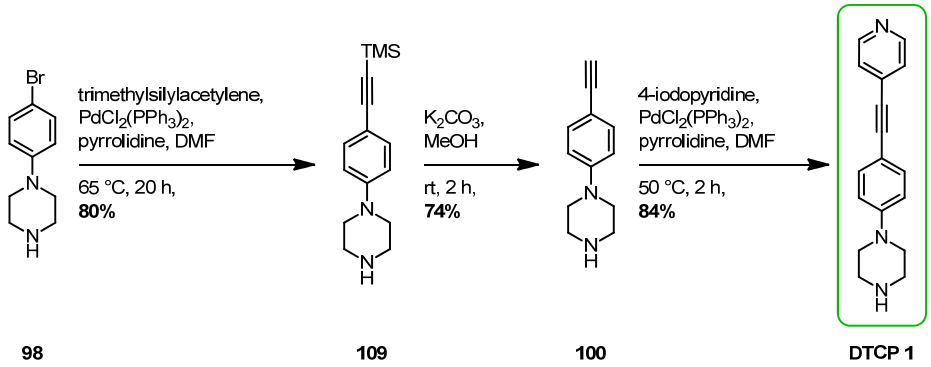

Scheme 89. Synthesis sequence to target compound **DTCP 1.**

To summarize, the pyridine-based structure **DTCP 1** was successfully synthesized in three steps without amine protection chemistry in an overall yield of 50%. **DTCP 1** was fully characterized by NMR spectroscopy (^1H and ^{13}C), EI-MS and EA. Following this modular synthetic strategy the next **DTCP**s were envisaged.

The initial protection of the piperazine proved to cause problems during the deprotection of the Boc-group in the presence of acetylene units. However, the isolated and characterized (^{1}H- and ^{13}C-NMR and EI-MS) ketone product **106**, which was formed during the attempt to deprotect the amine with trifluoroacetic acid, was also sent to the Material Science Laboratory SONY for surface investigations.

*Synthesis of **DTCP 2***

Target compound **DTCP 2** bears the most electron deficient top arene unit compared to the other **DTCP**s (**DTCP 1** and **DTCP 3**-**5**). Due to this property the synthetic route via intermediate **100** (see *Scheme 83*) was chosen, as for **DTCP 1**. The nitro group is an electron withdrawing substituent and if it is incorporated in *para*-position to the aryl halogen it would activate the aryl moiety for the oxidative addition process in cross-coupling reactions. Mechanistically 1-halo-4-nitrobenzene would act as the organic electrophile.

As compound **100** was previously synthesized, it was suggested to react it in a Sonogashira cross-coupling reaction with the commercially available 1-iodo-4-nitrobenzene. Liang *et al.* reported on modified palladium-catalyzed Sonogashira cross-coupling reactions under copper-, amine and solvent-free conditions.[361] They had performed several screenings of phenylacetylenes with aryl halides, including 1-iodo-4-nitrobenzene and 1-bromo-4-nitrobenzene, affording the desired products in high yields and in short reaction times. Thus, the same regents and conditions were applied for the reaction of compound **100** with 1-iodo-4-nitrobenzene (*Scheme 90*). To the starting materials were added tetrabutylammonium fluoride trihydrate as base and subsequently $PdCl_2(PPh_3)_2$ as catalyst. The reaction mixture was heated to 80 °C for one hour and afterwards purified by column chromatography. The desired target molecule **DTCP 2** was isolated as a reddish solid in a yield of 61%.

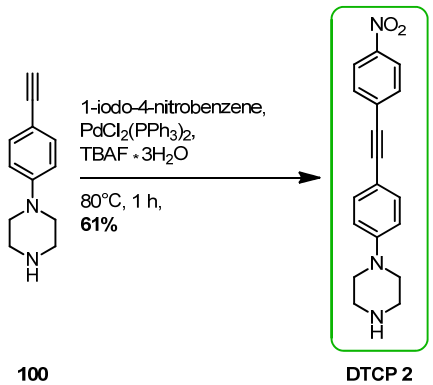

Scheme 90. Sonogashira cross-coupling reaction to target structure **DTCP 2**.

The nitro compound **DTCP 2** was successfully synthesized in two steps. With acetylene building block **100** in hand only one additional step was required (overall yield of 36%). This step included a copper-, amine and solvent-free reaction using a palladium catalyst and tetrabutylammonium fluoride as base. The characterization of **DTCP 2** was accomplished by ^{1}H- and ^{13}C-NMR spectroscopy and EI-MS.

The next three target structures **DTCP 3**, **DTCP 4** and **DTCP 5** have electron donating substituents on the molecular backbone. Due to these similarities the same synthetic route to the target compounds was proposed. The *N*,*N*-dimethyl, julolidine and the alkoxy aryl moieties will bear the free acetylene unit for the envisaged coupling with the commercially available 1-(4-bromophenyl)piperazine (**98**).

*Synthesis of **DTCP 3***

A one step synthesis to **DTCP 3** was performed with the commercially available 4-ethynyl-*N*,*N*-dimethylaniline (**110**) and 1-(4-bromophenyl)piperazine (**98**). In a copper free Sonogashira cross-coupling reaction the compound **98**, 1.5 equivalents of compound **110** and pyrrolidine were dissolved in dry *N*,*N*-dimethylformamide. The solution was degassed and thereafter catalytic amounts of $PdCl_2(PPh_3)_2$ were added under an inert atmosphere. The reaction mixture was stirred at 70 °C for 22 hours. After workup and purification by column chromatography the desired target molecule **DTCP 3** was isolated as a brownish solid in a yield of 56%. Compound **DTCP 3** was characterized by ^{1}H- and ^{13}C-NMR spectroscopy and EI-MS.

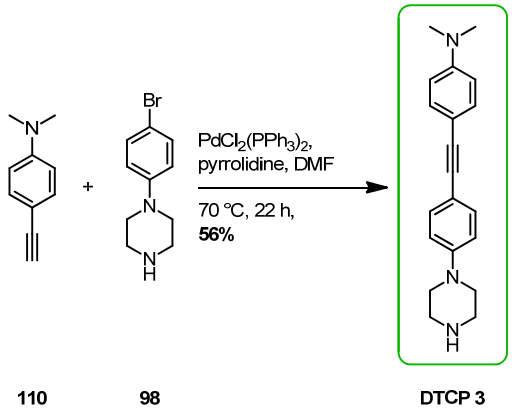

Scheme 91. Synthesis of target molecule **DTCP 3**.

*Synthesis of **DTCP 4***

The julolidine-phenylene-acetylene moiety had to be synthesized first before performing the cross-coupling reaction with compound **98**. The first synthesis step was the bromination of julolidine (**111**) (*Scheme 92*). This was performed with 2,4,4,6-tetrabromo-2,5-cyclohexadienone in dichloromethane. Following a literature procedure[362] the addition of one equivalent of the bromine source was performed at -10 °C and afterwards it was stirred at room temperature for 2.5 hours. After basic workup and purification by column chromatography the brominated julolidine **112** was obtained as a colorless liquid in a yield of 42%. After bromination the attachment of the acetylene was performed. Compound **112** was dissolved in triethylamine, which served as base and simultaneously as solvent and the solution was degassed. Afterwards an excess of trimethylsilylacetylene, the catalyst $Pd(PPh_3)_4$ and the co-catalyst copper iodide were added under an inert atmosphere and the resulting reaction mixture was stirred at 75 °C for 17 hours. After workup and purification by column chromatography the desired acetylene intermediate **113** was obtained as a yellowish viscous liquid in a yield of 91%.

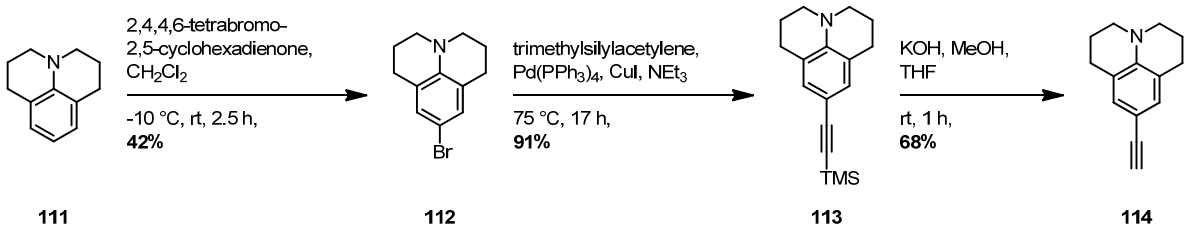

Scheme 92. Bromination of julolidine (**111**), attachment of the acetylene and subsequent cleavage of the TMS-protecting group afforded intermediate **114**.

The deprotection of the TMS-group of compound **113** was accomplished with potassium hydroxide in a methanol/tetrahydrofuran solvent mixture at room temperature in one hour. After workup and purification by column chromatography compound **114** was obtained as a yellow oil in a yield of 68%. The last step to target structure **DTCP 4** was a Sonogashira cross-coupling reaction applying the previously reported copper free reagents and conditions. The acetylene **114** and 1.3 equivalents of 1-(4-bromophenyl)piperazine (**98**) were dissolved in *N*,*N*-dimethylformamide, and pyrrolidine and $PdCl_2(PPh_3)_2$ were then added after degassing the solution. The corresponding reaction mixture was stirred at 70 °C for 22 hours (*Scheme 93*). After workup and purification by column chromatography the aimed julolidine structure **DTCP 4** was isolated as a brownish solid in a yield of 52%. The julolidine compound **DTCP 4** was synthesized in a total of four steps in an overall yield of 14% and it was characterized by ^{1}H- and ^{13}C-NMR spectroscopy and EI-MS.

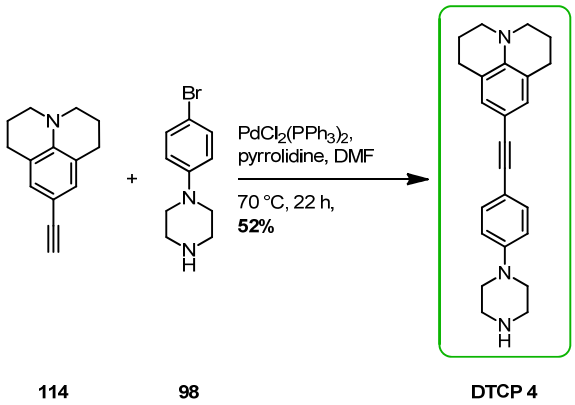

Scheme 93. A Sonogashira cross-coupling reaction to the target julolidine compound **DTCP 4**.

*Synthesis of **DTCP 5***

Target compound **DTCP 5** was synthesized in four steps starting from the commercially available 4-bromophenol (**115**) (*Scheme 94*). 4-Bromophenol performed an S_N2-reaction with commercially available 1-bromoheptane in the presence of potassium carbonate. 4-Bromophenol (**115**), a slight excess of 1-bromoheptane, potassium carbonate and catalytic amounts of potassium iodide were added in dry tetrahydrofuran into a microwave vial. The vial was exposed to microwave irradiation at 170 °C for 1 hour. After workup the crude product was not further purified to afford 1-bromo-4-(heptyloxy)benzene (**116**) as a colorless solid in a yield of 72%. The next reaction was a Sonogashira cross-coupling reaction of compound **116** with trimethylsilylacetylene. Compound **116** and triethylamine were dissolved in dry tetrahydrofuran. After degassing the solution catalytic amounts of $PdCl_2(PPh_3)_2$ and copper iodide were added under inert atmosphere. The reaction mixture was stirred at 70 °C for 20 hours and after workup and purification by column chromatography the acetylene intermediate **117** was isolated as a yellowish oil in a yield of 47%. Subsequent cleavage of the TMS-protecting group was performed with potassium carbonate in a methanol solution. After workup and purification by column chromatography the desired deprotected acetylene **118** was isolated as a colorless liquid in a yield of 93%.

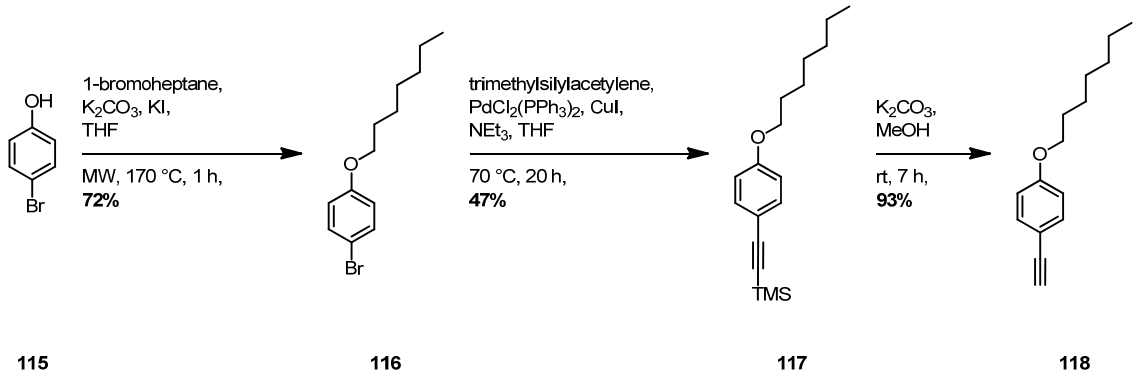

Scheme 94. Synthesis sequence to acetylene **118**.

The last step to target compound **DTCP 5** was the cross-coupling of acetylene **118** with 1-(4-bromophenyl)piperazine (**98**). The catalyst $PdCl_2(PPh_3)_2$ and the base pyrrolidine were used again, as they proved to be adequate when using piperazine building blocks.

Acetylene **118**, pyrrolidine and a slight excess of compound **98** were dissolved in dry *N*,*N*-dimethylformamide. After degassing the solution catalytic amounts of $PdCl_2(PPh_3)_2$ were added under an inert atmosphere and the resulting reaction mixture was stirred at 65 °C for 20 hours. After workup and purification by column chromatography the desired alkoxy target compound **DTCP 5** was obtained as a yellowish solid in a yield of 41%.

DTCP 5 was synthesized in a total of four steps in an overall yield of 13%. The last step included once again the successfully applied copper free reagents for the Sonogashira cross-coupling reaction. **DTCP 5** was fully characterized by ^{1}H- and ^{13}C-NMR spectroscopy, EI-MS and EA.

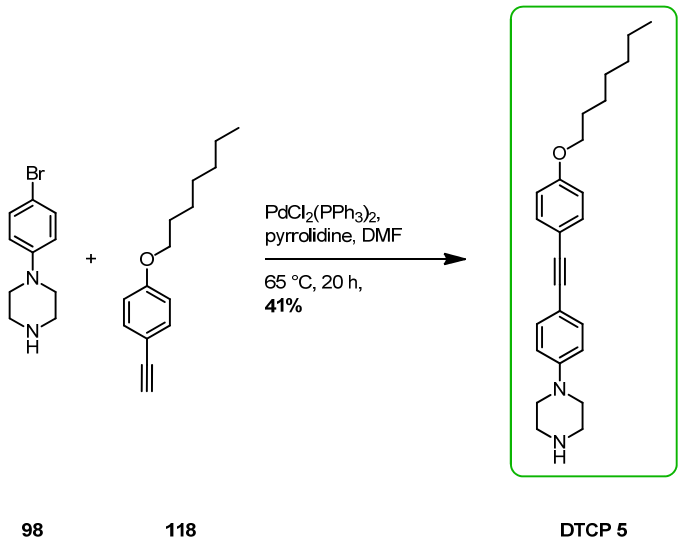

Scheme 95. Last step to target compound **DTCP 5**.

4.2 Touching Monolayers Approach

The integration of molecular films into electronic circuits and to tune the electronic properties of the resulting junction was at first proposed by Kuhn, Aviram and Ratner in the 1970s.[18,19,363] The first experimental realizations of electrode-SAM-electrode setups were presented in the 1990s.[21,364,365] The investigation of appealing devices that perform rectification are of special interest.[19] Conceptually, a rectifying system can be achieved in different ways. The molecular subunits should differ in electron density (electron rich and electron poor systems), but also different molecule-electrode contacts may provide unidirectional transport properties. In general, rectifying devices consist of molecular structures that are sandwiched between two electrodes. Such a built-up allows for electrical characterization of the molecular film and thus of the device performance. However, practically the devices often suffer from imperfections (pinholes[262,366]) in the film. In the strong electric field arising from the applied current, filament formation in the pinholes may result in short circuits. With this disadvantage of an electrode-SAM-electrode junction in mind a new device is designed. The device is based, as shown in *Scheme 96*, on an electrode-SAM/SAM-electrode junction, a touching monolayers approach. Two monolayers, which are prepared separately, will be brought in touching contact to each other forming a metal-film/film-metal junction. The considered advantage of this device is the minor probability of having film defects (pinholes) at identical lateral positions, thus dramatically decreasing the amount of short circuits during the electrical measurements. The applicability of this touching monolayer device will be tested with the assembly of molecules that differ in the architecture's backbone. The goal is to achieve a rectifying system with this new device setup. The unidirectional transport properties should arise here from the variation of the molecular backbone. Thus, the electrodes have to consist of the same material and the structures have to be assembled with the help of identical anchoring groups. Profiting from the advantageous properties of dithiocarbamate linkers, i.e. stability and good electric contact to the metal (section 1.3.3), the use of gold electrodes is considered. To correlate the observed physical properties of a dithiocarbamate-SAM with the backbone structure of the dithiocarbamate molecule, comparable molecular densities within the SAM and similar lateral packing features are proposed. To keep the spatial requirements of the SAM-forming molecule as comparable as possible, the two heterocyclic amine derivatives **DTCP 1** and **DTCP 2** are considered (*Scheme 96*). Each target structure comprises a terminal nitrogen atom, which is integrated in a saturated six membered ring and is known to react with carbon disulfide to form the dithiocarbamate anchoring group (section 1.3.2).[44,262] While the matchable number and arrangement of atoms within both target structures is proposed to result in comparable spatial requirements within the SAM, considerable differences in the electron densities of their central aromatic subunits are expected. The electron withdrawing fluorine substituents reduce the electron density of the

aromatic core in **DTCP 7** considerably, whereas the central benzene subunit of **DTCP 6** is electron rich due to the electron donating alkoxy and dialkylamino substituents. The bottom monolayer represents the "electron deficient" part of the system and the top layer the "electron rich" part. Once both structures are assembled on the flat gold substrates, the top electrode will be flipped and brought in touching contact to the bottom monolayer, where the alkyl chains are expected to stabilize the electrode-film/film-electrode device due to *van der Waals* forces. The alkyl chains are suggested to intercalate. Furthermore, the area, in which the alkyl chains are in contact, can be varied mechanically. This area represents the bridge between the electron rich and poor part of the system. With this setup the insulating length can thus be varied and optimized. Finally, current/voltage measurements will give insight to the electronic properties of this setup. A correlation between the molecular structures and the rates of electron transport can then be made.

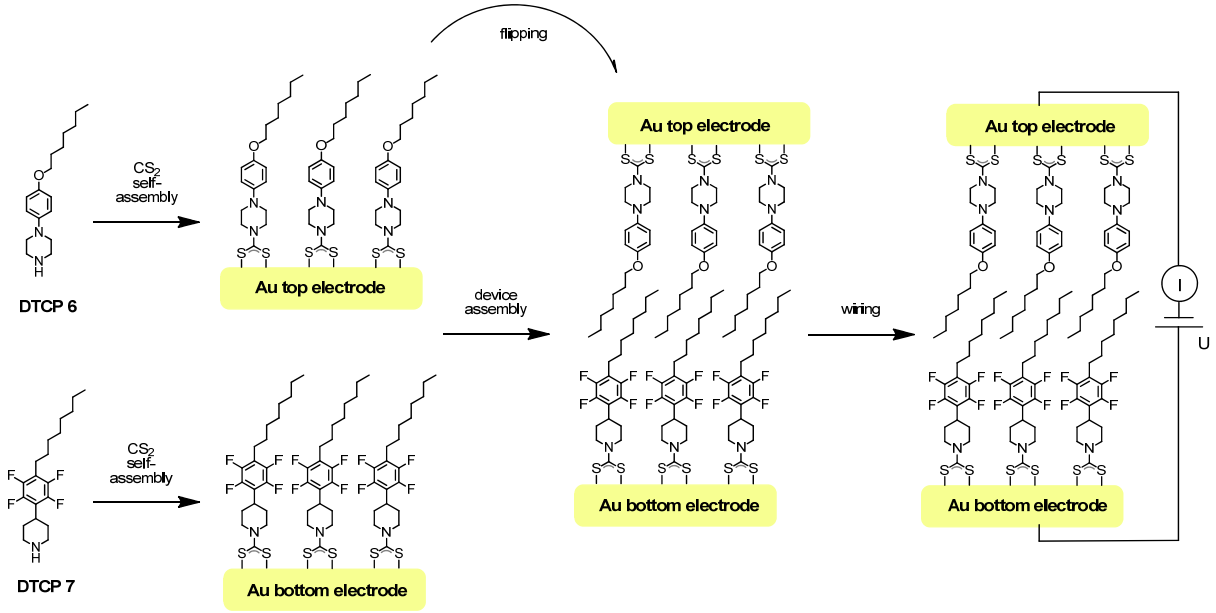

Scheme 96. Touching monolayer approach for the investigation of electrical rectification in an electrode-SAM/SAM-electrode junction.

As the expertise of flipping the top electrode and adjusting it towards the bottom electrode still gives room for improvement, another similar setup could be used in the mean time. This junction consists of a SAM supported on a gold film in contact with a second SAM on the surface of a Hg drop. With the Hg drop setup the screening of the electrical properties of a wide range of molecular structures is possible.[80] Especially, its simplicity in usage encouraged us to perform preliminary investigations. The bottom electrode and SAM will be kept as described above. For the top Hg electrode a thiol-based structure was designed, as the expertise with thiols on Hg droplets is well established.[47,81] The thiol-based target structure (**T1**) is depicted in *Scheme 97*. The biphenyl subunit and the methylene spacer between the biphenyl and the sulfur should

guarantee a tight packing and well ordered monolayer.[290,367–369] With this setup current-voltage characteristics of the device can be obtained. However, if the device shows rectification properties, it also has to be considered that the unidirectional transport properties could additionally arise from the different electrodes and different electrode-linker contacts. Before starting the practical research towards this appealing new setup, preliminary electronic characterization, such as work function measurements, of the individual SAMs will be performed.

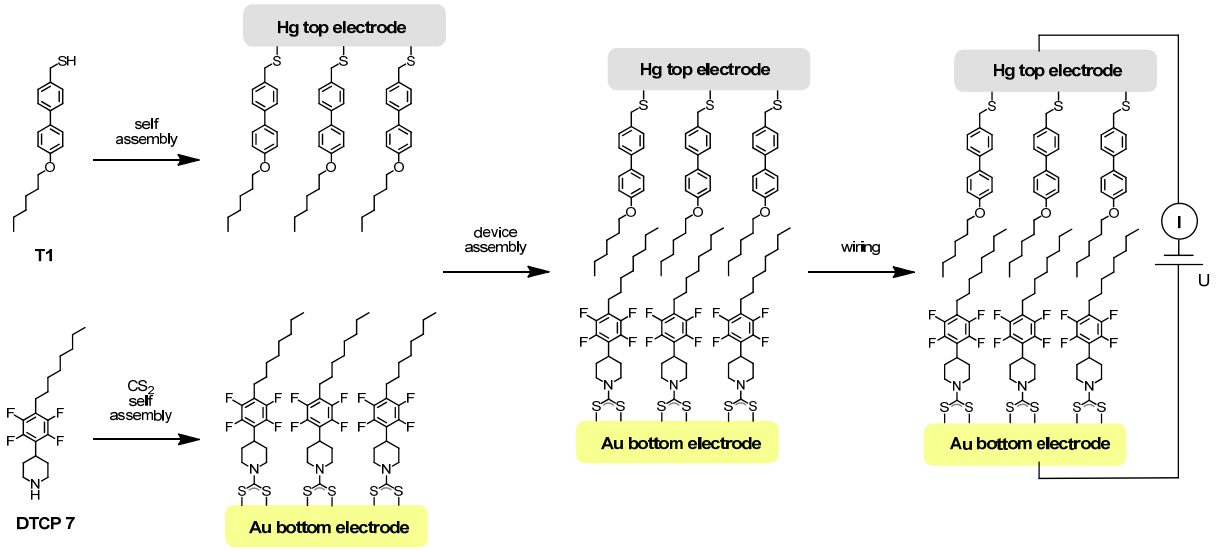

Scheme 97. Touching monolayer approach with a mercury drop set-up.

4.2.1 Synthesis and Characterization

As already described in the introduction (section 1.3.2) the formation of the dithiocarbamates can be performed *in situ* during the assembly process. Therefore, the targeted structures will be synthesized as the corresponding free amines (dithiocarbamate precursors, **DTCP**s) as shown in *Figure 46*.

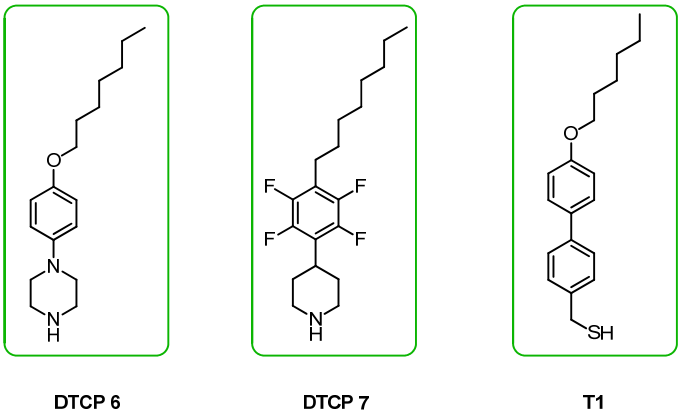

DTCP 6 DTCP 7 T1

Figure 46. Target compounds for the investigation of their electrical properties of the formed dithiocarbamate-SAMs and thiol-SAM.

*Synthesis of **DTCP 6***

The two step synthesis of target structure **DTCP 6** was initiated with the commercially available acetyl protected piperazine **119**. Starting material **119** underwent a S_N2 reaction with 1-bromoheptane in *N*,*N*-dimethylformamide using potassium carbonate as base (*Scheme 98*). The reaction was stirred at room temperature for 18 hours. After workup the crude was used directly in the next reaction step without further purification. Compound **120** was obtained quantitatively as a pinkish solid.

The deprotection of the piperazine moiety **120** was performed in an acidic media and under microwave irradiation. The precursor **120** was added to a microwave vial together with an aqueous hydrochloric acid solution and exposed to microwave irradiation at 120 °C for 20 minutes. The reaction mixture was then basified with an aqueous potassium carbonate solution. After extraction the crude was purified by column chromatography to give **DTCP 6** as a brownish solid in a yield of 92%.

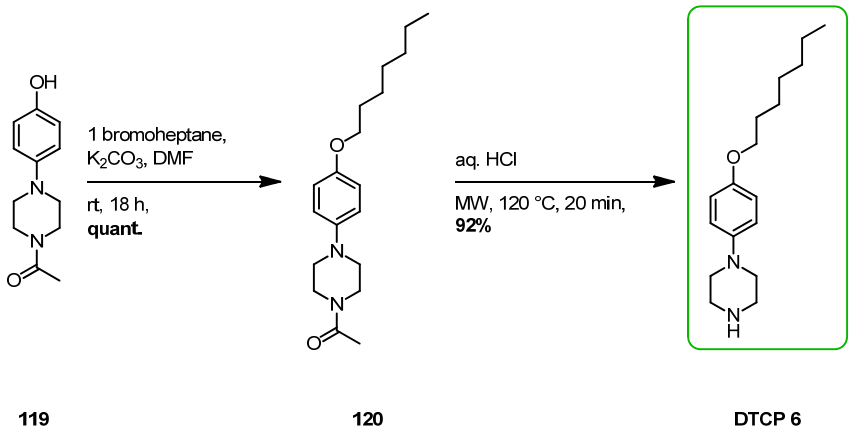

Scheme 98. Synthesis of target structure **DTCP 6** in two steps starting from acetyl protected piperazine **119**.

Target structure **DTCP 6** was synthesized in two steps and was fully characterized by NMR-spectroscopy (^{1}H- and ^{13}C-NMR), EI-MS, MALDI-ToF mass spectrometry and EA.

*Synthesis of **DTCP 7***

The synthetic access to the piperidine **DTCP 7** started with the commercially available benzyl carbamate protected 4-piperidinone **121** (*Scheme 99*). Following a literature procedure the enol-form of compound **121** was trapped as a triflate.[370] *N*-Benzyloxycarbonyl-4-piperidone (**121**) was dissolved in tetrahydrofuran and cooled to -78 °C. After dropwise addition of lithium bis(trimethylsilyl)amide (LiHMDS) and then treatment with *N*-phenyl-bis(trifluoromethane-sulfonimide) the reaction mixture was stirred at room temperature for 16 hours. The desired triflate **122** was isolated after aqueous workup and purification by column chromatography as a colorless solid in a yield of 43%. Substitution of the triflate group with a boronic ester provided a suitable precursor for a Suzuki-Miyaura cross-coupling reaction. The triflate **122** was then converted to the boronic acid derivative **123** with bis(pinacolato)diboron.[371] A literature procedure was adapted for the formation of the boronic ester **123** as follows: the triflate **122**, 1.1 equivalents of bis(pinacolato)diboron and the base potassium acetate were dissolved under inert atmosphere in dry dioxane. Afterwards catalytic amounts of dichloro(1,1'-bis(diphenyl-phosphino)ferrocene)palladium dichloromethane adduct (Pd Cl_2(dppf) ·CH_2Cl_2) and the ligand 1,1'-bis(diphenylphosphino)ferrocene (dppf) were added and stirred at 80 °C for 27 hours. After aqueous workup and purification by column chromatography the boronic ester **123** was isolated as a colorless solid in a yield of 72%.

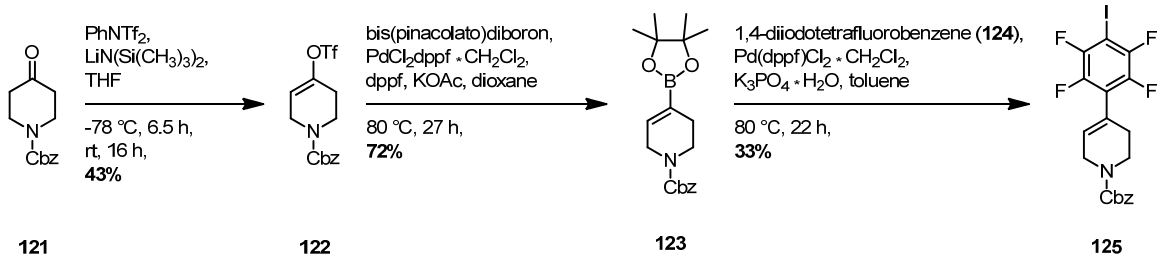

Scheme 99. Synthesis of the intermediate **125**.

Boronic ester **123** is an appropriate precursor for the following Suzuki-Miyaura cross-coupling reaction with 1,4-diiodotetrafluorobenzene (**124**). Sarwar *et al.* reported on the synthesis of the monosubstituted biphenyl compound **127**, starting from 1,4-diiodotetrafluorobenzene (**124**) and phenylboronic acid (**126**) (*Scheme 100*).[372] The reagents and conditions for that synthesis were adapted to the reaction of boronic ester **123** to afford the derivative **125**. $PdCl_2(dppf)\cdot CH_2Cl_2$ as catalyst and potassium phosphate tribasic monohydrate as base were added to a solution of the starting material **123** and 1.5 equivalents of 1,4-diiodotetrafluorobenzene (**124**) in toluene. The reaction mixture was stirred at 80 °C for 22 hours and after workup and purification by column chromatography compound **125** was obtained as a colorless solid in low yields of 33%. To the best of our knowledge Suzuki-Miyaura mono cross-coupling reactions of boronic derivatives with 1,4-diiodotetra-fluorobenzene were not reported to give high yields of the desired product.[372]

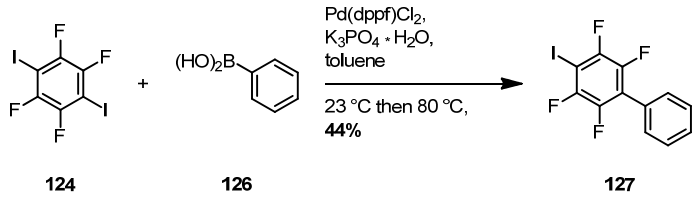

Scheme 100. Monocoupling of 1,4-diiodotetrafluorobenzene (**124**) with phenylboronic acid (**126**).

The alkyl chain was attached as the third and last building block. It was planned to introduce the carbon chain by a Sonogashira cross-coupling reaction. Compound **125** was converted to the acetylene derivative **128** (*Scheme 101*) using standard Sonogashira reagents, i.e. $Pd(PPh_3)_4$ as catalyst, copper iodide as co-catalyst and triethylamine, which acts as base and solvent. To the starting material **125** an excess of commercially available 1-octyne and subsequently the reagents were added and the reaction mixture was heated at 75 °C overnight. The desired alkynylated product **128** was obtained after purification by column chromatography as a brownish oil in a yield of 78%. With intermediate **128** in hand the target structure **DTCP 7** was considered to be formed in one last step. This step involved simultaneously three operations on different positions of compound **128** in a hydrogenation reaction: reduction of the triple bond of the carbon chain down to a single bond, saturation of the hydro pyridine unit and cleavage of the

benzyl carbamate protecting group. To compound **128** was added palladium on charcoal, acetic acid and ethanol. The reaction mixture was then exposed to 20 bar hydrogen pressure in an autoclave at room temperature for three days. After filtration, extraction and basic workup the remaining crude was purified by column chromatography to afford the desired target structure **DTCP 7** as a colorless solid in a yield of 79%. **DTCP 7** was synthesized in a total of five steps in an overall yield of 6%. Especially the last synthetic step proved to be appealing, as it included simultaneously three operations at three different positions. **DTCP 7** was fully characterized by NMR-spectroscopy (^{1}H-, ^{19}F- and ^{13}C-NMR), EI-MS and EA.

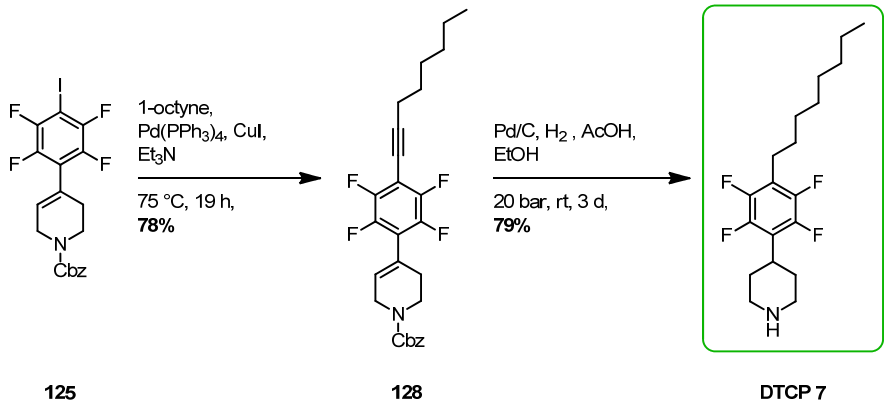

Scheme 101. Introduction of the carbon chain and subsequent hydrogenation of intermediate **128** to afford target compound **DTCP 7**.

*Synthesis of **T1***

The synthesis of target structure **T1** was initiated with commercially available 4'-hydroxy-4-biphenylcarboxylic acid (**129**) (*Scheme 102*). The attachment of the alkyl chain was performed with 1-bromohexane in basic media. Compound **129** was dissolved in an ethanol/water mixture and then a slight excess of 1-bromohexane, 2.1 equivalents of potassium hydroxide and catalytic amounts of potassium iodide were added. The reaction mixture was then stirred at reflux for 19 hours and after acidic workup the precipitate formed was filtered. The crude was recrystallized from glacial acetic acid to afford the intermediate **130** as a colorless solid in a yield of 59%. The carboxylic acid **130** was then reduced to the corresponding alcohol **131** with 3.0 equivalents of lithium aluminium hydride in dry tetrahydrofuran. After refluxing for 6 hours the reaction mixture was worked up and the crude product was purified by column chromatography to obtain the alcohol **131** as a colorless solid in a yield of 84%. In an Appel reaction[373] the introduction of the benzylic bromine was performed. The addition of triphenylphosphine and carbon tetrabromide to the benzylic alcohol **131** in dichloromethane gave after stirring at room temperature for 18 hours and purification by column

chromatography the desired intermediate **132** as a yellowish solid in a yield of 62%. These first three steps were performed adapting a literature procedure.[368]

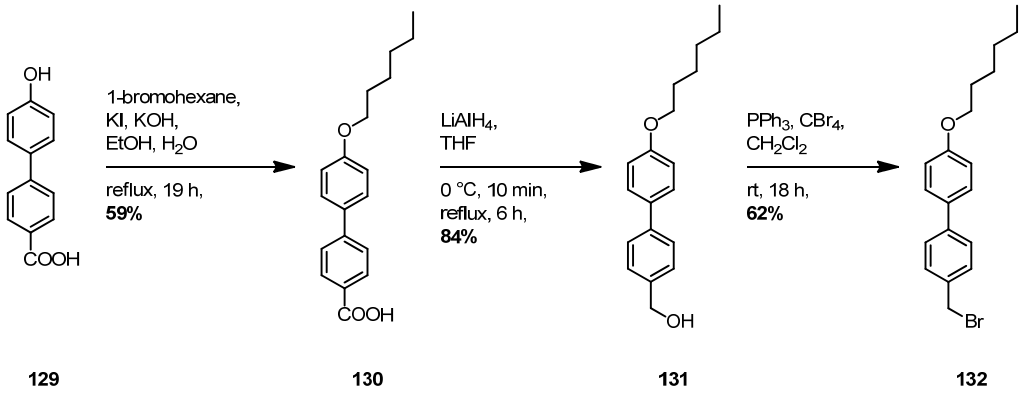

Scheme 102. Introduction of the alkyl chain, reduction of the acid **130** to the alcohol **131** and subsequent bromination afforded intermediate **132**.

The last two steps included the introduction of the sulfur functionality and the subsequent deprotection of the sulfur to the free thiol. The introduction of the sulfur functionality was achieved with trityl thiol and an excess of sodium hydride in tetrahydrofuran. The reaction mixture was stirred at room temperature for one hour and after workup and purification by column chromatography the desired trityl protected sulfur **133** was obtained as a brownish oil in a yield of 84%. The trityl protecting group was cleaved with trifluoroacetic acid in the presence of the cation scavenger triethylsilane in dichloromethane. The reaction mixture was stirred at room temperature for three hours. After quenching with an aqueous sodium hydrogen carbonate solution and purification by column chromatography the desired target compound **T1** was isolated as a colorless solid in a yield of 86%.

Target structure **T1** was synthesized in five steps in an overall yield of 22% and it was fully characterized by NMR-spectroscopy (^{1}H- and ^{13}C-NMR), EI-MS and EA.

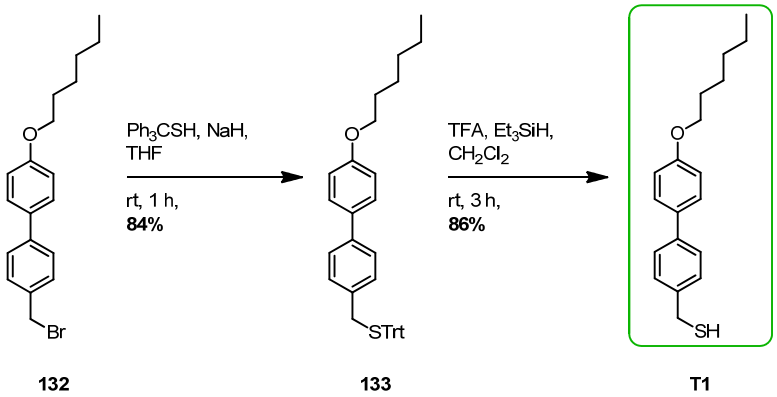

Scheme 103. Introduction of the sulfur functionality and subsequent deprotection of the sulfur to obtain the target structure **T1**.

4.3 SAM Formation and Work Function Investigations

For the tuning of the metal's work function several dithiocarbamate-based compounds were designed and synthesized. With these compounds surface investigations to characterize the properties of the corresponding SAMs were performed. An overview of the prepared monolayers on gold surfaces is depicted in *Scheme 104*. For the structure **DTC 5** drawn in gray the surface experiments are currently ongoing.

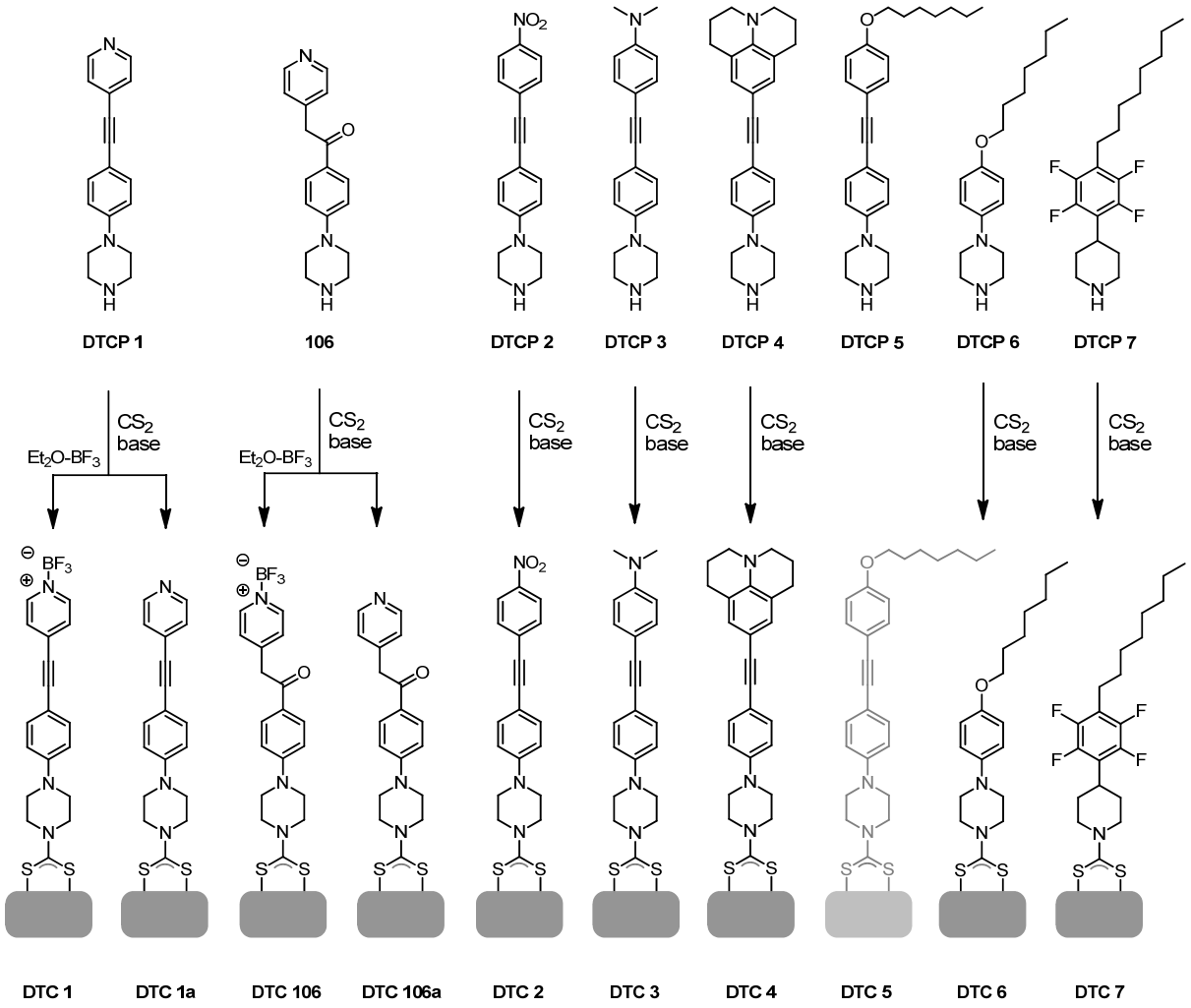

Scheme 104. Overview of the dithiocarbamate-based SAMs.

The SAM preparation from **DTCP 1**-**4**, **DTCP 6**, **DTCP 7** and **106** was performed *in situ*, i.e. the **DTCPs** were dissolved in ethanol and subsequently carbon disulfide, a base (triethylamine) and the gold substrate were added. After the assembly time the corresponding dithiocarbamate-based SAMs were investigated by XPS and the obtained values were compared with literature known values for alkanethiols. The XPS measurements suggested for all surfaces the chemisorption of the structures. The results were reproducible and did not depend on the assembly time. To afford **DTC 1** and **DTC 106**, the SAMs **DTC 1a** and **DTC 106a**, respectively,

were treated with boron trifuoride diethyletherate. Here the XPS results indicated a 40–50% conversion of the pyridine groups to the BF_3-complexes.

With the help of UPS the work function of the functionalized gold substrates was measured. In *Figure 47* the obtained values were plotted against the calculated dipole moment values of the structures obtained from DFT calculations. The values of the new structures are shown in color. The gray squares correspond to the values of structures that were measured by the Material Science Laboratory of SONY Deutschland GmbH in advance for preliminary investigations of dithiocarbamate-based SAMs. These structures were depicted in *Figure 43* (section 4.1). For these gray squares a linear fit was performed. As nicely shown in *Figure 47*, the new structures follow the trend that decreasing the dipole moment leads to an increase of the work function of the functionalized gold substrate. However, the measured work function value of the pyridine-BF_3-based SAM (red square) does not correlate with the value extrapolated (black circle) based on the fit to the data and did not exceed the work function of the clean gold (Φ = 5.1 eV). As the XPS measurements suggest that not all pyridine moieties of **DTC 1a** and **DTC 106a** bear the BF_3-group, an interpretation should be handled with care. Nevertheless, the tendency that the substitution of the building block that is located at the SAM's outer surface has an impact on the work function is demonstrated. Electron withdrawing substituents (such as $-NO_2$) increase the work function and electron donating groups (such as $-NMe_2$) at the outer part of the SAM decrease the metal's work function.

To conclude, the XPS measurements confirmed the SAM formation of all analyzed structures and the work function measurements by UPS are roughly consistent with the expected trend.

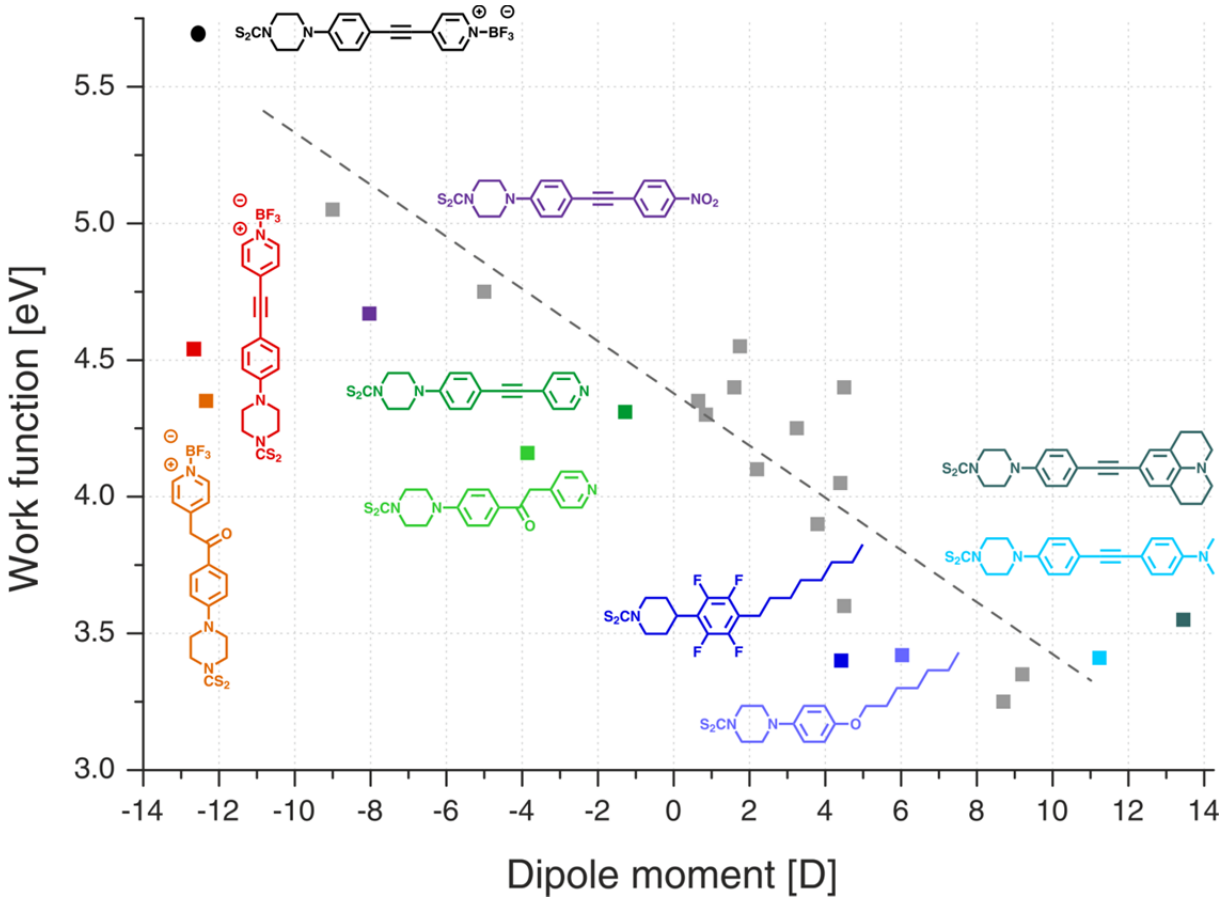

Figure 47. Plot of the work function against the calculated dipole moment. The work function value of the black structure (circle) is estimated and the work function values of the colored structures (squares) are obtained by UPS measurements. The gray squares correspond to the structures measured in advanced from the Material Science Labortory of SONY Deutschlang GmbH. The linear fit is done with the gray data points.

4.4 Summary and Conclusion

Several new dithiocarbamate-based structures were designed and synthesized (**DTCP 1**-**5**) for the purpose to tune the gold metal's work function (*Figure 48*). These structures have the same basic molecular motif, whereas the tail unit is varied implementing electron donating and withdrawing substituents. The integration of such substituents has an impact to the overall dipole moment of the molecular structure and thus on the functionalized metal's work function. The constant unit (acetylene-phenylene-piperazine structure) enabled a modular synthetic pathway to the target structures. The synthesis of each target molecule afforded one to a maximum of four steps. Molecule **106** was obtained during a reaction as side product. The surface investigations of this compound were also performed, as the ketone unit is a new interesting structural motif. Additional three target structures (**DTCP 6**, **DTCP 7**, and **T1**) were designed and successfully synthesized for the application in a new device setup that provides rectification (*Figure 48*). In this device two monolayers will be brought in touching contact to each other. **DTCP 6** and **DTCP 7** show structural similarities but different elemental compositions. **DTCP 7** was obtained in five steps starting from a commercially available piperidone derivative, **DTCP 6** was synthesized in two steps starting from the commercially available 1-acetyl-4-(4-hydroxyphenyl)piperazine and compound **T1** was assembled in five reaction steps starting from 4'-hydroxy-4-biphenylcarboxylic acid.

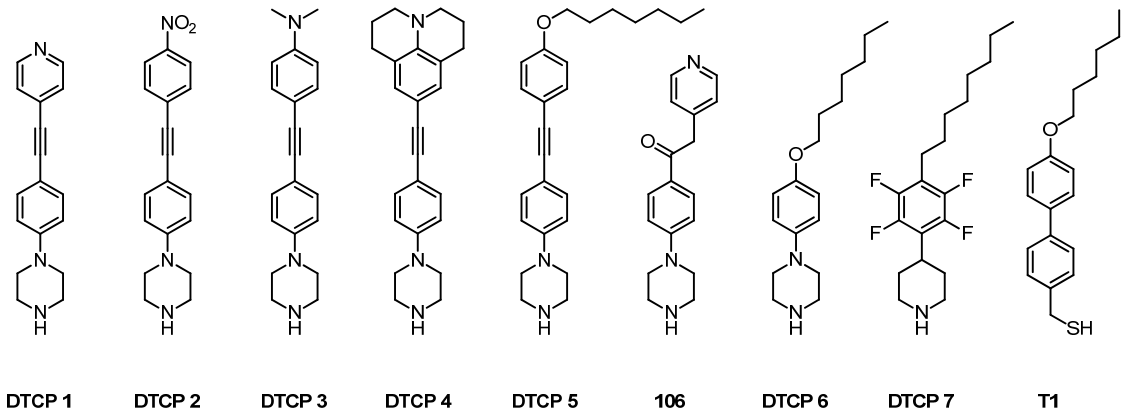

Figure 48. Synthesized compounds for the modulation of the metal's work function and the investigation of rectifying devices.

DTCP 1-**4**, **DTCP 6**, **DTCP 7** and compound **106** were assembled onto gold substrates by the *in situ* formation of the dithiocarbamate linker. The successful formation of all corresponding SAMs was confirmed by XPS analysis. Furthermore, these SAMs were investigated by UPS and the determined work function values showed the expected tendency that tailoring the dipole moment of the molecule has an influence on the surface potential. The investigations on the rectifying system are currently ongoing.

By investigating the surface properties of dithiocarbamate-based SAMs we hope to better estimate the required molecular components necessary to modify the metal's work function in order to improve the electronic communication between the metal electrode and the monolayer.

5 Summary and Outlook

In order to improve the device performance of metal-molecule junctions, the ambition of this thesis was the design and synthesis of tailor-made molecules to functionalize metallic substrates for surface investigations. In particular, the aim of tuning the metal's work function was set in the foreground.

In the introduction a general overview of surface characterization techniques and integration setups is provided and the molecular requirements are briefly discussed pointing out that molecular electronics is an interdisciplinary field between scientists from different backgrounds. Furthermore, a historical outline and the general chemistry and properties of azobenzenes and dithiocarbamates are introduced. These functional molecular units are attractive for their integration in self-assembled monolayers.

The synthetic effort for the synthesis of the azo compounds described in this thesis represents the starting point to the production of functionalized metal surfaces, which are investigated in the laboratories of our collaborators Prof. Dr. P. Samorì, Prof. Dr. B. Doudin, Prof. Dr. C. Wöll and Prof. Dr. M. A. Rampi. The implementation of the azo compounds on surfaces and devices gave an insight into their electronic properties. The modulation of the metal's work function is of special interest. However, the analysis of other aspects such as SAM formation, SAM crystallinity, SAM stability and SAM interactions are of fundamental need. The synthesis of the dithiocarbamate molecular rods represents the extention of studies previousely performed at the Material Science Laboratory of SONY Deutschland GmbH aiming at the development of a new class of dipolar molecules for the work function modification of noble metal surfaces. This work was performed in a close collaboration with Dr. F. von Wrochem and Dr. W. Ford from the Material Science Laboratory of SONY Deutschland GmbH.

Azobenzenes are often incorporated as light responsive components into monolayer matrices. The azo functionality undergoes photoisomerization and thus is able to adapt two conformational states. The reversible switching between these two isomers (*trans* and *cis*) is the reason that a terminal thiol functionalized biphenyl azobenzene (**CABP,** *Scheme 105*) found interest as a molecular switch in the literature. The aim to investigate this specific assembled azobiphenyl in more detail spurred us to improve its synthesis for the straightforward access of the compound. An efficient synthetic route to the acetyl protected derivative (**CABP-SAc**) was found, where the noteworthy synthetic step is the Mills reaction to form an asymmetric azo benzene for the subsequent selective Suzuki-Miyaura cross-coupling reactions.

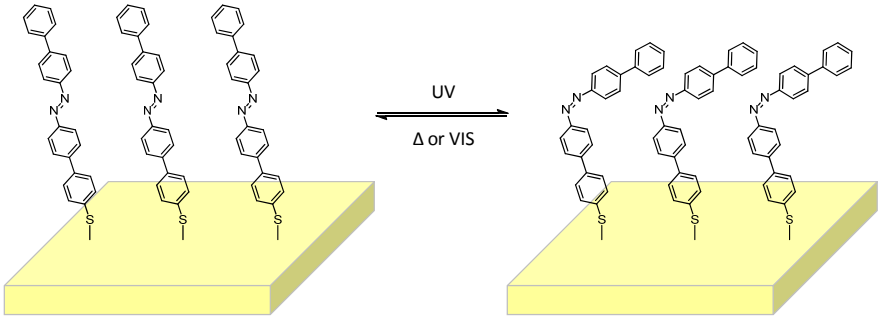

Scheme 105. Schematic representation of the **CABP** in its *trans*- and *cis*-form.

The **CABP-SAc** starting material was used for the functionalization on gold substrates and the resulting devices were investigated. One part of the investigations included the analysis of the work function. In comparative studies using different experimental techniques it was shown that a work function shift upon photoisomerization of the self assembled monolayer can be observed. Furthermore, the **CABP-SAc** was also tested in an organic field-effect transistor device. With this setup it was possible to optically and reversibly modulate for the first time the charge injection at the electrode-semiconductor interface. The decrease in tunneling barrier thickness from *trans* to *cis* revealed a higher current density in the *cis*-based device. Moreover, an optically switchable molecular device using microsphere based junctions provided a proof-of-principle experiment. It gave evidence for the **CABP**-based photoactive responsive molecular devices. Furthermore, the solvation and precipitation of gold nanoparticles coated with the azobiphenyl was optically and reversibly modulated in solution. These particles were also blended with a semiconductor and then implemented in a field-effect transistor device. The source-drain current through the channel could be gated electrically and optically, showing an improved performance and cyclability compared to the organic field-effect transistor reported above.

In order to broaden the scope of functional azobenzenes several new azo compounds were designed and synthesized. Issues like packing tightness of the resulting monolayer, switching strength of the chromophore, π-π-stacking of the aromatic units and conductance switching rations were considered. By applying a synthetic strategy that profits from modular building blocks several new azo compounds were successfully synthesized (**AZOP 1**-**5**, *Figure 49*).

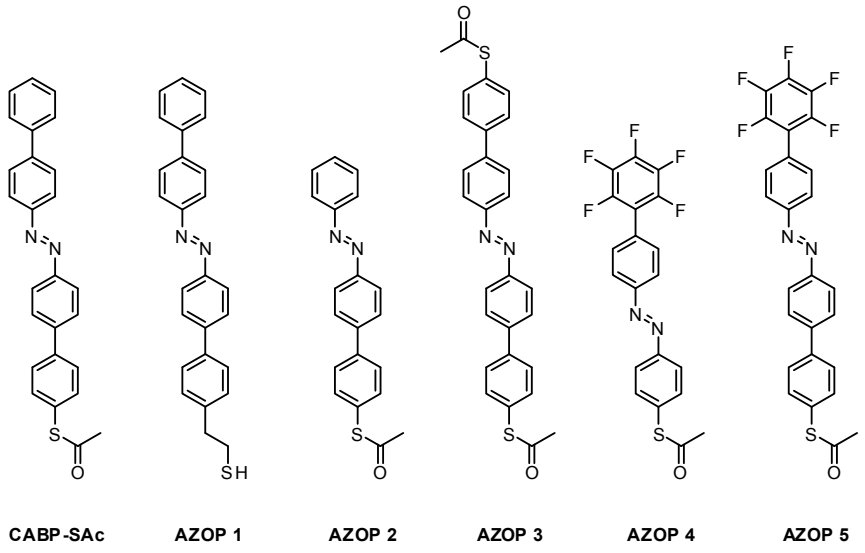

Figure 49. Synthesized azo compounds.

UV/Vis measurements and ^{1}H-NMR spectroscopy of these target compounds were performed, showing the time dependent photoisomerization process of the azo compounds in solution. The UV/Vis spectra were compared with each other and for **AZOP 2** and **AZOP 4** the solid state structures were measured by X-ray analysis. While the aromatic units of **AZOP 2** lie in the same plane, the arene units of **AZOP 4** are twisted to each other (*Figure 50*). **AZOP 4** was functionalized on gold surfaces and the metal's work function could be tuned photochemically. Furthermore an efficient organic light emitting diode based on **AZO 4** was presented. The other synthesized target compounds are currently under investigation in the research groups of Prof. Samorì, Prof. Wöll and Prof. Rampi.

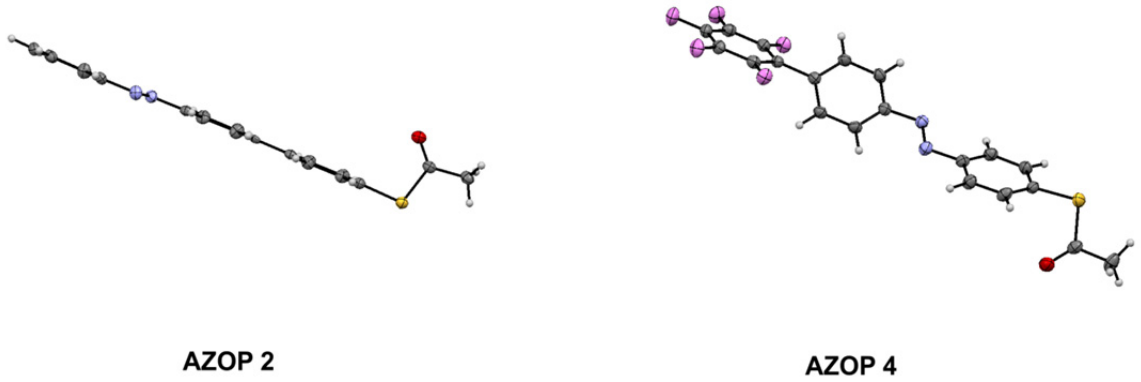

Figure 50. Solid state structures of *trans*-**AZOP 2** and *trans*-**AZOP 4**.

In collaboration with the Material Science Laboratory of SONY Deutschland GmbH in Stuttgart, Germany, the design and syntheses of dithiocarbamate-based structures were carried out. The advantages of dithiocarbamates over thiols as suitable anchoring groups on gold surfaces motivate for the investigations towards organic light-emitting diodes and thin-film transistors.

The SAM stability and the reduced charge injection barrier across the metal-molecule interface are of particular interest. In the emerging field of dithiocarbamates as functional units, fundamental investigations of the electron transport properties of the resulting devices are required. In particular, work function measurements and rectification issues in a new device setup are considered in this work. In *Figure 51* the successfully synthesized dithiocarbamate-based precursors for the mentioned investigations are depicted. As for the synthesis of the azo compounds, the synthesis of the dithiocarbamate-based structures profited from a modular synthetic strategy.

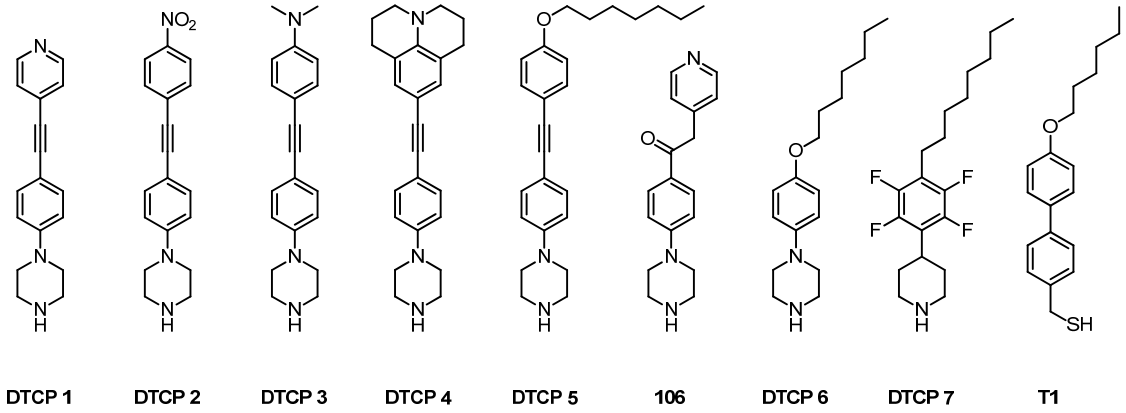

Figure 51. Synthesized piperazine-, piperidine- and thiol-based structures.

The chemisorption of **DTCP 1**-**4**, **DTCP 6**, **DTCP 7** and compound **106** on gold surfaces was proven by XPS measurements. Furthermore, UPS investigations of the corresponding devices showed that the dipole moment of the structures correlates with the modification of the work function value of the functionalized metal substrate (*Figure 52*). **DTCP 5** and **T1** are currently under investigation. **DTCP 6**, **DTCP 7** and **T1** were synthesized for its implementation in a mercury drop setup for rectification measurements.

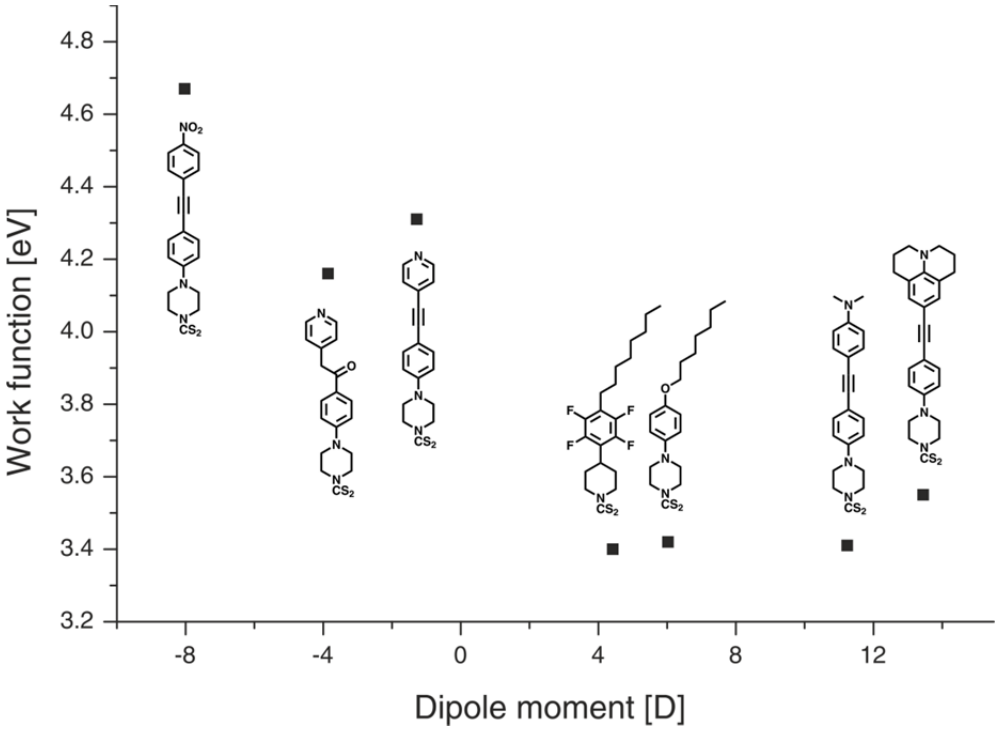

Figure 52. Plot of the work function against the calculated dipole moment of the synthesized structures.

In order to expand the knowledge of what factors influence the performance of a modified surface with organic molecules, extensive studies still have to be made. The potential of chemists to build up a manifold diversity of molecules allows for the development of an infinitively large molecular library to play around with. The fundamental research of surface functionalization is the basis for the development of future electronic devices based on molecular films.

Profiting from the gained knowledge within this research activity, new tailor-made structures can be proposed as an outlook. For example, the combination of azobenzenes and dithiocarbamate units in the same molecule could lead to interesting new device properties. Exploiting the isomerization capabilities of azobenzenes and the appealing stability and electronic properties of dithiocarbamate linkers, could effectively improve future device generations.

6 Experimental Part

6.1 General Remarks

Reagents and Solvents

All commercially available starting materials were of reagent grade and used as received from *Fluka AG* (Buchs, Switzerland), *Acros AG* (Basel, Switzerland), *Merck* (Darmstadt, Germany), *Alfa Aesar* (Karlsruhe, Germany), *ABCR* (Karlsruhe, Germany) and *Aldrich* (Buchs, Switzerland). The solvents for chromatography, crystallization and extraction were used in technical grade. Dry tetrahydrofuran, dry *N*,*N*-dimethylformamide, dry toluene, dry ethanol and dry dichloromethane were purchased from *Fluka*, stored over 4 Å molecular sieves, and handled under argon. For an inert atmosphere *Argon 4.8* from *PanGas AG* (Dagmersellen, Switzerland) was used.

Synthesis

All reactions with reagents which are sensitive to air or moisture were performed under an argon atmosphere using Schlenk technique, only dry solvents were used and the glassware was heated out before use.

^{1}H-Nuclear Magnetic Resonance (^{1}H-NMR)

Bruker DRX-NMR (500 MHz or 600 MHz), *Bruker DPX-NMR* (400 MHz) and *Bruker BZH-NMR* (250 MHz) instruments were used to record the spectra. Chemical shifts (δ) are reported in parts per million (ppm) relative to residual solvent peaks ($CDCl_3$: 7.26 ppm, CD_2Cl_2: 5.32 ppm) or trimethylsilane (TMS: 0.00 ppm), and coupling constants (*J*) are reported in Hertz (Hz). The bond distance of the coupling constant is stated with a superscript number (^{n}J). NMR solvents were obtained from *Cambridge Isotope Laboratories, Inc.* (Andover, MA, USA). The measurements were done at room temperature. The multiplicities are written as: s = singlet, d = doublet, t = triplet, q = quartet, quin = quintet, m = multiplet and s_{br} = broad singlet.

^{13}C-Nuclear Magnetic Resonance (^{13}C-NMR)

Bruker DRX-NMR (126 MHz or 151 MHz) and *Bruker DPX-NMR* (101 MHz) instruments were used to record the spectra. Chemical shifts (δ) are reported in parts per million (ppm) relative to residual solvent peaks ($CDCl_3$: 77.2 ppm, CD_2Cl_2: 54.0 ppm or TMS: 0.0 ppm). The measurements were done at room temperature. The multiplicities are written as: s = singlet, d = doublet, t = triplet, q = quartet, quin = quintet, m = multiplet. The coupling constants (*J*) are reported in Hertz (Hz). The bond distance of the coupling constant is stated with a superscript number (^{n}J).

^{19}F-Nuclear Magnetic Resonance (^{19}F-NMR)

A *Bruker DPX-NMR* (377 MHz) instrument was used to record the spectra. Chemical shifts (δ) are reported in parts per million (ppm), uncorrected. The measurements were done at room temperature. Coupling constants (*J*) are reported in Hertz (Hz). The bond distance of the coupling constant is stated with a superscript number (^{n}J). The multiplicities are written as: s = singlet, d = doublet, t = triplet, q = quartet, quin = quintet, m = multiplet.

Mass Spectrometry (MS)

Matrix Assisted Laser Desorption Ionization Time of Flight (MALDI-ToF) mass spectra were performed on an *Applied Bio Systems Voyager-De™ Pro* mass spectrometer or a *Bruker microflex* mass spectrometer. Electron Impact (EI) mass spectra were recorded on a *Finnigan MAT 95Q*. Fast Atom Bombardment (FAB) mass spectra were recorded on a *Finnigan MAT 8400*. Significant signals are given in mass units per charge (m/z) and the relative intensities are given in brackets. EI-MS and FAB-MS measurements were performed by Dr. H. Nadig.

Elemental Analysis (EA)

Elemental analyses were measured by W. Kirsch on a *Perkin-Elmer Analysator 240*. The values are given in mass percent.

Ultraviolet Spectroscopy (UV)

UV/Vis-spectra were recorded on a *UV-1800* spectrophotometer from *Shimadzu* using optical 114-*QS Hellma* cuvettes (10 mm light path) at room temperature and ambient conditions.

Thin Layer Chromatography (TLC)

Silica gel 60 F_{254} glass plates with a thickness of 0.25 mm from *Merck* were used. For detection a UV lamp (8 Watt) with 254 nm or 366 nm was used.

Column Chromatography (CC)

For CC *silica gel 60* (particle size 40-63 µm) from *Merck* or *silica gel 60* (particle size 40-63 µm) from *Fluka* was used.

Microwave Reactions

Microwave reactions were carried out in an *Initiator 8* (400 W) from *Biotage*.

6.2 Synthetic Procedures

1-Bromo-4-nitrosobenzene (13)[173]

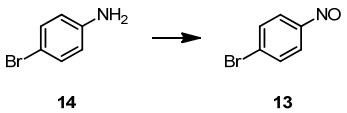

14 13

4-Bromoaniline (**14**, 3.50 g, 20.3 mmol, 1.0 eq.) was dissolved in dichloromethane (50 mL) and then a solution of Oxone® ($2KHSO_5 \cdot KHSO_4 \cdot K_2SO_4$) (25.0 g, 40.7 mmol, 2.0 eq.) in water (200 mL) was added. The reaction mixture was stirred under an argon atmosphere at room temperature for 5 hours. Afterwards the phases were separated and the aqueous layer was extracted with dichloromethane. The collected organic layers were washed with an aqueous HCl-solution (1 M), a saturated aqueous $NaHCO_3$-solution, water and brine and then dried over $MgSO_4$. The solvent was removed under reduced pressure and the remaining green crude product (**13**, C_6H_4BrNO, 3.80 g) was used without further purification in the next reaction step.

1-(4-Bromophenyl)-2-(4-iodophenyl)diazene (11)[173]

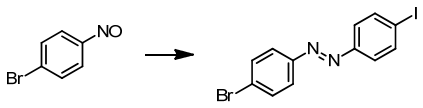

13 **11**

The crude 1-bromo-4-nitrosobenzene (**13**, 3.80 g) was dissolved in acetic acid (160 mL) and then 4-iodoaniline (4.45 g, 20.3 mmol) was added. The reaction mixture was stirred under an argon atmosphere at room temperature for 42 hours. The orange precipitate was collected and washed with acetic acid and water. After drying, the solid was purified by column chromatography (silica gel, ethyl acetate/*n*-hexane 1:20) to obtain azo compound **11** ($C_{12}H_8BrIN_2$, 6.21 g, 79% over two steps) as an orange solid.

TLC R_f = 0.78 (ethyl acetate/*n*-hexane 1:20).

^{1}H-NMR (400 MHz, $CDCl_3$, δ/ppm): 7.87 (d, $^3J_{HH}$ = 8.7 Hz, 2H), 7.79 (d, $^3J_{HH}$ = 8.7 Hz, 2H), 7.65 (d, $^3J_{HH}$ = 8.8 Hz, 2H), 7.64 (d, $^3J_{HH}$ = 8.7 Hz, 2H).

^{13}C-NMR (101 MHz, $CDCl_3$, δ/ppm): 151.7, 151.1, 138.4, 132.4, 125.8, 124.5, 124.4, 98.1.

MS (EI, m/z): 385.9 (77%, M^+), 231.0 (59%), 203.0 (100%), 183.0 (30%), 155.0 (56%), 76.1 (70%), 50.0 (21%).

EA calculated: C = 37.24, H = 2.08, N = 7.24,
found: C = 37.04, H = 2.00, N = 7.17.

1-([1,1'-Biphenyl]-4-yl)-2-(4-bromophenyl)diazene (10)

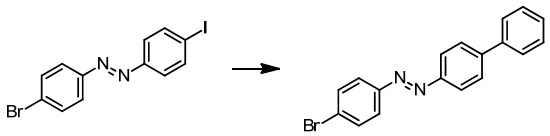

11 10

To 1-(4-bromophenyl)-2-(4-iodophenyl)diazene (**11**, 2.24 g, 5.78 mmol, 1.0 eq.), phenylboronic acid (0.94 g, 7.74 mmol, 1.3 eq.) and potassium carbonate (1.60 g, 11.6 mmol, 2.0 eq.), dry ethanol (40 mL) and dry toluene (60 mL) were added under an argon atmosphere. The reaction mixture was degassed by purging argon through the solution. Afterwards $Pd(PPh_3)_4$ (200 mg, 0.17 mmol, 3 mol%) was added and the mixture was stirred at 50 °C for 18 hours. Afterwards water was added to the reaction mixture, which was then extracted with ethyl acetate (3x). The collected organic layers were washed with water (3x) and brine and then dried over $MgSO_4$. The solvent was removed under reduced pressure and the crude product was purified by column chromatography (silica gel, dichloromethane/cyclohexane 1:2) to obtain azo compound **10** ($C_{18}H_{13}BrN_2$, 1.87 g, 96%) as an orange solid.

TLC R_f = 0.64 (dichloromethane/cyclohexane 1:2).

^{1}H-NMR (400 MHz, $CDCl_3$, δ/ppm): 8.00 (d, $^3J_{HH}$ = 8.6 Hz, 2H), 7.82 (d, $^3J_{HH}$ = 8.7 Hz, 2H), 7.76 (d, $^3J_{HH}$ = 8.7 Hz, 2H), 7.66 (m, 4H), 7.48 (m, 2H), 7.40 (t, $^3J_{HH}$ = 7.3 Hz, 1H).

^{13}C-NMR (126 MHz, $CDCl_3$, δ/ppm): 151.6, 151.5, 144.0, 140.1, 132.4, 128.9, 128.0, 127.2, 127.2, 125.4, 124.4, 123.5.

MS (EI, m/z): 336.0 (32%, M^+), 153.1 (100%).

EA calculated: C = 64.11, H = 3.89, N = 8.31,
found: C = 63.81, H = 3.98, N = 8.26.

(2-((4-Bromophenyl)thio)ethyl)trimethylsilane (16)[272]

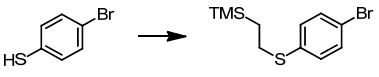

15 16

4-Bromothiophenol (**15**, 6.20 g, 32.8 mmol, 1.0 eq,), vinyltrimethylsilane (5.72 mL, 39.4 mmol, 1.2 eq.) and di-*tert*-butyl peroxide (905 µl, 4.92 mmol, 15 mol%) were added under an argon atmosphere into a pressure tube. The pressure tube was sealed and heated to 100 °C in an oil bath for 5 hours. The reaction mixture was cooled to room temperature, diluted with *n*-hexane and washed with an aqueous NaOH-solution (1 M) (2x). The collected aqueous layers were extracted with *n*-hexane (3x) and the collected organic layers were dried over $MgSO_4$. The solvent was removed under reduced pressure to obtain a liquid which was purified by vacuum distillation. (2-((4-Bromophenyl)thio)ethyl)trimethylsilane (**16**, $C_{11}H_{17}BrSSi$, 8.25 g, 87%) was isolated as a colorless liquid.

^{1}H-NMR (400 MHz, $CDCl_3$, δ/ppm): 7.39 (d, $^3J_{HH}$ = 8.6 Hz, 2H), 7.16 (d, $^3J_{HH}$ = 8.6 Hz, 2H), 2.93 (m, 2H), 0.91 (m, 2H), 0.04 (s, 9H).

^{13}C-NMR (101 MHz, $CDCl_3$, δ/ppm): 136.5, 131.8, 130.4, 119.4, 29.7, 16.8, 1.8.

MS (EI, m/z): 288.1 (7%, M^+), 73.1 (100%).

EA calculated: C = 45.67, H = 5.92,
found: C = 45.53, H = 6.00.

Tris(4-((2-(trimethylsilyl)ethyl)thio)phenyl)-boroxine (17)[273]

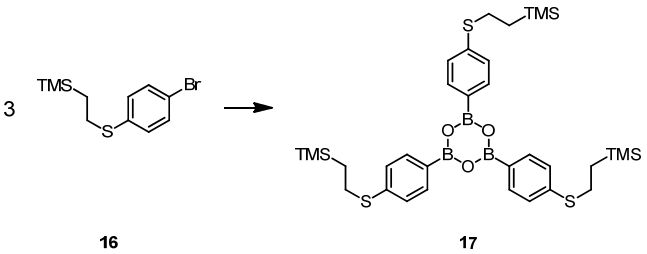

(2-((4-Bromophenyl)thio)ethyl)trimethylsilane (**16**, 8.07 g, 27.9 mmol, 1.0 eq.) was dissolved under an argon atmosphere in dry tetrahydrofuran (40 mL) in a dry Schlenk-tube. The solution was degassed by purging argon through it and was cooled to -78 °C. *n*-Butyllithium (1.6 M in *n*-hexane, 27.9 mL, 1.6 eq.) was added dropwise. During the addition of *n*-butyllithium the solution turned from colorless to yellow. The solution was stirred at -78 °C for 30 minutes. Afterwards triisopropyl borate (33.3 mL, 145 mmol, 5.2 eq.) was added dropwise and the solution became colorless again. The reaction mixture was stirred at -78 °C for 2 hours and then at -15 °C. At this point, further tetrahydrofuran (20 mL) was added, since the formed precipitate inhibited the stirring. After 2.5 hours the cooling bath was removed and the reaction mixture was stirred at room temperature for 48 hours. The reaction mixture was quenched with water and then concentrated under reduced pressure to almost only the water phase. An extraction was then performed with diethyl ether (3x). The collected organic layers were washed with water (3x) and brine and then dried over $MgSO_4$. The crude product was recrystallized from *n*-hexane to afford boroxine **17** ($C_{33}H_{51}B_3O_3S_3Si_3$, 4.22 g, 64%) as a colorless powder.

^{1}H-NMR (400 MHz, $CDCl_3$, δ/ppm): 8.10 (d, $^3J_{HH}$ = 8.2 Hz, 6H), 7.36 (d, $^3J_{HH}$ = 8.2 Hz, 6H), 3.05 (m, 6H), 1.00 (m, 6H), 0.08 (s, 27H).

^{13}C-NMR (101 MHz, $CDCl_3$, δ/ppm): 143.9, 136.0, 126.5, 28.2, 16.7, -1.6.

MS (EI, m/z): 708.3 (7%, M^+), 101.1 (18%), 73.0 (100%).

EA calculated: C = 55.93, H = 7.25,
found: C = 55.81, H = 7.27.

1-([1,1'-Biphenyl]-4-yl)-2-(4'-((2-(trimethylsilyl)ethyl)thio)-[1,1'-biphenyl]-4-yl)-diazene (18)

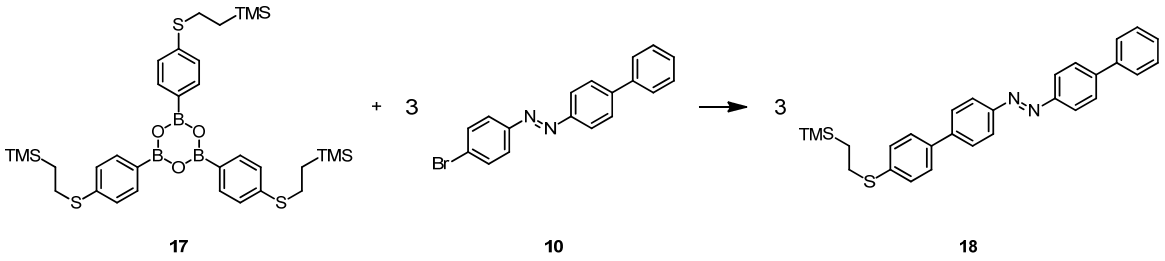

17 10 18

1-([1,1'-Biphenyl]-4-yl)-2-(4-bromophenyl)diazene (**10**, 323 mg, 0.96 mmol, 1.0 eq.), boroxine **17** (292 mg, 0.41 mmol, 0.4 eq.), potassium carbonate (264 mg, 1.92 mmol, 2.0 eq.), $Pd(PPh_3)_4$ (55 mg, 0.06 mmol, 5 mol%), dry ethanol (20 mL) and dry toluene (20 mL) were added under an argon atmosphere to a flask. The reaction mixture was stirred at 60 °C for 3 hours. After cooling the reaction mixture to room temperature water was added. The reaction mixture was extracted with ethyl acetate (3x) and the collected organic layers were washed with brine and then dried over $MgSO_4$. The solvent was removed under reduced pressure and the crude product was purified by column chromatography (silica gel, dichloromethane/*n*-hexane 1:2) to obtain azo compound **18** ($C_{29}H_{30}N_2SSi$, 359 mg, 80%) as an orange solid.

TLC R_f = 0.46 (dichloromethane/*n*-hexane 1:2).

^{1}H-NMR (400 MHz, $CDCl_3$, δ/ppm): 8.02 (d, $^3J_{HH}$ = 8.6 Hz, 2H), 8.02 (d, $^3J_{HH}$ = 8.6 Hz, 2H), 7.77 (d, $^3J_{HH}$ = 8.6 Hz, 2H), 7.75 (d, $^3J_{HH}$ = 8.6 Hz, 2H), 7.68 (d, $^3J_{HH}$ = 7.1 Hz, 2H), 7.61 (d, $^3J_{HH}$ = 8.4 Hz, 2H), 7.49 (m, 2H), 7.40 (m, 3H), 3.03 (m, 2H), 0.98 (m, 2H), 0.07 (s, 9H).

^{13}C-NMR (101 MHz, $CDCl_3$, δ/ppm): 151.9, 151.8, 143.7, 143.0, 140.2, 137.5, 137.4, 129.0, 128.9, 127.9, 127.8, 127.5, 127.44, 127.2, 123.5, 123.4, 29.4, 16.9, -1.7.

MS (EI, m/z): 466.2 (93%, M^+), 438.1 (41%), 257.1 (54%), 153.1 (71%), 73.1 (100%).

EA calculated: C = 74.63, H = 6.48, N = 6.00,
found: C = 74.55, H = 6.49, N = 5.81.

(4'-([1,1'-Biphenyl]-4-yldiazenyl)-[1,1'-biphenyl]-4-yl) ethanethioate (CABP-SAc)

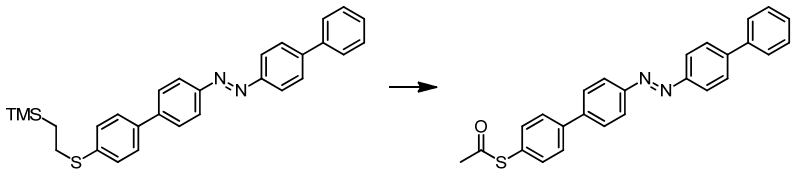

18 CABP-SAc

Precursor **18** (244 mg, 0.52 mmol, 1.0 eq.) was dissolved under an argon atmosphere in dry tetrahydrofuran (40 mL) and degassed by purging argon through the solution. A tetra-*n*-butylammonium fluoride (3.00 mL, 10.1 mmol, 19 eq.) was then added at once and the reaction mixture stirred at room temperature for 1.5 hours. After the addition of tetra-*n*-butylammonium fluoride the solution turned from orange to deep purple. The mixture was then cooled to 0 °C and acetyl chloride (4.0 mL), which was degassed before by purging argon through it, was added in one portion. Again the solution turned from deep purple back to orange and it was stirred for 1 hour. The reaction mixture was then quenched slowly with water and then extracted with ethyl acetate (3x). The collected organic layers were washed with brine and subsequently dried over $MgSO_4$. The solvent was removed under reduced pressure and the crude product was purified by column chromatography (silica gel, dichloromethane/*n*-hexane 1:1) to obtain target structure **CABP-SAc** ($C_{26}H_{20}N_2OS$, 154 mg, 72%) as an orange solid.

TLC R_f = 0.40 (dichloromethane/*n*-hexane 1:1).

^{1}H-NMR (400 MHz, $CDCl_3$, δ/ppm): 8.03 (m, 4H), 7.77 (m, 4H), 7.70 (m, 4H), 7.51 (m, 4H), 7.41 (t, $^3J_{HH}$ = 7.3 Hz, 1H), 2.47 (s, 3H).

^{13}C-NMR ^{13}C-shifts determined from HSQC and HMBC experiments; (151 MHz, $CDCl_3$, δ/ppm): 194.0, 152.2, 151.8, 143.9, 142.6, 141.4, 140.2, 134.9, 128.9, 128.0, 127.9, 127.5, 127.2, 123.5, 30.7.

MS (EI, m/z): 408.1 (86%, M^+), 366.1 (57%), 185.0 (57%), 153.1 (100%).

EA calculated: C = 76.44, H = 4.93, N = 6.86,
found: C = 76.16, H = 5.21, N = 6.73.

1-([1,1'-Biphenyl]-4-yl)-2-(4'-vinyl-[1,1'-biphenyl]-4-yl)diazene (20)

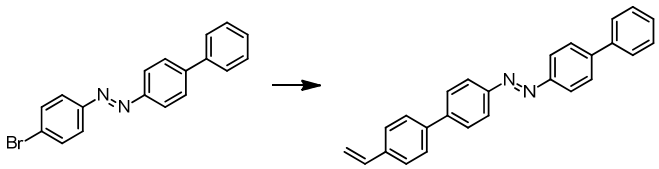

10 20

1-([1,1'-Biphenyl]-4-yl)-2-(4-bromophenyl)diazene (**10**, 186 mg, 0.55 mmol, 1.0 eq.), 4-vinylbenzeneboronic acid (122 mg, 0.83 mmol, 1.5 eq.), potassium carbonate (152 mg, 1.10 mmol, 2.0 eq.), dry toluene (5 mL) and dry ethanol (5 mL) were added under an argon atmosphere into a dry 25 mL-Schlenk-tube. The reaction mixture was degassed with the freeze-pump-thaw method. Afterwards $Pd(PPh_3)_4$ (32.0 mg, 0.03 mmol, 5 mol%) was added and the reaction mixture was stirred at 60 °C for 45 minutes. The mixture was diluted with dichloromethane and washed with water (3x) and brine and the organic layer was dried over $MgSO_4$. The solvent was removed under reduced pressure and the crude product was purified by column chromatography (silica gel, dichloromethane/cyclohexane 1:2) to afford azo compound **20** ($C_{26}H_{20}N_2$, 179 mg, 90%) as an orange solid.

TLC R_f = 0.54 (dichloromethane/cyclohexane 1:2).

^{1}H-NMR (400 MHz, $CDCl_3$, δ/ppm): 8.03 (m, 4H), 7.77 (m, 4H), 7.67 (m, 4H), 7.50 (m, 4H), 7.41 (m, 1H), 6.78 (dd, $^3J_{HH}$ = 17.7, $^3J_{HH}$ = 11.0 Hz, 1H), 5.83 (d, $^3J_{HH}$ = 17.6 Hz, 1H), 5.31 (d, $^3J_{HH}$ = 10.9 Hz, 1H).

MS (EI, m/z): 360.2 (100%, M^+), 179.2 (93%,), 153.1 (81%).

EA calculated: C = 86.64, H = 5.59, N = 7.77,
found: C = 86.23, H = 6.03, N = 7.46.

1-([1,1'-Biphenyl]-4-yl)-2-(4'-(2-((2-(trimethylsilyl)ethyl)thio)ethyl)-[1,1'-biphenyl]-4-yl)diazene (21)

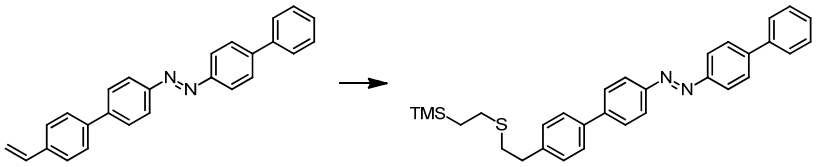

20 21

1-([1,1'-Biphenyl]-4-yl)-2-(4'-vinyl-[1,1'-biphenyl]-4-yl)diazene (**20**, 136 mg, 0.38 mmol, 1.0 eq.) and dry toluene (14 mL) were added under an argon atmosphere into a pressure tube and the solution was degassed by purging argon through it. Afterwards 2-trimethylsilylethanethiol (0.09 mL, 0.57 mmol, 1.5 eq.) and di-*tert*-butyl peroxide (0.04 mL, 0.16 mmol, 0.5 eq.) were added and the sealed tube was then heated at 130 °C for 68 hours. The solvent was removed under reduced pressure after cooling down to room temperature and the crude product was purified by column chromatography (silica gel, dichloromethane/*n*-hexane 3:5). Azo compound **21** ($C_{31}H_{34}N_2SSi$, 100 mg, 54%) was isolated as an orange solid.

TLC R_f = 0.30 (dichloromethane/*n*-hexane 3:5).

^{1}H-NMR (400 MHz, $CDCl_3$, δ/ppm): 8.02 (d, $^3J_{HH}$ = 8.6 Hz, 2H), 8.01 (d, $^3J_{HH}$ = 8.6 Hz, 2H), 7.76 (d, $^3J_{HH}$ = 8.5 Hz, 2H), 7.75 (d, $^3J_{HH}$ = 8.4 Hz, 2H), 7.68 (d, $^3J_{HH}$ = 7.1 Hz, 2H), 7.62 (d, $^3J_{HH}$ = 8.2 Hz, 2H), 7.48 (m, 2H), 7.41 (t, $^3J_{HH}$ = 7.3 Hz, 1H) 7.33 (d, $^3J_{HH}$ = 8.2 Hz, 2H), 2.95 (m, 2H), 2.85 (m, 2H), 2.58 (m, 2H), 0.88 (m, 2H), 0.02 (s, 9H).

^{13}C-NMR (101 MHz, $CDCl_3$, δ/ppm): 151.9, 151.8, 143.7, 143.5, 140.6 140.2, 138.2, 129.1, 128.9, 127.8, 127.6, 127.2, 127.2, 123.4, 123.3, 36.0, 33.3, 27.9, 17.4, -1.8.

MS (EI, m/z): 494.2 (100%, M^+), 347.2 (31%,), 153.1 (64%), 73.1 (59%).

EA calculated: C = 75.26, H = 6.93, N = 5.66,
found: C = 75.49, H = 6.91, N = 5.80.

1-([1,1'-Biphenyl]-4-yl)-2-(4'-(2-((2-(trimethylsilyl)ethyl)thio)ethyl)-[1,1'-biphenyl]-4-yl)diazene (22)

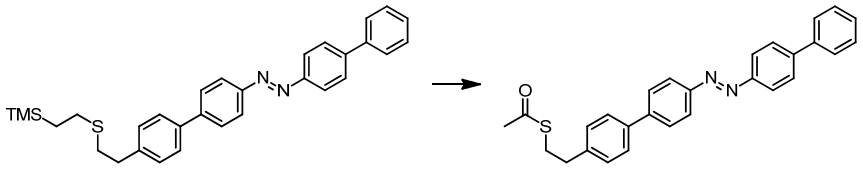

21 22

Azo compound **21** (285 mg, 0.58 mmol, 1.0 eq.) was dissolved under an argon atmosphere in dry dichloromethane (20 mL) and the solution was degassed by purging argon through it. Then acetyl chloride (1.50 mL, 21.0 mmol, 37 eq.) and silver tetrafluoroborate (336 mg, 1.73 mmol, 3.0 eq.) were added and stirred at room temperature for 3 hours. The reaction mixture was quenched with a saturated aqueous $NaHCO_3$-solution. After dilution with dichloromethane the organic layer was washed with water (3x) and then dried over $MgSO_4$. The solvent was removed under reduced pressure and the crude product was purified by column chromatography (silica gel, dichloromethane) to afford azo compound **22** ($C_{28}H_{24}N_2OS$, 226 mg, 90%) as an orange solid.

TLC R_f = 0.50 (dichloromethane).

^{1}H-NMR (400 MHz, $CDCl_3$, δ/ppm): 8.03 (d, $^3J_{HH}$ = 8.6 Hz, 2H), 8.02 (d, $^3J_{HH}$ = 8.6 Hz, 2H), 7.77 (d, $^3J_{HH}$ = 8.6 Hz, 2H), 7.76 (d, $^3J_{HH}$ = 8.6 Hz, 2H), 7.68 (d, $^3J_{HH}$ = 7.1 Hz, 2H), 7.63 (d, $^3J_{HH}$ = 8.2 Hz, 2H), 7.49 (m, 2H), 7.40 (t, $^3J_{HH}$ = 7.5 Hz, 1H), 7.34 (d, $^3J_{HH}$ = 8.3 Hz, 2H), 3.18 (m, 2H), 2.94 (m, 2H), 2.36 (s, 3H).

^{13}C-NMR (101 MHz, $CDCl_3$, δ/ppm): 195.7, 151.9, 151.8, 143.7, 143.4, 140.2, 139.8, 138.4, 129.2, 128.9, 127.9, 127.8, 127.6, 127.3, 127.2, 123.4, 123.4, 35.5, 30.7, 30.4.

MS (EI, m/z): 436.1 (89%, M^+), 360.2 (74%), 179.1 (93%), 153.1 (100%), 43.0 (13%).

EA calculated: C = 77.03, H = 5.54, N = 6.42,
found: C = 76.83, H = 5.54, N = 6.37.

UV/Vis ($CHCl_3$, λ_{max}/nm, (ε/L · mol^{-1} · cm^{-1})): 243 (13900), 365 (20100).

2-(4'-([1,1'-Biphenyl]-4-yldiazenyl)-[1,1'-biphenyl]-4-yl)ethanethiol (AZOP 1)

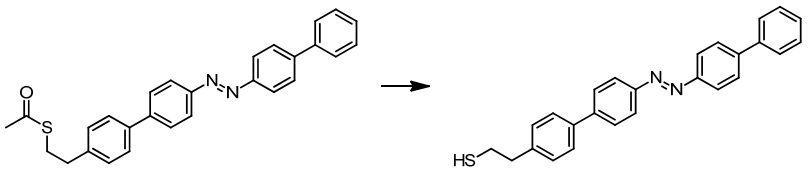

22 AZOP 1

Compound **22** (161 mg, 0.37 mmol) was dissolved under an argon atmosphere in dry chloroform (30 mL) and dry methanol (15 mL) and the solution was degassed by purging argon through it. Two small spatula tips of tetrabutylammonium cyanide were added and then the reaction mixture was stirred at room temperature for 4 hours. Further three spatula tips of tetrabutylammonium cyanide were added and the mixture was continued to stir for 18 hours. After addition of water and the separation of the phases the organic layer was washed with a saturated aqueous NH_4Cl-solution (2x) and dried over $MgSO_4$. The solvent was removed under reduced pressure and the crude product was purified by column chromatography (silica gel, dichloromethane/*n*-hexane 1:1) to afford target structure **AZOP 1** ($C_{26}H_{22}N_2S$, 105 mg, 72%) as an orange solid.

TLC R_f = 0.45 (dichloromethane/*n*-hexane 1:1).

^{1}H-NMR (400 MHz, $CDCl_3$, δ/ppm): 8.03 (d, $^3J_{HH}$ = 8.6 Hz, 2H), 8.02 (d, $^3J_{HH}$ = 8.6 Hz, 2H), 7.77 (d, $^3J_{HH}$ = 8.6 Hz, 2H), 7.76 (d, $^3J_{HH}$ = 8.5 Hz, 2H), 7.68 (d, $^3J_{HH}$ = 7.1 Hz, 2H), 7.63 (d, $^3J_{HH}$ = 8.2 Hz, 2H), 7.49 (m, 2H), 7.40 (t, $^3J_{HH}$ = 7.4 Hz, 1H) 7.32 (d, $^3J_{HH}$ = 8.1 Hz, 2H), 3.00 (m, 2H), 2.86 (m, 2H), 1.44 (t, $^3J_{HH}$ = 7.8 Hz, 1H).

^{13}C-NMR (101 MHz, $CDCl_3$, δ/ppm): 151.9, 151.8, 143.7, 143.4, 140.2, 139.7, 138.5, 129.3, 128.9, 127.9, 127.8, 127.6, 127.3, 127.2, 123.4, 123.4, 39.9, 26.0.

MS (EI, m/z): 394.2 (97%, M^+), 213.1 (73%), 179.1 (22%), 165.2 (20%), 153.1 (100%).

EA calculated: C = 79.15, H = 5.62, N = 7.10,
found: C = 78.93, H = 5.64, N = 7.00.

UV/Vis ($CHCl_3$, λ_{max}/nm, (ε/L · mol^{-1} · cm^{-1})): 245 (9000), 365 (16500).

Nitrosobenzene (24)

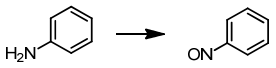

23 **24**

Aniline (**23**, 15.0 g, 161 mmol, 1.0 eq.) was dissolved in dichloromethane (400 mL) and then a solution of $2KHSO_5 \cdot KHSO_4 \cdot K_2SO_4$ (Oxone®, 198 g, 322 mmol, 2.0 eq.) in water (1.6 L) was added. The reaction mixture was stirred under an argon atmosphere at room temperature for 16 hours. Afterwards the phases were separated and the aqueous layer was extracted with dichloromethane (3x). The collected organic layers were washed with an aqueous HCl-solution (1 M), a saturated aqueous $NaHCO_3$-solution, water and brine and then dried over $MgSO_4$. The solvent was removed under reduced pressure and the remaining green crude product (**24**, C_6H_5NO, 19.7 g) was used without further purification in the next reaction step.

1-(4-Bromophenyl)-2-phenyldiazene (25)

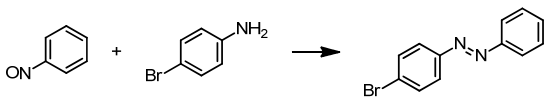

24 **14** **25**

Crude nitrosobenzene (**24**, 6.23 g) and 4-bromoaniline (**14**, 10.0 g, 58.1 mmol) were dissolved in acetic acid (200 mL) and stirred under an argon atmosphere at room temperature for 20 hours. Additional nitrosobenzene (**24**, 6.43 g) was added and stirred for further 24 hours. The addition of further nitrosobenzene (**24**, 6.30 g) was repeated and stirred again for 24 hours. The mixture was diluted with water and carefully neutralized with a saturated aqueous $NaHCO_3$-solution. An extraction was performed with ethyl acetate (3x) and the collected organic layers were dried over $MgSO_4$. The solvent was removed under reduced pressure and the crude product was purified by column chromatography (silica gel, dichloromethane/cyclohexane 1:2) to afford compound **25** ($C_{12}H_9BrN_2$, 6.46 g, 57% over two steps) as an orange solid.

TLC R_f = 0.53 (dichloromethane/cyclohexane 1:2).

^{1}H-NMR (400 MHz, $CDCl_3$, δ/ppm): 7.91 (m, 2H), 7.80 (d, $^3J_{HH}$ = 8.7 Hz, 2H), 7.65 (d, $^3J_{HH}$ = 8.7 Hz, 2H), 7.51 (m, 3H).

^{13}C-NMR (101 MHz, $CDCl_3$, δ/ppm): 152.5, 151.3, 132.3, 131.3, 129.2 125.4, 124.4, 122.9.

MS (EI, m/z): 260.0 (49%, M^+), 184.9 (21%), 154.9 (51%), 152.1 (17%), 105.0 (34%), 77.0 (100%), 51.0 (17%).

EA calculated: C = 55.20, H = 3.47, N = 10.73,
found: C = 55.24, H = 3.55, N = 10.75.

1-Phenyl-2-(4'-((2-(trimethylsilyl)ethyl)thio)-[1,1'-biphenyl]-4-yl)diazene (26)

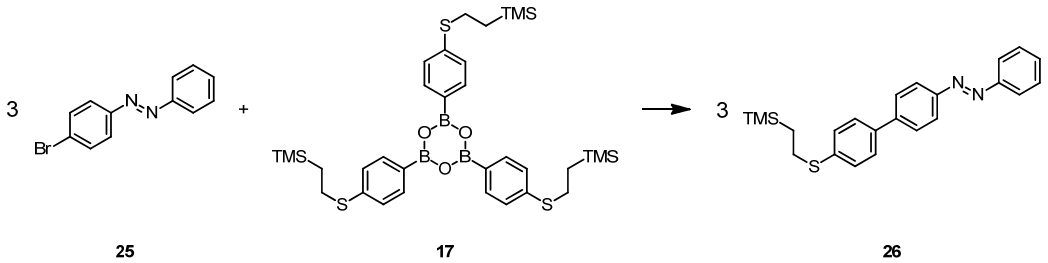

25 17 26

1-(4-Bromophenyl)-2-phenyldiazene (**25**, 2.00 g 7.66 mmol, 1.0 eq.), boroxine **17** (2.34 g, 3.30 mmol, 0.4 eq.), potassium carbonate (2.12 g, 15.3 mmol, 2.0 eq.), dry ethanol (40 mL) and dry toluene (40 mL) were added under an argon atmosphere into a dry flask and the resulting reaction mixture was degassed by purging argon through the solution. Then $Pd(PPh_3)_4$ (442 mg, 0.38 mmol, 5 mol%) was added and the reaction mixture was heated at 50 °C for 3 hours. The reaction mixture was diluted with water and an extraction with ethyl acetate (3x) was performed. The organic layer was washed with water (3x) and brine and then dried over $MgSO_4$. The solvent was removed under reduced pressure and the crude product was purified by column chromatography (silica gel, dichloromethane/cyclohexane 1:2) to obtain azo compound **26** ($C_{23}H_{26}N_2SSi$, 2.79 g, 93%) as an orange solid.

TLC R_f = 0.44 (dichloromethane/cyclohexane 1:2).

^{1}H-NMR (400 MHz, $CDCl_3$, δ/ppm): 8.00 (d, $^3J_{HH}$ = 8.5 Hz, 2H), 7.94 (d, $^3J_{HH}$ = 7.1 Hz, 2H), 7.74 (d, $^3J_{HH}$ = 8.5 Hz, 2H), 7.60 (d, $^3J_{HH}$ = 8.3 Hz, 2H), 7.52 (m, 3H), 7.39 (d, $^3J_{HH}$ = 8.3 Hz, 2H), 3.02 (m, 2H), 0.98 (m, 2H), 0.07 (s, 9H).

^{13}C-NMR (101 MHz, $CDCl_3$, δ/ppm): 152.8, 151.7, 143.0, 137.5, 137.3, 131.0, 129.1, 128.9, 127.5, 127.4, 123.5, 122.86, 29.3, 16.8, -1.7.

MS (EI, m/z): 390.2 (42%, M^+), 362.2 (24%), 257.1 (53%), 77.1 (21%), 73.1 (100%).

EA calculated: C = 70.72, H = 6.71, N = 7.17,
found: C = 70.77, H = 6.90, N = 7.23.

***S*-(4'-(phenyldiazenyl)-[1,1'-biphenyl]-4-yl) ethanethioate (AZOP 2)**

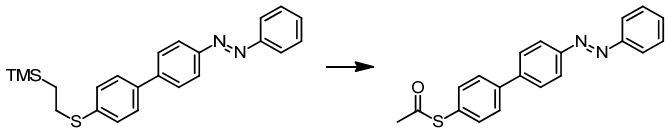

26 AZOP 2

Compound **26** (103 mg, 0.27 mmol, 1.0 eq.) was dissolved under an argon atmosphere in dry tetrahydrofuran (10 mL) and the solution was degassed by purging argon through it. Then tetrabutylammonium fluoride (1 M in THF, 0.34 mL, 0.34 mmol, 1.3 eq.) was added and the reaction mixture turned from orange to deep purple. The reaction mixture was stirred at room temperature for 1 hour. Afterwards the flask was cooled with an ice bath and acetyl chloride (1.00 mL, 11.2 mmol, 42 eq.) was added and the reaction mixture turned back to orange. After 10 minutes the ice bath was removed and the reaction mixture was stirred at room temperature for 44 hours. Afterwards it was slowly quenched with water and an extraction with dichloromethane (3x) was performed. The collected organic layers were washed with water (3x) and brine and then dried over $MgSO_4$. The solvent was removed under reduced pressure and the crude product was purified by column chromatography (silica gel, dichloromethane/*n*-hexane 1:1) to obtain target compound **AZOP 2** ($C_{20}H_{16}N_2OS$, 44 mg, 50%) as an orange solid.

TLC R_f = 0.62 (dichloromethane/*n*-hexane 1:1).

^{1}H-NMR (400 MHz, $CDCl_3$, δ/ppm): 8.01 (d, $^3J_{HH}$ = 8.5 Hz, 2H), 7.95 (d, $^3J_{HH}$ = 7.1 Hz, 2H), 7.76 (d, $^3J_{HH}$ = 8.5 Hz, 2H), 7.71 (d, $^3J_{HH}$ = 8.3 Hz, 2H), 7.52 (m, 5H), 2.46 (s, 3H).

^{13}C-NMR (101 MHz, $CDCl_3$, δ/ppm): 194.0, 152.7, 152.1, 142.6, 141.3, 134.9, 131.1, 129.1, 128.0, 127.9, 127.5, 123.5, 122.9, 30.3.

MS (EI, m/z): 332.1 (89%, M^+), 290.1 (56%), 227.1 (18%), 185.1 (100%), 152.1 (60%), 77.1 (40%), 43.0 (15%).

EA calculated: C = 72.26, H = 4.85, N = 8.43,
found: C = 72.00, H = 4.93, N = 8.48.

UV/Vis ($CHCl_3$, λ_{max}/nm, (ε/L · mol^{-1} · cm^{-1})): 241 (11200), 345 (26000), 441 (1100).

Crystal data	formula	$C_{20}H_{16}N_2OS$
	formula weight	332.43
	Z, calculated density	4, 1.375 Mg · m^{-3}
	F(000)	696
	description and size of crystal	yellow needle, 0.020 · 0.130 · 0.270 mm^3
	absorption coefficient	0.210 mm^{-1}
	min/max transmission	0.97 / 1.00
	temperature	123K
	radiation (wavelength)	Mo K_α (λ = 0.71073 Å)
	Crystal system, space group	orthorhombic, P 2_1 2_1 2_1
	a	5.8535(2) Å
	b	7.4207(3) Å
	c	36.9723(14) Å
	α	90°
	β	90°
	γ	90°
	V	1605.97(10) $Å^3$
	min/max Θ	2.203° / 27.552°
	number of collected reflections	11905
	number of independent refections	3627 (merging r = 0.043)
	number of observed reflections	2692 (I>2.0σ(I))
	number of refined parameters	218
	r	0.0527
	rW	0.0613
	goodness of fit	1.0393

1,2-Bis(4'-((2-(trimethylsilyl)ethyl)thio)-[1,1'-biphenyl]-4-yl)diazene (27)

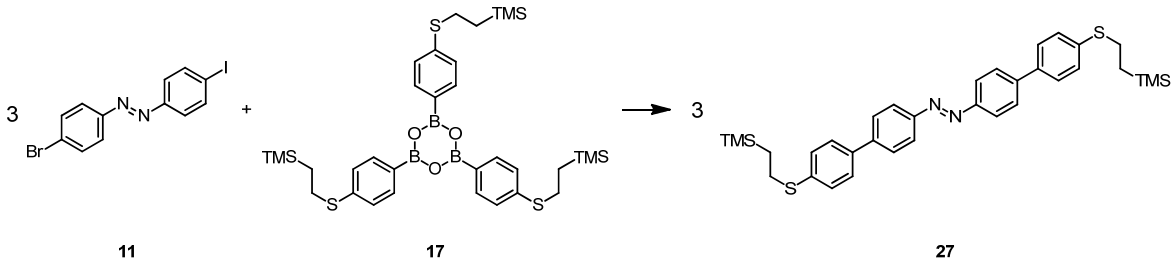

11 17 27

1-(4-Bromophenyl)-2-(4-iodophenyl)diazene (**11**, 203 mg, 0.52 mmol, 1.0 eq.), boroxine **17** (293 mg, 0.41 mmol, 0.8 eq.), potassium carbonate (145 mg, 1.05 mmol, 2.0 eq.), dry ethanol (20 mL) and dry toluene (20 mL) were added under an argon atmosphere into a dry flask and the resulting reaction mixture was degassed by purging argon through the solution. $Pd(PPh_3)_4$ (30 mg, 0.03 mmol, 5 mol%) was added and the reaction mixture was heated at 70 °C for 22 hours. After dilution of the reaction mixture with water it was extracted with ethyl acetate (3x). The organic layers were then washed with water (3x) and brine and dried over $MgSO_4$. The solvent was removed under reduced pressure and the crude product was purified by column chromatography (silica gel, dichloromethane/cyclohexane 1:1) to afford compound **27** ($C_{34}H_{42}N_2S_2Si_2$, 227 mg, 72%) as an orange solid.

TLC R_f = 0.43 (dichloromethane/cyclohexane 1:1).

^{1}H-NMR (400 MHz, $CDCl_3$, δ/ppm): 8.01 (d, $^3J_{HH}$ = 8.5 Hz, 4H), 7.75 (d, $^3J_{HH}$ = 8.5 Hz, 4H), 7.61 (d, $^3J_{HH}$ = 8.3 Hz, 4H), 7.40 (d, $^3J_{HH}$ = 8.3 Hz, 4H), 3.03 (m, 4H), 0.98 (m, 4H), 0.07 (s, 18H).

^{13}C-NMR (101 MHz, $CDCl_3$, δ/ppm): 151.8, 143.0, 137.5, 137.4, 128.9, 127.5, 127.4, 123.5, 29.4, 16.9, -1.7.

MS (EI, m/z): 598.2 (47%, M^+), 542.1 (13%), 257.0 (25%), 73.0 (100%).

EA calculated: C = 68.17, H = 7.07, N = 4.68,
found: C = 68.26, H = 7.18, N = 4.71.

_S,S'_-(diazene-1,2-diylbis([1,1'-biphenyl]-4',4-diyl)) diethanethioate (AZOP 3)

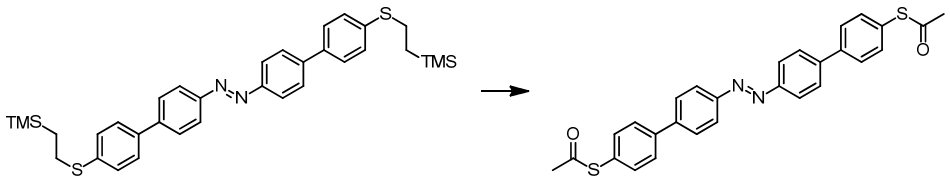

27 AZOP 3

Compound **27** (149 mg, 0.25 mmol, 1.0 eq.) was dissolved under an argon atmosphere in dry tetrahydrofuran and the solution was degassed by purging argon through it. Then tetrabutylammonium fluoride (1 M in THF, 5.00 mL, 5.00 mmol, 20 eq.) was added and the reaction mixture turned from orange to deep purple. The reaction mixture was stirred at room temperature for 1.5 hours. Afterwards the flask was cooled with an ice bath and acetyl chloride (5.0 mL) was added and the reaction mixture turned back to orange. Before removing the ice bath the reaction mixture was stirred for 10 minutes and then for 18 hours at room temperature. Afterwards it was slowly quenched with water. An extraction with dichloromethane (3x) was performed and the collected organic layers were washed with water (3x) and brine and dried over $MgSO_4$. The solvent was removed under reduced pressure and the crude product was purified by column chromatography (silica gel, dichloromethane) to obtain target compound **AZOP 3** ($C_{28}H_{22}N_2O_2S_2$, 42 mg, 35%) as an orange solid.

TLC R_f = 0.46 (dichloromethane).

^{1}H-NMR (400 MHz, $CDCl_3$, δ/ppm): 8.03 (d, $^3J_{HH}$ = 8.5 Hz, 4H), 7.77 (d, $^3J_{HH}$ = 8.5 Hz, 4H), 7.71 (d, $^3J_{HH}$ = 7.9 Hz, 4H), 7.52 (d, $^3J_{HH}$ = 8.3 Hz, 4H), 2.47 (s, 6H).

^{13}C-NMR (101 MHz, $CDCl_3$, δ/ppm): 194.0, 152.2, 142.7, 141.3, 134.9, 128.0, 127.9, 127.6, 123.5, 30.3.

MS (EI, m/z): 482.1 (49%, M^+), 440.1 (53%), 398.0 (47%), 227.0 (20%), 185.0 (100%), 152.0 (72%), 43.0 (18%).

EA calculated: C = 69.68, H = 4.59, N = 5.80,
found: C = 69.52, H = 4.60, N = 5.81.

UV/Vis ($CHCl_3$, λ_{max}/nm, (ε/L · mol^{-1} · cm^{-1})): 246 (20700), 365 (37900).

N-((4-(2-(Trimethylsilyl)ethyl)thio)phenyl)-phthalimide (30)

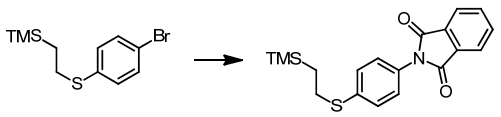

16 30

(2-((4-Bromophenyl)thio)ethyl)trimethylsilane (**16**, 1.29 g, 4.45 mmol, 1.0 eq.), phthalimide (786 mg, 5.34 mmol, 1.2 eq.), copper(I) oxide (382 mg, 2.67 mmol, 0.6 eq.) and 2,4,6-collidine (10 mL) were added under an argon atmosphere into a flask and the reaction mixture was heated to reflux for 30 hours. The reaction mixture was then cooled to room temperature and diluted with dichloromethane and washed with an aqueous HCl-solution (1 M) and with water. The organic layer was dried over $MgSO_4$ and the solvent was removed under reduced pressure. The resulting crude product was purified by column chromatography (silica gel, dichloromethane/*n*-hexane 2:1) to afford *N*-((4-(2-(trimethylsilyl)ethyl)thio)phenyl)phthalimide (**30**, $C_{19}H_{21}NO_2SSi$, 1.22 g, 77%) as a yellowish solid.

TLC R_f = 0.51 (dichloromethane/*n*-hexane 2:1).

^{1}H-NMR (400 MHz, $CDCl_3$, δ/ppm): 7.96 (m, 2H), 7.80 (m, 2H), 7.39 (m, 4H), 3.00 (m, 2H), 0.97 (m, 2H), 0.06 (s, 9H).

^{13}C-NMR (101 MHz, $CDCl_3$, δ/ppm): 167.2, 137.8, 134.4, 131.7, 129.1, 128.9, 126.8, 123.8, 29.4, 16.8, -1.7.

MS (EI, m/z): 355.1 (18%, M^+), 327.1 (67%), 312.1 (22%), 73.1 (100%).

EA calculated: C = 64.19, H = 5.95, N = 3.94,
found: C = 64.13, H = 6.08, N = 3.95.

4-((2-(Trimethylsilyl)ethyl)thio)aniline (31)

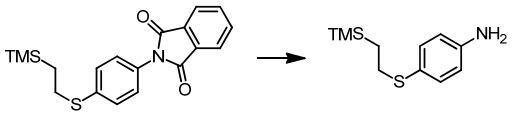

30 **31**

N-((4-(2-(Trimethylsilyl)ethyl)thio)phenyl)-phthalimide (**30**, 1.43 g, 4.03 mmol, 1.0 eq.) was dissolved under an argon atmosphere in dry dichloromethane (60 mL), dry tetrahydrofuran (10 mL) and dry methanol (10 mL). Then hydrazine monohydrate (1.96 mL, 40.3 mmol, 10 eq.) was added at once and the resulting reaction mixture was stirred at 50 °C for 30 minutes. Afterwards the reaction mixture was cooled to room temperature and the precipitate formed was filtered off. The filtrate was washed with an aqueous NaOH-solution (1 M) and the aqueous layer was extracted with dichloromethane (3x). The collected organic layers were washed with water (3x) and dried over $MgSO_4$. The solvent was removed under reduced pressure and the crude product was purified by column chromatography (silica gel, ethyl acetate/*n*-hexane 1:2) to obtain 4-((2-(trimethylsilyl)ethyl)thio)aniline (**31**, $C_{11}H_{19}NSSi$, 909 mg, quant.) as a colorless liquid.

TLC R_f = 0.58 (ethyl acetate/*n*-hexane 1:2).

^{1}H-NMR (400 MHz, $CDCl_3$, δ/ppm): 7.22 (d, $^3J_{HH}$ = 8.4 Hz, 2H), 6.63 (d, $^3J_{HH}$ = 8.4 Hz, 2H), 3.68 (s_{br}, 2H), 2.81 (m, 2H), 0.85 (m, 2H), -0.01 (s, 9H).

^{13}C-NMR (101 MHz, $CDCl_3$, δ/ppm): 145.5, 133.6, 123.9, 115.4, 32.1, 17.1, -1.9.

MS (EI, m/z): 225.1 (35%, M^+), 197.1 (54%), 182.0 (28%), 166.0 (18%), 73.0 (100%).

1-(4-bromophenyl)-2-(4-((2-(trimethylsilyl)ethyl)thio)phenyl)diazene (32)

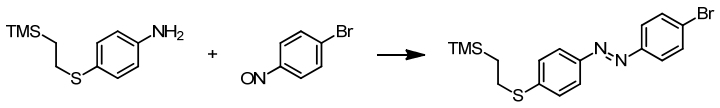

31 13 32

4-((2-(Trimethylsilyl)ethyl)thio)aniline (**31**, 248 mg, 1.10 mmol, 1.0 eq) and the crude 1-bromo-4-nitrosobenzene (**13**, 468 mg) were added to acetic acid (14 mL) and the reaction mixture was stirred at room temperature for 5.5 hours. The reaction mixture was carefully neutralized with a saturated aqueous $NaHCO_3$-solution and subsequently an extraction with ethyl acetate (3x) was performed. The collected organic layers were washed with water (3x) and dried over $MgSO_4$. The solvent was removed under reduced pressure and the crude product was purified by column chromatography (silica gel, dichloromethane/*n*-hexane 1:2) to afford azo compound **32** ($C_{17}H_{21}BrN_2SSi$, 145 mg, 40%) as an orange solid.

TLC R_f = 0.67 (dichloromethane/*n*-hexane 1:2).

^{1}H-NMR (400 MHz, $CDCl_3$, δ/ppm): 7.85 (d, $^3J_{HH}$ = 8.7 Hz, 2H), 7.78 (d, $^3J_{HH}$ = 8.8 Hz, 2H), 7.64 (d, $^3J_{HH}$ = 8.8 Hz, 2H), 7.36 (d, $^3J_{HH}$ = 8.7 Hz, 2H), 3.05 (m, 2H), 0.99 (m, 2H), 0.08 (s, 9H).

***tert*-Butyl(4-nitrophenyl)sulfane (36)**[330]

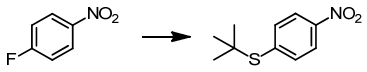

35 **36**

1-Fluoro-4-nitrobenzene (**35**, 3.20 mL, 302 mmol, 1.0 eq.) and sodium *tert*-butyl sulfide (5.62 g, 50.0 mmol, 1.7 eq.) were dissolved in dry *N*,*N*-dimethylformamide (120 mL). The reaction mixture was stirred under an argon atmosphere at room temperature for 2 hours. The reaction mixture was then poured into brine (200 mL) and extracted with *tert*-butyl methyl ether (3x). The combined organic layers were washed with water (3x) and then dried over $MgSO_4$. The solvent was removed under reduced pressure and the crude product was purified by column chromatography (silica gel, dichloromethane/*n*-hexane 1:5) to afford *tert*-butyl(4-nitrophenyl)-sulfane (**36**, $C_{10}H_{13}NO_2S$, 5.91 g, 93%) as an orange solid.

TLC R_f = 0.19 (dichloromethane/*n*-hexane 1:5).

^{1}H-NMR (400 MHz, $CDCl_3$, δ/ppm): 8.17 (d, $^3J_{HH}$ = 8.7 Hz, 2H), 7.67 (d, $^3J_{HH}$ = 8.8 Hz, 2H), 1.36 (s, 9H).

4-(*tert*-Butylthio)aniline (37)[330]

36 **37**

tert-Butyl(4-nitrophenyl)sulfane (**36**, 5.50 g, 26.0 mmol, 1.0 eq.) was dissolved in ethanol (110 mL). Hydrochloric acid (36%, 3 mL) and tin powder (6.19 g, 52.1 mmol, 2.0 eq.) were added to the solution. The reaction mixture was stirred at room temperature for 2.5 hours. After neutralization with an aqueous NaOH-solution (1 M) the reaction mixture was extracted with toluene (3x). The solvent was removed under reduced pressure and the crude product was purified by column chromatography (silica gel, dichloromethane/*n*-hexane 2:1) to obtain 4-(*tert*-butylthio)aniline (**37**, $C_{10}H_{15}NS$, 2.54 g, 83%) as a yellowish solid.

TLC R_f = 0.29 (dichloromethane/*n*-hexane 2:1).

^{1}H-NMR (400 MHz, $CDCl_3$, δ/ppm): 7.30 (d, $^3J_{HH}$ = 8.5 Hz, 2H), 6.63 (d, $^3J_{HH}$ = 8.5 Hz, 2H), 3.77 (s_{br}, 2H), 1.24 (s, 9H).

1-(4-Bromophenyl)-2-(4-(*tert*-butylthio)phenyl)diazene (38)

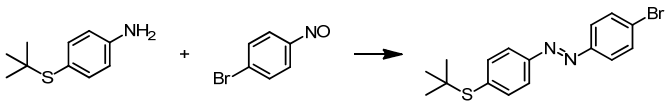

37 13 38

The crude 1-bromo-4-nitrosobenzene (**13**, 922 mg) was dissolved in acetic acid (60 mL) and 4-(*tert*-butylthio)aniline (**37**, 896 mg, 0.49 mmol) was added. The reaction mixture was stirred under an argon atmosphere at room temperature for 22 hours. The orange precipitate was removed by filtration and to the filtrate a saturated aqueous $NaHCO_3$-solution was slowly added. The filtrate was then extracted with ethyl acetate (3x). The initially removed precipitate was added to the collected organic layers. The solvent was removed under reduced pressure and the crude product was purified by column chromatography (silica gel, dichloromethane/*n*-hexane 1:1) to obtain azo compound **38** ($C_{16}H_{17}BrN_2S$, 705 mg, 41% over two steps) as an orange solid.

TLC R_f = 0.65 (dichloromethane/*n*-hexane 1:1).

^{1}H-NMR (400 MHz, $CDCl_3$, δ/ppm): 7.86 (d, $^3J_{HH}$ = 8.5 Hz, 2H), 7.80 (d, $^3J_{HH}$ = 8.7 Hz, 2H), 7.66 (m, 4H), 1.34 (s, 9H).

^{13}C-NMR (101 MHz, $CDCl_3$, δ/ppm): 152.3, 151.3, 137.9, 136.9, 132.4, 125.7, 124.4, 122.7, 46.8, 31.1.

MS (EI, m/z): 348.1 (27%, M^+), 292.0 (80%), 185.0 (18%), 155.0 (40%), 137.0 (100%), 109.0 (92%), 57.1 (70%), 41.1 (20%).

EA calculated: C = 55.02, H = 4.91, N = 8.02,
found: C = 54.80, H = 4.83, N = 7.95.

1-(4-(*tert*-Butylthio)phenyl)-2-(2',3',4',5',6'-pentafluoro-[1,1'-biphenyl]-4-yl)diazene (39)

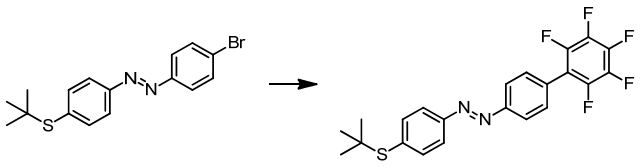

38 39

1-(4-Bromophenyl)-2-(4-(*tert*-butylthio)phenyl)diazene (**38**, 306 mg, 0.88 mmol, 1.0 eq.), pentafluorophenylboronic acid (210 mg, 0.99 mmol, 1.1 eq.), silver oxide (243 mg, 1.10 mmol, 1.2 eq.), $Pd_2(dba)_2$ (40 mg, 0.04 mmol, 5 mol%), tri-*tert*-butylphosphine (0.03 mL, 0.12 mmol, 14 mol%), cesium fluoride (266 mg, 1.75 mmol, 2.0 eq.) and dry *N*,*N*-dimethylformamide (10 mL) were added under an argon atmosphere into a microwave vial. The vial was exposed to microwave irradiation at 180 °C for 10 minutes. The reaction mixture was then cooled to room temperature and poured into water and then extracted with ethyl acetate (3x). The collected organic layers were washed with water and then filtered over Celite®. The solvent was removed under reduced pressure and the crude product was purified by column chromatography (silica gel, dichloromethane/*n*-hexane 1:5) to obtain compound **39** ($C_{22}H_{17}F_5N_2S$, 284 mg, 74%) as an orange solid.

TLC R_f = 0.35 (dichloromethane/*n*-hexane 1:5).

^{1}H-NMR (400 MHz, $CDCl_3$, δ/ppm): 8.04 (d, $^3J_{HH}$ = 8.6 Hz, 2H), 7.90 (d, $^3J_{HH}$ = 8.5 Hz, 2H), 7.70 (d, $^3J_{HH}$ = 8.5 Hz, 2H), 7.60 (d, $^3J_{HH}$ = 8.4 Hz, 2H), 1.35 (s, 9H).

^{19}F-NMR (377 MHz, $CDCl_3$, δ/ppm): -143.0 (dd, $^3J_{FF}$ = 23.0 Hz, $^4J_{FF}$ = 7.9 Hz, 2F), -154.7 (t, $^3J_{FF}$ = 21.6 Hz, 1F), -161.9 (td, $^3J_{FF}$ = 22.5 Hz, $^4J_{FF}$ = 8.5 Hz, 2F).

MS (EI, m/z): 436.1 (34%, M^+), 380.0 (100%), 243.0 (62%), 137.0 (58%), 109.0 (56%), 57.1 (34%).

EA calculated: C = 60.54, H = 3.93, N = 6.42,
found: C = 60.24, H = 4.08, N = 6.42.

(4-((2',3',4',5',6'-Pentafluoro-[1,1'-biphenyl]-4-yl)diazenyl)phenyl)ethanethioate (AZOP 4)

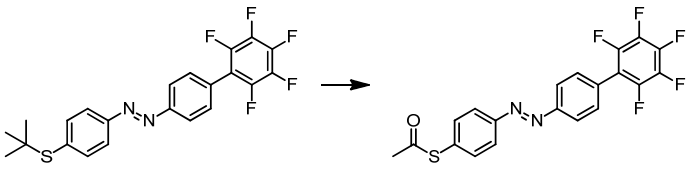

39 AZOP 4

Precursor **39** (44 mg, 0.10 mmol, 1.0 eq.) and acetyl chloride (2 mL) were dissolved in toluene (8 mL) and the solution was degassed by purging argon through it. Then boron tribromide (1M in CH_2Cl_2, 0.20 mL, 0.20 mmol, 2.0 eq.) was added dropwise and the reaction mixture was stirred at room temperature for 3 hours. Afterwards the mixture was cooled with an ice bath and it was quenched with cold water. The phases were separated and the aqueous layer was extracted with toluene (3x). The combined organic layers were washed with water (3x) and dried over $MgSO_4$. The solvent was removed under reduced pressure and the crude product was purified by column chromatography (silica gel, ethyl acetate/*n*-hexane 1:20) to obtain target structure **AZOP 4** ($C_{20}H_{11}F_5N_2OS$, 18 mg, 42%) as an orange solid.

TLC R_f = 0.17 (ethyl acetate/*n*-hexane 1:20).

^{1}H-NMR (400 MHz, $CDCl_3$, δ/ppm): 8.05 (d, $^3J_{HH}$ = 8.6 Hz, 2H), 7.99 (d, $^3J_{HH}$ = 8.6 Hz, 2H), 7.59 (m, 4H), 2.48 (s, 3H).

^{19}F-NMR (377 MHz, $CDCl_3$, δ/ppm): -143.8 (m, 2F), -155.6 (t, $^3J_{FF}$ = 20.7 Hz, 1F), -162.8 (m, 2F).

^{13}C-NMR ^{13}C-shifts determined from HSQC and HMBC experiments; due to C-F coupling, C-atoms adjacent to F-atoms were not identified; (126 MHz, CD_2Cl_2, δ/ppm): 193.1, 152.5, 151.1, 135.2, 135.1, 131.8, 131.2, 129.2, 123.4, 123.1, 30.1.

MS (EI, m/z): 422.0 (61%, M^+), 380.1 (100%), 243.0 (72%), 137.0 (43%), 109.0 (54%), 43.0 (36%).

EA calculated: C = 56.87, H = 2.62, N = 6.63,
found: C = 57.09, H = 2.88, N = 6.50.

UV/Vis ($CHCl_3$, λ_{max}/nm, (ε/L · mol^{-1} · cm^{-1})): 241 (12500), 341 (25600), 446 (900).

Crystal data	formula	$C_{20}H_{11}F_5N_2OS$
	formula weight	422.38
	Z, calculated density	2, 1.610 Mg · m^{-3}
	F(000)	428
	description and size of crystal	yellow needle, 0.040 · 0.070 · 0.260 mm^3
	absorption coefficient	0.252 mm^{-1}
	min/max transmission	0.98 / 0.99
	temperature	173K
	radiation (wavelength)	Mo K_α (λ = 0.71073 Å)
	Crystal system, space group	monoclinic, P c
	a	11.8019(4) Å
	b	6.2574(2) Å
	c	12.0048(4) Å
	α	90°
	β	100.662(2)°
	γ	90°
	V	871.24(5) $Å^3$
	min/max Θ	1.756° / 30.029°
	number of collected reflections	11812
	number of independent refections	5011 (merging r = 0.025)
	number of observed reflections	3991 (I>2.0σ(I))
	number of refined parameters	263
	r	0.0337
	rW	0.0473
	goodness of fit	0.9762

4-Boc-amino-(2',3',4',5',6'-pentafluoro[1,1'-biphenyl]) (41)

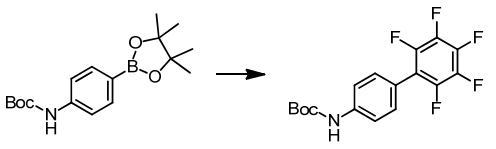

40 41

A mixture of 4-Boc-amino-(1-(4,4,5,5-tetramethyl-1,3,2-dioxaborolan-2-yl)benzene) (**40,** 102 mg, 0.32 mmol, 1.0 eq.), iodopentafluorobenzene (0.06 mL, 0.45 mmol, 1.4 eq.), cesium carbonate (814 mg, 2.50 mmol, 7.8 eq.) and dry toluene (40 mL) was degassed by purging argon through the solution. Then $Pd(PPh_3)_4$ (34 mg, 0.03 mmol, 9 mol%) was added under an argon atmosphere and the reaction mixture was heated to reflux for 30 hours. Afterwards water was added to the reaction mixture, which was extracted with ethyl acetate (3x). The collected organic layers were washed with water (3x) and brine and dried over $MgSO_4$. The solvent was removed under reduced pressure and the crude product was purified by column chromatography (silica gel, dichloromethane/*n*-hexane 2:1, ethyl acetate/*n*-hexane 1:5) to obtain 4-Boc-amino-(2',3',4',5',6'-pentafluoro[1,1'-biphenyl]) (**41**, $C_{17}H_{14}F_5NO_2$, 69 mg, 60%) as a colorless solid.

TLC R_f = 0.56 (dichloromethane/*n*-hexane 2:1),
R_f = 0.41 (ethyl acetate/*n*-hexane 1:5).

^{1}H-NMR (400 MHz, $CDCl_3$, δ/ppm): 7.50 (d, $^3J_{HH}$ = 8.7 Hz, 2H), 7.36 (d, $^3J_{HH}$ = 8.6 Hz, 2H), 6.59 (s, 1H), 1.54 (s, 9H).

^{19}F-NMR (377 MHz, $CDCl_3$, δ/ppm): -143.7 (dd, $^3J_{FF}$ = 23.3 Hz, $^4J_{FF}$ = 8.3 Hz, 2F), -156.4 (t, $^3J_{FF}$ = 21.2 Hz, 1F), -162.6 (td, $^3J_{FF}$ = 22.9 Hz, $^4J_{FF}$ = 8.4 Hz, 2F)

^{13}C-NMR (101 MHz, $CDCl_3$, δ/ppm): 181.6, 152.5, 139.4, 130.9, 118.4, 81.0, 28.3.

MS (EI, m/z): 359.1 (7%, M^+), 303.0 (76%), 285.0 (49%), 259.0 (100%), 57.1 (98%), 41.0 (19%).

EA calculated: C = 56.83, H = 3.93, N = 3.90,
found: C = 56.68, H = 3.92, N = 3.85.

2',3',4',5',6'-Pentafluoro-[1,1'-biphenyl]-4-amine (42)

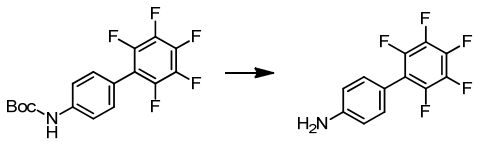

41 42

A mixture of 4-Boc-amino-(2',3',4',5',6'-pentafluoro[1,1'-biphenyl]) (**41**, 1.97 g, 5.48 mmol, 1.0 eq.) was dissolved in dichloromethane (300 mL). Then trifluoroacetic acid (10.0 mL, 131 mmol, 24 eq.) was added and the reaction mixture was heated to reflux for 1 hour. The mixture was then cooled to room temperature and neutralized carefully with a water/triethylamine mixture (1:5). The phases were separated and the organic layer was washed with water (3x) and brine and dried over $MgSO_4$. The solvent was removed under reduced pressure and without further purification 2',3',4',5',6'-pentafluoro-[1,1'-biphenyl]-4-amine (**42**, $C_{12}H_6F_5N$, 1.39 g, 98%) was obtained as a colorless solid.

^{1}H-NMR (400 MHz, $CDCl_3$, δ/ppm): 7.22 (d, $^3J_{HH}$ = 8.5 Hz, 2H), 6.77 (d, $^3J_{HH}$ = 8.6 Hz, 2H), 3.87 (s_{br}, 2H).

^{19}F-NMR (377 MHz, $CDCl_3$, δ/ppm): -145.0 (dd, $^3J_{FF}$ = 23.6 Hz, $^4J_{FF}$ = 8.4 Hz, 2F), -158.6 (t, $^3J_{FF}$ = 20.8 Hz, 1F), -164.1 (td, $^3J_{FF}$ = 23.7 Hz, $^4J_{FF}$ = 8.2 Hz, 2F).

MS (EI, m/z): 259.1 (100%, M^+).

EA calculated: C = 55.61, H = 2.33, N = 5.40,
found: C = 55.63, H = 2.63, N = 5.23.

1-(4-Bromophenyl)-2-(2',3',4',5',6'-pentafluoro-[1,1'-biphenyl]-4-yl)diazene (43)

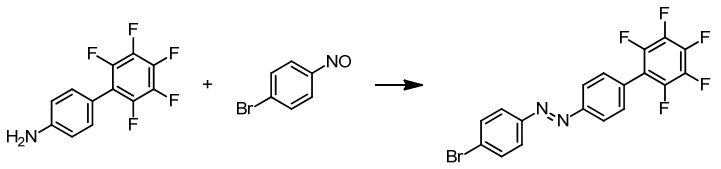

42 13 43

The crude 1-bromo-4-nitrosobenzene (**13**, 1.76 g,) and 2',3',4',5',6'-pentafluoro-[1,1'-biphenyl]-4-amine (**42**, 1.39 g, 5.38 mmol) were dissolved in acetic acid (200 mL) and stirred at room temperature for 29 hours. The reaction mixture was carefully neutralized with a saturated aqueous $NaHCO_3$-solution. Then an extraction with dichloromethane (3x) was performed and the collected organic layers were washed with water (3x) and brine and dried over $MgSO_4$. The solvent was removed under reduced pressure and the crude product was purified by column chromatography (silica gel, dichloromethane/*n*-hexane 1:5) to afford azo compound **43** ($C_{18}H_8BrF_5N_2$, 2.05 g, 89% over two steps) as an orange solid.

TLC R_f = 0.48 (dichloromethane/*n*-hexane 1:5).

^{1}H-NMR (400 MHz, $CDCl_3$, δ/ppm): 8.03 (d, $^3J_{HH}$ = 8.5 Hz, 2H), 7.84 (d, $^3J_{HH}$ = 8.7 Hz, 2H), 7.68 (d, $^3J_{HH}$ = 8.6 Hz, 2H), 7.60 (d, $^3J_{HH}$ = 8.3 Hz, 2H).

^{19}F-NMR (377 MHz, $CDCl_3$, δ/ppm): -143.0 (dd, $^3J_{FF}$ = 22.9 Hz, $^4J_{FF}$ = 8.1 Hz, 2F), -154.7 (t, $^3J_{FF}$ = 21.0 Hz, 1F), -161.9 (td, $^3J_{FF}$ = 22.2 Hz, $^4J_{FF}$ = 7.9 Hz, 2F).

^{13}C-NMR (101 MHz, $CDCl_3$, δ/ppm): 152.5, 151.3, 132.5, 131.1, 129.1, 126.0, 124.5, 123.2.

MS (EI, m/z): 426.0 (48%, M^+), 243.0 (100%), 224.0 (23%), 182.9 (21%), 155.0 (42%).

EA calculated: C = 50.61, H = 1.89, N = 6.56,
found: C = 50.35, H = 1.92, N = 6.76.

(4-Bromophenyl)(*tert*-butyl)sulfane (44)

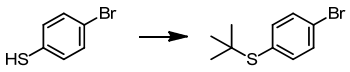

15 44

To a slurry reaction mixture of 4-bromothiophenol (**15**, 11.0 g, 58.2 mmol, 1.0 eq.) and 2-chloro-2-methylpropane (50.0 mL, 0.46 mol, 7.9 eq.) three spatula tips of aluminium trichloride were added. The reaction mixture was stirred under an argon atmosphere at room temperature for 2 hours and then quenched with water. The reaction mixture was extracted with *n*-hexane (3x) and the collected organic layers were dried over $MgSO_4$. The solvent was removed under reduced pressure and without further purification (4-bromophenyl)(*tert*-butyl)sulfane (**44**, $C_{10}H_{13}BrS$, 13.6 g, 96%) was obtained as a yellow viscous liquid.

^{1}H-NMR (400 MHz, $CDCl_3$, δ/ppm): 7.46 (d, $^3J_{HH}$ = 8.5 Hz, 2H), 7.38 (d, $^3J_{HH}$ = 8.5 Hz, 2H), 1.28 (s, 9H).

^{13}C-NMR (101 MHz, $CDCl_3$, δ/ppm): 139.1, 132.1, 131.8, 123.7, 46.3, 31.1.

MS (EI, m/z): 244.0 (14%, M^+), 189.9 (100%), 109.0 (36%), 57.1 (60%).

EA calculated: C = 48.99, H = 5.34,
found: C = 49.19, H = 5.41.

Tris(4-((*tert*-butyl)thio)phenyl)-boroxine (45)

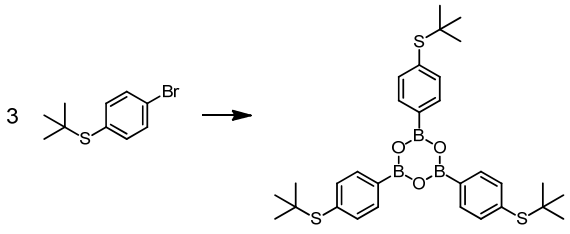

44 **45**

(4-Bromophenyl)(*tert*-butyl)sulfane (**44**, 2.98 g, 12.2 mmol, 1.0 eq.) was dissolved under an argon atmosphere in dry tetrahydrofuran (5 mL) in a dry Schlenk-tube. The solution was degassed by purging argon through it and cooled to -78 °C before adding *n*-butyllithium (1.6 M in *n*-hexane, 12.2 mL, 1.6 eq.) dropwise. The reaction mixture was stirred at -78 °C for 25 minutes. Afterwards triisopropyl borate (14.5 mL, 63.2 mmol, 5.2 eq.) was added dropwise and the reaction mixture was stirred at -78 °C for further 40 minutes. At this point, further tetrahydrofuran (10 mL) was added, since the formed precipitate inhibited the stirring. After 2 hours the cooling bath was removed and the reaction mixture was stirred at room temperature for 17 hours. The reaction mixture was quenched with water and then concentrated under reduced pressure to almost only the water phase. An extraction was then performed with diethyl ether (3x). The collected organic layers were washed with water (3x) and brine and then dried over $MgSO_4$. The solvent was removed under reduced pressure and the crude product was recrystallized from *n*-hexane to afford boroxine **45** ($C_{30}H_{39}B_3O_3S_3$, 1.43 g, 61%) as a colorless solid.

^{1}H-NMR (400 MHz, $CDCl_3$, δ/ppm): 8.18 (d, $^3J_{HH}$ = 8.1 Hz, 2H), 7.68 (d, $^3J_{HH}$ = 8.1 Hz, 2H), 1.35 (s, 9H).

^{13}C-NMR (101 MHz, $CDCl_3$, δ/ppm): 138.5, 136.6, 135.5, 46.6, 31.1.

MS (EI, m/z): 576.2 (12%, M^+), 407.9 (100%), 57.1 (98%).

EA calculated: C = 62.53, H = 6.82,
found: C = 62.62, H = 6.72.

1-(4'-(*tert*-Butylthio)-[1,1'-biphenyl]-4-yl)-2-(2',3',4',5',6'-pentafluoro-[1,1'-biphenyl]-4-yl)diazene (46)

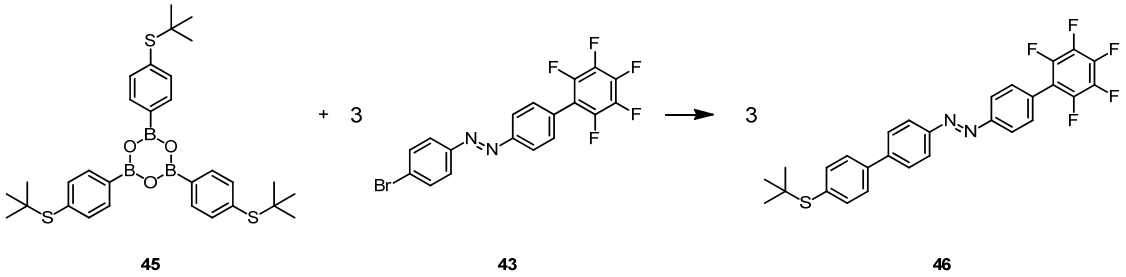

Boroxine **45** (85 mg, 0.15 mmol, 0.4 eq.), azo compound **43** (180 mg, 0.42 mmol, 1.0 eq.), potassium carbonate (117 mg, 0.84 mmol, 2.0 eq.), dry ethanol (10 mL) and dry toluene (10 mL) were added into a flask and the reaction mixture was degassed by purging argon thround gh the solution. Afterwards $Pd(PPh_3)_4$ (24 mg, 0.02 mmol, 5 mol%) was added under an argon atmosphere and the reaction mixture was stirred at 60 °C for 1 hour. After dilution with dichloromethane the organic layer was washed with water (3x) and brine and dried over $MgSO_4$. The solvent was removed under reduced pressure and the crude product was purified by column chromatography (silica gel, dichloromethane/cyclohexane 1:2) to obtain azo compound **46** ($C_{18}H_8BrF_5N_2$, 208 mg, 96%) as an orange solid.

TLC R_f = 0.27 (dichloromethane/cyclohexane 1:2).

^{1}H-NMR (400 MHz, $CDCl_3$, δ/ppm): 8.05 (m, 4H), 7.78 (d, $^3J_{HH}$ = 8.6 Hz, 2H), 7.62 (m, 6H), 1.34 (s, 9H).

^{19}F-NMR (377 MHz, $CDCl_3$, δ/ppm): -142.7 (dd, $^3J_{FF}$ = 23.0 Hz, $^4J_{FF}$ = 8.2 Hz, 2F), -154.6 (t, $^3J_{FF}$ = 20.9 Hz, 1F), -161.8 (td, $^3J_{FF}$ = 22.6 Hz, $^4J_{FF}$ = 8.0 Hz, 2F).

^{13}C-NMR (126 MHz, $CDCl_3$, δ/ppm): 152.8, 151.9, 143.4, 140.3, 137.9, 132.8, 131.1, 127.8, 127.2, 123.7, 123.1, 120.7, 46.3, 31.0.

MS (EI, m/z): 512.1 (39%, M^+), 456.1 (92%), 243.0 (36%), 185.0 (100%), 152.1 (49%), 57.1 (16%).

EA calculated: C = 65.62, H = 4.13, N = 5.47,
found: C = 65.72, H = 4.28, N = 5.13.

1-(2',3',4',5',6'-Pentafluoro-[1,1'-biphenyl]-4-yl)-2-(4'-((2-(trimethylsilyl)ethyl)thio)-[1,1'-biphenyl]-4-yl)diazene (47)

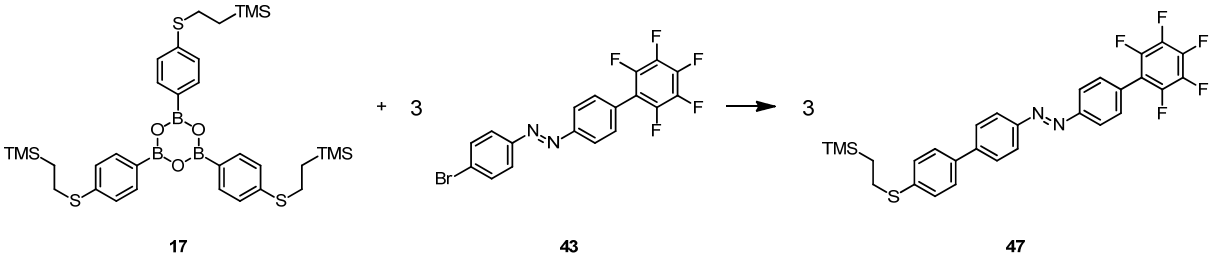

17 43 47

Boroxine **17** (116 mg, 0.23 mmol, 0.4 eq.), azo compound **43** (250 mg, 0.59 mmol, 1.0 eq.), potassium carbonate (161 mg, 1.17 mmol, 2.0 eq.), dry ethanol (20 mL) and dry toluene (20 mL) were added into a flask and the reaction mixture was degassed by purging argon through the solution. Afterwards $Pd(PPh_3)_4$ (34 mg, 0.03 mmol, 5 mol%) was added and the reaction mixture was stirred at 60 °C for 45 minutes. After dilution with dichloromethane the organic layer was washed with water (3x) and brine and then dried over $MgSO_4$. The solvent was removed under reduced pressure and the crude product was purified by column chromatography (silica gel, dichloromethane/cyclohexane 1:2) to obtain azo compound **47** ($C_{29}H_{25}F_5N_2SSi$, 319 mg, 98%) as an orange solid.

TLC R_f = 0.53 (dichloromethane/cyclohexane 1:2).

^{1}H-NMR (400 MHz, $CDCl_3$, δ/ppm): 8.05 (d, $^3J_{HH}$ = 8.7 Hz, 2H), 8.03 (d, $^3J_{HH}$ = 8.6 Hz, 2H), 7.76 (d, $^3J_{HH}$ = 8.6 Hz, 2H), 7.61 (d, $^3J_{HH}$ = 8.4 Hz, 2H), 7.60 (d, $^3J_{HH}$ = 8.6 Hz, 2H), 7.40 (d, $^3J_{HH}$ = 8.4 Hz, 2H), 3.03 (m, 2H), 0.99 (m, 2H), 0.07 (s, 9H).

^{19}F-NMR (377 MHz, $CDCl_3$, δ/ppm): -143.0 (dd, $^3J_{FF}$ = 23.0 Hz, $^4J_{FF}$ = 8.2 Hz, 2F), -154.9 (t, $^3J_{FF}$ = 20.9 Hz, 1F), -162.0 (td, $^3J_{FF}$ = 22.8 Hz, $^4J_{FF}$ = 8.1 Hz, 2F).

^{13}C-NMR (126 MHz, $CDCl_3$, δ/ppm): 152.8, 151.6, 143.5, 137.7, 137.2, 131.1, 128.9, 128.7, 127.5, 127.5, 123.7, 123.1, 29.3, 16.8, -1.73.

MS (EI, m/z): 556.2 (35%, M^+), 528.2 (27%), 257.1 (36%), 243.0 (20%), 73.0 (100%).

EA calculated: C = 62.57, H = 4.53, N = 5.03,
found: C = 62.59, H = 4.75, N = 4.91.

_S_-(4'-((2',3',4',5',6'-Pentafluoro-[1,1'-biphenyl]-4-yl)diazenyl)-[1,1'-biphenyl]-4-yl) ethanethioate (AZOP 5)

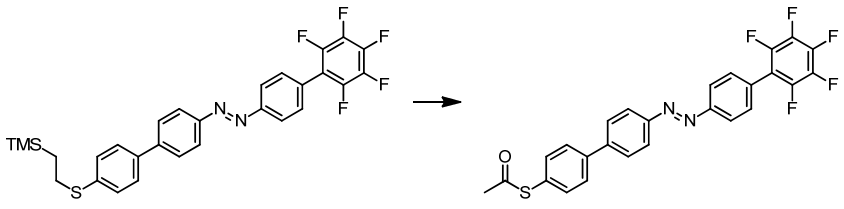

Compound **47** (18 mg, 0.03 mmol, 1.0 eq.) and acetyl chloride (1 mL) were dissolved under an argon atmosphere in dry dichloromethane (5 mL). Then silver tetrafluoroborate (76 mg, 0.39 mmol, 12 eq.) was added and the reaction mixture turned immediately from orange to dark blue and then dark red. After stirring at room temperature for 20 minutes the reaction mixture was quenched with water. The phases were separated and the organic layer was washed with water (3x) and brine and then dried over $MgSO_4$. The solvent was removed under reduced pressure and the crude product was purified by column chromatography (silica gel, dichloromethane/*n*-hexane 1:1) to obtain target structure **AZOP 5** ($C_{26}H_{15}F_5N_2OS$, 13 mg, 83%) as an orange solid.

TLC R_f = 0.22 (dichloromethane/*n*-hexane 1:1).

^{1}H-NMR (400 MHz, $CDCl_3$, δ/ppm): 8.06 (d, $^3J_{HH}$ = 8.4 Hz, 2H), 8.05 (d, $^3J_{HH}$ = 8.3 Hz, 2H), 7.78 (d, $^3J_{HH}$ = 8.5 Hz, 2H), 7.72 (d, $^3J_{HH}$ = 8.4 Hz, 2H), 7.61 (d, $^3J_{HH}$ = 8.4 Hz, 2H), 7.53 (d, $^3J_{HH}$ = 8.3 Hz, 2H), 2.47 (s, 3H).

^{19}F-NMR (377 MHz, $CDCl_3$, δ/ppm): -142.7 (dd, $^3J_{FF}$ = 23.4 Hz, $^4J_{FF}$ = 8.4 Hz, 2F), -154.6 (t, $^3J_{FF}$ = 20.6 Hz, 1F), -161.7 (m, 2F).

^{13}C-NMR ^{13}C-shifts determined from HSQC and HMBC experiments; due to C-F coupling, C-atoms adjacent to F-atoms were not identified; (126 MHz, $CDCl_3$, δ/ppm): 128.7, 152.7, 152.0, 143.0, 141.2, 127.5, 194.0, 123.3, 123.4, 128.0, 127.9, 131.1, 134.9, 30.1.

MS (EI, m/z): 498.1 (58%, M^+), 456.1 (62%), 243.0 (40%), 185.0 (100%), 152.0 (58%), 43.0, (21%).

UV/Vis ($CHCl_3$, λ_{max}/nm, (ε/L · mol^{-1} · cm^{-1})): 243 (20400), 355 (42500), 439 (1800).

5-Phenyl-2,2'-bithiophene (53)

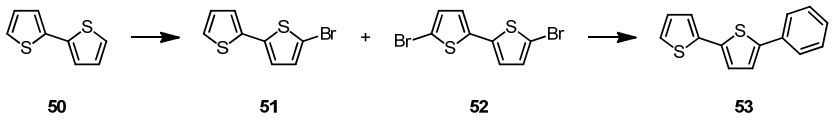

50 51 52 53

2,2'-Bithiophene (**50**, 11.5 g, 69.4 mmol, 1.0 eq.) was dissolved in chloroform (100 mL) and the reaction mixture was cooled to -35 °C. Then acetic acid (1.0 mL) was added followed by *N*-bromosuccinimide (12.4 g, 69.4 mmol, 1.0 eq.). The reaction mixture was kept at -35 °C for 1.5 hours without stirring. The precipitate formed (succinimide) was removed by filtration. The filtrate was washed successively with an aqueous NaOH-solution (1%) and then water. The solvent was removed and the remaining crude mixture (unreacted starting material **50**, the desired monobrominated bithiophene **51** and the dibrominated bithiophene **52**) was re-dissolved in toluene (70 mL) and water (20 mL). To the mixture phenylboronic acid (16.4 g, 134 mmol, 1.9 eq.), sodium carbonate (14.6 g, 138 mmol, 2.0 eq.) and $Pd(PPh_3)_4$ (2.20 g, 1.90 mmol, 3 mol%) were added and it was heated to 110 °C for 2.5 hours. After cooling down to room temperature an extraction with ethyl acetate (3x) followed. The collected organic layers were washed with brine and dried over $MgSO_4$. The solvent was removed under reduced pressure and the crude product was purified by column chromatography (silica gel, *n*-hexane) to afford 5-phenyl-2,2'-bithiophene (**53**, $C_{14}H_{10}S_2$, 7.05 g, 42% over two steps) as a colorless solid.

TLC R_f = 0.34 (*n*-hexane).

^{1}H-NMR (400 MHz, $CDCl_3$, δ/ppm): 7.60 (m, 2H), 7.38 (m, 2H), 7.28 (t, $^3J_{HH}$ = 7.4 Hz, 1H), 7.21 (m, 3H), 7.14 (d, $^3J_{HH}$ = 3.8 Hz, 1H), 7.02 (dd, $^3J_{HH}$ = 5.1 Hz, $^3J_{HH}$ = 3.6 Hz, 1H).

^{13}C-NMR (101 MHz, $CDCl_3$, δ/ppm): 143.1, 137.4, 136.7, 134.1, 128.9, 127.9, 127.6, 125.6, 124.6, 124.4, 123.7, 123.6.

MS (EI, m/z): 242.0 (100%, M^+).

EA calculated: C = 69.38, H = 4.16,
found: C = 69.13, H = 4.38.

5-Bromo-5'-phenyl-2,2'-bithiophene (55)

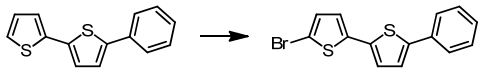

53 55

5-Phenyl-2,2'-bithiophene (**53**, 333 mg, 1.37 mmol, 1.0 eq.) was dissolved in chloroform (5 mL) and the solution was cooled to -35 °C. Then acetic acid (0.05 mL) and subsequently *N*-bromosuccinimide (245 mg, 1.37 mmol, 1.0 eq.) were added under an argon atmosphere and stirred at -35 °C for 3 hours. The reaction mixture was diluted with chloroform and the organic layer was washed with water (3x) and then dried over $MgSO_4$. The solvent was removed under reduced pressure and the crude product was purified by column chromatography (silica gel, *n*-hexane) to obtain 5-bromo-5'-phenyl-2,2'-bithiophene (**55**, $C_{14}H_9BrS_2$, 315 mg, 72%) as a yellowish solid.

TLC R_f = 0.43 (*n*-hexane).

^{1}H-NMR (400 MHz, $CDCl_3$, δ/ppm): 7.59 (m, 2H), 7.39 (m, 2H), 7.29 (t, $^3J_{HH}$ = 7.4 Hz, 1H), 7.21 (d, $^3J_{HH}$ = 3.8 Hz, 1H), 7.08 (d, $^3J_{HH}$ = 3.8 Hz, 1H), 6.98 (d, $^3J_{HH}$ = 3.8 Hz, 1H), 6.94 (d, $^3J_{HH}$ = 3.8 Hz, 1H).

^{13}C-NMR (101 MHz, $CDCl_3$, δ/ppm): 143.7, 138.9, 135.6, 133.8, 130.7, 129.0, 127.8, 125.7, 124.9, 123.8, 123.7, 110.9.

MS (EI, m/z): 321.9 (100%, M^+), 197.0 (44%).

EA calculated: C = 52.34, H = 2.82,
found: C = 52.57, H = 2.90.

4,4,5,5-Tetramethyl-2-(5'-phenyl-[2,2'-bithiophen]-5-yl)-1,3,2-dioxaborolane (56)

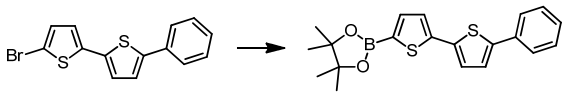

55 **56**

5-Bromo-5'-phenyl-2,2'-bithiophene (**55**, 361 mg, 1.12 mmol, 1.0 eq.) was dissolved under an argon atmosphere in dry tetrahydrofuran (20 mL) in a dry flask. The solution was cooled to -78 °C before adding *n*-butyllithium (1.6 M in *n*-hexane, 0.84 mL, 1.35 mmol, 1.2 eq.) dropwise. After the addition the reaction mixture was stirred at -78 °C for 1.5 hours. The solution turned from yellow to green and then to orange. Afterwards 2-*iso*propoxy-4,4,5,5-tetramethyl-1,3,2-dioxaborolane (0.28 mL, 1.35 mmol, 1.2 eq.) was added at once at -78 °C and stirred for 45 minutes. The cooling bath was then removed and the reaction mixture was slowly quenched with water. An extraction with dichloromethane (3x) followed and the collected organic layers were washed with water (3x) and dried over $MgSO_4$. The solvent was removed under reduced pressure and the remaining crude product was purified by column chromatography (silica gel, dichloromethane/*n*-hexane 1:5) to afford compound **56** ($C_{20}H_{21}BO_2S_2$, 97 mg, 23%) as dark green solid.

TLC R_f = 0.48 (dichloromethane/*n*-hexane 1:5).

^{1}H-NMR (400 MHz, $CDCl_3$, δ/ppm): 7.60 (m, 2H), 7.54 (m, 1H), 7.39 (m, 2H), 7.30 (m, 2H), 7.22 (m, 2H), 1.36 (s, 12H).

1-(4-Bromophenyl)-2-(4'-((2-(trimethylsilyl)ethyl)thio)-[1,1'-biphenyl]-4-yl)diazene (19)

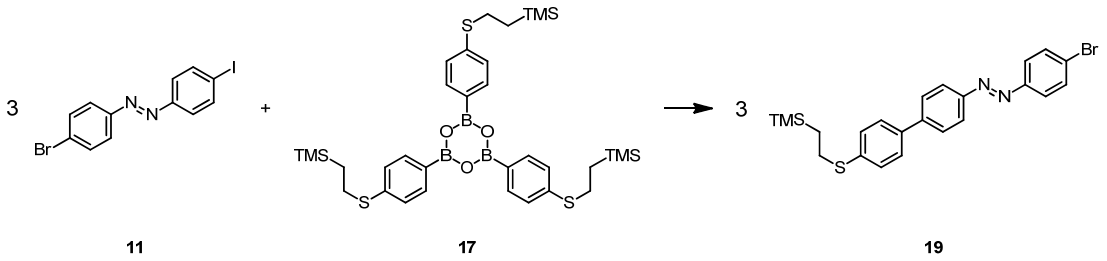

11 **17** **19**

Under an argon atmosphere 1-(4-bromophenyl)-2-(4-iodophenyl)diazene (**11**, 1.85 g, 4.78 mmol, 1.0 eq.), boroxine **17** (1.46 g, 2.06 mmol, 0.4 eq.), potassium carbonate (1.32 g, 9.57 mmol, 2.0 eq.), dry ethanol (60 mL) and dry toluene (30 mL) were added into a flask and the reaction mixture was degassed by purging argon through the solution. Then $Pd(PPh_3)_4$ (276 mg, 0.24 mmol, 5 mol%) was added and the reaction mixture was stirred at 50 °C for 24 hours. After addition of water an extraction with ethyl acetate (3x) was performed and the collected organic layers were dried over $MgSO_4$. The solvent was removed under reduced pressure and the crude product was purified by column chromatography (silica gel, dichloromethane/*n*-hexane 1:2) to obtain azo compound **19** ($C_{23}H_{25}BrN_2SSi$, 2.15 g, 96%) as an orange solid.

TLC R_f = 0.42 (dichloromethane/*n*-hexane 1:2)

^{1}H-NMR (400 MHz, $CDCl_3$, δ/ppm): 7.99 (d, $^3J_{HH}$ = 8.5 Hz, 2H), 7.82 (d, $^3J_{HH}$ = 8.7 Hz, 2H), 7.73 (d, $^3J_{HH}$ = 8.5 Hz, 2H), 7.66 (d, $^3J_{HH}$ = 8.7 Hz, 2H), 7.60 (d, $^3J_{HH}$ = 8.4 Hz, 2H), 7.39 (d, $^3J_{HH}$ = 8.4 Hz, 2H), 3.02 (m, 2H), 0.98 (m, 2H), 0.07 (s, 9H).

^{13}C-NMR (101 MHz, $CDCl_3$, δ/ppm): 151.7, 151.6, 143.5, 137.8, 137.3, 132.5, 129.0, 127.6, 127.6, 125.5, 124.5, 123.7, 29.4, 17.0, -1.6.

MS (EI, m/z): 470.1 (18%, M^+), 442.1 (16%), 257.1 (33%), 73.0 (100%).

1-(4-Bromophenyl)-2-(4-(4,4,5,5-tetramethyl-1,3,2-dioxaborolan-2-yl)phenyl)diazene (59)

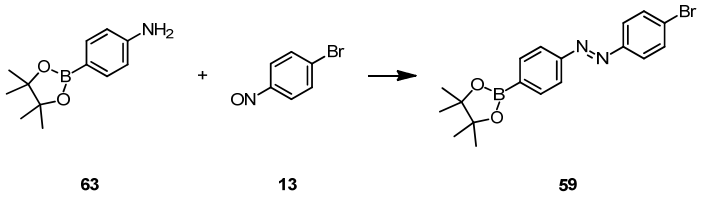

63 13 59

The crude 1-bromo-4-nitrosobenzene (**13**, 4.56 g) was dissolved in acetic acid (200 mL) and then 4-(4,4,5,5-tetramethyl-1,3,2-dioxaborolan-2-yl)aniline (**63**, 1.36 g, 6.21 mmol, 1.0 eq) was added. The reaction mixture was stirred under an argon atmosphere at room temperature for 20 hours. The reaction mixture was diluted with water and extracted with ethyl acetate (3x). The collected organic layers were washed with water (3x) and dried over $MgSO_4$. The solvent was removed under reduced pressure and the crude product was purified by column chromatography (silica gel, dichloromethane) to afford azo compound **59** ($C_{18}H_{20}BBrN_2O_2$, 366 mg, 15%) as an orange solid.

TLC R_f = 0.71 (dichloromethane).

^{1}H-NMR (400 MHz, $CDCl_3$, δ/ppm): 7.96 (d, $^3J_{HH}$ = 8.4 Hz, 2H), 7.88 (d, $^3J_{HH}$ = 8.4 Hz, 2H), 7.81 (d, $^3J_{HH}$ = 8.8 Hz, 2H), 7.65 (d, $^3J_{HH}$ = 8.8 Hz, 2H), 1.37 (s, 12H).

^{13}C-NMR (101 MHz, $CDCl_3$, δ/ppm): 154.2, 151.4, 135.7, 132.4, 125.6, 124.5, 122.1, 84.1, 24.91.

MS (EI, m/z): 386.1 (31%, M^+), 203.1 (100%), 155.0 (25%), 83.1 (20%).

5,5'-Diiodo-2,2'-bithiophene (64)

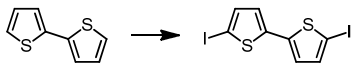

50 64

2,2'-Bithiophene (**50**, 1.56 g, 9.40 mmol, 1.0 eq.) and *N*-iodosuccinimide (5.29 g, 23.5 mmol, 2.5 eq.) were dissolved in methanol (140 mL) and acetic acid was added (1.6 mL). The reaction mixture was stirred under an argon atmosphere at room temperature for 7 hours. A white precipitate was formed and the flask was placed in the fridge overnight to ensure the complete precipitation of the product. The crude solid was collected and then washed with cold methanol. Without further purification the solid was dried under high vacuum to obtain 5,5'-diiodo-2,2'-bithiophene (**64**, $C_8H_4I_2S_2$, 3.41 g, 87%) as a colorless solid.

^{1}H-NMR (400 MHz, $CDCl_3$, δ/ppm): 7.15 (d, $^3J_{HH}$ = 3.8 Hz, 2H), 6.78 (d, $^3J_{HH}$ = 3.8 Hz, 2H).

^{13}C-NMR (101 MHz, $CDCl_3$, δ/ppm): 142.0, 137.7, 125.5, 72.5.

MS (EI, m/z): 417.8 (100%, M^+), 290.9 (13%), 246.9 (16%), 164.0 (15%), 82.0 (12%).

EA calculated: C = 22.98, H = 0.96,
found: C = 23.00, H = 0.96.

5-Iodo-5'-phenyl-2,2'-bithiophene (60)

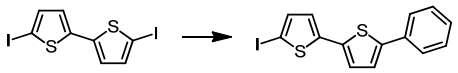

64 60

5,5'-Diiodo-2,2'-bithiophene (**64**, 921 mg, 2.20 mmol, 2.0 eq.), phenyl boronic acid (134 mg, 1.10 mmol, 1.0 eq.), potassium carbonate (457 mg, 3.30 mmol, 3.0 eq.), $Pd(PPh_3)_4$ (64 mg, 0.06 mmol, 5 mol%), dry methanol (10 mL) and dry toluene (10 mL) were added under an argon atmosphere into a microwave vial. The reaction mixture was irradiated at 100 °C for 8 minutes and afterwards it was diluted with water and then extracted with ethyl acetate (3x). The collected organic layers were washed with water (3x) and dried over $MgSO_4$. The solvent was removed under reduced pressure and the crude product was purified by column chromatography (silica gel, *n*-hexane) to afford 5-iodo-5'-phenyl-2,2'-bithiophene (**60**, $C_{14}H_9IS_2$, 129 mg, 32%) as colorless solid.

TLC R_f = 0.42 (*n*-hexane).

^{1}H-NMR (400 MHz, $CDCl_3$, δ/ppm): 7.58 (m, 2H), 7.38 (m, 2H), 7.29 (t, $^3J_{HH}$ = 7.4 Hz, 1H), 7.21 (d, $^3J_{HH}$ = 3.8 Hz, 1H), 7.16 (d, $^3J_{HH}$ = 3.8 Hz, 1H), 7.08 (d, $^3J_{HH}$ = 3.8 Hz, 1H), 6.86 (d, $^3J_{HH}$ = 3.8 Hz, 1H).

^{13}C-NMR (101 MHz, $CDCl_3$, δ/ppm): 143.7, 143.3, 137.7, 135.5, 133.8, 129.0, 127.8, 125.7, 125.0, 124.9, 123.7, 71.8.

MS (EI, m/z): 367.9 (100%, M^+), 197.0 (39%).

4-Boc-amino-(5'-phenyl-[2,2'-bithiophen]-5-yl)benzene (66)

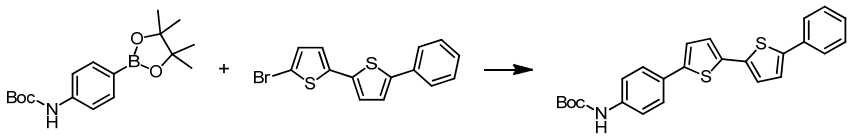

65 55 66

5-Iodo-5'-phenyl-2,2'-bithiophene (**60**, 56 mg, 0.18 mmol, 1.0 eq.), 4-Boc-amino-(4,4,5,5-tetramethyl-1,3,2-dioxaborolan-2-yl)benzene (**65**, 123 mg, 0.39 mmol, 2.2 eq.), potassium carbonate (97 mg, 0.70 mmol, 4.0 eq.), dry ethanol (10 mL) and dry toluene (10 mL) were added into a flask and the reaction mixture was degassed by purging argon through the solution. Then $Pd(PPh_3)_4$ (20 mg, 0.02 mmol, 10 mol%) was added under an argon atmosphere and the reaction mixture was heated at 80 °C for 1 hour. The reaction mixture was then diluted with water and an extraction was performed with dichloromethane (3x). The collected organic layers were dried over $MgSO_4$. The solvent was removed under reduced pressure and the crude product was purified by column chromatography (silica gel, dichloromethane/cyclohexane 2:1) to obtain bithiophene compound **66** ($C_{25}H_{23}NO_2S_2$, 23 mg, 31%) as a yellow solid.

TLC R_f = 0.54 (dichloromethane/cyclohexane 2:1).

^{1}H-NMR (400 MHz, $CDCl_3$, δ/ppm): 7.61 (m, 2H), 7.53 (m, 2H), 7.39 (m, 4H), 7.29 (m, 1H), 7.24 (m, 1H), 7.15 (m, 3H), 6.51 (s_{br}, 1H), 1.54 (s, 9H).

4-(5'-Phenyl-[2,2'-bithiophen]-5-yl)aniline (62)

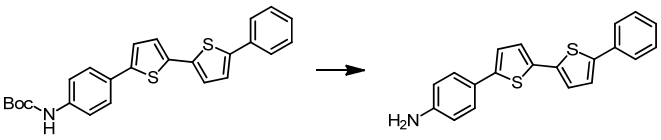

66 62

Bithiophene compound **66** (19 mg, 0.04 mmol, 1.0 eq.) was dissolved in dichloromethane (30 mL) and then trifluoroacetic acid (0.33 mL, 4.31 mmol, 100 eq.) was added. The reaction mixture was stirred at room temperature for 2 hours and then at 45 °C for further 2 hours. The solvent and the excess of trifluoroacetic acid were removed under reduced pressure and the remaining greenish solid was dissolved in a triethylamine/dichloromethane mixture (1:5) and stirred for a while. To the mixture water was then added and an extraction with dichloromethane (3x) was performed. The collected organic layers were dried over $MgSO_4$. The solvent was removed under reduced pressure and the crude product was purified by column chromatography (silica gel, dichloromethane/cyclohexane 2:1) to afford 4-(5'-phenyl-[2,2'-bithiophen]-5-yl)aniline (**62**, $C_{20}H_{15}NS_2$, 9 mg, 60%) as a greenish solid.

TLC R_f = 0.26 (dichloromethane/cyclohexane 2:1).

^{1}H-NMR (400 MHz, $CDCl_3$, δ/ppm): 7.60 (m, 2H), 7.40 (m, 4H), 7.28 (m, 1H), 7.23 (d, $^3J_{HH}$ = 3.6 Hz, 1H), 7.13 (m, 2H), 7.07 (d, $^3J_{HH}$ = 3.7 Hz, 1H), 6.70 (d, $^3J_{HH}$ = 8.3 Hz, 2H), 1.54 (s_{br}, 2H).

5,5-Dimethyl-2-(4-octylphenyl)-1,3,2-dioxaborinane (68)

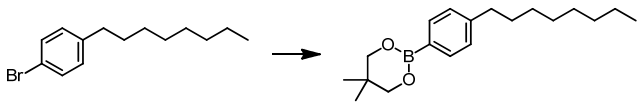

67 68

1-Bromo-4-octylbenzene (**67**, 803 mg, 2.98 mmol, 1.0 eq.) and dry tetrahydrofuran (25 mL) were added under an argon atmosphere to a dry flask, which was then cooled to -78 °C. Afterwards *n*-butyllithium (1.6 M in *n*-hexane, 2.24 mL, 3.58 mmol, 1.2 eq.) was added over a period of 10 minutes and then stirred at -78 °C for 30 minutes. Trimethyl borate (0.43 mL, 3.88 mmol, 1.3 eq.) was then added over a period of 10 minutes and the reaction mixture was continued to stir at -78 °C for further 50 minutes. After removal of the cooling bath the reaction mixture was quenched and neutralized with an aqueous HCl-solution (1 M). The reaction mixture was extracted with diethyl ether (3x) and the collected organic layers were washed with water (3x) and brine and dried over $MgSO_4$. The solvent was removed under reduced pressure and the crude product was dried under high vacuum conditions for 2 hours. The crude product was dissolved under an argon atmosphere in dry dichloromethane (20 mL) and 2,2-dimethyl-1,3-propanediol (264 mg, 2.54 mmol, 0.9 eq.) was added. The reaction mixture was stirred at room temperature for 2.5 hours. The solvent was removed under reduced pressure and the remaining crude product was purified by column chromatography (silica gel, dichloromethane/*n*-hexane 1:1) to obtain 5,5-mimethyl-2-(4-octylphenyl)-1,3,2-dioxaborinane (**68**, $C_{19}H_{31}BO_2$, 155 mg, 20%) as a colorless solid.

TLC R_f = 0.25 (dichloromethane/*n*-hexane 1:1).

^{1}H-NMR (400 MHz, $CDCl_3$, δ/ppm): 7.71 (d, $^3J_{HH}$ = 7.9 Hz, 2H), 7.17 (d, $^3J_{HH}$ = 7.9 Hz, 2H), 3.76 (s, 4H), 2.60 (m, 2H), 1.59 (m, 2H), 1.25 (m, 10H), 1.02 (s, 6H), 0.87 (t, $^3J_{HH}$ = 6.8 Hz, 3H).

^{13}C-NMR (101 MHz, $CDCl_3$, δ/ppm): 145.7, 133.8, 127.8, 72.3, 36.2, 31.9, 31.4, 29.5, 29.4, 29.3, 22.7, 21.9, 14.1.

MS (EI, m/z): 302.2 (36%, M^+), 203.1 (100%).

EA calculated: C = 75.50, H = 10.34,
found: C = 75.60, H = 10.33.

2-(4-Iodocyclopenta-1,3-dien-1-yl)-5-(4-octylphenyl)thiophene (83)

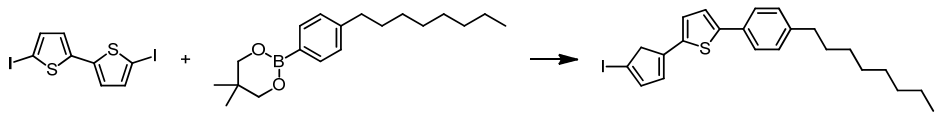

64 68 83

5,5'-Diiodo-2,2'-bithiophene (**64**, 185 mg, 0.44 mmol, 1.1 eq.), boronic ester **68** (121 mg, 0.40 mmol, 1.0 eq.), potassium carbonate (111 mg, 0.80 mmol, 2.0 eq.), dry ethanol (10 mL) and dry toluene (10 mL) were added under an argon atmosphere into a flask and the mixture was degassed by purging argon through the solution. Then $PdCl_2(PPh_3)_2$ (14 mg, 0.02 mmol, 5 mol%) was added and the reaction mixture was stirred at room temperature for 20 hours. The solvent was removed under reduced pressure and the remaining crude product mixture was purified by column chromatography (silica gel, *n*-hexane) to afford bithiophene compound **83** ($C_{23}H_{27}IS$, 33 mg, 17%) as a greenish solid.

TLC R_f = 0.34 (*n*-hexane).

^{1}H-NMR (400 MHz, $CDCl_3$, δ/ppm): 7.49 (d, $^3J_{HH}$ = 8.2 Hz, 2H), 7.19 (d, $^3J_{HH}$ = 8.1 Hz, 2H), 7.16 (m, 4H), 7.07 (d, $^3J_{HH}$ = 3.8 Hz, 1H), 6.85 (d, $^3J_{HH}$ = 3.8 Hz, 1H), 2.61 (m, 2H), 1.62 (m, 2H), 1.29 (m, 10H), 0.88 (t, $^3J_{HH}$ = 6.8 Hz, 3H).

tert-Butyl-2-iodobenzoate (73)[338]

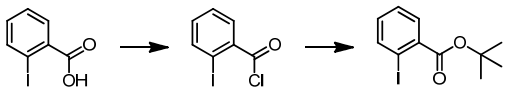

71 72 73

2-Iodobenzoic acid (**71**, 10.3 g, 41.7 mmol, 1.0 eq.) was dissolved in dichloromethane (100 mL) and then oxalyl chloride (2.0 M in CH_2Cl_2, 25.0 mL, 50.0 mmol, 1.2 eq.) was added, followed by a drop of *N*,*N*-dimethylformamide. Gas formation was observed and the milky reaction mixture was stirred at room temperature for 2.5 hours until it clarified. The solvent was removed under reduced pressure carefully, as 2-iodobenzoyl chloride (**72**) has a boiling point at 105 °C. The remaining yellowish crude liquid was not characterized, but subsequently used for the next reaction to *tert*-butyl-2-iodobenzoate (**73**): *tert*-Butanol (4.63 g, 62.5 mmol, 1.5 eq.) was dissolved in dry tetrahydrofuran (50 mL) in a dry flask under an argon atmosphere. The flask was cooled to -78 °C before adding *n*-butyllithium (1.6 M in *n*-hexane, 39.1 mL, 62.5 mmol, 1.5 eq.) dropwise and then stirred for 5 minutes. In the mean time, the crude mixture of compound **72** was dissolved in dry tetrahydrofuran (50 mL) and slowly added to the cooled reaction mixture, which was stirred at -78 °C for additional 20 minutes. The cooling bath was removed and the reaction mixture was stirred at room temperature for 2.5 hours. The reaction mixture was quenched with water and extracted with ethyl acetate (3x). The collected organic layers were washed with water (3x) and brine and dried over $MgSO_4$. The solvent was removed under reduced pressure and the crude product was purified by column chromatography (silica gel, ethyl acetate/cyclohexane 1:20) to afford *tert*-butyl-2-iodobenzoate (**73**, $C_{11}H_{13}IO_2$, 12.1 g, 96% over two steps) as a yellowish liquid.

TLC R_f = 0.55 (ethyl acetate/cyclohexane 1:20).

^{1}H-NMR (400 MHz, $CDCl_3$, δ/ppm): 7.94 (dd, $^3J_{HH}$ = 7.9 Hz, $^4J_{HH}$ = 1.1 Hz, 1H), 7.68 (dd, $^3J_{HH}$ = 7.7 Hz, $^4J_{HH}$ = 1.7 Hz, 1H), 7.37 (td, $^3J_{HH}$ = 7.6 Hz, $^4J_{HH}$ = 1.2 Hz, 1H), 7.10 (td, $^3J_{HH}$ = 7.6 Hz, , $^4J_{HH}$ = 1.7 Hz, 1H), 1.62 (s, 9H).

^{13}C-NMR (101 MHz, $CDCl_3$, δ/ppm): 166.2, 140.9, 137.4, 131.9, 130.5, 127.8, 93.4, 82.6, 28.2.

MS (EI, m/z): 304.0 (9%, M^+), 247.9 (100%), 230.9 (45%), 76.0 (10%), 57.1 (13%).

EA calculated: C = 43.44, H = 4.31,
found: C = 43.46, H = 4.25.

2-Bromo-5-((4-(4,4,5,5-tetramethyl-1,3,2-dioxaborolan-2-yl)phenyl)diazenyl)pyridine (76)

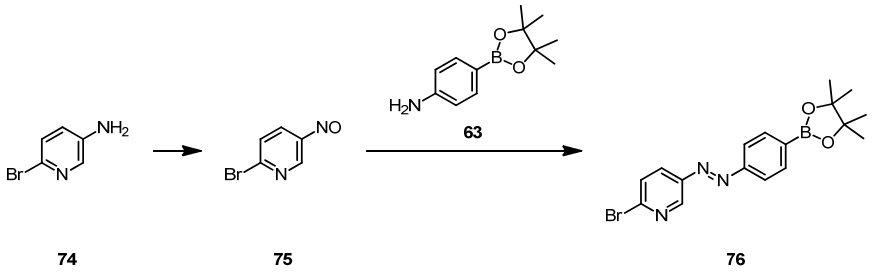

74 75 76

6-Bromopyridin-3-amine (**74**, 5.58 g, 32.3 mmol, 1.0 eq.) was dissolved in dichloromethane (100 mL) and then a solution of Oxone® ($2KHSO_5 \cdot KHSO_4 \cdot K_2SO_4$) (39.7 g, 64.5 mmol, 2.0 eq.) in water (300 mL) was added. The reaction mixture was stirred under an argon atmosphere at room temperature for 19 hours. Afterwards the phases were separated and the aqueous layer was extracted with dichloromethane (3x). The collected organic layers were washed with a saturated aqueous $NaHCO_3$-solution, water and brine and dried over $MgSO_4$. The solvent was removed under reduced pressure and the remaining green crude product (**75**) was purified by column chromatography (silica gel, ethyl acetate/cyclohexane 1:1) to obtain a solid **75** ($C_5H_3BrN_2O$, 3.24 g), which was not characterized, but immediately used in the next reaction to azo compound **76**: To 4-(4,4,5,5-tetramethyl-1,3,2-dioxaborolan-2-yl)aniline (**63**, 3.80 g, 17.3 mmol) and 2-bromo-5-nitrosopyridine (**75**, 3.24 g), acetic acid (200 mL) was added and the reaction mixture was stirred at room temperature for 3 days. The reaction mixture was carefully neutralized with a saturated aqueous $NaHCO_3$-solution and extrated with ethyl acetate (3x). The collected organic layers were washed with water (3x) and then dried over $MgSO_4$. The solvent was removed under reduced pressure and the crude product was purified by column chromatography (silica gel, dichloromethane) to afford azo compound **76** ($C_{17}H_{19}BBrN_3O_2$, 1.45 g, 12% over two steps) as an orange solid.

TLC R_f = 0.93 (ethyl acetate/cyclohexane 1:1), compound **75**,
R_f = 0.30 (dichloromethane), compound **76**.

^{1}H-NMR (400 MHz, $CDCl_3$, δ/ppm): 8.98 (d, $^3J_{HH}$ = 2.3 Hz, 1H), 8.02 (dd, $^3J_{HH}$ = 8.5 Hz, $^4J_{HH}$ = 2.6 Hz, 1H), 7.97 (d, $^3J_{HH}$ = 8.4 Hz, 2H), 7.91 (d, $^3J_{HH}$ = 8.4 Hz, 2H), 7.62 (d, $^3J_{HH}$ = 8.5 Hz, 1H), 1.38 (s, 12H).

^{13}C-NMR (101 MHz, $CDCl_3$, δ/ppm): 154.0, 148.2, 147.2, 144.2, 135.8, 129.0, 128.7, 122.3, 84.2, 24.9.

MS (EI, m/z): 387.1 (20%, M^+), 203.1 (100%), 83.1 (22%).

tert-Butyl-4'-((6-bromopyridin-3-yl)diazenyl)-[1,1'-biphenyl]-2-carboxylate (77)

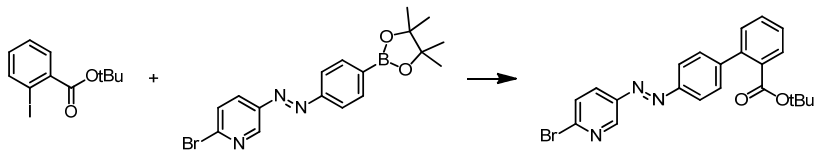

73 **76** **77**

Four microwave vials were each charged with the following mixture: *tert*-butyl-2-iodobenzoate (**73**, 940 mg, 3.1 mmol, 30 eq.), azo compound **76** (40 mg, 0.1 mmol, 1.0 eq.), sodium carbonate (1 M in H_2O, 10.0 mL, 97 eq.), $PdCl_2(PPh_3)_2$ (3.6 mg, 5 µmol, 5 mol%) and tetrahydrofuran (10 mL). The vials were irradiated in a microwave under an argon atmosphere at 40 °C for 45 minutes. To all four reaction mixtures water was added and the mixtures were poured together. Then an extraction with ethyl acetate (3x) was performed. The collected organic layers were dried over $MgSO_4$. The solvent was removed under reduced pressure and the crude product was purified by column chromatography (silica gel, ethyl acetate/cyclohexane 1:20) to afford azo compound **77** ($C_{22}H_{20}BrN_3O_2$, 77 mg, 43%) as an orange solid.

TLC R_f = 0.34 (ethyl acetate/cyclohexane 1:20).

^{1}H-NMR (400 MHz, $CDCl_3$, δ/ppm): 8.98 (d, $^3J_{HH}$ = 2.5 Hz, 1H), 8.05 (dd, $^3J_{HH}$ = 8.5 Hz, $^2J_{HH}$ = 2.6 Hz, 1H), 7.99 (d, $^3J_{HH}$ = 8.5 Hz, 2H), 7.85 (dd, $^3J_{HH}$ = 7.7 Hz, $^4J_{HH}$ = 1.3 Hz, 1H), 7.63 (d, $^3J_{HH}$ = 8.5 Hz, 1H), 7.53 (td, $^3J_{HH}$ = 7.5 Hz, $^4J_{HH}$ = 1.5 Hz, 1H), 7.49 (d, $^3J_{HH}$ = 8.5 Hz, 2H), 7.45 (td, $^3J_{HH}$ = 6.9 Hz, $^4J_{HH}$ = 1.3 Hz, 1H), 7.37 (dd, $^3J_{HH}$ = 7.6 Hz, $^4J_{HH}$ = 1.1 Hz, 1H), 1.30 (s, 9H).

^{13}C-NMR (101 MHz, $CDCl_3$, δ/ppm): 167.8, 151.6, 148.3, 147.4, 146.2, 144.2, 141.2, 132.9, 131.1, 130.6, 130.2, 129.8, 129.2, 128.9, 128.0, 123.2, 81.8, 27.9.

MS (EI, m/z): 437.1 (5%, M^+), 381.0 (32%), 197.1 (100%), 152.1 (12%), 57.1 (8%).

Methyl-4-bromo-3-hydroxybenzoate (79)[339]

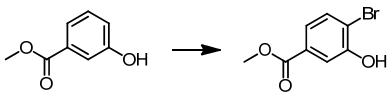

78 79

Methyl-3-hydroxybenzoate (**78**, 24.4 g, 160 mmol, 1.0 eq.) was dissolved in acetic acid (100 mL). Bromine (8.21 mL, 160 mmol, 1.0 eq.) was slowly added and the reaction mixture was stirred at room temperature for 5.5 hours. The reaction mixture was then diluted with water and an extraction with ethyl acetate (3x) was performed. The collected organic layers were washed with a saturated aqueous $NaHCO_3$-solution and dried over $MgSO_4$. The solvent was removed under reduced pressure and the crude product was purified by column chromatography (silica gel, dichloromethane) to obtain methyl-4-bromo-3-hydroxybenzoate (**79**, $C_8H_7BrO_3$, 13.5 g, 36%) as a colorless solid.

TLC R_f = 0.42 (dichloromethane).

^{1}H-NMR (400 MHz, $CDCl_3$, δ/ppm): 7.69 (d, $^4J_{HH}$ = 1.9 Hz, 1H), 7.54 (d, $^3J_{HH}$ = 8.3 Hz, 1H), 7.47 (dd, $^3J_{HH}$ = 8.3 Hz, $^4J_{HH}$ = 2.0 Hz, 1H), 5.97 (s_{br}, 1H, OH), 3.92 (s, 3H).

^{13}C-NMR (101 MHz, $CDCl_3$, δ/ppm): 166.4, 152.5, 132.3, 131.2, 122.7, 117.1, 115.6, 52.5.

MS (EI, m/z): 230.0 (50%, M^+), 198.9 (100%), 170.9 (17%), 63.0 (14%).

EA calculated: C = 41.59, H = 3.05,
found: C = 41.41, H = 2.99.

2-Bromo-5-(hydroxymethyl)phenol (80)[340]

79 **80**

Methyl-4-bromo-3-hydroxybenzoate (**79**, 3.03 g, 13.1 mmol, 1.0 eq.) was dissolved in dry dichloromethane (150 mL) and the solution was cooled to 0 °C. Afterwards diisobutylaluminium hydride (1.0 M in THF, 43.3 mL, 43.3 mmol, 3.3 eq.) was slowly added. The ice bath was then removed and the reaction mixture was stirred under an argon atmosphere at room temperature for 3 hours. The reaction mixture was quenched with a saturated aqueous potassium sodium tartrate solution (100 mL) and subsequently a saturated aqueous NH_4Cl-solution (60 mL) was added. The biphasic solution was stirred at room temperature overnight. The layers were then separated and the aqueous layer was extracted with dichloromethane (3x). The collected organic layers were dried over $MgSO_4$. The solvent was removed under reduced pressure and the remaining product was not further purified to obtain 2-bromo-5-(hydroxymethyl)phenol (**80**, $C_7H_7BrO_2$, 2.30 g, 86%) as a colorless solid.

^{1}H-NMR (400 MHz, $CDCl_3$, δ/ppm): 7.44 (d, $^3J_{HH}$ = 8.2 Hz, 1H), 7.04 (d, $^4J_{HH}$ = 2.0 Hz, 1H), 6.82 (dd, $^3J_{HH}$ = 8.2 Hz, $^4J_{HH}$ = 2.0 Hz, 1H), 5.51 (s_{br}), 4.64 (d, $^3J_{HH}$ = 6.0 Hz, 2H), 1.66 (t, $^3J_{HH}$ = 6.0 Hz, 1H).

^{13}C-NMR (101 MHz, $CDCl_3$, δ/ppm): 152.4, 142.6, 132.1, 120.1, 114.4, 109.1, 64.5.

MS (EI, m/z): 202.0 (100%, M^+), 172.9 (19%), 123.1 (36%), 95.1 (91%), 77.0 (45%).

EA calculated: C = 41.41, H = 3.47,
found: C = 41.12, H = 3.34.

2-Bromo-5-(bromomethyl)phenol (81)[340]

80 81

2-Bromo-5-(hydroxymethyl)phenol (**80**, 2.30 g, 11.4 mmol, 1.0 eq.) was suspended in chloroform (60 mL). The solution was cooled to 0 °C and phosphorus tribromide (0.53 mL, 5.67 mmol, 0.5 eq.) was added over a period of 25 minutes. After the addition the reaction mixture was continued to stir at 0 °C for 1 hour and then at room temperature for 2 hours. The reaction mixture was then poured into ice water and an extraction with dichloromethane (3x) was performed. The collected organic layers were dried over $MgSO_4$. The solvent was removed under reduced pressure and the crude product was purified by column chromatography (silica gel, ethyl acetate/dichloromethane 1:10) to obtain 2-bromo-5-(bromomethyl)phenol (**81**, $C_7H_6Br_2O$, 2.36 g, 78%) as a colorless solid.

TLC R_f = 0.86 (ethyl acetate/dichloromethane 1:10)

^{1}H-NMR (400 MHz, $CDCl_3$, δ/ppm): 7.42 (d, $^3J_{HH}$ = 8.2 Hz, 1H), 7.05 (d, $^4J_{HH}$ = 2.1 Hz, 1H), 6.84 (dd, $^3J_{HH}$ = 8.2 Hz, $^4J_{HH}$ = 2.1 Hz, 1H), 5.53 (s_{br}), 4.39 (s, 2H).

^{13}C-NMR (101 MHz, $CDCl_3$, δ/ppm): 152.3, 139.3, 132.3, 122.4, 116.6, 110.2, 32.2.

MS (EI, m/z): 265.9 (23%, M^+), 185.0 (100%), 77.0 (18%).

EA calculated: C = 31.62, H = 2.27,
found: C = 31.67, H = 2.23.

(2-Bromo-5-(bromomethyl)phenoxy)(*tert*-butyl)dimethylsilane (82)

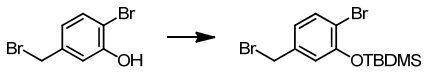

81 **82**

2-Bromo-5-(bromomethyl)phenol (**81**, 1.59 g, 5.96 mmol, 1.0 eq.) was dissolved under an argon atmosphere in dry *N*,*N*-dimethylformamide (20 mL). *tert*-Butyldimethylsilyl chloride (1.08 g, 7.16 mmol, 1.2 eq.) and subsequently imidazole (1.02 g, 14.9 mmol, 2.5 eq.) were added. The reaction mixture was stirred at room temperature for 3 hours and afterwards poured into *tert*-butylmethylether. The organic layer was washed with water (3x) and brine and dried over $MgSO_4$. The solvent was removed under reduced pressure and the crude product was purified by column chromatography (silica gel, dichloromethane/cyclohexane 1:10) to afford compound **82** ($C_{13}H_{20}Br_2OSi$, 1.11 g, 49%) as colorless liquid.

TLC R_f = 0.51 (dichloromethane/cyclohexane 1:10).

^{1}H-NMR (400 MHz, $CDCl_3$, δ/ppm): 7.48 (d, $^3J_{HH}$ = 8.1 Hz, 1H), 6.89 (d, $^4J_{HH}$ = 2.0 Hz, 1H), 6.84 (dd, $^3J_{HH}$ = 8.1 Hz, $^4J_{HH}$ = 2.1 Hz, 1H), 4.49 (s, 2H), 1.05 (s, 9H), 0.26 (s, 6H).

^{13}C-NMR (101 MHz, $CDCl_3$, δ/ppm): 153.0, 138.1, 133.8, 122.6, 120.5, 115.7, 45.7, 25.9, 18.6, -4.0.

(2-Bromo-5-((tritylthio)methyl)phenoxy)(*tert*-butyl)dimethylsilane (83)

82 **83**

(2-Bromo-5-(bromomethyl)phenoxy)(*tert*-butyl)dimethylsilane (**82**, 203 mg, 0.53 mmol, 1.0 eq.) and triphenylmethanethiol (221 mg, 0.80 mmol, 1.5 eq.) were dissolved under an argon atmosphere in dry tetrahydrofuran (10 mL). Then sodium hydride (60% dispersion in mineral oil, 107 mg, 2.66 mmol, 5.0 eq.) was added in small portions and the resulting reaction mixture was stirred at room temperature for 2 hours. Afterwards water was slowly added to quench the reaction mixture and an extraction with ethyl acetate (3x) was performed. The collected organic layers were washed with water (3x) and brine and dried over $MgSO_4$. The solvent was removed under reduced pressure and the crude product was purified by column chromatography (silica gel, dichloromethane/cyclohexane 1:10) to afford compound **83** ($C_{32}H_{35}BrOSSi$, 268 mg, 87%) as a colorless solid.

TLC R_f = 0.33 (dichloromethane/cyclohexane 1:10).

^{1}H-NMR (400 MHz, $CDCl_3$, δ/ppm): 7.45 (m, 6H), 7.28 (m, 10H), 6.64 (d, $^4J_{HH}$ = 1.9 Hz, 1H), 6.58 (dd, $^3J_{HH}$ = 8.1 Hz, $^4J_{HH}$ = 2.0 Hz, 1H), 3.21 (s, 2H), 1.03 (s, 9H), 0.23 (s, 6H).

^{13}C-NMR (101 MHz, $CDCl_3$, δ/ppm): 152.7, 144.8, 138.0, 133.4, 129.8, 128.2, 127.0, 123.3, 121.2, 114.1, 67.8, 36.6, 26.0, 18.6, -4.0.

(3-(Benzyloxy)-4-bromobenzyl)(trityl)sulfane (90)

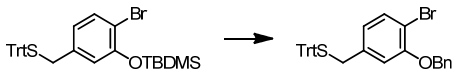

83 **90**

To a suspension of cesium fluoride (443 mg, 2.91 mmol, 2.0 eq.) in dry *N*,*N*-dimethylformamide (3 mL), compound **83** (839 mg, 1.46 mmol, 1.0 eq.) in dry *N*,*N*-dimethylformamide (6 mL) was added under an argon atmosphere. Subsequently benzyl bromide (0.21 mL, 1.75 mmol, 1.2 eq.) dissolved in dry *N*,*N*-dimethylformamide (3 mL) was added and the reaction mixture was stirred at room temperature for 3 days. The reaction mixture was quenched with an aqueous phosphate buffer (pH 7-8) and an extraction with diethyl ether (3x) was performed. The collected organic layers were dried over $MgSO_4$. The solvent was removed under reduced pressure and the crude product was purified by column chromatography (silica gel, dichloromethane/*n*-hexane 1:2) to obtain (3-(benzyloxy)-4-bromobenzyl)(trityl)sulfane (**90**, $C_{33}H_{27}BrOS$, 470 mg, 83%) as a yellowish solid.

TLC R_f = 0.39 (dichloromethane/*n*-hexane 1:2).

^{1}H-NMR (400 MHz, $CDCl_3$, δ/ppm): 7.36 (m, 21H), 6.66 (d, $^4J_{HH}$ = 1.6 Hz, 1H), 6.60 (dd, $^3J_{HH}$ = 8.1 Hz, $^4J_{HH}$ = 1.7 Hz, 1H), 5.07 (s, 2H), 3.28 (s, 2H).

^{13}C-NMR (101 MHz, $CDCl_3$, δ/ppm): 155.0, 144.6, 138.1, 136.5, 133.2, 129.6, 128.6, 128.0, 127.9, 127.1, 126.8, 122.8, 114.53, 111.0, 70.8, 67.6, 36.7.

(2-(Benzyloxy)-4-((tritylthio)methyl)phenyl)boronic acid (91)

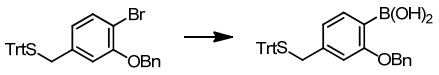

90 **91**

(3-(Benzyloxy)-4-bromobenzyl)(trityl)sulfane (**90**, 144 mg, 0.26 mmol, 1.0 eq.) was dissolved under an argon atmosphere in dry tetrahydrofuran (5 mL) in a dry flask, which was then cooled to -78 °C. *n*-Butyllithium (1.6 M in *n*-hexane, 0.20 mL, 0.31 mmol, 1.2 eq.) was added dropwise and the reaction mixture was stirred at -78 °C for 30 minutes. Trimethyl borate (0.04 mL, 0.34 mmol, 1.3 eq.) was added dropwise and the reaction mixture was stirred at -78 °C for additional 40 minutes and at room temperature for 50 minutes. The reaction was quenched with a saturated aqueous NH_4Cl-solution and the resulting solution was stirred vigorously for 20 minutes. An extraction with diethyl ether (3x) was performed and the collected organic layers were dried over anhydrous Na_2SO_4. The solvent was removed under reduced pressure and the crude product was purified by column chromatography (silica gel, dichloromethane) to afford boronic acid **91** ($C_{33}H_{29}BO_3S$, 16 mg, 12%) as a colorless solid.

TLC R_f = 0.11 (dichloromethane).

^{1}H-NMR (500 MHz, $CDCl_3$, δ/ppm): 7.71 (d, $^3J_{HH}$ = 7.5 Hz, 1H), 7.46 (m, 6H), 7.41 (m, 4H), 7.31 (m, 7H), 7.23 (m, 3H), 6.81 (dd, $^3J_{HH}$ = 7.5 Hz, $^4J_{HH}$ = 1.3 Hz, 1H), 6.70 (d, $^4J_{HH}$ = 1.0 Hz, 1H), 5.59 (s, 2H), 5.05 (s, 2H), 3.34 (s, 2H).

^{13}C-NMR (126 MHz, $CDCl_3$, δ/ppm): 163.9, 144.6, 142.6, 137.0, 135.9, 129.6, 129.0, 128.6, 128.0, 127.9, 126.8, 122.2, 111.8, 70.7, 67.6, 37.1.

***tert*-Butyl 4'-((6-(2-(benzyloxy)-4-((tritylthio)methyl)phenyl)pyridin-3-yl)diazenyl)-[1,1'-biphenyl]-2-carboxylate (93)**

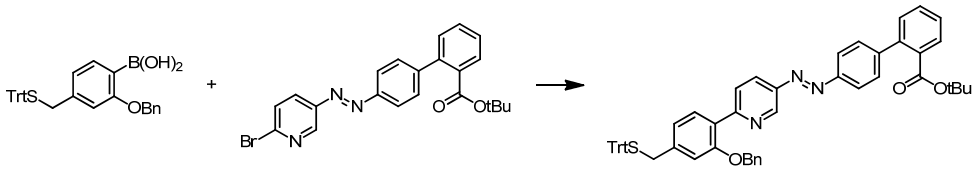

91 **77** **93**

Boronic acid **91** (16 mg, 0.03 mmol, 1.0 eq.), azo compound **77** (13 mg, 0.03 mmol, 1.0 eq.), potassium carbonate (8 mg, 0.06 mmol, 2.0 eq.), dry ethanol (2 mL) and dry toluene (2 mL) were added into a flask and the mixture was degassed by purging argon through the solution. Afterwards $PdCl_2(PPh_3)_2$ (1 mg, 2 µmol, 5 mol%) was added under an argon atmosphere and the reaction mixture was stirred at 60 °C for 19 hours. The solvent was removed under reduced pressure and the resulting crude mixture was purified by column chromatography (silica gel, ethyl acetate/*n*-hexane 1:5) to afford azo compound **93** ($C_{55}H_{47}N_3O_3S$, 25 mg, 98%) as an orange solid.

TLC R_f = 0.34 (ethyl acetate/*n*-hexane 1:5).

^{1}H-NMR (400 MHz, $CDCl_3$, δ/ppm): 9.27 (d, $^4J_{HH}$ = 2.2 Hz, 1H), 8.09 (m, 2H), 8.00 (d, $^3J_{HH}$ = 8.5 Hz, 2H), 7.88 (d, $^3J_{HH}$ = 7.9 Hz, 1H), 7.85 (dd, $^3J_{HH}$ = 7.7 Hz, $^4J_{HH}$ = 1.2 Hz, 1H), 7.48 (m, 10H), 7.32 (m, 15H), 6.91 (dd, $^3J_{HH}$ = 7.9 Hz, $^4J_{HH}$ = 1.3 Hz, 1H), 6.83 (d, $^4J_{HH}$ = 1.2 Hz, 1H), 5.10 (s, 2H), 3.40 (s, 2H), 1.29 (s, 9H).

1-Boc-4-(4-bromophenyl)piperazine (102)

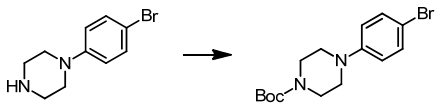

98 102

Commercially available 1-(4-bromophenyl)piperazine (**98**, 3.80 g, 15.8 mmol, 1.0 eq.) was dissolved in dichloromethane (100 mL) and the solution was cooled to 0 °C. Boc anhydride (3.44 g, 15.8 mmol, 1.0 eq.) was added and the corresponding reaction mixture was stirred at 0 °C for 2 hours. The solvent was then removed under reduced pressure and the resulting crude product was dissolved in ethyl acetate. The organic layer was washed with water (2x) and dried over $MgSO_4$. The solvent was removed under reduced pressure and the remaining product was not further purified to obtain 1-Boc-4-(4-bromophenyl)piperazine (**102**, $C_{15}H_{21}BrN_2O_2$, 5.33 g, quant.) as a colorless solid.

^{1}H-NMR (400 MHz, $CDCl_3$, δ/ppm): 7.35 (d, $^3J_{HH}$ = 9.0 Hz, 2H), 6.79 (d, $^3J_{HH}$ = 9.0 Hz, 2H), 3.57 (m, 4H), 3.09 (m, 4H), 1.48 (s, 9H).

^{13}C-NMR (101 MHz, $CDCl_3$, δ/ppm): 154.7, 150.3, 132.0, 118.2, 112.4, 80.0, 49.2, 28.4.

MS (EI, m/z): 340.1 (39%, M^+), 286.0 (98%), 284.0 (100%), 210.0 (46%), 57.1 (36%).

EA calculated: C = 52.80, H = 6.20, N = 8.21,
found: C = 52.91, H = 6.24, N = 8.30.

1-Boc-4-(4-((trimethylsilyl)ethyny)phenyl)piperazine (103)

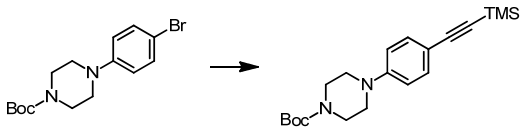

102 **103**

1-Boc-4-(4-bromophenyl)piperazine (**102**, 161 mg, 0.47 mmol, 1.0 eq.) and pyrrolidine (2.00 mL, 24.4 mmol, 52 eq.) were dissolved under an argon atmosphere in dry *N*,*N*-dimethylformamide (10 mL) in a dry Schlenk-tube and the solution was degassed with the freeze-pump-thaw method. Then ethynyltrimethylsilane (0.13 mL, 0.94 mmol, 2.0 eq.) and $Pd(PPh_3)_4$ (27 mg, 0.02 mmol, 5 mol%) were added and the reaction mixture was heated at 70°C for 2 days. The reaction mixture was then cooled to room temperature and diluted with water. An extraction with dichloromethane (3x) was performed and the collected organic layers were washed with water (3x) and then dried over $MgSO_4$. The solvent was removed under reduced pressure and the crude product was purified by column chromatography (silica gel, ethyl acetate/cyclohexane 1:5) to obtain 1-Boc-4-(4-((trimethylsilyl)ethyny)phenyl)piperazine (**103**, $C_{20}H_{30}N_2O_2Si$, 134 mg, 79%) as a yellow solid.

TLC R_f = 0.43 (ethyl acetate/cyclohexane 1:5).

^{1}H-NMR (400 MHz, $CDCl_3$, δ/ppm): 7.37 (d, $^3J_{HH}$ = 8.9 Hz, 2H), 6.80 (d, $^3J_{HH}$ = 8.9 Hz, 2H), 3.56 (m, 4H), 3.17 (m, 4H), 1.48 (s, 9H), 0.23 (s, 9H).

^{13}C-NMR (101 MHz, $CDCl_3$, δ/ppm): 154.7, 150.9, 133.1, 115.4, 113.7, 105.6, 92.3, 80.0, 48.4, 28.4, 0.1.

MS (EI, m/z): 358.3 (38%, M^+), 302.2 (100%), 216.2 (33%), 186.1 (15%).

EA calculated: C = 67.00, H = 8.43, N = 7.81,
found: C = 67.03, H = 8.40, N = 7.81.

1-Boc-4-(4-ethynylphenyl)piperazine (104)

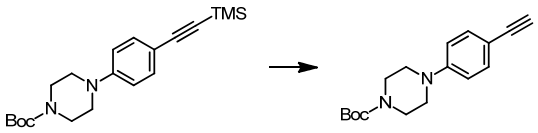

103 **104**

1-Boc-4-(4-((trimethylsilyl)ethyny)phenyl)piperazine (**103**, 717 mg, 2.00 mmol, 1.0 eq.) was dissolved under an argon atmosphere in dry methanol (50 mL) and then potassium carbonate (428 mg, 3.10 mmol, 1.6 eq.) was added. The reaction mixture was stirred at room temperature for 1.5 hours. The mixture was diluted with water and an extraction with ethyl acetate (3x) was performed. The organic collected layers were washed with water (2x) and dried over $MgSO_4$. The solvent was removed under reduced pressure and the remaining crude product was purified by column chromatography (silica gel, ethyl acetate/cyclohexane 1:5) to afford 1-Boc-4-(4-ethynylphenyl)piperazine (**104**, $C_{17}H_{22}N_2O_2$, 538 mg, 94%) as a colorless solid.

TLC R_f = 0.38 (ethyl acetate/cyclohexane 1:5).

^{1}H-NMR (400 MHz, $CDCl_3$, δ/ppm): 7.39 (d, $^3J_{HH}$ = 8.8 Hz, 2H), 6.83 (d, $^3J_{HH}$ = 8.9 Hz, 2H), 3.57 (m, 4H), 3.18 (m, 4H), 2.99 (s, 1H), 1.48 (s, 9H).

^{13}C-NMR (101 MHz, $CDCl_3$, δ/ppm): 154.7, 151.1, 133.3, 115.4, 112.6, 84.0, 80.0, 75.6, 48.4, 28.4.

MS (EI, m/z): 286.2 (40%, M^+), 230.1 (100%), 156.1 (41%), 144.1 (28%).

EA calculated: C = 71.30, H = 7.74, N = 9.78,
found: C = 71.25, H = 7.93, N = 9.72.

1-Boc-4-(4-(pyridin-4-ylethynyl)phenyl)piperazine (105)

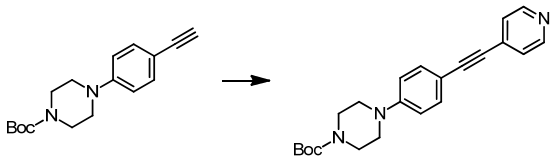

104 105

1-Boc-4-(4-ethynylphenyl)piperazine (**104**, 156 mg, 0.54 mmol, 1.2 eq.), 4-bromopyridine hydrochloride (88 mg, 0.45 mmol, 1.0 eq.) and pyrrolidine (2.00 mL, 24.4 mmol, 54 eq.) were dissolved under an argon atmosphere in dry *N*,*N*-dimethylformamide (10 mL) in a dry Schlenk-tube and the solution was degassed with the freeze-pump-thaw method. $PdCl_2(PPh_3)_2$ (16 mg, 0.02 mmol, 5 mol%) was added and the reaction mixture was heated at 70°C for 14 hours. The reaction mixture was then cooled to room temperature and diluted with water. An extraction with ethyl acetate (3x) was performed and the collected organic layers were washed with water (2x) and brine dried over $MgSO_4$. The solvent was removed under reduced pressure and the crude product was purified by column chromatography (silica gel, ethyl acetate/cyclohexane 1:1) to obtain 1-Boc-4-(4-(pyridin-4-ylethynyl)phenyl)piperazine (**105**, $C_{22}H_{25}N_3O_2$, 124 mg, 75%) as a yellowish solid.

TLC R_f = 0.30 (ethyl acetate/cyclohexane 1:1).

^{1}H-NMR (400 MHz, $CDCl_3$, δ/ppm): 8.57 (d, $^3J_{HH}$ = 6.1 Hz, 2H), 7.45 (d, $^3J_{HH}$ = 8.9 Hz, 2H), 7.34 (d, $^3J_{HH}$ = 6.1 Hz, 2H), 6.87 (d, $^3J_{HH}$ = 8.9 Hz, 2H), 3.59 (m, 4H), 3.24 (m, 4H), 1.49 (s, 9H).

^{13}C-NMR (101 MHz, $CDCl_3$, δ/ppm): 154.7, 151.3, 149.7, 133.2, 132.0, 125.3, 115.3, 112.3, 94.9, 85.7, 80.1, 48.1, 28.4.

MS (EI, m/z): 363.2 (49%, M^+), 307.1 (100%), 233.1 (27%), 221.1 (52%), 206.1 (16%).

EA calculated: C = 72.70, H = 6.93, N = 11.56,
found: C = 72.72, H = 7.00, N = 11.43.

1-(4-(Piperazin-1-yl)phenyl)-2-(pyridin-4-yl)ethanone (106)

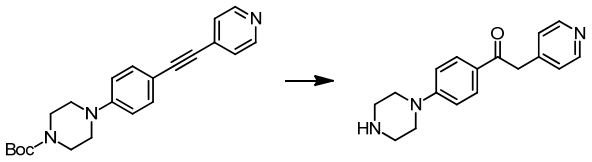

105 **106**

1-Boc-4-(4-(pyridin-4-ylethynyl)phenyl)piperazine (**105**, 79 mg, 0.22 mmol) was dissolved in dry tetrahydrofuran (5 mL) under an argon atmosphere and then trifluoroacetic acid (1 mL) was added. With the addition of trifluoroacetic acid the reaction mixture turned from yellow to orange. The reaction mixture was stirred at room temperature for 1.5 hours. Additional trifluoroacetic acid (2 mL) was added after 30 minutes and again after 2 hours. The reaction mixture was stirred for additional 1.5 hours. The solvent and the excess of trifluoroacetic acid were removed under reduced pressure. The resulting crude product was dissolved in dichloromethane and the organic layer was washed with an aqueous K_2CO_3-solution (3x) and water and dried over $MgSO_4$. The solvent was removed and the crude was purified by column chromatography (silica gel, ethanol/chloroform/NH_4OH 1:10:0.1) to afford 1-(4-(piperazin-1-yl)phenyl)-2-(pyridin-4-yl)ethanone (**106**, $C_{17}H_{19}N_3O$) as a colorless solid.

TLC R_f = 0.28 (ethanol/chloroform/NH_4OH 1:10:0.1).

^{1}H-NMR (400 MHz, $CDCl_3$, δ/ppm): 8.54 (d, $^3J_{HH}$ = 5.8 Hz, 2H), 7.91 (d, $^3J_{HH}$ = 8.9 Hz, 2H), 7.21 (d, $^3J_{HH}$ = 5.8 Hz, 2H), 6.87 (d, $^3J_{HH}$ = 9.0 Hz, 2H), 4.20 (s, 2H), 3.36 (m, 4H), 3.05 (m, 4H), 1.77 (s_{br}, 1H).

^{13}C-NMR (101 MHz, $CDCl_3$, δ/ppm): 194.0, 154.7, 149.9, 144.4, 130.7, 126.2, 124.8, 113.3, 48.2, 45.8, 44.1.

MS (EI, m/z): 281.2 (38%, M^+), 239.2 (100%), 189.1 (82%), 132.1 (18%), 119.1 (18%).

1-(4-((Trimethylsilyl)ethynyl)phenyl)piperazine (109)

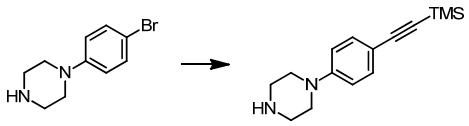

98 **109**

Commercially available 1-(4-bromophenyl)piperazine (**98**, 3.76 g, 15.6 mmol, 1.0 eq.) and pyrrolidine (4.00 mL, 48.7 mmol, 3.1 eq.) were dissolved under an argon atmosphere in dry *N*,*N*-dimethylformamide (30 mL) in a dry Schlenk-tube and the solution was degassed with the freeze-pump-thaw method. Then ethynyltrimethylsilane (8.82 mL, 62.4 mmol, 4.0 eq.) and $PdCl_2(PPh_3)_2$ (547 mg, 0.78 mmol, 5 mol%) were added and the reaction mixture was heated at 65 °C for 20 hours. The reaction mixture was cooled to room temperature and diluted with water. An extraction with ethyl acetate (3x) was performed and the collected organic layers were washed with water (3x) and dried over $MgSO_4$. The solvent was removed under reduced pressure and the crude product was purified by column chromatography (silica gel, ethanol/chloroform/NH_4OH 1:10:0.1) to obtain 1-(4-((trimethylsilyl)ethynyl)phenyl)piperazine (**109**, $C_{15}H_{22}N_2Si$, 3.23 g, 80%) as a yellow solid.

TLC R_f = 0.17 (ethanol/chloroform/NH_4OH 1:10:0.1).

^{1}H-NMR (400 MHz, $CDCl_3$, δ/ppm): 7.36 (d, $^3J_{HH}$ = 8.9 Hz, 2H), 6.80 (d, $^3J_{HH}$ = 8.9 Hz, 2H), 3.17 (m, 4H), 3.01 (m, 4H), 1.59 (s_{br}, 1H), 0.23 (s, 9H).

^{13}C-NMR (101 MHz, $CDCl_3$, δ/ppm): 151.7, 133.3, 115.1, 113.3, 106.1, 92.2, 49.6, 46.2, 0.3.

MS (EI, m/z): 258.2 (33%, M^+), 216.2 (100%).

EA calculated: C = 69.71, H = 8.58, N = 10.84,
found: C = 69.33, H = 8.24, N = 10.63.

1-(4-Ethynylphenyl)piperazine (100)

109 **100**

1-(4-((Trimethylsilyl)ethynyl)phenyl)piperazine (**109**, 176 mg, 0.68 mmol, 1.0 eq.) was dissolved under an argon atmosphere in dry methanol (20 mL) and then potassium carbonate (157 mg, 1.14 mmol, 1.7 eq.) was added. The reaction mixture was stirred at room temperature for 2 hours and the solvent was removed under reduced pressure. The resulting crude product was purified by column chromatography (silica gel, ethanol/chloroform/NH_4OH 1:10:0.1) to obtain 1-(4-ethynylphenyl)piperazine (**100**, $C_{12}H_{14}N_2$, 94 mg, 74%) as a yellowish solid.

TLC R_f = 0.33 (ethanol/chloroform/NH_4OH 1:10:0.1).

^{1}H-NMR (400 MHz, $CDCl_3$, δ/ppm): 7.39 (d, $^3J_{HH}$ = 8.9 Hz, 2H), 6.83 (d, $^3J_{HH}$ = 8.9 Hz), 3.19 (m, 4H), 3.02 (m, 4H), 2.98 (s, 1H), 1.65 (s_{br}, 1H).

^{13}C-NMR (101 MHz, $CDCl_3$, δ/ppm): 151.7, 133.2, 115.0, 112.0, 84.3, 75.4, 49.4, 46.0).

MS (EI, m/z): 186.1 (37%, M^+), 144.1 (100%).

EA calculated: C = 77.38, H = 7.58, N = 15.04,
found: C = 77.04, H = 7.64, N = 14.64.

1-(4-(Pyridin-4-ylethynyl)phenyl)piperazine (DTCP 1)

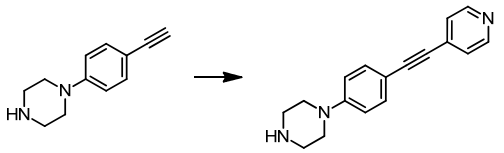

100 DTCP 1

1-(4-Ethynylphenyl)piperazine (**100**, 203 mg, 1.09 mmol, 1.0 eq.) and pyrrolidine (1.50 mL, 1.42 mmol, 1.3 eq.) were dissolved under an argon atmosphere in dry *N*,*N*-dimethylformamide (10 mL) in a dry Schlenk-tube and the solution was degassed with the freeze-pump-thaw method. Then 4-iodopydridine (290 mg, 1.42 mmol, 1.3 eq.) and $PdCl_2(PPh_3)_2$ (38 mg, 0.05 mmol, 5 mol%) were added and the reaction mixture was stirred at room temperature for 2 hours and at 50 °C for further 2 hours. The reaction mixture was cooled to room temperature and diluted with water and an extraction with dichloromethane (3x) was performed. The collected organic layers were washed with water (3x) and dried over $MgSO_4$. The solvent was removed under reduced pressure and the crude product was purified by column chromatography (silica gel, ethanol/chloroform/NH_4OH 1:10:0.1) to obtain target compound 1-(4-(pyridin-4-ylethynyl)phenyl)piperazine (**DTCP 1**, $C_{17}H_{17}N_3$, 240 mg, 84%) as a yellowish solid.

TLC R_f = 0.28 (ethanol/chloroform/NH_4OH 1:10:0.1).

^{1}H-NMR (500 MHz, $CDCl_3$, δ/ppm): 8.56 (d, $^3J_{HH}$ = 6.0 Hz, 2H), 7.44 (d, $^3J_{HH}$ = 8.8 Hz, 2H), 7.34 (d, $^3J_{HH}$ = 6.0 Hz, 2H), 6.87 (d, $^3J_{HH}$ = 8.9 Hz, 2H), 3.23 (m, 4H), 3.03 (m, 4H), 1.67 (s_{br}, 1H).

^{13}C-NMR (126 MHz, $CDCl_3$, δ/ppm): 151.9, 149.7, 133.1, 132.1, 125.3, 114.8, 111.6, 95.2, 85.5, 49.1, 46.0.

MS (EI, m/z): 263.1 (45%, M^+), 221.1 (100%).

EA calculated: C = 77.54, H = 6.51, N = 15.96,
found: C = 77.17, H = 6.61, N = 15.62.

1-(4-((4-Nitrophenyl)ethynyl)phenyl)piperazine (DTCP 2)

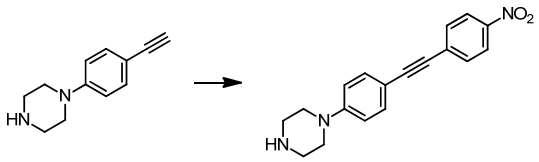

100 DTCP 2

1-(4-Ethynylphenyl)piperazine (**100**, 87.6 mg, 0.47 mmol, 1.2 eq.), 1-iodo-4-nitrobenzene (98 mg, 0.39 mmol, 1.0 eq.), tetrabutylammonium fluoride trihydrate (371 mg, 1.18 mmol, 3.0 eq.) and $PdCl_2(PPh_3)_2$ (8 mg, 0.01 mmol, 3 mol%) were heated under an argon atmosphere at 80 °C for 1 hour. Then dry tetrahydrofuran (2 mL) was added and the reaction mixture was stirred at 80 °C for 30 minutes. The reaction mixture was cooled to room temperature and tetrahydrofuran was removed under reduced pressure. The resulting crude mixture was purified by column chromatography (silica gel, ethanol/chloroform/NH_4OH 1:10:0.1) to obtain target structure 1-(4-((4-nitrophenyl)ethynyl)-phenyl)piperazine (**DTCP 2**, $C_{18}H_{17}N_3O_2$, 73 mg, 61%) as a reddish solid.

TLC R_f = 0.29 (ethanol/chloroform/NH_4OH 1:10:0.1).

^{1}H-NMR (400 MHz, $CDCl_3$, δ/ppm): 8.20 (d, $^3J_{HH}$ = 8.9 Hz), 7.61 (d, $^3J_{HH}$ = 8.9 Hz, 2H), 7.45 (d, $^3J_{HH}$ = 8.9 Hz), 6.88 (d, $^3J_{HH}$ = 8.9 Hz, 2H), 3.24 (m, 4H), 3.04 (m, 4H), 1.63 (s_{br}, 1H).

^{13}C-NMR (101 MHz, $CDCl_3$, δ/ppm): 152.0, 146.5, 133.1, 131.8, 131.1, 123.6, 114.8, 111.6, 96.2, 86.6, 49.1, 46.0.

MS (EI, m/z): 307.1 (38%, M^+), 265.1 (100%).

EA calculated: C = 70.34, H = 5.57, N = 13.67,
found: C = 69.85, H = 5.72, N = 13.36.

_N_,_N_-Dimethyl-4-((4-(piperazin-1-yl)phenyl)ethynyl)aniline (DTCP 3)

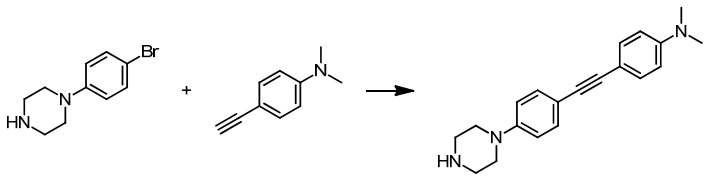

98 110 DTCP 3

Commercially available 1-(4-bromophenyl)piperazine (**98**, 332 mg, 1.38 mmol, 1.0 eq.), 4-ethynyl-*N*,*N*-dimethylaniline (**110**, 300 mg, 2.07 mmol, 1.5 eq.) and pyrrolidine (2.0 mL, 24.4 mmol, 17.7 eq.) were dissolved under an argon atmosphere in dry *N*,*N*-dimethylformamide (6 mL) in a dry Schlenk-tube and degassed with the freeze-pump-thaw method. Then $PdCl_2(PPh_3)_2$ (48 mg, 0.07 mmol, 5 mol%) was added and the reaction mixture was stirred at 70 °C for 22 hours. The reaction mixture was cooled to room temperature and diluted with water. An extraction with dichloromethane (3x) was performed. The collected organic layers were washed with water (3x) and dried over $MgSO_4$. The solvent was removed under reduced pressure and the crude product was purified by column chromatography (silica gel, ethanol/chloroform/NH_4OH 1:10:0.1) to afford target structure *N*,*N*-dimethyl-4-((4-(piperazin-1-yl)phenyl)ethynyl)aniline (**DTCP 3**, $C_{20}H_{23}N_3$, 237 mg, 56%) as a brownish solid.

TLC R_f = 0.24 (ethanol/chloroform/NH_4OH 1:10:0.1).

^{1}H-NMR (500 MHz, $CDCl_3$, δ/ppm): 7.39 (m, 4H), 6.86 (d, $^3J_{HH}$ = 8.9 Hz, 2H), 6.65 (d, $^3J_{HH}$ = 8.9 Hz, 2H), 3.23 (m, 4H), 3.08 (m, 4H), 2.98 (s, 6H), 2.38 (s_{br}, 1H).

^{13}C-NMR (101 MHz, $CDCl_3$, δ/ppm): 150.9, 149.8, 132.5, 132.3, 115.3, 114.5, 111.9, 110.8, 88.8, 87.6, 49.7, 46.1, 40.3.

MS (EI, m/z): 305.2 (93%, M^+), 263.2 (100%), 248.1 (28%).

9-Bromo-julolidine (112)[362]

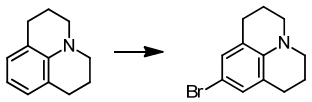

111 112

Commercially available julolidine (**111**, 1.69 g, 9.78 mmol, 1.0 eq.) was dissolved under an argon atmosphere in dry dichloromethane (25 mL) and the solution was cooled to -10 °C. Then 2,4,4,6-tetrabromo-2,5-cyclohexadienone (4.01 g, 9.78 mmol, 1.0 eq.) was added in small portions such that the temperature of the solution was maintained below 0 °C. After the addition the reaction mixture was stirred at room temperature for 2.5 hours. The solution was then washed with an aqueous NaOH-solution (1 M) and with brine. After drying the organic layer over $MgSO_4$ the solvent was removed under reduced pressure. The resulting crude product was purified by column chromatography (silica gel, dichloromethane/cyclohexane 1:5) to afford 9-bromo-julolidine (**112**, $C_{12}H_{14}BrN$, 1.04 g, 42%) as a colorless solid.

TLC R_f = 0.28 (dichloromethane/cyclohexane 1:5)

^{1}H-NMR (400 MHz, $CDCl_3$, δ/ppm): 6.86 (s, 2H), 3.10 (m, 4H), 2.70 (m, 4H), 1.93 (m, 4H).

^{13}C-NMR (101 MHz, $CDCl_3$, δ/ppm): 141.9, 129.2, 123.6, 107.1, 49.8, 27.5, 21.8.

MS (EI, m/z): 251.0 (100%, M^+), 170.1 (52%).

EA calculated: C = 57.16, H = 5.60, N = 55.5,
found: C = 57.14, H = 5.72, N = 5.65.

9-(Trimethylsilyl)ethynyl-julolidine (113)

112 **113**

9-Bromo-julolidine (**112**, 1.03 g, 4.10 mmol, 1.0 eq.) was dissolved under an argon atmosphere in triethylamine (10 mL) in a Schlenk-tube and the solution was degassed with the freeze-pump-thaw method. Then trimethylsilylacetylene (2.32 mL, 16.4 mmol, 4.0 eq.), $Pd(PPh_3)_4$ (237 mg, 0.21 mmol, 5 mol%) and copper iodide (39 mg, 0.21 mmol, 5 mol%) were added and the reaction mixture was stirred at room temperature for 1.5 hours and then at 75 °C for 17 hours. Afterwards the reaction mixture was diluted with water and an extraction with ethyl acetate (3x) was performed. The collected organic layers were washed with water (3x) and dried over $MgSO_4$. The solvent was removed under reduced pressure and the crude product was purified by column chromatography (silica gel, dichloromethane/cyclohexane 1:2) to afford 9-(trimethyl-silyl)ethynyl-julolidine (**113**, $C_{17}H_{23}NSi$, 1.01 g, 91%) as a yellow viscous liquid.

TLC R_f = 0.51 (dichloromethane/cyclohexane 1:2).

^{1}H-NMR (400 MHz, $CDCl_3$, δ/ppm): 6.90 (m, 2H), 3.15 (m, 4H), 2.68 (m, 4H), 1.92 (m, 4H), 0.20 (s, 9H).

^{13}C-NMR (126 MHz, $CDCl_3$, δ/ppm): 143.3, 130.8, 121.0, 108.8, 107.3, 90.6, 50.1, 27.7, 21.9, 0.5.

MS (EI, m/z): 269.2 (100%, M^+), 254.2 (58%), 126.6 (16%).

EA calculated: C = 75.78, H = 8.60, N = 5.20,
found: C = 75.50, H = 8.18, N = 5.46.

9-Ethynyl-julolidine (114)

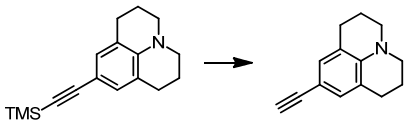

113 **114**

9-(Trimethylsilyl)ethynyl-julolidine (**113**, 260 mg, 0.97 mmol, 1.0 eq.) was dissolved in dry methanol (5 mL) and dry tetrahydrofuran (5 mL). Then potassium hydroxide (158 mg, 2.82 mmol, 2.9 eq.) was added and the reaction mixture was stirred at room temperature for 1 hour. The reaction mixture was diluted with water and extracted with ethyl acetate (3x). The collected organic layers were washed with water (3x) and then dried over $MgSO_4$. The solvent was removed under reduced pressure and the crude product was purified by column chromatography (silica gel, ethyl acetate /cyclohexane 1:20) to afford 9-ethynyl-julolidine (**114**, $C_{14}H_{15}N$, 129 mg, 68%) as a yellow oil.

TLC R_f = 0.47 (ethyl acetate /cyclohexane 1:20).

^{1}H-NMR (400 MHz, $CDCl_3$, δ/ppm): 6.92 (s, 2H), 3.17 (m, 4H), 2.91(s, 1H), 2.69 (m, 4H), 1.93 (m, 4H).

9-((4-(Piperazin-1-yl)phenyl)ethynyl)-julolidine (DTCP 4)

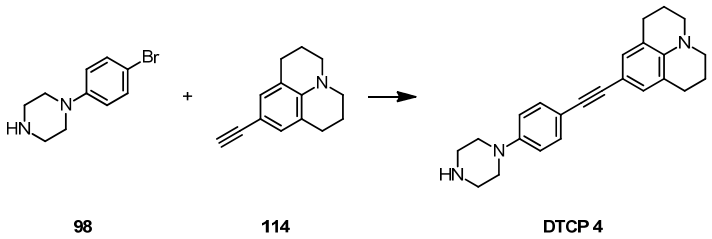

98 114 DTCP 4

9-Ethynyl-julolidine (**114**, 121 mg, 0.50 mmol, 1.0 eq.), commercially available 1-(4-bromophenyl)piperazine (**98**, 129 mg, 0.65 mmol, 1.3 eq.) and pyrrolidine (1.5 mL, 18.3 mmol, 37 eq.) were dissolved under an argon atmosphere in dry *N*,*N*-dimethylformamide (6 mL) in a dry Schlenk-tube and the solution was degassed with the freeze-pump-thaw method. Then $PdCl_2(PPh_3)_2$ (18 mg, 0.03 mmol, 5 mol%) was added and the reaction mixture was stirred at 70 °C for 22 hours. Afterwards the reaction mixture was cooled to room temperature and diluted with water. An extraction with dichloromethane (3x) was performed and the collected organic layers were washed with water (3x) and dried over $MgSO_4$. The solvent was removed under reduced pressure and the resulting crude product was purified by column chromatography (silica gel, ethanol/chloroform/NH_4OH 1:10:0.1) to obtain target structure 9-((4-(piperazin-1-yl)phenyl)ethynyl)-julolidine (**DTCP 4**, $C_{24}H_{27}N_3$, 93 mg, 52%) as a brownish solid.

TLC R_f = 0.30 (ethanol/chloroform/NH_4OH 1:10:0.1).

^{1}H-NMR (400 MHz, $CDCl_3$, δ/ppm): 7.36 (d, $^3J_{HH}$ = 8.8 Hz, 2H), 6.90 (s, 2H), 6.84 (d, $^3J_{HH}$ = 8.8 Hz, 2H), 3.17 (m, 8H), 3.03 (m, 4H), 2.72 (m, 4H), 1.96 (m, 5H).

^{13}C-NMR (126 MHz, $CDCl_3$, δ/ppm): 150.6, 142.6, 132.2, 130.0, 121.0, 115.4, 114.9, 109.4, 89.3, 86.9, 49.9, 49.5, 45.8, 27.5, 21.8.

MS (EI, m/z): 357.2 (100%, M^+), 315.1 (52%), 300.1 (25%), 157.6 (19%).

1-Bromo-4-(heptyloxy)benzene (116)

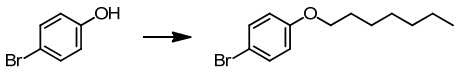

115 116

Commercially available 4-bromophenol (**115**, 2.16 g, 12.5 mmol, 1.0 eq.), commercially available 1-bromoheptane (2.55 mL, 16.2 mmol, 1.3 eq.), potassium carbonate (3.44 g, 24.9 mmol, 2.0 eq.), potassium iodide (103 mg, 0.62 mmol, 5 mol%) and dry tetrahydrofuran (15 mL) were added under an argon atmosphere into a microwave vial. The resulting reaction mixture was exposed to microwave irradiation at 170 °C for 1 hour. The reaction mixture was diluted water and extracted with ethyl acetate (3x). The collected organic layers were washed with water, an aqueous NaOH-solution (1 M) and thereafter again with water (3x). The organic phase was dried over $MgSO_4$ and the solvent was removed under reduced pressure. The product was not further purified and it was dried under high vacuum conditions to afford 1-bromo-4-(heptyloxy)benzene (**116**, $C_{13}H_{19}BrO$, 2.43 g, 72%) as a colorless liquid.

^{1}H-NMR (400 MHz, $CDCl_3$, δ/ppm): 7.35 (d, $^3J_{HH}$ = 9.0 Hz, 2H), 6.77 (d, $^3J_{HH}$ = 9.0 Hz, 2H), 3.91 (t, $^3J_{HH}$ = 6.6 Hz, 2H), 1.77 (m, 2H), 1.44 (m, 2H), 1.33 (m, 6H), 0.89 (t, $^3J_{HH}$ = 6.8 Hz, 3H).

^{13}C-NMR (101 MHz, $CDCl_3$, δ/ppm): 158.3, 132.2, 116.3, 112.5, 68.3, 31.8, 29.2, 29.0, 26.0, 22.6, 14.1.

MS (EI, m/z): 272.1 (17%), 270.1 (18%, M^+), 173.9 (99%), 171.9 (100%), 57.1 (22%).

EA calculated: C = 57.58, H = 7.06,
found: C = 57.67, H = 6.90.

((4-(Heptyloxy)phenyl)ethynyl)trimethylsilane (117)

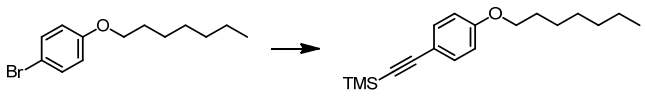

116 117

1-Bromo-4-(heptyloxy)benzene (**116**, 1.10 g, 4.06 mmol, 1.0 eq.) and triethylamine (5.00 mL, 35.9 mmol, 8.9 eq.) were dissolved in dry tetrahydrofuran (15 mL) and the solution was degassed by purging argon through it. Then trimethylsilylacetylene (1.15 mL, 8.11 mmol, 2.0 eq.), $PdCl_2(PPh_3)_2$ (142 mg, 0.20 mmol, 5 mol%) and a spatula tip of copper iodide were added and the resulting reaction mixture was stirred at 70 °C for 20 hours. After cooling to room temperature it was diluted with water and an extraction with ethyl acetate (3x) was performed. The collected organic layers were washed with water (3x) and brine and dried over $MgSO_4$. The solvent was removed under reduced pressure and the crude product was purified by column chromatography (silica gel, cyclohexane) to afford ((4-(heptyloxy)phenyl)ethynyl)trimethylsilane (**117**, $C_{18}H_{28}OSi$, 554 mg, 47%) as a yellowish viscous liquid.

TLC R_f = 0.15 (cyclohexane).

^{1}H-NMR (400 MHz, $CDCl_3$, δ/ppm): 7.38 (d, $^3J_{HH}$ = 8.9 Hz, 2H), 6.80 (d, $^3J_{HH}$ = 8.9 Hz, 2H), 3.94 (t, $^3J_{HH}$ = 6.6 Hz, 2H), 1.77 (m, 2H), 1.44 (m, 2H), 1.32 (m, 6H), 0.89 (t, $^3J_{HH}$ = 6.9 Hz, 3H), 0.23 (s, 9H).

^{13}C-NMR (101 MHz, $CDCl_3$, δ/ppm): 159.6, 133.7, 115.2, 114.6, 105.6, 92.5, 68.3, 32.0, 29.4, 29.3, 26.2, 22.8, 14.3, 0.3.

MS (EI, m/z): 288.2 (41%, M^+), 273.2 (28%), 190.1 (30%), 175.1 (100%).

EA calculated: C = 74.94, H = 9.78,
found: C = 74.94, H = 9.76.

1-Ethynyl-4-(heptyloxy)benzene (118)

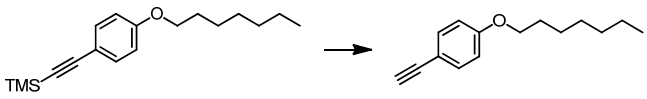

117 118

((4-(Heptyloxy)phenyl)ethynyl)trimethylsilane (**117**, 443 mg, 1.54 mmol, 1.0 eq.) was dissolved under an argon atmosphere in dry methanol (20 mL) and then potassium carbonate (425 mg, 3.07 mmol, 2.0 eq.) was added. The reaction mixture was stirred at room temperature for 24 hours. Afterwards further dry methanol (10 mL) and potassium carbonate (1.70 g, 12.3 mmol, 7.9 eq.) were added and the reaction mixture was stirred at room temperature for 4 hours. Thereafter further dry methanol (10 mL) was added and the reaction mixture was continued to stir for 3 hours. Dilution with water and an extraction with ethyl acetate (3x) were subsequently performed. The collected organic layers were washed with water (3x) and dried over $MgSO_4$. The solvent was removed under reduced pressure and the crude product was purified by column chromatography (silica gel, dichloromethane/cyclohexane 1:9) to afford 1-ethynyl-4-(heptyloxy)benzene (**118**, $C_{15}H_{20}O$, 309 mg, 93%) as a colorless liquid.

TLC R_f = 0.49 (dichloromethane/cyclohexane 1:9).

^{1}H-NMR (400 MHz, $CDCl_3$, δ/ppm): 7.41 (d, $^3J_{HH}$ = 8.8 Hz, 2H), 6.82 (d, $^3J_{HH}$ = 8.2 Hz, 2H), 3.95 (t, $^3J_{HH}$ = 6.6 Hz, 2H), 2.98 (s, 1H), 1.77 (m, 2H), 1.44 (m, 2H), 1.32 (m, 6H), 0.89 (t, $^3J_{HH}$ = 6.9 Hz, 3H).

^{13}C-NMR (101 MHz, $CDCl_3$, δ/ppm): 159.6, 133.6, 114.5, 113.8, 83.8, 75.6, 68.1, 31.8, 29.2, 29.1, 26.0, 22.6, 14.1.

MS (EI, m/z): 216.2 (28%, M^+), 118.1 (100%).

1-(4-((4-(Heptyloxy)phenyl)ethynyl)phenyl)piperazine (DTCP 5)

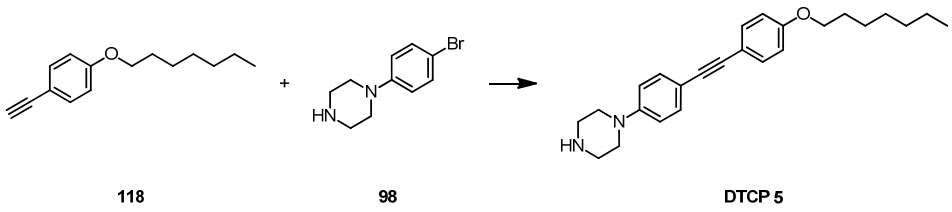

118 98 DTCP 5

1-Ethynyl-4-(heptyloxy)benzene (**118**, 216 mg, 1.00 mmol, 1.2 eq.), commercially available 1-(4-bromophenyl)piperazine (**98**, 201 mg, 0.83 mmol, 1.0 eq.) and pyrrolidine (3.00 mL, 36.5 mmol, 41 eq.) were dissolved under an argon atmosphere in dry *N*,*N*-dimethylformamide (10 mL) in a dry Schlenk-tube and the solution was degassed with the freeze-pump-thaw method. Then $PdCl_2(PPh_3)_2$ (29 mg, 0.04 mmol, 5 mol%) was added and the reaction mixture was heated to 65 °C for 20 hours. After cooling the reaction mixture to room temperature it was diluted with water and extracted with ethyl acetate (3x). The collected organic layers were washed with water (3x) and brine and dried over $MgSO_4$. The solvent was removed under reduced pressure and the resulting crude mixture was purified by column chromatography (silica gel, ethanol/chloroform/NH_4OH 1:10:0.1) to afford target structure 1-(4-((4-(heptyloxy)phenyl)-ethynyl)phenyl)piperazine (**DTCP 5**, $C_{25}H_{32}N_2O$, 130 mg, 41%) as a yellowish solid.

TLC R_f = 0.40 (ethanol/chloroform/NH_4OH 1:10:0.1).

^{1}H-NMR (400 MHz, $CDCl_3$, δ/ppm): 7.42 (d, $^3J_{HH}$ = 8.8 Hz, 2H), 7.40 (d, $^3J_{HH}$ = 8.9 Hz, 2H), 6.86 (d, $^3J_{HH}$ = 8.9 Hz, 2H), 6.84 (d, $^3J_{HH}$ = 8.8 Hz, 2H), 3.96 (t, $^3J_{HH}$ = 6.6 Hz, 2H), 3.18 (m, 4H), 3.03 (m, 4H), 1.78 (m, 2H), 1.45 (m, 2H), 1.33 (m, 6H), 0.89 (t, $^3J_{HH}$ = 6.9 Hz, 3H).

^{13}C-NMR (101 MHz, $CDCl_3$, δ/ppm): 158.9, 151.1, 132.8, 132.5, 115.7, 115.2, 114.5, 113.8, 88.4, 87.8, 68.1, 49.6, 46.1, 31.8, 29.2, 29.1, 26.0, 22.6, 14.1.

MS (EI, m/z): 376.2 (72%, M^+), 334.2 (100%).

EA calculated: C = 79.75, H = 8.57, N = 7.44,
found: C = 79.72, H = 8.62, N = 7.53.

1-(4-(4-(Heptyloxy)phenyl)piperazin-1-yl)ethanone (120)

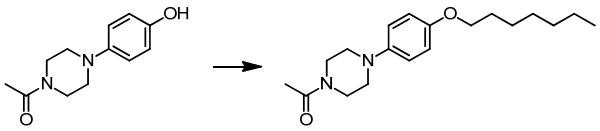

119 120

Commercially available 1-acetyl-4-(4-hydroxyphenyl)piperazine (**119**, 3.40 g, 15.4 mmol, 1.0 eq.), was dissolved under an argon atmosphere in dry *N*,*N*-dimethylformamide (40 mL) and then 1-bromoheptane (2.91 mL, 18.5 mmol, 1.2 eq.) and potassium carbonate (2.77 g, 20.1 mmol, 1.3 eq.) were added. The resulting reaction mixture was stirred at room temperature for 18 hours. Afterwards the reaction mixture was diluted with water and extracted with ethyl acetate (3x). The collected organic layers were washed with an aqueous NaOH-solution (1 M) and with water (3x) and then dried over $MgSO_4$. The solvent was removed under reduced pressure and the product was dried to afford 1-(4-(4-(heptyloxy)phenyl)piperazin-1-yl)ethanone (**120**, $C_{19}H_{30}N_2O_2$, 4.92 g, quant.) without further purification as a pinkish solid.

^{1}H-NMR (400 MHz, $CDCl_3$, δ/ppm): 6.87 (m, 4H), 3.91 (t, $^3J_{HH}$ = 6.6 Hz, 2H), 3.76 (m, 2H), 3.61 (m, 2H), 3.03 (m, 4H), 2.13 (s, 3H), 1.75 (m, 2H), 1.44 (m, 2H), 1.30 (m, 6H), 0.89 (t, $^3J_{HH}$ = 6.9 Hz, 3H).

^{13}C-NMR (126 MHz, $CDCl_3$, δ/ppm): 169.0, 154.0, 145.1, 118.9, 115.2, 68.4, 51.3, 50.9, 46.4, 41.5, 31.8, 29.4, 29.1, 26.0, 22.6, 21.4, 14.1.

MS (EI, m/z): 318.2 (100%, M^+), 246.2 (43%), 219.2 (30%), 148.1 (42%).

EA calculated: C = 71.66, H = 9.49, N = 8.80,
found: C = 71.69, H = 9.15, N = 8.65.

1-(4-(Heptyloxy)phenyl)piperazine (DTCP 6)

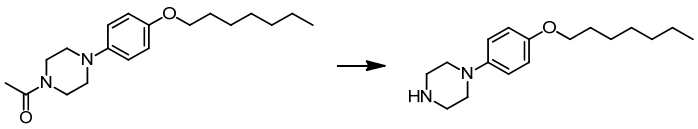

120 DTCP 6

1-(4-(4-(Heptyloxy)phenyl)piperazin-1-yl)ethanone (**120**, 137 mg, 0.43 mmol, 1.0 eq.) was dissolved in an aqueous hydrochloric solution (1 M in H_2O, 10.0 mL, 10.0 mmol, 23 eq.) in a microwave vial. The reaction mixture was exposed to microwave irradiation under stirring at 120 °C for 20 minutes. After cooling down to room temperature the reaction mixture was basified with an aqueous K_2CO_3-solution. The basic aqueous layer was then extracted with ethyl acetate (3x). The collected organic layers were then washed with an aqueous K_2CO_3-solution and water (3x) and then dried over $MgSO_4$. The solvent was removed under reduced pressure to obtain the desired 1-(4-(heptyloxy)phenyl)piperazine (**DTCP 6**, $C_{17}H_{28}N_2O$, 109 mg, 92%) without further purification as a colorless solid.

^{1}H-NMR (400 MHz, $CDCl_3$, δ/ppm): 6.86 (m, 4H), 3.90 (t, $^3J_{HH}$ = 6.6 Hz, 2H), 3.03 (s_{br}, 8H), 1.75 (m, 2H), 1.57 (s_{br}, 1H), 1.44 (m, 2H), 1.30 (m, 6H), 0.89 (t, $^3J_{HH}$ = 6.9 Hz, 3H).

^{13}C-NMR (101 MHz, $CDCl_3$, δ/ppm): 153.4, 146.1, 118.2, 115.1, 68.4, 52.0, 46.3, 31.8, 29.4, 29.1, 26.0, 22.6, 14.1.

MS (EI) (m/z): 276.2 (34%, M^+), 234.2 (100%), 136.1 (15%).

EA calculated: C = 73.84, H = 10.21, N = 10.13,
found: C = 73.63, H = 9.98, N = 10.00.

1-Cbz-4-(((trifluoromethyl)sulfonyl)oxy)-1,2,3,6-tetrahydropyridine (122)[370]

121 **122**

Commercially available 1-Cbz-4-piperidone (**121**, 2.18 g, 9.33 mmol, 1.0 eq.) was dissolved under an argon atmosphere in dry tetrahydrofuran (50 mL) in a dry flask, which was cooled to -78 °C. Lithium bis(trimethylsilyl)amide (1 M in THF, 10.3 mL, 10.3 mmol, 1.1 eq.) was added dropwise to the solution and the resulting reaction mixture was stirred at -78 °C for 30 minutes. Thereafter *N*-phenyl-bis(trifluoromethanesulfonimide) (5.00 g, 14.0 mmol, 1.5 eq.) was added at once and stirred at -78 °C for further 6.5 hours and at room temperature for 16 hours. The reaction mixture was then quenched with water and extracted with diethyl ether (3x). The combined organic layers were dried over $MgSO_4$. The solvent was removed under reduced pressure and the crude product was purified by column chromatography (silica gel, ethyl acetate/cyclohexane 1:5) to afford triflate **122** ($C_{14}H_{14}F_3NO_5S$, 1.47 g, 43%).

TLC R_f = 0.37 (ethyl acetate/cyclohexane 1:5).

^{1}H-NMR (400 MHz, $CDCl_3$, δ/ppm): 7.35 (m, 5H), 5.78 (m, 1H), 5.16 (s, 2H), 4.13 (m, 2H), 3.75 (m, 2H), 2.46 (m, 2H).

1-Cbz-4-(4,4,5,5-tetramethyl-1,3,2-dioxaborolan-2-yl)-1,2,3,6-tetrahydropyridine (123)[371]

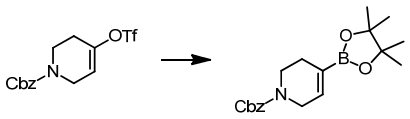

122 **123**

1-Cbz-4-(((trifluoromethyl)sulfonyl)oxy)-1,2,3,6-tetrahydropyridine (**122**, 1.46 g, 4.00 mmol, 1.0 eq.) was dissolved under an argon atmosphere in dry dioxane (20 mL) in a dry Schlenk-tube and the solution was degassed with the freeze-pump-thaw method. Then bis(pinacolato)diboron (1.12 g, 4.40 mmol, 1.1 eq.), potassium acetate (1.18 g, 12.0 mmol, 3.0 eq.), $PdCl_2(dppf)\cdot CH_2Cl_2$ (98 mg, 0.12 mmol, 3 mol%) and 1,1'-bis(diphenylphosphino)ferrocene (67 mg, 0.12 mmol, 3 mol%) were added and the resulting reaction mixture was stirred at 80 °C for 27 hours. The reaction mixture was then quenched with water and extracted with dichloromethane (3x). The combined organic layers were dried over $MgSO_4$. The solvent was removed under reduced pressure and the crude product was purified by column chromatography (silica gel, ethyl acetate/cyclohexane 1:5) to afford boronic ester **123** ($C_{19}H_{26}BNO_4$, 982 mg, 72%) as a colorless solid.

TLC R_f = 0.31 (ethyl acetate/cyclohexane 1:5).

^{1}H-NMR (400 MHz, $CDCl_3$, δ/ppm): 7.33 (m, 5H), 6.47 (d, $^3J_{HH}$ = 29.0 Hz, 1H), 5.15 (s, 2H), 4.03 (m, 2H), 3.52 (m, 2H), 2.25 (m, 2H), 1.26 (s, 12H).

MS (EI, m/z): 343.2 (15%, M^+), 252.2 (42%), 108.1 (19%), 91.1 (100%).

1-Cbz-4-(2,3,5,6-tetrafluoro-4-iodophenyl)-1,2,3,6-tetrahydropyridine (125)

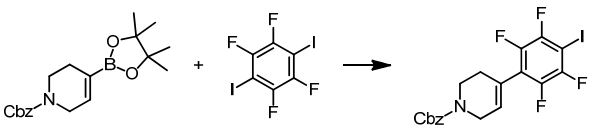

123 **124** **125**

Boronic ester **123** (239 mg, 0.70 mmol, 1.0 eq.) and commercially available 1,4-diiodotetrafluoro-benzene (**124**, 419 mg, 1.04 mmol, 1.5 eq.) were dissolved under an argon atmosphere in dry toluene (6 mL) in a Schlenk-tube and the resulting solution was degassed with the freeze-pump-thaw method. Afterwards $PdCl_2(dppf)\cdot CH_2Cl_2$ (6 mg, 7 µmol, 1 mol%) and potassium phosphate tribasic monohydrate (320 mg, 1.39 mmol, 2.0 eq.) were added and the reaction mixture was stirred at 80 °C for 22 hours. After removal of the solvent under reduced pressure the remaining crude mixture was purified by column chromatography (silica gel, ethyl acetate/cyclohexane 1:10) to afford compound **125** ($C_{19}H_{14}F_4INO_2$, 115 mg, 33%) as a colorless solid.

TLC R_f = 0.20 (ethyl acetate/cyclohexane 1:10).

^{1}H-NMR (500 MHz, $CDCl_3$, δ/ppm): 7.37 (m, 5H), 5.92 (m, 1H), 5.19 (s, 2H), 4.18 (m, 2H), 3.73 (m, 2H), 2.45 (m, 2H).

^{19}F-NMR (376 MHz, $CDCl_3$, δ/ppm): -120.9 (m, 2F), -140.4 (m, 2F).

MS (FAB, m/z): 492(26%, $[M+H]^+$), 91.0 (100%).

EA calculated: C = 46.46, H = 2.87, N = 2.85,
found: C = 46.41, H = 2.97, N = 2.97.

1-Cbz-4-(2,3,5,6-tetrafluoro-4-(oct-1-yn-1-yl)phenyl)-1,2,3,6-tetrahydropyridine (128)

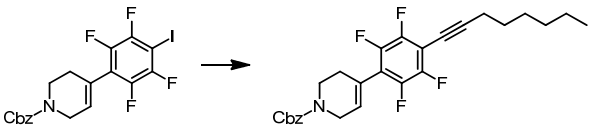

Compound **125** (214 mg, 0.44 mL, 1.0 eq.) was dissolved in triethylamine (10 mL) in a dry Schlenk-tube and the solution was degassed with the freeze-pump-thaw method. Then commercially available 1-octyne (0.19 mL, 1.31 mmol, 3.0 eq.), $Pd(PPh_3)_4$ (15 mg, 0.01 mmol, 3 mol%) and copper iodide (5 mg, 0.03 mmol, 6 mol%) were added under an argon atmosphere and the reaction mixture was stirred at 65 °C for 19 hours. The reaction mixture was diluted with water and an extraction with dichloromethane (3x) was performed. The collected organic extracts were washed with water (3x) and dried over $MgSO_4$. The solvent was removed under reduced pressure and the resulting crude product was purified by column chromatography (silica gel, ethyl acetate/cyclohexane 1:10) to afford compound **128** ($C_{27}H_{27}F_4NO_2$, 160 mg, 78%) as a brownish oil.

TLC R_f = 0.31 (ethyl acetate/cyclohexane 1:10).

^{1}H-NMR (400 MHz, $CDCl_3$, δ/ppm): 7.35(m, 5H), 5.91 (m, 1H), 5.19 (s, 2H), 4.18 (m, 2H), 3.72 (m, 2H), 2.50 (t, $^3J_{HH}$ = 7.0 Hz, 2H), 2.44 (m, 2H), 1.64 (m, 2H), 1.47 (m, 2H), 1.32 (m, 4H), 0.90 (t, $^3J_{HH}$ = 6.9 Hz, 3H).

^{19}F-NMR (377 MHz, $CDCl_3$, δ/ppm): -138.5 (m, 2F), -143.5 (m, 2F).

MS (FAB, m/z): 473.2 (21%, M^+), 472.2 (65%), 428.2 (42%), 382.2 (16%), 91.0 (100%).

4-(2,3,5,6-Tetrafluoro-4-octylphenyl)piperidine (DTCP 7)

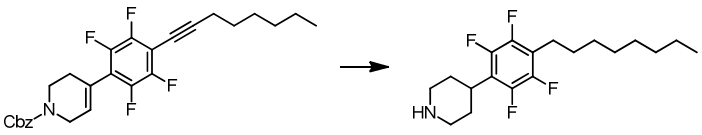

128 DTCP 7

Compound **128** (112 mg, 0.24 mmol, 1.0 eq.), palladium on activated carbon (10 wt%, 24 mg, 0.02 mmol, 0.1 eq.), acetic acid (0.5 mL) and ethanol (6 mL) were added into a 10 mL sample glass, which was then put into an autoclave. Under hydrogen pressure of 20 bar the reaction mixture was stirred at room temperature for 3 days. The reaction mixture was diluted with dichloromethane and the resulting solution was then washed with an aqueous NaOH-solution (1 M). The organic layer was dried over $MgSO_4$ and the solvent was then removed under reduced preesure. The remaining crude product was purified by column chromatography (silica gel, ethanol/chloroform/NH_4OH 1:10:0.1) to afford target structure **DTCP 7** ($C_{19}H_{27}F_4N$, 65 mg, 79%) as a colorless solid.

TLC R_f = 0.41 (ethanol/chloroform/NH_4OH 1:10:0.1).

^{1}H-NMR (500 MHz, $CDCl_3$, δ/ppm): 3.19 (m, 2H), 3.12 (m, 1H), 2.73 (m, 2H), 2.67 (m, 2H), 2.01 (m, 2H), 1.70 (m, 2H), 1.58 (m, 3H), 1.29 (m, 10H), 0.88 (t, $^3J_{HH}$ = 6.9 Hz, 3H).

^{19}F-NMR (377 MHz, $CDCl_3$, δ/ppm): -145.0 (m, 2F), -146.1 (m, 2F).

^{13}C-NMR (126 MHz, $CDCl_3$, δ/ppm): 145.8 (m), 143.9 (m), 120.9 (t, $^2J_{CF}$ = 16.2 Hz), 118.4 (t, $^2J_{CF}$ = 18.8 Hz), 47.2, 34.1, 31.9, 31.4, 29.3, 29.3, 29.2, 22.7, 22.6, 14.1.

MS (EI, m/z): 345.2 (100%, M^+), 325.2 (23%), 83.1 (46%), 56.1 (46%), 43.1 (40%).

EA calculated: C = 66.07, H = 7.88, N = 4.06,
found: C = 65.98, H = 7.83, N = 4.13.

4'-Hexyloxy-4-biphenylcarboxylic acid (130)[374]

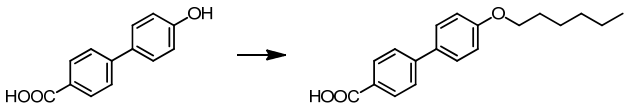

129 **130**

Commercially available 4'-hydroxy-4-biphenylcarboxylic acid (**129**, 5.06 g, 23.6 mmol, 1.0 eq.), 1-bromohexane (4.33 mL, 30.7 mmol, 1.3 eq.), potassium hydroxide (2.78 g, 49.6 mmol, 2.1 eq.), potassium iodide (196 mg, 1.18 mmol, 5 mol%), ethanol (350 mL) and water (35 mL) were added under an argon atmosphere into a flask and the reaction mixture was stirred to reflux for 19 hours. Afterwards the solution was cooled to room temperature and then an aqueous KOH-solution (15 w%, 12 mL) was added and the reaction mixture was stirred again to reflux for 2 hours. After cooling down to room temperature the reaction mixture was acidified with an aqueous HCl-solution (1 M). The precipitate formed was collected by filtration and then recrystallized from acetic acid. A further recrystallization from ethanol was performed to obtain 4'-hexyloxy-4-biphenylcarboxylic acid (**130**, $C_{19}H_{22}O_3$, 4.10 g, 59%) as a colorless solid.

^{1}H-NMR (400 MHz, $CDCl_3$, δ/ppm): 12.93 (s_{br}, 1H), 7.99 (d, $^3J_{HH}$ = 8.5 Hz, 2H), 7.75 (d, $^3J_{HH}$ = 8.5 Hz, 2H), 7.67 (d, $^3J_{HH}$ = 8.8 Hz, 2H), 7.04 (d, $^3J_{HH}$ = 8.8 Hz, 2H), 4.01 (t, $^3J_{HH}$ = 6.5 Hz, 2H), 1.72 (m, 2H), 1.42 (m, 2H), 1.31 (m, 4H), 0.88 (t, $^3J_{HH}$ = 7.1 Hz, 3H).

^{13}C-NMR (101 MHz, $CDCl_3$, δ/ppm): 167.1, 158.9, 143.9, 131.0, 129.8, 128.7, 128.0, 126.0, 114.9, 67.5, 30.9, 28.5, 25.1, 22.0, 13.8.

MS (EI, m/z): 298.2 (28%, M^+), 214.1 (100%).

EA calculated: C = 76.48, H = 7.43,
found: C = 76.11, H = 7.53.

4'-Hexyloxy-4-biphenylmethanol (131)

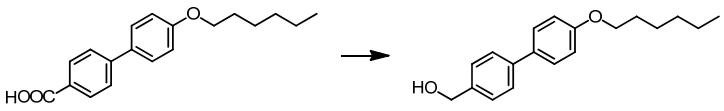

130 131

4'-Hexyloxy-4-biphenylcarboxylic acid (**130**, 3.84 g, 12.9 mmol, 1.0 eq.) was dissolved under an argon atmosphere in dry tetrahydrofuran (200 mL) in a dry flask. This solution was added slowly to a previously prepared and cooled (0 °C) solution of lithium aluminium hydride (1.0 M in THF, 38.6 mmol, 3.0 eq.). After addition and removal of the cooling bath the reaction mixture was stirred to reflux for 6 hours and then cooled to room temperature. Subsequently the reaction mixture was quenched with water (2 mL). An aqueous NaOH-solution (15 wt%, 2 mL) and water (2 mL) were added and the precipitate formed was filtered off. The solvent of the filtrate was removed under reduced pressure. The resulting solid was purified by column chromatography (silica gel, ethyl acetate/cyclohexane 1:2) to afford 4'-hexyloxy-4-biphenyl-methanol (**131**, $C_{19}H_{24}O_2$, 3.07 g, 84%) as a colorless solid.

TLC R_f = 0.39 (ethyl acetate/cyclohexane 1:2).

^{1}H-NMR (400 MHz, $CDCl_3$, δ/ppm): 7.55 (d, $^3J_{HH}$ = 8.3 Hz, 2H), 7.51 (d, $^3J_{HH}$ = 8.9 Hz, 2H), 7.41 (d, $^3J_{HH}$ = 8.4 Hz, 2H), 6.96 (d, $^3J_{HH}$ = 8.8 Hz, 2H), 4.72 (d, $^3J_{HH}$ = 5.9 Hz, 2H), 3.99 (t, $^3J_{HH}$ = 6.6 Hz, 2H), 1.80 (m, 2H), 1.70 (t, $^3J_{HH}$ = 5.9 Hz, 1H), 1.45 (m, 2H), 1.34 (m, 4H), 0.91 (t, $^3J_{HH}$ = 7.0 Hz, 3H).

^{13}C-NMR (101 MHz, $CDCl_3$, δ/ppm): 158.8, 140.3, 139.2, 133.1, 128.0, 127.5, 126.9, 114.8, 68.1, 65.2, 31.6, 29.3, 25.7, 22.6, 14.1.

MS (EI, m/z): 284.2 (70%, M^+), 200.1 (100%), 183.1 (17%), 171.0 (19%).

EA calculated: C = 80.24, H = 8.51,
found: C = 80.01, H = 8.56.

4'-Hexyloxy-4-biphenylbromomethane (132)

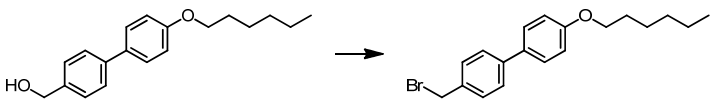

131 **132**

4'-Hexyloxy-4-biphenylmethanol (**131**, 2.57 g, 9.04 mmol, 1.0 eq.) and carbon tetrabromide (3.00 g, 9.04 mmol, 1.0 eq.) were dissolved under an argon atmosphere in dry dichloromethane (160 mL) in a dry flask. To this solution, a solution of triphenylphosphine (2.37 g, 9.04 mmol, 1.0 eq.) in dry dichloromethane (20 mL) was slowly added. The resulting reaction mixture was stirred at room temperature for 18 hours. The solution was then concentrated under reduced pressure and the residue was passed through a short plug of silica gel with *n*-hexane as an eluent. The solvent was then removed under reduced pressure to afford 4'-hexyloxy-4-biphenylbromomethane (**132**, $C_{19}H_{23}BrO$, 1.94 g, 62%) as a yellowish solid.

^{1}H-NMR (400 MHz, $CDCl_3$, δ/ppm): 7.51 (m, 4H), 7.42 (d, $^3J_{HH}$ = 8.2 Hz, 2H), 6.96 (d, $^3J_{HH}$ = 8.8 Hz, 2H), 4.53 (s, 2H), 3.99 (t, $^3J_{HH}$ = 6.6 Hz, 2H), 1.79 (m, 2H), 1.47 (m, 2H), 1.34 (m, 4H), 0.91 (t, $^3J_{HH}$ = 7.0 Hz, 3H).

^{13}C-NMR (101 MHz, $CDCl_3$, δ/ppm): 159.0, 141.1, 136.0, 132.7, 129.5, 128.1, 127.0, 114.8, 68.1, 33.6, 31.6, 29.2, 25.7, 22.6, 14.1.

MS (EI, m/z): 346.1 (8%, M^+), 267.2 (100%), 183.1 (64%).

EA calculated: C = 65.71, H = 6.67,
found: C = 65.78, H = 6.74.

4'-Hexyloxy-4-biphenyltritylthiomethane (133)

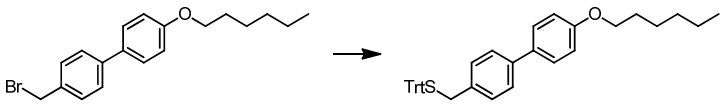

132 **133**

4'-Hexyloxy-4-biphenylbromomethane (**132**, 166 mg, 0.48 mmol, 1.0 eq.) and triphenylmethanethiol (197 mg, 0.72 mmol, 1.5 eq.) were dissolved under an argon atmosphere in dry tetrahydrofuran (15 mL) in a dry flask. Then sodium hydride (60% dispersion in mineral oil, 95.8 mg, 2.40 mmol, 5.0 eq.) was added in small portions and the reaction mixture was stirred at room temperature for 1 hour. Afterwards the reaction mixture was carefully quenched with water and an extraction with ethyl acetate (3x) was performed. The collected organic layers were washed with water (3x) and dried over $MgSO_4$. The solvent was removed under reduced pressure and the crude product was purified by column chromatography (silica gel, dichloromethane/*n*-hexane 1:5) to afford 4'-hexyloxy-4-biphenyltritylthiomethane (**133**, $C_{38}H_{38}OS$, 217 mg, 84%) as a brownish oil.

TLC R_f = 0.36 (dichloromethane/*n*-hexane 1:5).

^{1}H-NMR (400 MHz, $CDCl_3$, δ/ppm): 7.47 (m, 8H), 7.42 (d, $^3J_{HH}$ = 8.0 Hz, 2H), 7.31 (m, 6H), 7.23 (m, 3H), 7.17 (d, $^3J_{HH}$ = 8.0 Hz, 2H), 6.94 (d, $^3J_{HH}$ = 8.6 Hz, 2H), 3.98 (t, $^3J_{HH}$ = 6.5 Hz, 2H), 3.34 (s, 2H), 1.79 (m, 2H), 1.47 (m, 2H), 1.34 (m, 4H), 0.91 (t, $^3J_{HH}$ = 6.5 Hz, 3H).

^{13}C-NMR (126 MHz, $CDCl_3$, δ/ppm): 158.7, 144.7, 139.7, 135.3, 133.4, 129.6, 129.4, 128.0, 127.9, 126.8, 126.7, 114.7, 68.2, 67.4, 36.7, 31.6, 29.3, 25.7, 22.6, 14.1.

MS (FAB, m/z): 542.2 (1%, M^+), 243.1 (100%).

4'-Hexyloxy-4-biphenylmethanethiol (T1)

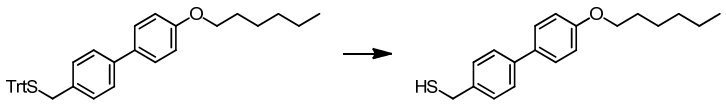

133 T1

4'-Hexyloxy-4-biphenyltritylthiomethane (**133**, 342 mg, 0.63 mmol, 1.0 eq.) and triethylsilane (0.15 mL, 0.95 mmol, 1.5 eq.) were dissolved under an argon atmosphere in dry dichloromethane (7.0 mL) in a dry flask. Then trifluoroacetic acid (280 µl, 4 vol.-% related to CH_2Cl_2) was slowly added and the reaction mixture was stirred at room temperature for 3 hours. Subsequently the reaction mixture was quenched with a saturated aqueous $NaHCO_3$-solution and an extraction with dichloromethane (3x) was performed. The collected organic layers were dried over $MgSO_4$ and the solvent was removed under reduced pressure. The resulting crude product was purified by column chromatography (silica gel, dichloromethane/cyclohexane 3:5) to afford target structure 4'-hexyloxy-4-biphenylmethanethiol (**T1**, $C_{19}H_{24}OS$, 162 mg, 86%) as a colorless solid.

TLC R_f = 0.45 (dichloromethane/cyclohexane 3:5).

^{1}H-NMR (400 MHz, $CDCl_3$, δ/ppm): 7.50 (m, 4H), 7.36 (d, $^3J_{HH}$ = 8.2 Hz, 2H), 6.96 (d, $^3J_{HH}$ = 8.8 Hz, 2H), 3.99 (t, $^3J_{HH}$ = 6.6 Hz, 2H), 3.78 (d, $^3J_{HH}$ = 7.5 Hz, 2H), 1.80 (m, 3H), 1.48 (m, 2H), 1.35 (m, 4H), 0.91 (t, $^3J_{HH}$ = 7.0 Hz, 3H).

^{13}C-NMR (101 MHz, $CDCl_3$, δ/ppm): 158.8, 139.7, 139.5, 133.0, 128.4, 128.0, 127.0, 114.8, 68.1, 31.6, 29.3, 28.7, 25.7, 22.6, 14.1.

MS (EI, m/z): 300.2 (51%, M^+), 267.2 (100%), 183.1 (99%).

EA calculated: C = 75.95, H = 8.05,
found: C = 75.81, H = 7.99.

7 Abbreviations

A	Ampere
Abs	absorbance
Ac	acetyl
aq.	aqueous
au	atomic units
AZOP	AZO precursor
Boc	*tert*-butoxycarbonyl
Bn	benzyl
br	broad
Bu	butyl
BZ	benzene
C	concentration
CABP	“classical” azobiphenyl
cAFM	contact atomic force microscopy
Cbz	carboxybenzyl
CC	column chromatography
cd	Candela
cm	centimeter
CV	cyclic voltammetry
d	duplet
dba	dibenzylideneacetone
dppf	1,1'-bis(diphenylphosphino)-ferrocene
D	Debye
DDT	dodecanethiol
DIBAL-H	diisobutylaluminium hydride
DMF	*N*,*N*-dimethylformamide
DTC	dithiocarbamate
DTCP	dithiocarbamate precursor
EA	electroabsorption
EA	elemental analysis
EI	electron impact
EL	electroluminescence
eq.	equivalent
EQE	external quantum efficiency
Et	ethyl
eV	electron volt
FAB	fast atom bombardment
FBZ	hexafluorobenzene
F8BT	poly(9,9’-dioctylfluorene-alt-benzothiadiazole)
h	hour
HMBC	heteronuclear multiple bond co-herence
HMQC	heteronuclear multiple quantum coherence
Hz	Hertz
ITO	indium tin oxide
I	current
IR	infrared
J	current density
J	Joule
k	kilo
KP	Kelvin probe
KPFM	Kelvin probe force microscopy
L	luminance
LB	Langmuir-Blodgett
LED	light-emitting diode
LiHMDS	lithium bis(trimethylsilyl)amide
LUMO	lowest unoccupied molecular orbital
m	milli
m	meter
m	multiplet
M	mega
M	metal
M	molar
MALDI	matrix-assisted laser desorption ionization
Me	methyl
min	minute

mol	mole
MS	mass spectrometry
MW	microwave
m/z	mass per charge
n	nano
NBS	*N*-bromosuccinimide
NIS	*N*-iodosuccinimide
NMR	nuclear magnetic resonance
NP	nanoparticle
OFET	organic field-effect transistor
OLED	organic light-emitting diode
OPE	oligo phenylene ethynylene
OTf	triflate
Oxone®	$2KHSO_5 \cdot KHSO_4 \cdot K_2SO_4$
PDIF-CN_2	*N,N'*-1H,1H-perfluorobutyl-dicyanoperylenecarboxydiimide
PG	protecting group
Ph	phenyl
P3HT	poly(3-hexylthiophene)
PL	photoluminescence
PMDTA	pentamethyldiethylenetriamine
ppm	parts per million
Pr	propyl
PS	photoelectron spectroscopy
q	quartet
quant.	quantitative
R	ratio
R_f	retention factor
rt	room temperature
s	singlet
SAM	self-assembled monolayer
s_{br}	broad singlet
SEF	stretched exponential function
S_N	nucleophilic substitution
SPR	surface plasmon resonance
STEM	scanning transmission electron microscopy
STM	scanning tunneling microscopy
t	triplet
t	*tert*
TATA	triazatriangulenium
TBACN	tetrabutylammonium cyanide
TBAF	tetrabutylammonium fluoride
TBDMCl	*tert*-butyldimethylsilyl chloride
TBDMS	*tert*-butyldimethylsilyl
TBME	*tert*-butylmethylether
TBDMS	*tert*-butyldimethylsilyl
TEM	transition electron microscopy
Tf	trifluoromethanesulfonyl
TFA	trifluoroacetic acid
TFT	thin film transistor
THF	tetrahydrofuran
TLC	thin layer chromatography
TMEDA	tetramethylethylenediamine
TMS	tetramethylsilane
ToF	time of flight
Trt	trityl
UPS	ultraviolet photoelectron spectroscopy
UV	ultraviolet
V	Volt
Vis	visible
vol.-%	volume percent
W	Watt
wt%	weight percent
XPS	X-ray photoelectron spectroscopy
Å	Angstrom
°C	Celsius
δ	chemical shift
λ	wavelength
µ	micro
µ	mobility
Φ	work function

8 Literature

[1] L. Meng, X. Zhang, Q. Lu, Z. Fei, P. J. Dyson, *Biomaterials* **2012**, *33*, 1689–1698.

[2] D. Papakostas, F. Rancan, W. Sterry, U. Blume-Peytavi, A. Vogt, *Arch. Dermatol. Res.* **2011**, *303*, 533–550.

[3] K. Saha, S. S. Agasti, C. Kim, X. Li, V. M. Rotello, *Chem. Rev.* **2012**, *112*, 2739–2779.

[4] Y. Cui, S. N. Kim, R. R. Naik, M. C. McAlpine, *Acc. Chem. Res.* **2012**, *45*, 696–704.

[5] P. Uhlmann, H. Merlitz, J. Sommer, M. Stamm, *Macromol. Rapid Commun.* **2009**, *30*, 732–740.

[6] A. Olivier, F. Meyer, J.-M. Raquez, P. Damman, P. Dubois, *Prog. Polym. Sci.* **2012**, *37*, 157–181.

[7] M. Tada, Y. Iwasawa, *Chem. Commun.* **2006**, 2833–2844.

[8] C. Hess, *ChemPhysChem* **2009**, *10*, 319–326.

[9] F. Cicoira, C. Santato, *Adv. Funct. Mater.* **2007**, *17*, 3421–3434.

[10] R. H. Friend, R. W. Gymer, A. B. Holmes, J. H. Burroughes, R. N. Marks, C. Taliani, D. D. C. Bradley, D. A. D. Santos, J. L. Brédas, M. Lögdlund, et al., *Nature* **1999**, *397*, 121–128.

[11] R. J. P. Corriu, A. Mehdi, C. Reyé, *J. Mater. Chem.* **2005**, *15*, 4285–4294.

[12] S. Garoff, *Thin Solid Films* **1987**, *152*, 49–66.

[13] F. Tao, S. L. Bernasek, G.-Q. Xu, *Chem. Rev.* **2009**, *109*, 3991–4024.

[14] J. G. Kushmerick, D. B. Holt, J. C. Yang, J. Naciri, M. H. Moore, R. Shashidhar, *Phys. Rev. Lett.* **2002**, *89*, 086802(4).

[15] J. Chen, M. A. Reed, A. M. Rawlett, J. M. Tour, *Science* **1999**, *286*, 1550–1552.

[16] B. Xu, N. J. Tao, *Science* **2003**, *301*, 1221–1223.

[17] L. A. Bumm, J. J. Arnold, M. T. Cygan, T. D. Dunbar, T. P. Burgin, L. Jones, D. L. Allara, J. M. Tour, P. S. Weiss, *Science* **1996**, *271*, 1705–1707.

[18] H. Kuhn, D. Möbius, *Angew. Chem. Int. Ed.* **1971**, *10*, 620–637.

[19] A. Aviram, M. A. Ratner, *Chem. Phys. Lett.* **1974**, *29*, 277–283.

[20] C. Joachim, J. K. Gimzewski, A. Aviram, *Nature* **2000**, *408*, 541–548.

[21] R. M. Metzger, *Accounts of Chemical Research* **1999**, *32*, 950–957.

[22] C. P. Collier, G. Mattersteig, E. W. Wong, Y. Luo, K. Beverly, J. Sampaio, F. M. Raymo, J. F. Stoddart, J. R. Heath, *Science* **2000**, *289*, 1172–1175.

[23] Y. Luo, C. P. Collier, J. O. Jeppesen, K. A. Nielsen, E. DeIonno, G. Ho, J. Perkins, H. Tseng, T. Yamamoto, J. F. Stoddart, et al., *ChemPhysChem* **2002**, *3*, 519–525.

[24] M. Mayor, H. B. Weber, *Chimia* **2002**, *56*, 494–499.

[25] J. A. Zasadzinski, R. Viswanathan, L. Madsen, J. Garnaes, D. K. Schwartz, *Science* **1994**, *263*, 1726–1733.

[26] A. Ulman, *Chem. Rev.* **1996**, *96*, 1533–1554.

[27] J. C. Love, L. A. Estroff, J. K. Kriebel, R. G. Nuzzo, G. M. Whitesides, *Chem. Rev.* **2005**, *105*, 1103–1170.

[28] G. M. Whitesides, J. P. Mathias, C. T. Seto, *Science* **1991**, *254*, 1312–1319.

[29] F. Schreiber, *Prog. Surf. Sci.* **2000**, *65*, 151–257.

[30] D. G. Castner, B. D. Ratner, *Surf. Sci.* **2002**, *500*, 28–60.

[31] R. L. McCreery, A. J. Bergren, *Adv. Mater.* **2009**, *21*, 4303–4322.

[32] A. Danilov, S. Kubatkin, S. Kafanov, P. Hedegard, N. Stuhr-Hansen, K. Moth-Poulsen, T. Bjornholm, *Nano Lett.* **2007**, *8*, 1–5.

[33] Y. Xue, S. Datta, M. A. Ratner, *J. Chem. Phys.* **2001**, *115*, 4292.

[34] L. Venkataraman, J. E. Klare, C. Nuckolls, M. S. Hybertsen, M. L. Steigerwald, *Nature* **2006**, *442*, 904–907.

[35] F. Chen, X. Li, J. Hihath, Z. Huang, N. Tao, *J. Am. Chem. Soc.* **2006**, *128*, 15874–15881.

[36] S. Wu, M. T. González, R. Huber, S. Grunder, M. Mayor, C. Schönenberger, M. Calame, *Nat. Nanotechnol.* **2008**, *3*, 569–574.

[37] J. M. Seminario, A. G. Zacarias, J. M. Tour, *J. Am. Chem. Soc.* **1999**, *121*, 411–416.
[38] J. Sagiv, *J. Am. Chem. Soc.* **1980**, *102*, 92–98.
[39] O. M. Magnussen, B. M. Ocko, M. Deutsch, M. J. Regan, P. S. Pershan, D. Abernathy, G. Grübel, J.-F. Legrand, *Nature* **1996**, *384*, 250–252.
[40] G. S. Tulevski, M. B. Myers, M. S. Hybertsen, M. L. Steigerwald, C. Nuckolls, *Science* **2005**, *309*, 591–594.
[41] J. A. M. Simoes, J. L. Beauchamp, *Chem. Rev.* **1990**, *90*, 629–688.
[42] F. Tournus, S. Latil, M. I. Heggie, J.-C. Charlier, *Phys. Rev. B* **2005**, *72*, 075431(5).
[43] D. Vonlanthen, Biphenyl-Cyclophanes, Dissertation, University of Basel, **2010**.
[44] Y. Zhao, W. Pérez-Segarra, Q. Shi, A. Wei, *J. Am. Chem. Soc.* **2005**, *127*, 7328–7329.
[45] P. Morf, F. Raimondi, H.-G. Nothofer, B. Schnyder, A. Yasuda, J. M. Wessels, T. A. Jung, *Langmuir* **2006**, *22*, 658–663.
[46] Cao, A. Díaz, R. Cao, A. Otero, R. Cea, M. C. Rodríguez-Argüelles, C. Serra, *J. Am. Chem. Soc.* **2007**, *129*, 6927–6930.
[47] F. von Wrochem, D. Gao, F. Scholz, H.-G. Nothofer, G. Nelles, J. M. Wessels, *Nat. Nanotechnol.* **2010**, *5*, 618–624.
[48] G. D. Thorn, R. A. Ludwig, *The Dithiocarbamates and Related Compounds*, Elsevier Publishing Company, **1962**.
[49] N. Koch, *ChemPhysChem* **2007**, *8*, 1438–1455.
[50] O. T. Hofmann, D. A. Egger, E. Zojer, *Nano Lett.* **2010**, *10*, 4369–4374.
[51] H. Ishii, K. Sugiyama, E. Ito, K. Seki, *Adv. Mater.* **1999**, *11*, 605–625.
[52] G. M. Rangger, L. Romaner, G. Heimel, E. Zojer, *Surf. Interface Anal.* **2008**, *40*, 371–378.
[53] B. de Boer, A. Hadipour, M. M. Mandoc, T. van Woudenbergh, P. W. M. Blom, *Adv. Mater.* **2005**, *17*, 621–625.
[54] D. M. Alloway, M. Hofmann, D. L. Smith, N. E. Gruhn, A. L. Graham, Colorado, V. H. Wysocki, T. R. Lee, P. A. Lee, N. R. Armstrong, *J. Phys. Chem. B* **2003**, *107*, 11690–11699.
[55] H. Vázquez, R. Oszwaldowski, P. Pou, J. Ortega, R. Pérez, F. Flores, A. Kahn, *Europhys. Lett.* **2004**, *65*, 802–808.
[56] S. Braun, M. P. de Jong, W. Osikowicz, W. R. Salaneck, *Appl. Phys. Lett.* **2007**, *91*, 202108(3).
[57] G. Heimel, L. Romaner, J.-L. Brédas, E. Zojer, *Surf. Sci.* **2006**, *600*, 4548–4562.
[58] S. Braun, W. R. Salaneck, M. Fahlman, *Adv. Mater.* **2009**, *21*, 1450–1472.
[59] Y. Lee, B. Carsten, L. Yu, *Langmuir* **2008**, *25*, 1495–1499.
[60] D. Cahen, A. Kahn, *Adv. Mater.* **2003**, *15*, 271–277.
[61] A. Natan, Y. Zidon, Y. Shapira, L. Kronik, *Phys. Rev. B* **2006**, *73*, 193310(4).
[62] A. Natan, L. Kronik, H. Haick, R. T. Tung, *Adv. Mater.* **2007**, *19*, 4103–4117.
[63] D. Cornil, Y. Olivier, V. Geskin, J. Cornil, *Adv. Funct. Mater.* **2007**, *17*, 1143–1148.
[64] R. M. Metzger, *Chem. Rev.* **2003**, *103*, 3803–3834.
[65] A. S. Martin, J. R. Sambles, G. J. Ashwell, *Phys. Rev. Lett.* **1993**, *70*, 218–221.
[66] D. Gao, F. Scholz, H. G. Nothofer, W. E. Ford, U. Scherf, J. M. Wessels, A. Yasuda, F. von Wrochem, *Journal of the American Chemical Society* **2011**.
[67] B. L. Feringa, *J. Org. Chem.* **2007**, *72*, 6635–6652.
[68] B. L. Feringa, *Molecular Switches*, Wiley-VCH, **2001**.
[69] J. Leblond, A. Petitjean, *ChemPhysChem* **2011**, *12*, 1043–1051.
[70] M. Iyoda, M. Hasegawa, H. Enozawa, *Chem. Lett.* **2007**, *36*, 1402–1407.
[71] N. Fuentes, A. Martín-Lasanta, L. Álvarez de Cienfuegos, M. Ribagorda, A. Parra, J. M. Cuerva, *Nanoscale* **2011**, *3*, 4003–4014.
[72] H. Tavana, A. W. Neumann, *Adv. Colloid Interface Sci.* **2007**, *132*, 1–32.
[73] D. Briggs, M. P. Seah, *Practical Surface Analysis: Auger and X-Ray Photoelectron Spectroscopy*, Wiley-vch, **1995**.

[74] P. Morf, Self-Assembled Monolayers Beyond Thiols: Dithiocarbamates – from pure layers to ternary assembly systems, Dissertation, University of Basel, **2007**.
[75] F. von Wrochem, Electron Structure and Charge Transport Properties of Thiols and Dithiocarbamates in Self-Assembled Monolayers, Dissertation, University of Basel, **2007**.
[76] G. Ertl, J. Küppers, *Low Energy Electrons and Surface Chemistry*, Wiley-VCH, **1985**.
[77] J. H. D. Eland, *Photoelectron Spectroscopy : An Introduction to Ultraviolet Photoelectron Spectroscopy in the Gas Phase*, Butterworths, **1974**.
[78] N. Knöpfel, T. Olbricht, A. Schweig, *Chemie in unserer Zeit* **1971**, *5*, 65–77.
[79] A. Einstein, *Annalen der Physik* **1905**, *322*, 132–148.
[80] R. E. Holmlin, R. Haag, M. L. Chabinyc, R. F. Ismagilov, A. E. Cohen, A. Terfort, M. A. Rampi, G. M. Whitesides, *J. Am. Chem. Soc.* **2001**, *123*, 5075–5085.
[81] F. C. Simeone, M. A. Rampi, *Chimia* **2010**, *64*, 362–369.
[82] V. Ferri, M. Elbing, G. Pace, M. D. Dickey, M. Zharnikov, P. Samorì, M. Mayor, M. A. Rampi, *Angew. Chem. Int. Ed.* **2008**, *47*, 3407–3409.
[83] H. Zollinger, *Color Chemistry : Syntheses, Properties and Applications of Organic Dyes and Pigments*, Wiley-VCH, **1987**.
[84] W. Müller, *Handbuch der Farbenchemie : Grundlagen, Technik, Anwendungen*, Ecomed, **2000**.
[85] J. F. Osma, V. Saravia, J. L. Toca-Herrera, S. R. Couto, *J. Hazard. Mater.* **2007**, *147*, 900–905.
[86] K. Hunger, W. Rieper, R. Raue, K. Kunde, A. Engel, in *Ullmann's Encyclopedia of Industrial Chemistry*, Wiley-VCH Verlag GmbH & Co. KGaA, **2000**.
[87] A. A. Beharry, G. A. Woolley, *Chem. Soc. Rev.* **2011**, *40*, 4422–4437.
[88] J.-I. Anzai, T. Osa, *Tetrahedron* **1994**, *50*, 4039–4070.
[89] A. Archut, F. Vögtle, L. De Cola, G. C. Azzellini, V. Balzani, P. S. Ramanujam, R. H. Berg, *Chem. Eur. J.* **1998**, *4*, 699–706.
[90] S. Shinkai, T. Minami, Y. Kusano, O. Manabe, *J. Am. Chem. Soc.* **1983**, *105*, 1851–1856.
[91] N. Tamaoki, *Adv. Mater.* **2001**, *13*, 1135–1147.
[92] K. Ichimura, *Chem. Rev.* **2000**, *100*, 1847–1874.
[93] Z. Yu, S. Hecht, *Angew. Chem. Int. Ed.* **2011**, *50*, 1640–1643.
[94] M. R. Banghart, M. Volgraf, D. Trauner, *Biochemistry* **2006**, *45*, 15129–15141.
[95] T. Kudernac, N. Katsonis, W. R. Browne, B. L. Feringa, *J. Mater. Chem.* **2009**, *19*, 7168–7177.
[96] N. Katsonis, M. Lubomska, M. M. Pollard, B. L. Feringa, P. Rudolf, *Prog. Surf. Sci.* **2007**, *82*, 407–434.
[97] Z. F. Liu, K. Hashimoto, A. Fujishima, *Nature* **1990**, *347*, 658–660.
[98] T. Ikeda, O. Tsutsumi, *Science* **1995**, *268*, 1873–1875.
[99] T. Hugel, *Science* **2002**, *296*, 1103–1106.
[100] H. Koshima, N. Ojima, H. Uchimoto, *J. Am. Chem. Soc.* **2009**, *131*, 6890–6891.
[101] J. A. Delaire, K. Nakatani, *Chem. Rev.* **2000**, *100*, 1817–1846.
[102] M.-M. Russew, S. Hecht, *Adv. Mater.* **2010**, *22*, 3348–3360.
[103] W. R. Browne, B. L. Feringa, *Annu. Rev. Phys. Chem.* **2009**, *60*, 407–428.
[104] S. Hagen, F. Leyssner, D. Nandi, M. Wolf, P. Tegeder, *Chem. Phys. Lett.* **2007**, *444*, 85–90.
[105] M. Alemani, M. V. Peters, S. Hecht, K.-H. Rieder, F. Moresco, L. Grill, *J. Am. Chem. Soc.* **2006**, *128*, 14446–14447.
[106] M. J. Comstock, N. Levy, A. Kirakosian, J. Cho, F. Lauterwasser, J. H. Harvey, D. A. Strubbe, J. M. J. Fréchet, D. Trauner, S. G. Louie, et al., *Phys. Rev. Lett.* **2007**, *99*, 038301(4).
[107] J. Henzl, M. Mehlhorn, H. Gawronski, K. Rieder, K. Morgenstern, *Angew. Chem. Int. Ed.* **2006**, *45*, 603–606.
[108] S. D. Evans, S. R. Johnson, H. Ringsdorf, L. M. Williams, H. Wolf, *Langmuir* **1998**, *14*, 6436–6440.
[109] K. Tamada, H. Akiyama, T.-X. Wei, S.-A. Kim, *Langmuir* **2003**, *19*, 2306–2312.
[110] B. Baisch, D. Raffa, U. Jung, O. M. Magnussen, C. Nicolas, J. Lacour, J. Kubitschke, R. Herges, *J. Am. Chem. Soc.* **2008**, *131*, 442–443.
[111] D. S. Sidhaye, S. Kashyap, M. Sastry, S. Hotha, B. L. V. Prasad, *Langmuir* **2005**, *21*, 7979–7984.

[112] P. Ahonen, D. J. Schiffrin, J. Paprotny, K. Kontturi, *Phys. Chem. Chem. Phys.* **2007**, *9*, 651–658.
[113] R. Klajn, K. J. . Bishop, M. Fialkowski, M. Paszewski, C. J. Campbell, T. P. Gray, B. A. Grzybowski, *Science* **2007**, *316*, 261–264.
[114] R. Klajn, K. J. M. Bishop, B. A. Grzybowski, *Proc. Natl. Acad. Sci.* **2007**, *104*, 10305–10309.
[115] N. Ishii, F. Fitrilawati, A. Manna, H. Akiyama, Y. Tamada, K. Tamada, *Biosci. Biotechnol. Biochem.* **2008**, *72*, 124–131.
[116] C. Luo, F. Zuo, Z. Zheng, X. Cheng, X. Ding, Y. Peng, *Macromol. Rapid Commun.* **2008**, *29*, 149–154.
[117] T. Kawai, S. Nakamura, A. Sumi, T. Kondo, *Thin Solid Films* **2008**, *516*, 8926–8931.
[118] R. Klajn, P. J. Wesson, K. J. M. Bishop, B. A. Grzybowski, *Angew. Chem. Int. Ed.* **2009**, *48*, 7035–7039.
[119] A. Housni, Y. Zhao, Y. Zhao, *Langmuir* **2010**, *26*, 12366–12370.
[120] C. Raimondo, F. Reinders, U. Soydaner, M. Mayor, P. Samorì, *Chem. Commun.* **2010**, *46*, 1147–1149.
[121] C. Julius Berend, *Practical Organic Chemistry*, Macmillan And Co, **1920**.
[122] G. S. Hartley, *Nature* **1937**, *140*, 281–281.
[123] H. H. Jaffé, S.-J. Yeh, R. W. Gardner, *J. Mol. Spectrosc.* **1958**, *2*, 120–136.
[124] D. L. Beveridge, H. H. Jaffé, *J. Am. Chem. Soc.* **1966**, *88*, 1948–1953.
[125] J. Griffiths, *Chem. Soc. Rev.* **1972**, *1*, 481–493.
[126] G. M. Wyman, *Chem. Rev.* **1955**, *55*, 625–657.
[127] H. P. Latscha, H. A. Klein, *Chemie-Basiswissen*, Springer, **1995**.
[128] H. Rau, *Angew. Chem.* **1973**, *85*, 248–258.
[129] P. De Maria, A. Fontana, C. Gasbarri, G. Siani, P. Zanirato, *ARKAT* **2009**, *8*, 16–29.
[130] G. S. Kumar, D. Neckers, *Chem. Rev.* **1989**, *89*, 1915–1925.
[131] I. Conti, M. Garavelli, G. Orlandi, *J. Am. Chem. Soc.* **2008**, *130*, 5216–5230.
[132] T. Ishikawa, T. Noro, T. Shoda, *J. Chem. Phys.* **2001**, *115*, 7503–7512.
[133] A. Cembran, F. Bernardi, M. Garavelli, L. Gagliardi, G. Orlandi, *J. Am. Chem. Soc.* **2004**, *126*, 3234–3243.
[134] G. Granucci, M. Persico, *Theor. Chem. Acc.* **2006**, *117*, 1131–1143.
[135] E. Wei-Guang Diau, *J. Chem. Phys.* **2004**, *108*, 950–956.
[136] D. H. Waldeck, *Chem. Rev.* **1991**, *91*, 415–436.
[137] Z. Smedarchina, *Chem. Phys. Lett.* **1985**, *116*, 538–542.
[138] J. J. de Lange, J. M. Robertson, I. Woodward, *Proc. R. Soc. Lond. A* **1939**, *171*, 398 –410.
[139] G. C. Hampson, J. M. Robertson, *J. Chem. Soc.* **1941**, 409–413.
[140] R. Hermann, in *Photoreactive Organic Thin Films: Photoisomerization of Azobenzenes*, Academic Press, **2002**.
[141] G. S. Hartley, R. J. W. L. Fèvre, *J. Chem. Soc.* **1939**, 531–535.
[142] D. J. W. Bullock, C. W. N. Cumper, A. I. Vogel, *J. Chem. Soc.* **1965**, 5316–5323.
[143] E. Merino, *Chem. Soc. Rev.* **2011**, *40*, 3835–3853.
[144] J. Merrington, M. James, M. Bradley, *Chem. Commun.* **2002**, 140–141.
[145] C. A. Hunter, L. D. Sarson, *Tetrahedron Lett.* **1996**, *37*, 699–702.
[146] A. Tsuge, T. Moriguchi, S. Mataka, M. Tashiro, *J. Chem. Soc., Perkin Trans. 1* **1993**, 2211–2215.
[147] J. Y. Kim, G. Kim, C. R. Kim, S. H. Lee, J. H. Lee, J. S. Kim, *J. Org. Chem.* **2003**, *68*, 1933–1937.
[148] R. F. Nystrom, W. G. Brown, *J. Am. Chem. Soc.* **1948**, *70*, 3738–3740.
[149] R. O. Hutchins, D. W. Lamson, L. Rua, C. Milewski, B. Maryanoff, *J. Org. Chem.* **1971**, *36*, 803–806.
[150] W. Wei, T. Tomohiro, M. Kodaka, H. Okuno, *J. Org. Chem.* **2000**, *65*, 8979–8987.
[151] A. Khan, S. Hecht, *Chem. Eur. J.* **2006**, *12*, 4764–4774.
[152] C. Karunakaran, P. N. Palanisamy, *J. Mol. Catal. A: Chem.* **2001**, *172*, 9–17.
[153] H. Olsen, J. P. Snyder, *J. Am. Chem. Soc.* **1977**, *99*, 1524–1536.
[154] H. K. Hombrecher, K. Lüdtke, *Tetrahedron* **1993**, *49*, 9489–9494.
[155] S. M. Mehta, M. V. Vakilwala, *J. Am. Chem. Soc.* **1952**, *74*, 563–564.
[156] K. Kinoshita, *Bull. Chem. Soc. Jpn.* **1959**, *32*, 777–780.
[157] K. H. Schündehütte, *Methoden der organischen Chemie*, Thieme, **1965**.

[158] K. Ueno, S. Akiyoshi, *J. Am. Chem. Soc.* **1954**, *76*, 3670–3672.
[159] Y. Ogata, Y. Takagi, *J. Am. Chem. Soc.* **1958**, *80*, 3591–3595.
[160] B. G. Gowenlock, G. B. Richter-Addo, *Chem. Rev.* **2004**, *104*, 3315–3340.
[161] E. Bosch, J. K. Kochi, *J. Org. Chem.* **1994**, *59*, 5573–5586.
[162] W. L. Waters, P. G. Marsh, *J. Org. Chem.* **1975**, *40*, 3344–3349.
[163] A. Maltha, S. C. van Wermeskerken, B. Brunet, V. Ponec, *J. Mol. Catal.* **1994**, *93*, 305–316.
[164] S. Meijers, T. P. P. van der Hoeven, V. Ponec, J. P. Jacobs, H. H. Brongersma, *J. Catal.* **1996**, *161*, 459–464.
[165] M. H. Davey, V. Y. Lee, R. D. Miller, T. J. Marks, *J. Org. Chem.* **1999**, *64*, 4976–4979.
[166] H. Z. Caro, *Angew. Chem.* **1898**, *11*, 845–46.
[167] J. W. Gorrod, *Tetrahedron Lett.* **1968**, *9*, 6155–6158.
[168] E. Bamberger, F. Tschirner, *Berichte der Deutschen Chemischen Gesellschaft* **1899**, *32*, 342–355.
[169] S. J. Wratten, H. Fujiwara, R. T. Solsten, *J. Agric. Food Chem.* **1987**, *35*, 484–491.
[170] L. D. Nunno, S. Florio, P. E. Todesco, *J. Chem. Soc. C* **1970**, 1433–1434.
[171] Z. Zhu, J. H. Espenson, *J. Org. Chem.* **1995**, *60*, 1326–1332.
[172] B. Priewisch, K. Rück-Braun, *J. Org. Chem.* **2005**, *70*, 2350–2352.
[173] B. C. Yu, Y. Shirai, J. M. Tour, *Tetrahedron* **2006**, *62*, 10303–10310.
[174] "Non-Chlorine Shock Oxidizer from DuPont," can be found under http://www2.dupont.com/Pool_Care/en_US/products/benefits.html, **2012**.
[175] B. G. Gowenlock, G. B. Richter-Addo, *J. Chem. Educ.* **2008**, *85*, 1243–1245.
[176] N. Henningsen, K. J. Franke, G. Schulze, I. Fernández-Torrente, B. Priewisch, K. Rück-Braun, J. I. Pascual, *ChemPhysChem* **2007**, *9*, 71–73.
[177] B. Priewisch, Photoschaltbare Aminosäuren Synthese, photochrome Eigenschaften und Einbau in peptidische Grb2-SH2 Antagonisten, Dissertation, Technische Universität Berlin, **2006**.
[178] K. Rück-Braun, S. Kempa, B. Priewisch, A. Richter, S. Seedorff, L. Wallach, *Synthesis* **2009**, *24*, 4256–4267.
[179] Y.-K. Lim, K.-S. Lee, C.-G. Cho, *Org. Lett.* **2003**, *5*, 979–982.
[180] F. Paul, J. Patt, J. F. Hartwig, *J. Am. Chem. Soc.* **1994**, *116*, 5969–5970.
[181] A. S. Guram, S. L. Buchwald, *J. Am. Chem. Soc.* **1994**, *116*, 7901–7902.
[182] Y.-K. Lim, J.-W. Jung, H. Lee, C.-G. Cho, *J. Org. Chem.* **2004**, *69*, 5778–5781.
[183] Z. Wang, R. T. Skerlj, G. J. Bridger, *Tetrahedron Lett.* **1999**, *40*, 3543–3546.
[184] H.-M. Kang, J.-W. Jung, C.-G. Cho, *J. Org. Chem.* **2006**, *72*, 679–682.
[185] H.-M. Kang, Y.-K. Lim, I.-J. Shin, H.-Y. Kim, C.-G. Cho, *Org. Lett.* **2006**, *8*, 2047–2050.
[186] I. Shimao, S. Oae, *Bull. Chem. Soc. Jpn.* **1983**, *56*, 643–644.
[187] D. A. Blackadder, C. Hinshelwood, *J. Chem. Soc.* **1957**, 2904–2906.
[188] Y. Ogata, Y. Nakagawa, M. Inaishi, *Bull. Chem. Soc. Jpn.* **1981**, *54*, 2853–2854.
[189] E. F. V. Scriven, H. Suschitzky, G. V. Garner, *Tetrahedron Lett.* **1973**, *14*, 103–106.
[190] P. E. Laibinis, G. M. Whitesides, D. L. Allara, Y. T. Tao, A. N. Parikh, R. G. Nuzzo, *J. Am. Chem. Soc.* **1991**, *113*, 7152–7167.
[191] W. B. Caldwell, D. J. Campbell, K. Chen, B. R. Herr, C. A. Mirkin, A. Malik, M. Durbin, P. Dutta, K. Huang, *J. Am. Chem. Soc.* **1995**, *117*, 6071–6082.
[192] H. Wolf, H. Ringsdorf, E. Delamarche, T. Takami, H. Kang, B. Michel, C. Gerber, M. Jaschke, H.-J. Butt, E. Bamberg, *J. Phys. Chem.* **1995**, *99*, 7102–7107.
[193] M. Jaschke, H. Schönherr, H. Wolf, H.-J. Butt, E. Bamberg, M. K. Besocke, H. Ringsdorf, *J. Phys. Chem.* **1996**, *100*, 2290–2301.
[194] K. Tamada, J. Nagasawa, F. Nakanishi, K. Abe, T. Ishida, M. Hara, W. Knoll, *Langmuir* **1998**, *14*, 3264–3271.
[195] S. C. B. Mannsfeld, T. W. Canzler, T. Fritz, H. Proehl, K. Leo, S. Stumpf, G. Goretzki, K. Gloe, *J. Phys. Chem. B* **2002**, *106*, 2255–2260.

[196] C. Gahl, R. Schmidt, D. Brete, E. R. McNellis, W. Freyer, R. Carley, K. Reuter, M. Weinelt, *J. Am. Chem. Soc.* **2010**, *132*, 1831–1838.
[197] B. Stiller, G. Knochenhauer, E. Markava, D. Gustina, I. Muzikante, P. Karageorgiev, L. Brehmer, *Mater. Sci. Eng., C* **1999**, *8-9*, 385–389.
[198] D. G. Walter, D. J. Campbell, C. A. Mirkin, *J. Phys. Chem. B* **1999**, *103*, 402–405.
[199] J. Zhang, J. K. Whitesell, M. A. Fox, *Chem. Mater.* **2001**, *13*, 2323–2331.
[200] K. Tamada, H. Akiyama, T. X. Wei, *Langmuir* **2002**, *18*, 5239–5246.
[201] S. Yasuda, T. Nakamura, M. Matsumoto, H. Shigekawa, *J. Am. Chem. Soc.* **2003**, *125*, 16430–16433.
[202] H. Akiyama, K. Tamada, J. Nagasawa, K. Abe, T. Tamaki, *J. Phys. Chem. B* **2003**, *107*, 130–135.
[203] R. Micheletto, M. Yokokawa, M. Schroeder, D. Hobara, Y. Ding, T. Kakiuchi, *Appl. Surf. Sci.* **2004**, *228*, 265–270.
[204] Z. Wang, A.-M. Nygård, M. J. Cook, D. A. Russell, *Langmuir* **2004**, *20*, 5850–5857.
[205] P. Ahonen, T. Laaksonen, D. J. Schiffrin, K. Kontturi, *Phys. Chem. Chem. Phys.* **2007**, *9*, 4898–4901.
[206] L. F. N. Ah Qune, H. Akiyama, T. Nagahiro, K. Tamada, A. T. S. Wee, *Appl. Phys. Lett.* **2008**, *93*, 083109(3).
[207] A. S. Kumar, T. Ye, T. Takami, B. C. Yu, A. K. Flatt, J. M. Tour, P. S. Weiss, *Nano Lett.* **2008**, *8*, 1644–1648.
[208] R. Wang, T. Iyoda, L. Jiang, D. A. Tryk, K. Hashimoto, A. Fujishima, *J. Electroanal. Chem.* **1997**, *438*, 213–219.
[209] U. Jung, O. Filinova, S. Kuhn, D. Zargarani, C. Bornholdt, R. Herges, O. Magnussen, *Langmuir* **2010**, *26*, 13913–13923.
[210] Y. B. Zheng, J. L. Payton, C.-H. Chung, R. Liu, S. Cheunkar, B. K. Pathem, Y. Yang, L. Jensen, P. S. Weiss, *Nano Lett.* **2011**, *11*, 3447–3452.
[211] M. Ito, T. X. Wei, P.-L. Chen, H. Akiyama, M. Matsumoto, K. Tamada, Y. Yamamoto, *J. Mater. Chem.* **2005**, *15*, 478–483.
[212] U. Siemeling, C. Bruhn, F. Bretthauer, M. Borg, F. Träger, F. Vogel, W. Azzam, M. Badin, T. Strunskus, C. Wöll, *Dalton Trans.* **2009**, 8593–8604.
[213] S. Wagner, F. Leyssner, C. Kördel, S. Zarwell, R. Schmidt, M. Weinelt, K. Rück-Braun, M. Wolf, P. Tegeder, *Phys. Chem. Chem. Phys.* **2009**, *11*, 6242–6248.
[214] D. Takamatsu, Y. Yamakoshi, K. Fukui, *J. Phys. Chem. B* **2006**, *110*, 1968–1970.
[215] B. Baisch, D. Raffa, U. Jung, O. M. Magnussen, C. Nicolas, J. Lacour, J. Kubitschke, R. Herges, *J. Am. Chem. Soc.* **2008**, *131*, 442–443.
[216] R. Wang, T. Iyoda, D. A. Tryk, K. Hashimoto, A. Fujishima, *Langmuir* **1997**, *13*, 4644–4651.
[217] M. Han, T. Honda, D. Ishikawa, E. Ito, M. Hara, Y. Norikane, *J. Mater. Chem.* **2011**, *21*, 4696–4702.
[218] G. Pace, V. Ferri, C. Grave, M. Elbing, C. von Hänisch, M. Zharnikov, M. Mayor, M. A. Rampi, P. Samorì, *Proc. Natl. Acad. Sci.* **2007**, *104*, 9937–9942.
[219] M. Elbing, A. Błaszczyk, C. von Hänisch, M. Mayor, V. Ferri, C. Grave, M. A. Rampi, G. Pace, P. Samorì, A. Shaporenko, et al., *Adv. Funct. Mater.* **2008**, *18*, 2972–2983.
[220] J. M. Mativetsky, G. Pace, M. Elbing, M. A. Rampi, M. Mayor, P. Samorì, *J. Am. Chem. Soc.* **2008**, *130*, 9192–9193.
[221] E. Tirosh, E. Benassi, S. Pipolo, M. Mayor, M. Valášek, V. Frydman, S. Corni, S. R. Cohen, *Beilstein J. Nanotechnol.* **2011**, *2*, 834–844.
[222] H. Debus, *Justus Liebigs Annalen der Chemie* **1850**, *73*, 26–34.
[223] D. Coucouvanis, in *Progress in Inorganic Chemistry, The Chemistry of the Dithioacid and 1,1-Dithiolate Complexes*, John Wiley & Sons, Inc., **2007**.
[224] R. G. Mehta, J. Liu, A. Constantinou, C. F. Thomas, M. Hawthorne, M. You, C. Gerhäuser, J. M. Pezzuto, R. C. Moon, R. M. Moriarty, *Carcinogenesis* **1995**, *16*, 399–404.
[225] S. L. Cao, Y. P. Feng, Y. Y. Jiang, S. Y. Liu, G. Y. Ding, R. T. Li, *Bioorg. Med. Chem. Lett.* **2005**, *15*, 1915–1917.

[226] C. Gerhäuser, M. You, J. Liu, R. M. Moriarty, M. Hawthorne, R. G. Mehta, R. C. Moon, J. M. Pezzuto, *Cancer Res* **1997**, *57*, 272–278.
[227] H. D. Yin, S. C. Xue, *Appl. Organomet. Chem.* **2006**, *20*, 283–289.
[228] Zia-ur-Rehman, A. Shah, N. Muhammad, S. Ali, R. Qureshi, I. S. Butler, *J. Organomet. Chem.* **2009**, *694*, 1998–2004.
[229] A. Mohammad, C. Varshney, S. A. A. Nami, *Spectrochim. Acta, Part A* **2009**, *73*, 20–24.
[230] I. Rogachev, V. Kampel, V. Gusis, N. Cohen, J. Gressel, A. Warshawsky, *Pestic. Biochem. Physiol.* **1998**, *60*, 133–145.
[231] P. K. Gogoi, D. P. Phukan, D. K. Das, *Asian J. Chem.* **1999**, *11*, 1291–1295.
[232] T. Ueno, Y. Suzuki, S. Fujii, A. F. Vanin, T. Yoshimura, *Biochem. Pharmacol.* **2002**, *63*, 485–493.
[233] E. K. Abraham, P. Ramesh, R. Joseph, *J. Appl. Polym. Sci.* **2006**, *102*, 2055–2061.
[234] A. S. Sarpal, J. Christopher, S. Mukherjee, M. B. Patel, G. S. Kapur, *Lubrication Science* **2005**, *17*, 319–345.
[235] D. W. Bruce, in *Inorganic Materials, Metal-Containing Liquid Crystals*, **1992**.
[236] P. Espinet, M. A. Esteruelas, L. A. Oro, J. L. Serrano, E. Sola, *Coord. Chem. Rev.* **1992**, *117*, 215–274.
[237] N. Hoshino-Miyajima, *J. Chem. Soc., Chem. Commun.* **1993**, 1442–1444.
[238] D. J. Price, M. A. Wali, D. W. Bruce, *Polyhedron* **1997**, *16*, 315–320.
[239] J. D. E. T. Wilton-Ely, D. Solanki, G. Hogarth, *Eur. J. Inorg. Chem.* **2005**, *2005*, 4027–4030.
[240] E. R. Knight, N. H. Leung, A. L. Thompson, G. Hogarth, J. D. E. T. Wilton-Ely, *Inorg. Chem.* **2009**, *48*, 3866–3874.
[241] S.-W. Lai, M. G. . Drew, P. D. Beer, *J. Organomet. Chem.* **2001**, *637–639*, 89–93.
[242] O. D. Fox, M. G. B. Drew, P. D. Beer, *Angew. Chem. Int. Ed.* **2000**, *39*, 135–140.
[243] W. W. H. Wong, J. Cookson, E. A. L. Evans, E. J. L. McInnes, J. Wolowska, J. P. Maher, P. Bishop, P. D. Beer, *Chem. Commun.* **2005**, 2214–2216.
[244] P. Morf, N. Ballav, F. Nolting, F. von Wrochem, H.-G. Nothofer, A. Yasuda, J. M. Wessels, T. A. Jung, *ChemPhysChem* **2009**, *10*, 2212–2216.
[245] P. Morf, N. Ballav, M. Putero, F. von Wrochem, J. M. Wessels, T. A. Jung, *J. Phys. Chem. Lett.* **2010**, *1*, 813–816.
[246] H. Zhu, D. M. Coleman, C. J. Dehen, I. M. Geisler, D. Zemlyanov, J. Chmielewski, G. J. Simpson, A. Wei, *Langmuir* **2008**, *24*, 8660–8666.
[247] Z. Li, D. S. Kosov, *J. Phys. Chem. B* **2006**, *110*, 9893–9898.
[248] R. Chant, A. Hendrickson, R. Martin, N. Rohde, *Aust. J. Chem.* **1973**, *26*, 2533–2536.
[249] D. Lewis, S. Lippard, J. Zubieta, *Inorg. Chem.* **1972**, *11*, 823–828.
[250] J. M. Wessels, H.-G. Nothofer, W. E. Ford, F. von Wrochem, F. Scholz, T. Vossmeyer, A. Schroedter, H. Weller, A. Yasuda, *J. Am. Chem. Soc.* **2004**, *126*, 3349–3356.
[251] M. S. Vickers, J. Cookson, P. D. Beer, P. T. Bishop, B. Thiebaut, *J. Mater. Chem.* **2006**, *16*, 209–215.
[252] J. Sharma, R. Chhabra, H. Yan, Y. Liu, *Chem. Commun.* **n.d.**, 2140–2142.
[253] D. P. Cormode, J. J. Davis, P. D. Beer, *J. Inorg. Organomet. Polym. Mater.* **2007**, *18*, 32–40.
[254] F. Takami, K. Tokuyama, S. Wakahara, T. Maeda, *Chem. Pharm. Bull.* **1973**, *21*, 329–334.
[255] E. Humeres, N. A. Debacher, M. M. S. Sierra, J. D. Franco, A. Schutz, *J. Org. Chem.* **1998**, *63*, 1598–1603.
[256] S. P. Ewing, D. Lockshon, W. P. Jencks, *J. Am. Chem. Soc.* **1980**, *102*, 3072–3084.
[257] F. Liang, J. Tan, C. Piao, Q. Liu, *Synthesis* **2008**, *2008*, 3579–3584.
[258] J. Cookson, P. D. Beer, *Dalton Trans.* **2007**, 1459.
[259] G. Hogarth, in *Progress in Inorganic Chemistry, Transition Metal Dithiocarbamates* (Ed.: K.D. Karlin), John Wiley & Sons, Inc., **2005**.
[260] J. D. E. T. Wilton-Ely, D. Solanki, E. R. Knight, K. B. Holt, A. L. Thompson, G. Hogarth, *Inorg. Chem.* **2008**, *47*, 9642–9653.
[261] E. R. Knight, A. R. Cowley, G. Hogarth, J. D. E. T. Wilton-Ely, *Dalton Trans.* **2009**, 607–609.

[262] R. D. Weinstein, J. Richards, S. D. Thai, D. M. Omiatek, C. A. Bessel, C. J. Faulkner, S. Othman, G. K. Jennings, *Langmuir* **2007**, *23*, 2887–2891.
[263] L. Neelakantan, *J. Org. Chem.* **1958**, *23*, 938–939.
[264] F. A. Murphy, S. Suárez, E. Figgemeier, E. R. Schofield, S. M. Draper, *Chem. Eur. J.* **2009**, *15*, 5740–5748.
[265] S. Wang, R. C. Advincula, *Org. Lett.* **2001**, *3*, 3831–3834.
[266] M. Elbing, Funktionale Molekulare Bausteine, Dissertation, Universität Karlsruhe, **2004**.
[267] C. Vericat, M. E. Vela, G. Benitez, P. Carro, R. C. Salvarezza, *Chem. Soc. Rev.* **2010**, *39*, 1805–1834.
[268] K. Rößler, T. Rüffer, B. Walfort, R. Packheiser, R. Holze, M. Zharnikov, H. Lang, *J. Organomet. Chem.* **2007**, *692*, 1530–1545.
[269] A. De Meijere, F. Diederich, *Metal-Catalyzed Cross-Coupling Reactions*, Wiley-VCH, **2004**.
[270] F. Korte, *Methodicum Chimicum : A Critical Survey of Proven Methods and Their Application in Chemistry, Natural Science, and Medicine*, Academic Press, **1975**.
[271] P. G. M. Wuts, T. W. Greene, *Greene's Protective Groups in Organic Synthesis*, Wiley-VCH, **2007**.
[272] C. J. Yu, Y. Chong, J. F. Kayyem, M. Gozin, *J. Org. Chem.* **1999**, *64*, 2070–2079.
[273] S. Grunder, R. Huber, S. Wu, C. Schönenberger, M. Calame, M. Mayor, *Eur. J. Org. Chem.* **2010**, *5*, 833–845.
[274] D. G. Hall, *Boronic Acids: Preparation and Applications in Organic Synthesis and Medicine*, Wiley-VCH, **2005**.
[275] N. Crivillers, A. Liscio, F. Di Stasio, C. Van Dyck, S. Osella, D. Cornil, S. Mian, G. M. Lazzerini, O. Fenwick, E. Orgiu, et al., *Phys. Chem. Chem. Phys.* **2011**, *13*, 14302–14310.
[276] J. S. Kim, B. Lägel, E. Moons, N. Johansson, I. D. Baikie, W. R. Salaneck, R. H. Friend, F. Cacialli, *Synth. Met.* **2000**, *111–112*, 311–314.
[277] N. D. Orf, I. D. Baikie, O. Shapira, Y. Fink, *Appl. Phys. Lett.* **2009**, *94*, 113504(3).
[278] N. Crivillers, E. Orgiu, F. Reinders, M. Mayor, P. Samorì, *Adv. Mater.* **2011**, *23*, 1447–1452.
[279] D. J. Gundlach, J. E. Royer, S. K. Park, S. Subramanian, O. D. Jurchescu, B. H. Hamadani, A. J. Moad, R. J. Kline, L. C. Teague, O. Kirillov, et al., *Nat. Mater.* **2008**, *7*, 216–221.
[280] T. Dadosh, Y. Gordin, R. Krahne, I. Khivrich, D. Mahalu, V. Frydman, J. Sperling, A. Yacoby, I. Bar-Joseph, *Nature* **2005**, *436*, 677–680.
[281] J. Liao, L. Bernard, M. Langer, C. Schönenberger, M. Calame, *Adv. Mater.* **2006**, *18*, 2444–2447.
[282] S. J. van der Molen, J. Liao, T. Kudernac, J. S. Agustsson, L. Bernard, M. Calame, B. J. van Wees, B. L. Feringa, C. Schönenberger, *Nano Lett.* **2008**, *9*, 76–80.
[283] D. P. Long, C. H. Patterson, M. H. Moore, D. S. Seferos, G. C. Bazan, J. G. Kushmerick, *Appl. Phys. Lett.* **2005**, *86*, 153105(3).
[284] V. Faramarzi, C. Raimondo, F. Reinders, M. Mayor, P. Samorì, B. Doudin, *Appl. Phys. Lett.* **2011**, *99*, 233104(3).
[285] C. Raimondo, N. Crivillers, F. Reinders, F. Sander, M. Mayor, P. Samorì, *Proc. Natl. Acad. Sci.* **2012**, DOI 10.1073/pnas.201203848.
[286] H. Sirringhaus, P. J. Brown, R. H. Friend, M. M. Nielsen, K. Bechgaard, B. M. W. Langeveld-Voss, A. J. H. Spiering, R. a. J. Janssen, E. W. Meijer, P. Herwig, et al., *Nature* **1999**, *401*, 685–688.
[287] S. Ho Choi, B. Kim, C. D. Frisbie, *Science* **2008**, *320*, 1482–1486.
[288] V. Ruiz, P. G. Nicholson, S. Jollands, P. A. Thomas, J. V. Macpherson, P. R. Unwin, *J. Phys. Chem. B* **2005**, *109*, 19335–19344.
[289] P. Cyganik, M. Buck, W. Azzam, C. Wöll, *J. Phys. Chem. B* **2004**, *108*, 4989–4996.
[290] J. Liu, B. Schüpbach, A. Bashir, O. Shekhah, A. Nefedov, M. Kind, A. Terfort, C. Wöll, *Phys. Chem. Chem. Phys.* **2010**, *12*, 4459–4472.
[291] L. V. Schäfer, E. M. Müller, H. E. Gaub, H. Grubmüller, *Angew. Chem. Int. Ed.* **2007**, *46*, 2232–2237.
[292] M. Grandbois, M. Beyer, M. Rief, H. Clausen-Schaumann, H. E. Gaub, *Science* **1999**, *283*, 1727–1730.
[293] H. Grundberg, M. Andergran, U. J. Nilsson, *Tetrahedron Lett.* **1999**, *40*, 1811–1814.

[294] Y. Shirai, J. M. Guerrero, T. Sasaki, T. He, H. Ding, G. Vives, B.-C. Yu, L. Cheng, A. K. Flatt, P. G. Taylor, et al., *J. Org. Chem.* **2009**, *74*, 7885–7897.
[295] B. T. Holmes, A. W. Snow, *Tetrahedron* **2005**, *61*, 12339–12342.
[296] E. A. Meyer, R. K. Castellano, F. Diederich, *Angew. Chem. Int. Ed.* **2003**, *42*, 1210–1250.
[297] C. R. Patrick, G. S. Prosser, *Nature* **1960**, *187*, 1021–1021.
[298] R. T. Bailey, R. U. Ferri, *Spectrochim. Acta, Part A* **1980**, *36*, 69–74.
[299] J. S. W. Overell, G. S. Pawley, *Acta Crystallogr., Sect. B* **1982**, *38*, 1966–1972.
[300] J. H. Williams, J. K. Cockcroft, A. N. Fitch, *Angew. Chem. Int. Ed.* **1992**, *31*, 1655–1657.
[301] E. G. Cox, D. W. J. Cruickshank, J. a. S. Smith, *Proc. R. Soc. Lond. A* **1958**, *247*, 1–21.
[302] N. Boden, P. P. Davis, C. H. Stam, G. A. Wesselink, *Mol. Phys.* **1973**, *25*, 81–86.
[303] J. Hernández-Trujillo, M. Costas, A. Vela, *J. Chem. Soc., Faraday Trans.* **1993**, *89*, 2441–2443.
[304] C. A. Hunter, K. R. Lawson, J. Perkins, C. J. Urch, *J. Chem. Soc., Perkin Trans. 2* **2001**, 651–669.
[305] S. Tsuzuki, T. Uchimaru, M. Mikami, *J. Phys. Chem. A* **2006**, *110*, 2027–2033.
[306] J. Smith, R. Hamilton, Y. Qi, A. Kahn, D. D. C. Bradley, M. Heeney, I. McCulloch, T. D. Anthopoulos, *Adv. Funct. Mater.* **2010**, *20*, 2330–2337.
[307] S. Karpe, M. Oçafrain, K. Smaali, S. Lenfant, D. Vuillaume, P. Blanchard, J. Roncali, *Chem. Commun.* **2010**, *46*, 3657–3659.
[308] K. Smaali, S. Lenfant, S. Karpe, M. Oçafrain, P. Blanchard, D. Deresmes, S. Godey, A. Rochefort, J. Roncali, D. Vuillaume, *ACS Nano* **2010**, *4*, 2411–2421.
[309] S. Hotta, T. Yamao, *J. Mater. Chem.* **2011**, *21*, 1295–1304.
[310] Y. Liu, Y. Liu, X. Zhan, *Macromol. Chem. Phys.* **2011**, *212*, 428–443.
[311] F. Zhang, D. Wu, Y. Xu, X. Feng, *J. Mater. Chem.* **2011**, *21*, 17590–17600.
[312] A. Samokhvalov, *ChemPhysChem* **2011**, *12*, 2870–2885.
[313] D. W. Mosley, M. A. Sellmyer, E. J. Daida, J. M. Jacobson, *J. Am. Chem. Soc.* **2003**, *125*, 10532–10533.
[314] R. Valiokas, S. Svedhem, M. Östblom, S. C. T. Svensson, B. Liedberg, *J. Phys. Chem. B* **2001**, *105*, 5459–5469.
[315] E. Cooper, G. J. Leggett, *Langmuir* **1999**, *15*, 1024–1032.
[316] H.-H. Lee, Z. Ruželė, L. Malysheva, A. Onipko, A. Gutés, F. Björefors, R. Valiokas, B. Liedberg, *Langmuir* **2009**, *25*, 13959–13971.
[317] R. Arnold, W. Azzam, A. Terfort, C. Wöll, *Langmuir* **2002**, *18*, 3980–3992.
[318] S. Pawsey, M. McCormick, S. De Paul, R. Graf, Y. S. Lee, L. Reven, H. W. Spiess, *J. Am. Chem. Soc.* **2003**, *125*, 4174–4184.
[319] R. Valiokas, M. Östblom, S. Svedhem, S. C. T. Svensson, B. Liedberg, *J. Phys. Chem. B* **2002**, *106*, 10401–10409.
[320] R. K. Smith, S. M. Reed, P. A. Lewis, J. D. Monnell, R. S. Clegg, K. F. Kelly, L. A. Bumm, J. E. Hutchison, P. S. Weiss, *J. Phys. Chem. B* **2001**, *105*, 1119–1122.
[321] H. M. D. Bandara, T. R. Friss, M. M. Enriquez, W. Isley, C. Incarvito, H. A. Frank, J. Gascon, S. C. Burdette, *J. Org. Chem.* **2010**, *75*, 4817–4827.
[322] M. S. Gibson, R. W. Bradshaw, *Angew. Chem. Int. Ed.* **1968**, *7*, 919–930.
[323] R. G. R. Bacon, A. Karim, *J. Chem. Soc., Perkin Trans. 1* **1973**, 272–278.
[324] M. Sato, S. Ebine, S. Akabori, *Synthesis* **1981**, *1981*, 472–473.
[325] H. R. Ing, R. H. F. Manske, *J. Chem. Soc.* **1926**, 2348–2351.
[326] M. Havelková, M. Hocek, M. Česnek, D. Dvořák, *Synlett* **1999**, *1999*, 1145–1147.
[327] M. Havelková, D. Dvořak, M. Hocek, *Synthesis* **2001**, *2001*, 1704–1710.
[328] T. Korenaga, T. Kosaki, R. Fukumura, T. Ema, T. Sakai, *Org. Lett.* **2005**, *7*, 4915–4917.
[329] J. Kvíčala, M. Beneš, O. Paleta, V. Král, *J. Fluorine Chem.* **2010**, *131*, 1327–1337.
[330] A. Błaszczyk, M. Fischer, C. von Hänisch, M. Mayor, *Helv. Chim. Acta* **2006**, *89*, 1986–2005.
[331] N. Stuhr-Hansen, *Synth. Commun.* **2003**, *33*, 641–646.
[332] T. Pinault, F. Chérioux, B. Therrien, G. Süss-Fink, *Heteroatom Chem.* **2004**, *15*, 121–126.
[333] S. J. Shaw, K. J. Elgie, C. Edwards, R. W. Boyle, *Tetrahedron Lett.* **1999**, *40*, 1595–1596.

[334] S. Hotta, T. Katagiri, *J. Heterocycl. Chem.* **2003**, *40*, 845–850.
[335] P. Bäuerle, F. Würthner, G. Götz, F. Effenberger, *Synthesis* **1993**, *1993*, 1099–1103.
[336] J. J. Apperloo, L. B. Groenendaal, H. Verheyen, M. Jayakannan, R. A. J. Janssen, A. Dkhissi, D. Beljonne, R. Lazzaroni, J. Brédas, *Chem. Eur. J.* **2002**, *8*, 2384–2396.
[337] T. Cardolaccia, A. M. Funston, M. E. Kose, J. M. Keller, J. R. Miller, K. S. Schanze, *J. Phys. Chem. B* **2007**, *111*, 10871–10880.
[338] C. David, C. L. Franklin, P. R. Guzzo, L. S. Lin, J. Liu, M. M.-C. Lo, R. P. Nargund, I. K. Sebhat, *Preparation of Imidazole Derivatives as Bombesin Receptor Subtype-3 Modulators*, **2008**, U.S. Patent WO2008051404 A2.
[339] Z. Nie, C. Perretta, J. Lu, Y. Su, S. Margosiak, K. S. Gajiwala, J. Cortez, V. Nikulin, K. M. Yager, K. Appelt, et al., *J. Med. Chem.* **2005**, *48*, 1596–1609.
[340] S. A. Burkitt, M. G. Cardozo, T. D. Cushing, M. R. DeGraffenreid, X. Hao, X. Y. Jiao, M.-L. Smith, A. Smith, Y. Shin, S. P. Rasmussen, et al., *Antiinflammation Agents*, **2004**, U.S. Patent US2004/97485 A1.
[341] M. J. Burns, I. J. S. Fairlamb, A. R. Kapdi, P. Sehnal, R. J. K. Taylor, *Org. Lett.* **2007**, *9*, 5397–5400.
[342] C. Kleeberg, L. Dang, Z. Lin, T. B. Marder, *Angew. Chem. Int. Ed.* **2009**, *48*, 5350–5354.
[343] T. Oriyama, K. Noda, K. Yatabe, *Synlett* **1997**, *1997*, 701–703.
[344] B. W. Erickson, R. B. Merrifield, *J. Am. Chem. Soc.* **1973**, *95*, 3750–3756.
[345] R. S. Lott, V. S. Chauhan, C. H. Stammer, *J. Chem. Soc., Chem. Commun.* **1979**, 495–496.
[346] A. Mehta, R. Jaouhari, T. J. Benson, K. T. Douglas, *Tetrahedron Lett.* **1992**, *33*, 5441–5444.
[347] Y. Kiso, K. Ukawa, S. Nakamura, K. Ito, T. Akita, *Chem. Pharm. Bull.* **1980**, *28*, 673–676.
[348] S. F. Martin, K. X. Chen, C. T. Eary, *Org. Lett.* **1999**, *1*, 79–82.
[349] T. Akiyama, H. Hirofuji, S. Ozaki, *Tetrahedron Lett.* **1991**, *32*, 1321–1324.
[350] N. Crivillers, S. Osella, C. Van Dyck, G. M. Lazzerini, D. Cornil, A. Liscio, F. Di Stasio, S. Mian, O. Fenwick, F. Reinders, et al., *Adv. Mater.* **2012**, DOI 10.1002/adma.201201737.
[351] G. Lu, B. Cheng, H. Shen, Z. Chen, G. Yang, C. A. Marquette, L. J. Blum, O. Tillement, S. Roux, G. Ledoux, et al., *Appl. Phys. Lett.* **2006**, *88*, 023903(3).
[352] R. J. Klein, D. A. Fischer, J. L. Lenhart, *Langmuir* **2011**, *27*, 12423–12433.
[353] J. B. Schlenoff, M. Li, H. Ly, *J. Am. Chem. Soc.* **1995**, *117*, 12528–12536.
[354] Q. J. McCubbin, F. J. Stoddart, T. Welton, A. J. . White, D. J. Williams, *Inorg. Chem* **1998**, *37*, 3753–3758.
[355] S. Grunder, R. Huber, V. Horhoiu, M. T. González, C. Schönenberger, M. Calame, M. Mayor, *J. Org. Chem.* **2007**, *72*, 8337–8344.
[356] J. J. Li, *Name Reactions : A Collection of Detailed Reaction Mechanisms*, Springer, **2002**.
[357] T. Gibtner, F. Hampel, J. Gisselbrecht, A. Hirsch, *Chem. Eur. J.* **2002**, *8*, 408–432.
[358] G. Margraf, J. W. Bats, M. Wagner, H. W. Lerner, *Inorg. Chim. Acta* **2005**, *358*, 1193–1203.
[359] M. Alami, others, *Tetrahedron Lett.* **1993**, *34*, 6403–6406.
[360] V. A. Montes, R. Pohl, J. Shinar, P. Anzenbacher, *Chem. Eur. J.* **2006**, *12*, 4523–4535.
[361] Y. Liang, Y.-X. Xie, J.-H. Li, *J. Org. Chem.* **2006**, *71*, 379–381.
[362] H. Wang, Z. Lu, S. J. Lord, K. A. Willets, J. A. Bertke, S. D. Bunge, W. E. Moerner, R. J. Twieg, *Tetrahedron* **2007**, *63*, 103–114.
[363] B. Mann, H. Kuhn, *J. Appl. Phys.* **1971**, *42*, 4398–4405.
[364] G. J. Ashwell, *Thin Solid Films* **1990**, *186*, 155–165.
[365] C. M. Fischer, M. Burghard, S. Roth, K. v Klitzing, *Appl. Phys. Lett.* **1995**, *66*, 3331–3333.
[366] X. Lu, H. Yuan, G. Zuo, J. Yang, *Thin Solid Films* **2008**, *516*, 6476–6482.
[367] K. Rajalingam, L. Hallmann, T. Strunskus, A. Bashir, C. Wöll, F. Tuczek, *Phys. Chem. Chem. Phys.* **2010**, *12*, 4390–4399.
[368] S.-C. Chang, I. Chao, Y.-T. Tao, *J. Am. Chem. Soc.* **1994**, *116*, 6792–6805.
[369] F. von Wrochem, F. Scholz, A. Yasuda, J. M. Wessels, *J. Phys. Chem. C* **2009**, *113*, 12395–12401.

[370] M. V. Patel, T. Kolasa, K. Mortell, M. A. Matulenko, A. A. Hakeem, J. J. Rohde, S. L. Nelson, M. D. Cowart, M. Nakane, L. N. Miller, et al., *J. Med. Chem.* **2006**, *49*, 7450–7465.

[371] J. Levell, P. Astles, P. Eastwood, J. Cairns, O. Houille, S. Aldous, G. Merriman, B. Whiteley, J. Pribish, M. Czekaj, et al., *Bioorg. Med. Chem.* **2005**, *13*, 2859–2872.

[372] M. G. Sarwar, B. Dragisic, L. J. Salsberg, C. Gouliaras, M. S. Taylor, *J. Am. Chem. Soc.* **2010**, *132*, 1646–1653.

[373] R. Appel, R. Appel, *Angew. Chem.* **1975**, *87*, 863–874.

[374] G. W. Gray, J. B. Hartley, B. Jones, *J. Chem. Soc.* **1955**, 1412–1420.

9 Appendix

9.1 Contributions

All molecules were synthesized and characterized by Federica Reinders from the research group of Prof. Dr. Marcel Mayor. The described surface measurements were performed in the groups of Prof. Dr. Paolo Samorì and Prof. Dr. Bernard Doudin and at the Material Science Laboratory of SONY Deutschland GmbH in Stuttgart by Dr. Florian von Wrochem and Dr. William Ford.

9.2 Publications

Parts of the work presented in this thesis have been published in the following articles:

C. Raimondo, N. Crivillers, F. Reinders, F. Sander, M. Mayor, P. Samorì
Optically switchable organic field-effect transistors based on photoresponsive gold nanoparticles blended with poly(3-hexylthiophene)
Proc. Natl. Acad. Sci. **2012**, doi: 10.1073/pnas.201203848, accepted.

N. Crivillers, S. Osella, C. Van Dyck, G. M. Lazzerini, D. Cornil, A. Liscio, F. Di Stasio, S. Mian, O. Fenwick, F. Reinders, M. Neuburger, E. Treossi, M. Mayor, V. Palermo, F. Cacialli, J. Cornil, P. Samorì
Large Au work function shift induced by a novel perfluorinated azobenzene-based self-assembled monolayer
Adv. Mater. **2012**, doi: 10.1002/adma.201201737, online.

V. Faramarzi, C. Raimondo, F. Reinders, M. Mayor, P. Samorì, B. Doudin
Optically switchable molecular device using microsphere based junctions
Appl. Phys. Lett. **2011**, *99*, 233104-3.

N. Crivillers, A. Liscio, F. Di Stasio, C. Van Dyck, S. Osella, D. Cornil, S. Mian, G. M. Lazzerini, O. Fenwick, E. Orgiu, F. Reinders, S. Braun, M. Fahlman, M. Mayor, J. Cornil, V. Palermo, F. Cacialli and P. Samorì
Photoinduced work function changes by isomerization of a densely packed azobenzene-based SAM on Au: a joint experimental and theoretical study
Phys. Chem. Chem. Phys. **2011**, *13* (32), 14302-14310.

N. Crivillers, E. Orgiu, F. Reinders, M. Mayor, P. Samorì

Optical Modulation of the Charge Injection in an Organic Field-Effect Transistor Based on Photochromic Self-assembled-Monolayer Functionalized Electrodes

Adv. Mater. **2011**, *23*, 1447-1452.

C. Raimondo, F. Reinders, U. Soydaner, M. Mayor, P. Samorì

Light-responsive reversible solvation and precipitation of gold nanoparticles

Chem. Commun. **2010**, *46*, 1147-1149.

9.3 Cover Design

The cover of this book was designed by Federica Reinders.

Curriclum Vitae

Personal Information

Name	Federica Reinders
Date/place of birth	April 24th, 1982 in Sana'a, Yemen
Citizenship	German

Education

06/2008 – 07/2012	**PhD** work at the University of Basel, Department of Chemistry, Switzerland. Supervisor: Prof. Dr. Marcel Mayor. Thesis: "Azobenzenes and Dithiocarbamates in Molecular Film Devices".
04/2007 – 05/2008	**Master of Science (MSc)** in Chemistry, Institute of Organic Chemistry, University of Basel, Switzerland. Supervisor: Prof. Dr. Marcel Mayor. Thesis: "Molecular Building Blocks for a Touching Molecular Film Device".
10/2004 – 03/2007	**Bachelor of Science (BSc)** in Chemistry, University of Basel, Switzerland.
2002 – 2004	Chemistry studies at the University of Freiburg, Germany
1993 – 2002	**Abitur** at the Kant-Gymnasium in Weil am Rhein, Germany.

Publications

Optically switchable organic field-effect transistors based on photoresponsive gold nanoparticles blended with poly(3-hexylthiophene), C. Raimondo, N. Crivillers, F. Reinders, F. Sander, M. Mayor, P. Samorì, *Proc. Natl. Acad. Sci.* 2012, doi: 10.1073/pnas.201203848, accepted.

Large Au work function shift induced by a novel perfluorinated azobenzene-based self-assembled monolayer, N. Crivillers, S. Osella, C. Van Dyck, G. M. Lazzerini, D. Cornil, A. Liscio, F. Di Stasio, S. Mian, O. Fenwick, F. Reinders, M. Neuburger, E. Treossi, M. Mayor, V. Palermo, F. Cacialli, J. Cornil, P. Samorì, *Adv. Mater.* 2012, doi: 10.1002/adma.201201737, online.

Optically switchable molecular device using microsphere based junctions, V. Faramarzi, C. Raimondo, F. Reinders, M. Mayor, P. Samorì, B. Doudin, *Appl. Phys. Lett.* **2011**, *99*, 233104-3.

Photoinduced work function changes by isomerization of a densely packed azobenzene-based SAM on Au: a joint experimental and theoretical study, N. Crivillers, A. Liscio, F. Di Stasio, C. Van Dyck, S. Osella, D. Cornil, S. Mian, G. M. Lazzerini, O. Fenwick, E. Orgiu, F. Reinders, S. Braun, M. Fahlman, M. Mayor, J. Cornil, V. Palermo, F. Cacialli, P. Samorì, *Phys. Chem. Chem. Phys.* **2011**, *13* (32), 14302-14310.

Optical Modulation of the Charge Injection in an Organic Field-Effect Transistor Based on Photochromic Self-assembled-Monolayer Functionalized Electrodes, N. Crivillers, E. Orgiu, F. Reinders, M. Mayor, P. Samorì, *Adv. Mater.* **2011**, *23*, 1447-1452.

Light-responsive reversible solvation and precipitation of gold nanoparticles, C. Raimondo, F. Reinders, U. Soydaner, M. Mayor, P. Samorì, *Chem. Commun.* **2010**, *46*, 1147-1149.

The first complex of 4'-(4-methylthiophenyl)-2,2':6',2''-terpyridine – A model for terpylated self-assembled monolayers, E. C. Constable, C. E. Housecroft, E. Medlycott, M. Neuburger, F. Reinders, S. Reymann, S. Schaffner, *Inorg. Chem. Commun.* **2008**, *11*, 518-520.

Bis(4'-phenyl-2,2':6',2"-terpyridine)ruthenium(II): Holding the $\{Ru(tpy)_2\}^{2+}$ embraces at bay, E. C. Constable, C. E. Housecroft, E. Medlycott, M. Neuburger, F. Reinders, S. Reymann, S. Schaffner, *Inorg. Chem. Commun.* **2008**, *11*, 805-808.